UNIVERSITÄT ZU LÜBECK

From the Institute of Virology and Cell Biology
of the University of Lübeck
Director: Prof. Dr. Norbert Tautz

Functional characterization of nonstructural protein 2 of closely related *Flaviviridae* members

Dissertation
for Fulfillment of
Requirements
for the Doctoral Degree
of the University of Lübeck

from the Department of Natural Sciences

Submitted by
Thomas Walther
From Dresden

Lübeck 2021

First referee: Prof. Dr. Norbert Tautz

Second referee: Prof. Dr. Thomas Krey

Date of oral examination: 16.11.2021

Approved for printing: Lübeck, 18.11.2021

Parts of this work have been published:

Walther T. (2017). Experimentelle Charakterisierung des pestiviralen NS2 Membranproteins. Universität zu Lübeck.

Walther T., Fellenberg J., Klemens O., Isken O. and Tautz N. (2021). Membrane Topology of Pestiviral Nonstructural Protein 2 and determination of the minimal autoprotease domain. J Virol. 95. Accepted.

Parts of this work are prepared for publication:

Isken O., **Walther T.**, et al. and Tautz N. (2021). Identification of NS2 determinants stimulating intrinsic HCV NS2 protease activity. Manuscript in preparation.

Parts of this work were presented:

Tautz N., **Walther T.** (Presenter), Fellenberg J. Experimental determination of the BVDV NS2 membrane topology. 28th Annual Meeting of the Society for Virology, Würzburg 2018 (Oral presentation)

Walther T., Tautz N. Determination of the membrane topology of nonstructural protein 2 (NS2) of pestiviruses. 12th Student Symposium on Molecular Medicine, Ulm 2018 (Oral presentation)

Walther T., Isken O., Wong L., Tautz N. Identification of NS2 determinants stimulating intrinsic NS2 protease activity- molecular insights into the HCV NS2-NS3 autoprotease mechanism. 29th Annual Meeting of the Society for Virology, Düsseldorf 2019 (Poster presentation)

I Table of contents

II Abbreviations

°C	degree Celsius
µ	micro (10^{-6})
A	adenosine
aa	amino acid
Ab	antibody
ase	anti-sense
ATP	adenosinetriphosphate
BDV	Border Disease Virus
bp	base pairs
BSA	bovine serum albumine
BVDV	Bovine Viral Diarrhea Virus
C	”core”(nucleocapsid protein), cytosine
C terminus	carboxy terminus
cDNA	complementary DNA
cp	cytopathogenic
CPE	cytopathic effect
CSFV	Classical Swine Fever Virus
C-terminal	carboxy-terminal
CTP	cytosinetriphosphate
Cy3®	Cyanine 3
DAPI	4,6-diamidino-2-phenylindole
ddH_2O	double distilled water
DEPC	diethylepyrocarbonate
DMEM	Dulbecco’s Modified Eagle Medium
DNA	desoxyribonucleic acid
DNase	desoxyribonuclease
dNTP	desoxynucleosidetriphosphate
E	Envelope protein
E. coli	Escherichia coli
EDTA	ethylene diamine tetraacetic acid
EMCV	Encephalomyocarditis Virus
ER	Endoplasmatic Reticulum
EtOH	ethanol
F	Farad (unit of electric capacity)
Fig.	figure
FCS	fetal calf serum
g	gram, standard gravity
G	guanosine

G418	Geneticin
GTP	guanosinetriphosphate
h	hour, hours
HA	hemagglutinin
HCV	Hepatitis C Virus
HS	horse serum
HSP	heatshock protein
Huh	human hepatoma
IF	indirect immunofluorescence
IFN	Interferone
Ig	immunoglobulin
IRES	internal ribosomal entry site
IRF	Interferone Regulatory Factor
JBD	Jiv-binding domain
Jiv	J-domain-protein interacting with viral protein (DNAJC14)
k	kilo (10^3)
kb	kilobases
kDa	kilodalton
l	litre
LB	lysogeny broth
m	milli (10^{-3})
M	molar
mAb	monoclonal antibody
MBD	membrane binding domain
MD	mucosal disease
MDBK	“Madin Darby Bovien Kidney” cells
MEM	Minimal Essential Medium
min	minute, minutes
MOI	multiplicity of infection
mRNA	messenger RNA
MVA	Modified Virus Ankara
n	nano (10^{-9})
N terminus	amino terminus
ncp	non-cytopathogenic
nm	nanometer
N^{pro}	N-terminal protease
NS	nonstructural protein
nt	nucleotide
nt	Nukleotid
N-terminal	amino-terminal

NTPase	nukleosidtriphosphatase
OD	optical density
ORF	open reading frame
OST	oligosaccharyltransferase
P	phosphate
p	plasmid
PAGE	polyacrylamide gel electrophoresis
PBS	phosphate buffered saline
PBS-T	PBS with 0.05% Tween 20
PCR	polymerase chain reaction
pe	post electroporation
PEG	polyethyleneglycol
PFA	paraformaldehyde
Pfu	*Pyrococcus furiosus*
pi	post infection
PI	persitently infected
PM	Plasmamembran
PNGase	peptide-N-glycosidase
PO	(horseradish) peroxidase
RdRp	RNA dependent RNA polymerase
RNA	ribonucleic acid
RNase	ribonuclease
rns	ribonuclease secreted
rNTP	ribonukleosidetriphosphate
RT	room temperature, reverse transcription, reverse transcriptase
s	second, seconds
SCAM	Substituted Cystein Accessibility Method
SDS	sodiumdodecylsulfate
se	sense
SK6	“Swine Kidney” cells
ssRNA	single stranded RNA
T	thymidine
TAE	Tris-Acetate/EDTA
Taq	*Thermus aquaticus*
$TCID_{50}$	Tissue Culture Infectious Dose 50
TEMED	tetramethylethylenediamine
TM	transmembrane, transmembraneous, transmembrane domain, transmembrane helix, transmembrane segment
TMS	transmembrane segment
Tris	Tris(hydroxymethyl)aminomethane

TTP	thymidinetriphosphate
U	unit, uridine (nt)
Ubi	ubiquitin
UTR	untranslated region
UV	ultraviolet
V	volt
v/v	percent by volume
w/v	percent by weight
wt, WT	Wildtyp
X-Gal	5-bromo-4-chloro-3-indolyl-β-D-galactopyranoside
Zn	zink
α	anti, alpha
β	beta

1 Summary

Positive-strand RNA viruses of the *Flaviviridae* family encode a polyprotein that is cleaved by cellular and viral proteases into mature structural and nonstructural (NS) proteins. A special feature of *Flaviviridae* is the importance of NS proteins for both genome replication and virion morphogenesis. Nonstructural protein 2 (NS2) of Hepatitis C Virus (HCV) and pestiviruses plays a central role in their life cycles. First, NS2 catalyzes NS2-3 cleavage, releasing NS3 and thereby enabling the assembly of viral replicase. This process requires viral (in the case of HCV) or cellular (in the case of pestiviruses) cofactor-mediated NS2 protease activation. Second, NS2, either as free NS2 (HCV) or as uncleaved NS2-3 (pestiviruses), fulfills different roles in virion morphogenesis that are still incompletely characterized. Accordingly, a detailed knowledge of structural and functional properties of pestiviral and HCV NS2 as well as their uncleaved precursor proteins is imperative for a better understanding of these processes.

To overcome the lack of structural data on pestiviral NS2, a membrane topology model of bovine viral diarrhea virus 1 (BVDV-1) NS2 was determined using a substituted cysteine accessibility method (SCAM) assay. The determined BVDV NS2 topology, while overall comparable to that of HCV NS2, also revealed potentially important differences between the two molecules. This model was subsequently used to define the minimal pestiviral NS2 autoprotease domain. Here, it was shown that at least one transmembrane (TM) segment is essential for maintaining the residual activity of the BVDV-1 NS2 protease, whereas HCV and some hepaciviral NS2 are known to remain active in the absence of TM regions.

While structural data of the HCV NS2 protease domain and a membrane topology are available, the NS2 determinants that support activation of the NS2 protease by NS3 are still unknown. Based on the recent observation that a hydrophobic NS3 protease surface patch contains NS3 determinants mediating NS2 protease activation, two NS2 surface residues (F103 and L144) were identified in this work that, when mutated, stimulated the intrinsic NS2 protease activity in the absence of NS3. Further analyses of these NS2 determinants showed that (i) their stimulatory character is conserved among different HCV genotypes, (ii) both residues might employ different modes of action to contribute to the stimulation of the intrinsic NS2 protease activity and (iii) that optimal NS2-NS3 surface interactions are required for efficent NS3-mediated NS2 protease activation since mutations of these determinants are attenuating NS2-NS3 cleavage and RNA replication. An attractive hypothesis of this work is that mutations of these NS2 surface determinants (F103A and L144I) mimic structural changes occuring during NS2 protease stimulation by NS3.

Taken together, these studies provide a profound basis to further decipher the molecular mechanism of NS2 functions in the life cycle of hepaciviruses and pestiviruses, as well as to identify protein-protein interactions essential for NS2 functionality.

2 Zusammenfassung

Positivstrang-RNA-Viren der Familie *Flaviviridae* kodieren ein Polyprotein, das durch zelluläre und virale Proteasen in reife Struktur- und Nichtstrukturproteine (NSPs) gespalten wird. Eine Besonderheit der *Flaviviridae* ist die Bedeutung der NSPs sowohl für die Genomreplikation als auch für die Virionenmorphogenese. Das Nichtstrukturprotein 2 (NS2) spielt eine zentrale Rolle im Lebenszyklus des Hepatitis C Virus (HCV) und der Pestiviren. Zunächst katalysiert NS2 die Spaltung von NS2-3, wodurch NS3 freigesetzt und somit der Aufbau der viralen Replikase ermöglicht wird. Dieser Prozess erfordert die Aktivierung der NS2 Protease durch einen viralen (bei HCV) oder zellulären (bei Pestiviren) Kofaktor. Zweitens hat NS2, entweder als freies NS2 (HCV) oder als ungespaltenes NS2-3 (Pestiviren), essentielle, aber noch unvollständig charakterisierte Funktionen in der Virionmorphogenese. Dementsprechend ist eine detaillierte Kenntnis der strukturellen und funktionellen Eigenschaften von pestiviralem und HCV NS2 sowie der ungespaltenen Vorläuferproteine für ein besseres Verständnis dieser Prozesse unerlässlich.

Da bisher keine Strukturdaten des pestiviralen NS2 verfügbar sind, wurde ein Membrantopologie-Modell des NS2 des Virus der bovinen Virusdiarrhö 1 (BVDV-1) mit Hilfe eines *Substituted Cysteine Accessibility Method* (SCAM) Assays bestimmt. Die so ermittelte Topologie des BVDV NS2 war zwar insgesamt mit der des HCV NS2 vergleichbar, zeigte aber auch potenziell wichtige Unterschiede zwischen den beiden Molekülen. Dieses Modell wurde anschließend verwendet, um die minimale Autoproteasedomäne des pestiviralen NS2 zu definieren. Dabei wurde gezeigt, dass mindestens ein Transmembran (TM)-Segment essentiell ist, um eine Restaktivität der BVDV-1 NS2-Protease zu erhalten, während NS2 von HCV und einiger anderer Hepaciviren bekanntermaßen auch ohne TM-Regionen aktiv bleiben.

Während für das HCV NS2 Strukturdaten der Proteasedomäne und eine Membrantopologie verfügbar sind, sind die NS2-Determinanten, die die Aktivierung der NS2-Protease durch NS3 unterstützen, noch unbekannt. Ausgehend von der kürzlich gemachten Beobachtung, dass ein hydrophobe Oberfläche auf der NS3-Protease Determinanten enthält, die die Aktivierung der NS2-Protease vermitteln, wurden in dieser Arbeit zwei NS2-Oberflächenreste (F103 und L144) identifiziert, die, wenn sie mutiert wurden, die intrinsische NS2-Proteaseaktivität in Abwesenheit von NS3 stimulierten. Weitere Analysen dieser NS2-Determinanten zeigten, dass (i) ihr stimulierender Charakter zwischen verschiedenen HCV-Genotypen konserviert ist, (ii) beide Reste unterschiedliche Mechanismen nutzen könnten, um zur Stimulation der intrinsischen NS2-Proteaseaktivität beizutragen und (iii) dass optimale NS2-NS3-Oberflächeninteraktionen für eine wirksame NS3-vermittelte NS2-Proteaseaktivierung erforderlich sind, da Mutationen dieser Determinanten die NS2-NS3-

Spaltung und RNA-Replikation abschwächen. Eine attraktive Hypothese dieser Arbeit ist, dass Mutationen dieser NS2-Oberflächendeterminanten (F103A und L144I) strukturelle Veränderungen nachahmen, die während der Stimulation der NS2-Protease durch NS3 auftreten.

Zusammengenommen bieten diese Studien eine profunde Grundlage, um den molekularen Mechanismus der NS2-Funktionen im Lebenszyklus von Hepaciviren und Pestiviren weiter zu entschlüsseln sowie Protein-Protein-Interaktionen zu identifizieren, die für die NS2-Funktionalität wesentlich sind.

3 Introduction

3.1 Family *Flaviviridae*

The *Flaviviridae* family includes small enveloped viruses with a single-stranded RNA genome of positive polarity with a length of approximately 9-13 kb and is subdivided into the four genera *Flavivirus*, *Pestivirus*, *Hepacivirus*, and *Pegivirus* (Fig. 1) (Simmonds et al., 2017).

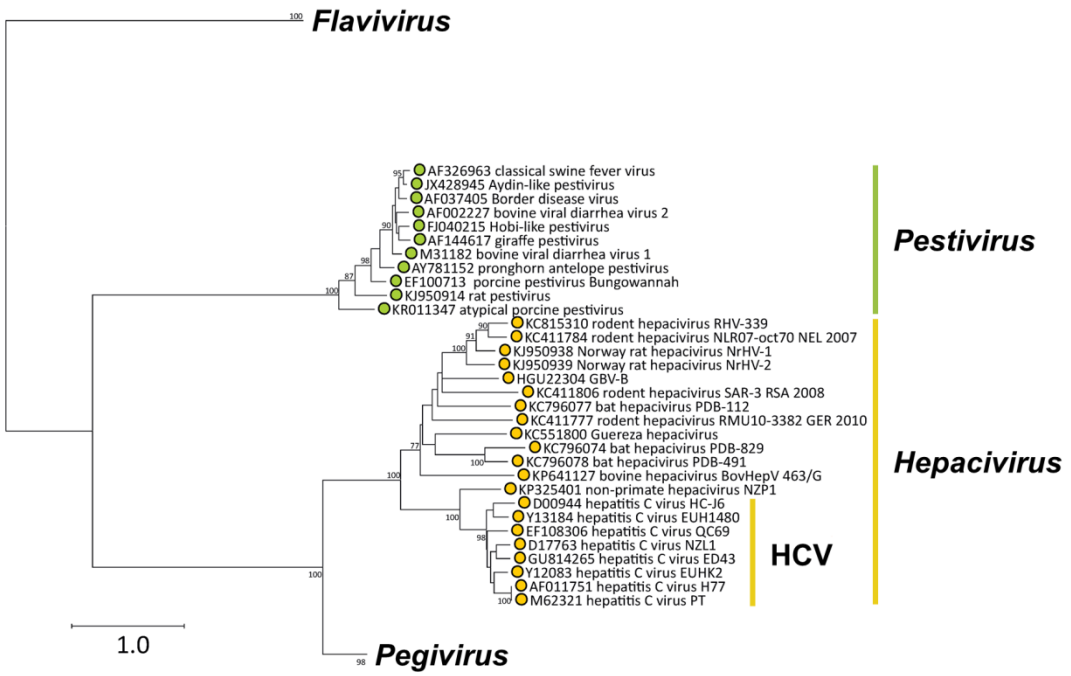

Fig. 1: *Flaviviridae* family. Phylogeny based on conserved amino acid sequences in the RNA-dependent RNA polymerase (NS5 or NS5B) (modified according to Simmonds et al., 2017)**.**

The genus *Flavivirus* includes human and animal pathogenic viruses that are transmitted by arthropods and accordingly, these viruses are often also refered to as Arboviruses (arthropod-borne viruses). Important human pathogens of this genus include yellow Fever Virus, Dengue Virus, Japanese Encephalitis Virus (Simmonds et al., 2017), and also Zika Virus, which was epidemic in 2015/16 (Wang et al., 2017).

The genus *Pegivirus* was introduced in 2011 in the *Flaviviridae* family (Stapleton et al., 2011). Many *Pegivirus* representatives cause persistent infections in humans and closely related primate species, such as chimpanzees. However, infections by pegiviruses have not been associated with disease (Simmonds et al., 2017). Due to numerous new discoveries of potential pegiviruses in other hosts, such as horses, pigs, rodents, and bats, the *Pegivirus* genus has been classified into the species Pegivirus A-K (Simmonds et al., 2017; Smith et al., 2016).

Historically, the *Hepacivirus* genus only comprised the important human pathogen Hepatitis C Virus (HCV), which causes severe liver damage as the result of a chronic infection (Simmonds et al., 2017). Because many potential hepaciviruses have been discovered in rodents, bats, cows, horses, and donkeys, among others, in recent years, the genus was proposed for re-grouping into the species Hepacivirus A-N in 2016 (Simmonds et al., 2017; Smith et al., 2016). Due to its prominent historical and medical importance, HCV was proposed to be listed as a separate species "Hepacivirus C" (Smith et al., 2016).

The *Pestivirus* genus comprises exclusively pathogenic animal viruses, that infect pigs, ruminants like cattle, sheep and goats, as well as wild ruminants (Simmonds et al., 2017). Recently, other potential pestiviruses have been isolated in antelope, giraffe, wild boar, and in atypical hosts, such as rats and bats, leading to the reclassification of the genus *Pestivirus* into the species Pestivirus A-K (Simmonds et al., 2017; Smith et al., 2017).

Because pestiviruses are closely related to HCV (Fig. 1; (Simmonds et al., 2017)), they have been used as HCV model system in cell culture (Lindenbach et al., 2005; Wakita et al., 2005; Zhong et al., 2005) and continue to serve as a reference for comparative studies of the viral life cycle between members of the *Flaviviridae* family.

Viral particles of hepaciviruses and pestiviruses consist of a cell-derived lipid bilayer incorporating two or three envelope (E) glycoprotein species, respectively, and surrounding a spherical capsid of the viral RNA genome complexed by the core (C) protein (Lindenbach et al., 2013). The genome encodes in a single open reading frame (ORF) for a large polyprotein which is processed by cellular and viral proteases into the mature viral structural and nonstructural (NS) proteins. The ORF of the viral RNA genome is flanked by a 5' and 3' untranslated region (UTR) (Lindenbach et al., 2013). Translation initiation at the genomic RNA occurs cap-independently via an internal ribosomal entry sites (IRES) present in the 5’ UTR (Simmonds et al., 2017). The structural proteins are located in the N-terminal portion of the polyprotein, followed by the nonstructural proteins in the remaining part of the polyprotein. The structural proteins are integral part of the virion while the NS proteins are not present in the virion. Nevertheless, they are important not only for RNA replication but also for virion morphogenesis (Lindenbach et al., 2013). Their critical role in particle assembly is mainly due to their ability to promote virion assembly by recruiting viral envelope proteins to the virus assembly sites via interactions between both structural and nonstructural proteins (Jirasko et al., 2010; Ma et al., 2011; Popescu et al., 2011). Some of the nonstructural proteins serve multiple functions and have different enzymatic activities such as serine protease, RNA helicase, NTPase, and RNA dependent RNA polymerase (RdRp) (Lindenbach et al., 2013). After translation and processing of the viral polyprotein replication of the viral RNA genome is initiated and occurs in close association with intracellular ER-

derived membranes in so-called replication compartments (Egger et al., 2002; Paul and Bartenschlager, 2015; Schmeiser et al., 2014). These replication compartments are formed by alterations of cellular membranes due to the expression of NS proteins and present a protected environment for efficient RNA synthesis. The *de novo* synthesized viral genome is subsequently packaged into virions in a multi-step process within the ER in close proximity to or directly on the surface to lipid droplets (LD). For release, the virions are transported to and released at the plasma membrane. In the case of HCV, detergent-resistant membranes (DRM) within the endoplasmic reticulum (ER) are one of the proposed particle assembly sites, as HCV assembly was shown to occur in the ER (Boson et al., 2011; Syed et al., 2017).

3.1.1 Pestiviruses

The genus *Pestivirus* includes ecologically and economically relevant animal pathogens, including Bovine Viral Diarrhea Virus (BVDV) and Classical Swine Fever Virus (CSFV). Transmission occurs through contact with infected secretions (respiratory droplets, urine, or feces). Infections can be subclinical or cause enteric, hemorrhagic, or wasting diseases, like bovine viral diarrhea, mucosal disease or classical swine fever (Tautz et al., 2015).

An unsual feature of pestiviruses is the appearance of two different biotypes in cell culture: while non-cytopathogenic (noncp) viruses replicate without altering cell morphology or viability at the light-microscopy level, the replication of cytopathogenic (cp) isolates causes the death of the infected cells in cell culture (Hoff and Donis, 1997; Jordan et al., 2002; Mathapati et al., 2010; Schmeiser et al., 2014). The noncp biotype in cell culture correlates with the ability of pestiviruses to temporally regulate their RNA replication efficiency (Lackner et al., 2004, 2005) and in cattle with their ability to establish life-long persistent infections (Baker, 1987; Bolin et al., 1985; Brownlie et al., 1989; Thiel et al., 1996). In contrast, cp strains, which always originate from their noncp counterpart, show a deregulated RNA replication (Mendez et al., 1998; Meyers et al., 1996; Tautz et al., 1999). Cp BVDV strains arise in persistently infected (pi) cattle often by RNA recombination and lead to the death of the pi animal (Tautz et al., 2015).

3.1.2 Hepatitis C Virus (HCV)

HCV was first identified in 1989 as the infectious agent of non-A, non-B hepatitis (NANBH) (Choo et al., 1989), which had already been recognized as leading cause of transfusion-acquired liver disease. In its host, the virus exists as a population of genetically distinct yet related variants, i.e. quasispecies, which are thought to arise through error-prone replication under permanent pressure of the immune system. As a result, the entire genome has high

sequence variability, with individual genotypes differing by up to 30% on nucleotide level (Bukh et al., 1995; Geller et al., 2016; Gomez et al., 1999; Kato, 2000; Martell et al., 1992). Currently, HCV is classified into seven genotypes with 67 subtypes based on phylogenetic and sequence analyses (Smith et al., 2014).

According to the WHO[1] an estimated 71 million people currently live with chronic HCV infection. The most common routes of infection are through contact with contaminated blood. The main routes of transmission are injection drug use and unhygienic medical practices, but sexual transmission and vertical transmission during birth is also possible (Alter, 2007). Acute infection is usually asymptomatic and may resolve spontaneously, depending on various virus- and host-related factors (Webster et al., 2015). However, in 80-85% of patients, the infection becomes persistent and establishes chronic hepatitis, which in turn can develop into cirrhosis and hepatocellular carcinoma (HCC) - the leading indications for liver transplantation (Chung and Baumert, 2014). In 2016, WHO estimated that approximately 399,000 deaths were caused by hepatitis C worldwide[1]. In recent years, research has made significant progress by developing all-oral Interferone (IFN)-free therapies based on HCV-specific direct-acting antivirals (DAAs) that achieve viral clearance in >90% of patients (Petta and Craxì, 2015). Still, a vaccine is urgently needed for prophylaxis, as patients remain at high risk for HCC even after viral clearance by DAA treatment (Huang et al., 2017).

3.2 Genome and polyprotein of HCV and pestiviruses

The genome of both, hepaci- and pestiviruses, consists of a single-stranded RNA with positive polarity (ss(+)RNA) that encodes one polyprotein in a single ORF and has neither a 5’ cap nor a 3’ poly-A tail (Lindenbach et al., 2013). The viral ORF is flanked by highly-structured 5’ and 3’ UTRs that have essential functions in translation initiation and viral RNA replication. Structures of the pestiviral and the hepaciviral genomes, the resulting polyproteins, and the mature viral proteins are shown in Fig. 2.

[1] https://www.who.int/news-room/fact-sheets/detail/hepatitis-c [last visited: 01.05.2021]

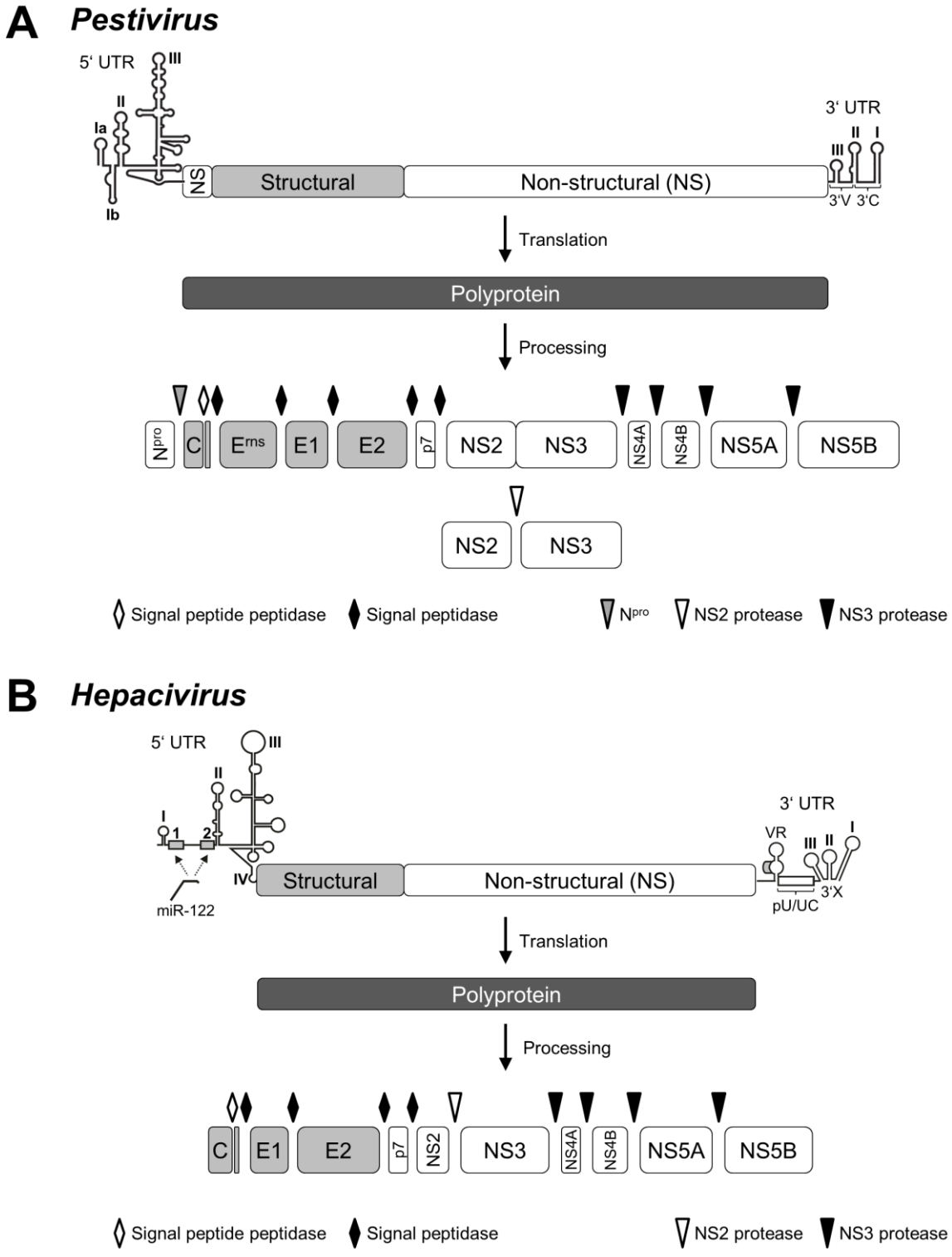

Fig. 2: Schematic representation of genome organization and polyprotein processing of the genera *Pestivirus* (A) and *Hepacivirus* (B). Both genomes comprise a single open reading frame flanked by highly structured untranslated regions (UTR). The coding regions and corresponding structural proteins in the genome are shown as gray boxes; the genome segments for the nonstructural proteins and corresponding proteins are depicted as white boxes. The cleavage sites of cellular proteases are marked by diamonds, and the cleavage sites of viral proteases are marked by triangles. UTRs were adapted and modified according to Lindenbach et al., 2007a (*Pestivirus*) and Niepmann, 2013 (*Hepacivirus*), respectively.

The 5‘ UTRs have an approx. size of 370-385 nt (pestiviruses) or 341 nt (HCV), respectively, forming four stem-loop structures (Pestiviruses: Ia, Ib, II, III; HCV: I-IV; Fig. 2), which serve a dual function in the viral life cycle (Lindenbach et al., 2013; Tautz et al., 2015). Stem-loop Ia of pestiviruses was shown to be important for translation initiation as well as viral RNA replication (Grassmann et al., 2005; Yu et al., 2000) and the 5’ UTR contains an IRES that recrutes the small ribosomal subunit to the site of translation initiation (Chon et al., 1998; Poole et al., 1995; Rijnbrand et al., 1997; Vassilev et al., 1997). For HCV, the stem-loops I and II are required for RNA replication (Friebe et al., 2001) and stem-loops II-IV form the IRES element that enables cap-independent initiation of translation (Honda et al., 1996; Piñeiro and Martinez-Salas, 2012; Tsukiyama-Kohara et al., 1992). In addition, the HCV 5' UTR contains two binding sequences for the liver-specific microRNA (miRNA, miR) miR-122 (Fig. 2B), whose binding stimulates translation, stabilizes the viral RNA and facilitates RNA replication, making this factor a key determinant of HCV cellular tropism (Jangra et al., 2010; Jopling et al., 2005).

The complex 3‘ UTRs have an approx. length of 185-276 nt (pestiviruses) or 225 nt (HCV), respectively (Lindenbach et al., 2013). The pestiviral 3' UTR can be devided into a variable (3’V) and highly-conserved (3’C) region and forms the three stem-loop structures SL I (3’C), II and III (3’V) (Deng and Brock, 1993; Yu et al., 1999; Fig. 2A). Lying between the ORF and the 3’C region, the 3’V region may serve as a spacer to prevent interference between RNA replication and translation (Deng and Brock, 1993). While the SL I, which is located at the very 3´ end of the genome, together with a conserved single-stranded segment between SL I and II is essential for replication, deletions of SL II or III are tolerated (Isken et al., 2004; Pankraz et al., 2005; Yu et al., 1999). Furthermore, the pestiviral 3' UTR was shown to be involved in the binding of host cell factors, which presumably serves to coordinate RNA replication and translation (Isken et al., 2003). Moreover, the cellular miRNA miR-17 was shown to bind to the spacer sequence upstream of SL I of the pestiviral 3' UTR, which was found to be critical for RNA replication (Kokkonos et al., 2020; Scheel et al., 2016). In the case of HCV, the 3‘ UTR consists a ~40 nt long variable region (VR), a polyuridine/polypyrimidine (pU/UC) tract and the highly-conserved 3’X domain, which forms three stem-loop structures (Kolykhalov et al., 1996; Tanaka et al., 1995, 1996; Fig. 2B). Mutagenesis studies showed that for RNA replication the 3’X domain and the 52 3’ nt of the pU/UC tract are essential (Friebe and Bartenschlager, 2002; Yi and Lemon, 2003b, 2003a).

The pestiviral genome is approx. 12.3 kb in length (Collett et al., 1988a, 1988b; Tautz et al., 2015). In certain cp strains, the genome can reach a size of 16.5 kb through naturally occurring recombination with cellular RNAs and duplications of viral sequences (Becher et al., 1999; Meyers et al., 1992). Translation of the ORF produces a polyprotein with a size of approx. 3900 aa that is processed co- and post-translationally into 12 viral proteins: N^{pro},

Core, E^{rns}, E1, E2, p7, (NS2-3), NS2, NS3, NS4A, NS4B, NS5A, NS5B (Fig. 2A; Tautz et al., 2015). The length of the HCV genome is 9.6 kb and translation of its ORF results in a polyprotein with 3011 aa in length (Choo et al., 1989, 1991). The co- and post-translational processing leads to ten mature viral proteins: Core, E1, E2, p7, NS2, NS3, NS4A, NS4B, NS5A, NS5B (Fig. 2B; Lindenbach et al., 2013).

Compared to other *Flaviviridae* genera, there is a striking difference in the arrangement of proteins in the pestiviral polyprotein, where the first protein encoded in the ORF is the NS protein N^{pro} (Tautz et al., 2015). This autoprotease cleaves itself cotranslationally from the polyprotein and thereby generates the N terminus of the nucleocapsid protein (Stark et al., 1993). N^{pro} is followed by the structural proteins: the nucleocapsid protein C and the glycosylated envelope proteins E^{rns}, which is also an unique feature of pestiviruses, E1 and E2 (Collett et al., 1991; Stark et al., 1990; Thiel et al., 1991). In the case of HCV, the polyprotein begins with the structural proteins C, E1 and E2 (Grakoui et al., 1993). In both viral systems, the order of nonstructural proteins is p7, NS2, NS3, NS4A, NS4B, NS5A, and NS5B which follow downstream of E2 (Lindenbach et al., 2013). The polyprotein processing of the structural proteins as well as between E2/p7 and p7/NS2 are carried out by the cellular ER-resident signal peptidase (Elbers et al., 1996; Hijikata et al., 1991, 1993a; Liu et al., 1997; Moradpour et al., 1996; Rümenapf et al., 1993). The pesti- and hepaciviral nucleocapsid protein C is further processed C-terminally by the signal peptide peptidase (Heimann et al., 2006; McLauchlan et al., 2002). Processing of the remaining polyprotein is carried out by viral proteases. The pesti- and hepaciviral NS2 cysteine protease catalyzes the cleavage of the NS2-3 precursor protein (Hijikata et al., 1993a, 1993b; Lackner et al., 2004). Cleavages downstream of NS3 are mediated by the serine protease activity in NS3, which forms the active protease complex together with its cofactor NS4A (Bartenschlager et al., 1994; Failla et al., 1994; Kolykhalov et al., 1994; Tautz et al., 1997; Wiskerchen and Collett, 1991; Xu et al., 1997).

3.2.1 Structural proteins

Structural proteins C, E^{rns} (only pestiviruses), E1 and E2 are those viral proteins that form the virus particle (Lindenbach et al., 2013). The cpasid protein C is an intrinsically unfolded protein that binds RNA nonspecifically and with low affinity due to its basic amino acid composition (Ivanyi-Nagy et al., 2008; Murray et al., 2008a). The glycoproteins E^{rns}, E1 and E2 are incorporated into the viral lipid envelope (Callens et al., 2016; Lindenbach and Rice, 2013). E1 and E2 form homo- and heterodimers via disulfide bridges and are essential for host cell entry (Deleersnyder et al., 1997; Dubuisson et al., 1994; Lindenbach and Rice, 2013; Ronecker et al., 2008; Wang et al., 2004).

In addition to its presence on the surface of the virion, the pestivirus-specific glycoprotein E^{rns}, is also secreted by infected cells (Hausmann et al., 2004; Rümenapf et al., 1993; Tews and Meyers, 2007). Secreted E^{rns} shows intrinsic RNase activity (rns = ribonuclease secreted) and is proposed to suppress the innate immune response against double-stranded RNA in the extracellular space (Iqbal et al., 2004; Magkouras et al., 2008; Mätzener et al., 2009).

3.2.2 Nonstructural proteins

The NS proteins are not detected in the virion, but are essential for viral replication as well as virion morphogenesis (Lindenbach et al., 2013).

N^{pro}, found only in pestiviruses, is an autoprotease that generates its C terminus to generate the authentic N terminus of the downstream capsid protein C (Stark et al., 1993). It also has an important function in inhibiting the host cell innate immune response. N^{pro} induces the polyubiquitinylation of interferon regulatory factor 3 (IRF-3) followed by its proteasomal degradation (Chen et al., 2007; Gottipati et al., 2016; Hilton et al., 2006). As a result, IRF-3-dependent activation of the Interferon-β promotor is blocked in pestivirus infected cells (Baigent et al., 2002; Ruggli et al., 2003).

p7 is a small integral membrane protein that is present in infected cells as an individual protein with a size of 7 kDa and as precursor proteins E2-p7 or in the case of HCV also as E2-p7-NS2, (Elbers et al., 1996; Harada et al., 2000; Lin et al., 1994; Pietschmann et al., 2002; Selby et al., 1994). p7 plays no role in RNA replication, however, mature p7 is essential for generation of infectious progeny (Harada et al., 2000; Sakai et al., 2003). Based on its hydrophobicity and its characteristics as an integral membrane protein with a charged central region, it has been proposed that p7 is a so-called viroporin, i.e., a small hydrophobic protein that oligomerizes in the host cell membrane and leads to the formation of hydrophilic pores (Harada et al., 2000). These proteins modify several cellular functions, including membrane permeability, Ca^{2+} homeostasis, membrane remodeling and glycoprotein trafficking (Griffin et al., 2003; Harada et al., 2000; Largo et al., 2014; Pavlovic et al., 2003; Premkumar et al., 2004). The pesti- and hepaciviral p7 proteins belong to the class II group of viroporins that form helix-turn-helix hairpin motifs with lumenal N and C termini (Nieva et al., 2012).

Since NS2 is the subject of this thesis, it is discussed in more detail in chapter 3.4.

NS3 is a 70 kDa (HCV) or 80 kDa (pestiviruses) multifunctional protein. It has an N-terminal serine protease domain of the chymotrypsin type and a C-terminal NTPase and helicase domain (Bartenschlager et al., 2004; Caruthers and McKay, 2002; Gorbalenya et al., 1989; Kim et al., 1996; Morikawa et al., 2011; Warrener and Collett, 1995; Xu et al., 1997). Association with the viral cofactor NS4A is required for full activity of the protease (Bartenschlager et al., 1994; Failla et al., 1994; Lin et al., 1995; Tautz et al., 2000; Xu et al., 1997). The NS3 protease generates the authentic NS3 C terminus *in cis* and the NS3/4A protease complex performs all downstream cleavages within the polyprotein *in trans* (Morikawa et al., 2011; Wiskerchen and Collett, 1991; Yao et al., 1999). In addition to its role in polyprotein processing, the HCV NS3/4A complex is important for evading the innate immune response by blocking activation of the IRF-3 and NF-κB transcription factors through cleavages of the cellular factors mitochondrial antiviral-signaling protein (MAVS) (also referred to as IPS-1, VISA, or Cardif), TRIF, and Importin β (Gagné et al., 2017; Li et al., 2005b; Meylan et al., 2005).

NS4A is an 8 kDa (HCV) or 10 kDa (pestiviruses) protein with a membrane-spanning, hydrophobic, N-terminal domain containing a short transmembrane segment (TMS) and a C-terminal, cytosolic domain (Lindenbach et al., 2013). Both regions are connected by a short, so-called kink-region (Lindenbach et al., 2007b). By binding to NS3, NS4A induces a classic serine protease conformation of the catalytic triad of the NS3 protease and rearranges the secondary structure of both the N-terminal part and catalytic site of the NS3 protease (Kim et al., 1996). Furthermore, it reduces the mobility of the global structure of the NS3 protease to provide a rigid and tight structure for the binding and hydrolysis of substrates (Kim et al., 1996). In addition to its function as a cofactor for the NS3 protease (Failla et al., 1994; Tanji et al., 1995; Tautz et al., 2000; Xu et al., 1997), NS4A is also a critical factor for virion morphogenesis (Dubrau et al., 2017; Kohlway et al., 2014; Liang et al., 2009; Moulin et al., 2007; Phan et al., 2011). For HCV NS4A, the C-terminal acidic domain was shown (i) to contribute to hyperphosphorylation of NS5A, thereby regulating viral replication (Lindenbach et al., 2007b), and (ii) to enhance NS3 helicase activity (Lindenbach et al., 2007b). In addition, interactions between NS4A and NS4B appear to control genome replication and the NS3/4A complex plays a role in virus assembly (Kohlway et al., 2014; Liang et al., 2009). Moreover, formation of NS4A TMS homodimers appears to be a prerequisite for efficient HCV replication and virus particle production, suggesting that NS3/4A dimers or oligomers are crucial for the viral life cycle (Kohlway et al., 2014). Apart from the ER, NS4A seems to target the NS3/4A complex to mitochondrial membranes or defined ER regions closely opposed to mitochondria and designated mitochondria-associated membranes (MAMS) (Horner et al., 2011). This localization plays an important role for blocking the IFN response by proteolytic cleavage of MAVS by NS3/4A (Horner et al., 2011). In pestiviruses, the

strength of surface interactions between the NS3 protease domain and the C-terminal domain of NS4A have been shown to regulate the switch between RNA replication and virion morphogenesis: while destabilization of this interaction resulted in a gain of function of the NS3/4A complex in particle formation, replicase assembly as a prerequisite of RNA replication requires a stable association between NS3 and the NS4A kink region (Dubrau et al., 2017).

NS4B is an approx. 27 kDa (HCV) or 35 kDa (pestiviruses) hydrophobic protein and an essential component of the viral replication complex (Collett et al., 1991; Grassmann et al., 2001; Gu and Rice, 2013). NS4B is an integral membrane protein associated with intracellular membranes that was shown to be involved in membrane alterations (Egger et al., 2002; Hügle et al., 2001; Weiskircher et al., 2009). A variety of topologies have been proposed for HCV NS4B with respect to the ER membrane and it is predicted that NS4B has between 4-6 TMS (Lundin et al., 2003). The N and C termini of NS4B are expected to reside in the cytoplasm (at least initially) because they are generated by the cytoplasmic NS3/4A protease complex (Hijikata et al., 1993a, 1993b). A membrane topology of pestiviral NS4B was determined by SCAM assay (Binder, 2016), e.g., an approach to study NS4B topology by introducing cysteine as a single amino acid substitute at defined different positions within native cysteine-free NS4B, which can be modified by PEG modification (PEGylation) when present in the cytoplasmic part of the protein (Van Geest and Lolkema, 2000; Zhu and Casey, 2007). Using this approach, it was shown that pestiviral NS4B has four TMS (Binder, 2016). Alternative topologies of the N-terminus were proposed for the NS4B proteins of both virus systems: an N-glycosylation motif introduced into the N-terminal segment of NS4B, predicted to be cytoplasmically oriented, was modified in a manner suggesting that it was translocated into the lumen in a fraction of the NS4B molecules (Langerwisch, 2015; Lundin et al., 2003, 2006).

NS5A is a protein of approx. 56 to 58 kDa that, like NS5 of members of the genus *Flavivirus*, is phosphorylated by cellular kinases. (Reed et al., 1997, 1998). While two phosphorylated isoforms (hypo- and hyperphosphorylated) can be distinguished for HCV NS5A by SDS-PAGE, pestiviral NS5A does not exhibit such differences in electrophoretic mobility (Kaneko et al., 1994; Tautz et al., 2015). It was shown that a fraction of NS5A localizes to the surface of lipid droplets (LD) (Isken et al., 2014; Miyanari et al., 2007; Shi et al., 2002). Zn^{2+}-binding motifs of NS5A have been shown to be critical for structural integrity of the protein and thereby also for viral replication (Tellinghuisen et al., 2004, 2006). Both pesti- and hepaciviral NS5A consist of a well-defined N-terminal and two intrinsically unstructured C-terminal domains connected by low-complexity sequences (Isken et al., 2014; Tellinghuisen et al., 2004, 2005, 2006). The C-terminal domains are in part dispensible for RNA replication and allow the insertion of heterologous protein sequences such as GFP or mCherry to perform

imaging studies in living cells (Appel et al., 2005; Isken et al., 2014; Moradpour et al., 2004). In the case of HCV NS5A, the C-terminal domain harbors determinants for virion morphogenesis (Tellinghuisen et al., 2008) and interactions between the casid protein C and NS5A at the LD surface of infected cells have been shown to be critical for virion morphogenesis (Miyanari et al., 2007). An N-terminal amphiphathic α-helix serves as a structural determinant for association of NS5A to intracellular membranes (Brass et al., 2007; Penin et al., 2004). This relatively weak membrane association most likely promotes efficient functional trans-complementation of both viral proteins (Appel et al., 2005; Grassmann et al., 2001).

The 68 kDa (HCV) or 77 kDa (pestiviruses) NS5B is the key enzyme in viral RNA replication, the RNA-dependent RNA polymerase (RdRp), and shows *de novo* polymerase activity *in vitro* (Behrens et al., 1996; Kao et al., 1999; Zhong et al., 1998, 2000). However, RNA replication *in vivo* requires the minimal viral replicase consisting of NS3 to NS5B (Behrens et al., 1998; Lohmann et al., 1999). In addition, NS5B has also been shown to play a role in virion morphogenesis (Aligeti et al., 2015; Ansari et al., 2004; Gouklani et al., 2012; Liang et al., 2009). Both NS5B proteins are anchored into cellular membranes by a C-terminal TM segment (Lai et al., 1999; Yamashita et al., 1998).

3.3 Lifecycle of HCV and pestiviruses

The general life cycle of members of the *Flaviviridae* family, and thus also of HCV and pestiviruses, is shown in Fig. 3. The viruses enter their host cells via receptor-mediated endocytosis. Next, the viral RNA genome is released into the cytoplasm and is subsequently used for translation of the viral polyprotein, which is co- and post-translationally processed by cellular and viral proteases to give rise to the mature viral proteins (Lindenbach and Rice, 2013; Murray et al., 2008b; Tautz et al., 2015). After viral replicase assembly at the 3’ end of the viral RNA, RNA replication of the viral genome occurs in association with ER membranes. In the late phase of infection, assembly of virions and egress of viral particles occurs via the secretory transport pathway (Fig. 3).

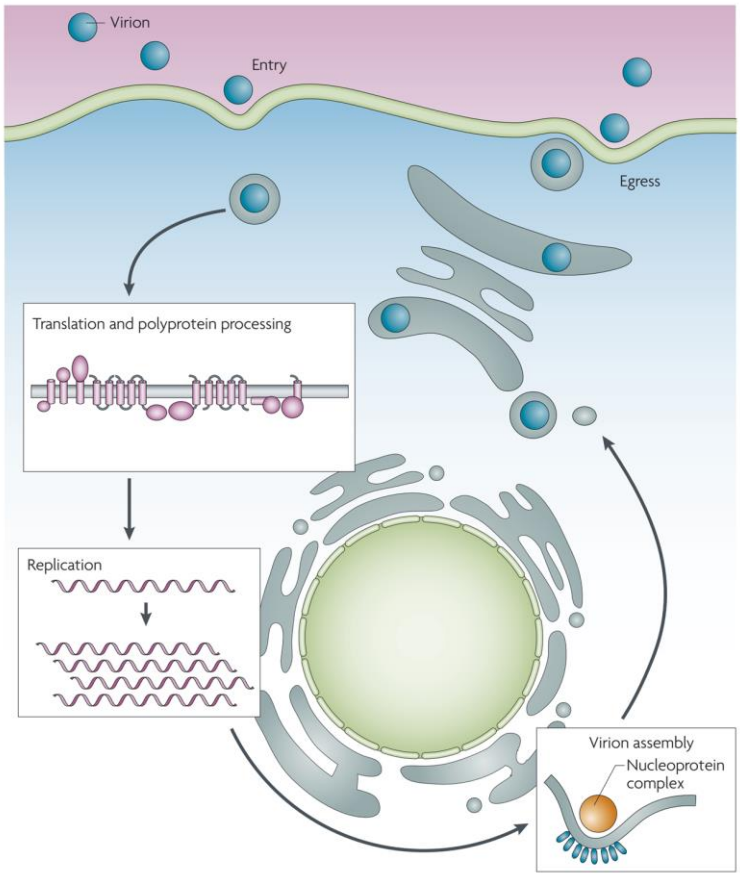

Fig. 3: Lifecycle of *Flaviviridae* (adapted from Murray et al., 2008b). Virus binding to host cell receptors and entry by clathrin-mediated endocytosis; uncoating and genome release into the cytoplasm; translation and polyprotein processing at ER membranes; replicase assembly and RNA replication at ER-derived membranes; packaging and virion assembly; release via the secretory pathway.

3.3.1 Cell entry

In the case of pestiviruses, the initial contact of the virion with the host cell is thought to occur through interaction of the glycoprotein E^{rns} with glycosaminoglycans (GAGs) on the cell surface (Iqbal and McCauley, 2002; Iqbal et al., 2000). The cellular surface protein CD46 serves as the primary receptor for binding of the BVDV virion via E2 to the host cell (Krey et al., 2006; Maurer et al., 2004). Nevertheless, other co-receptors besides CD46 are required for successful infection, as the sole expression of CD46 in non-permissive cells is not sufficient for BVDV infection (Maurer et al., 2004; Tscherne et al., 2008). Uptake of viral particles into the cell occurs by clathrin-mediated endocytosis (Grummer et al., 2004; Krey et al., 2005; Mathapati et al., 2010; Maurer et al., 2004). The low pH after acidification of the endosome finally triggers the release of the nucleocapsid into the cytosol by fusion of the virion envelope with the endosomal membrane (Krey et al., 2005; Mathapati et al., 2010).

Numerous host factors have been proposed to participate in the uptake of HCV into human hepatocytes, including GAGs as part of heparan sulfate proteoglycans (HSPGs), low-density-

lipoprotein receptor (LDLR) (Agnello et al., 1999), CD81 (Pileri et al., 1998), scavenger receptor class B member 1 (SCARB1) (Scarselli et al., 2002), the tight junction proteins claudin-1 (CLDN1) (Evans et al., 2007) and occludin (OCLN) (Liu et al., 2009; Ploss et al., 2009), the receptor tyrosine kinases epidermal growth factor receptor (EGFR) and ephrin receptor A2 (EphA2) (Lupberger et al., 2011), the cholesterol transporter Niemann-Pick C1-like 1 (NPC1L1) (Sainz et al., 2012), transferrin receptor 1 (TfR1) (Martin and Uprichard, 2013) and the cell death-inducing DFFA-like effector b (CIDEB) (Wu et al., 2014). The HCV entry process into its target cells (hepatocytes) is a complex sequence of interactions with these various factors (Lindenbach and Rice, 2013). As HCV virions circulate through the blood stream, the first low-affinity attachment to the basolateral surface of hepatocytes is mediated by the interaction of lipoviral HCV particles with GAGs in HSPGs and LDLRs (Agnello et al., 1999; Germi et al., 2002; Monazahian et al., 1999). Next, the viral particles interact with SCARB1 (Scarselli et al., 2002), which induces conformational changes in HCV E2, leading to binding of E2 to the tetraspanin CD81 (Bankwitz et al., 2010; Bertaux and Dragic, 2006; Petracca et al., 2000; Pileri et al., 1998; Scarselli et al., 2002; Thi et al., 2012; Zahid et al., 2013). CD81 binding activates signalling pathways via EGFR, Ras and Rho GTPases, triggering the lateral movement of bound virions along the cell surface towards tight junctions where HCV E2-CD81 interacts with the tight junction proteins CLDN1 and OCLN. Interaction of the HCV E2-CD81/CLDN1-complex initiates clathrin-mediated endocytosis (Brazzoli et al., 2008; Evans et al., 2007; Harris et al., 2010; Lupberger et al., 2011; Ploss et al., 2009). However, the exact roles of TfR1, NPC1L1, CLDN1 and OCLN during the entry process are not defined, but available data suggest that they are involved in steps post viral attachment and HCV binding to CD81. Furthermore, the host tropism of HCV entry into human hepatocytes is defined by human CD81 and OCLN (Dorner et al., 2011, 2013).

3.3.2 Replication of the viral RNA genome

The entire replication process of all representatives of the *Flaviviridae* takes place in the cytoplasm (Fig. 3). After release into the cytoplasm, the viral RNA genome, due to its structure, is used directly by the cellular translation machinery for translation of the viral polyprotein, which is processed co- and post-translationally by cellular and viral proteases (see 3.2). As with other ss(+)RNA viruses, RNA replication in HCV and pestiviruses starts with the synthesis of a complementary full-length negative-strand RNA (ss(-)RNA), resulting in partially or fully double-stranded RNAs termed replicative intermediate or replicative form, respectively. Subsequently, each ss(-)RNA is used as template for multiple rounds of ss(+)RNA genome synthesis, leading to an excess of newly generated positive-strand genomes (Ali et al., 2002; Gong et al., 1996, 1998; Quinkert et al., 2005).

Replication of the viral RNA genome occurs in close association with intracellular membrane structures derived from the ER (Lindenbach et al., 2013). The specific remodeling of the ER membrane to form locally shielded compartments in which viral RNA replication occurs is characteristic of many members of the *Flaviviridae* and shows parallels to other positive-strand RNA viruses (Neufeldt et al., 2018; Paul and Bartenschlager, 2015; Romero-Brey and Bartenschlager, 2014). In the case of HCV, double membrane vesicles (DMVs) are formed by protrusions of ER membranes. These HCV replication-induced membrane alterations were termed “membraneous web” (Egger et al., 2002; Ferraris et al., 2010; Gosert et al., 2003; Romero-Brey et al., 2012). In addition, HCV-induced DMVs have been shown to contain all NS proteins as well as the enzymatically active membrane-associated replicase complex. Accordingly, these structures are also referred to as replication factories (Romero-Brey and Bartenschlager, 2014; Romero-Brey et al., 2012). Although it is known that RNA replication of pestiviruses also occurs in close association with ER-derived membranes, the existence of similar ER remodeling has been proposed but not yet clearly demonstrated (Romero-Brey and Bartenschlager, 2014; Schmeiser et al., 2014; Weiskircher et al., 2009). Recently, it was demonstrated that HCV as well as BVDV rely on cellular miRNAs for a successful RNA replication process (Jopling et al., 2005; Masaki et al., 2015; Scheel et al., 2016). In the case of HCV, the liver-specific miR-122 binds to two binding sites within the 5’ UTR (Fig. 2B) thereby modulating the viral 5’ UTR structure and stabilizing the viral RNA genome for efficient RNA replication (Masaki et al., 2015; Schult et al., 2018; Sedano and Sarnow, 2014). Interestingly, it has been proposed that HCV RNA sequesters miR-122 and this may lead to inhibition of cellular miR-122 functions in HCV-infected cells, resulting in global de-repression of host miR-122 targets and creation of a fertile environment for long-term oncogenicity of HCV (Luna et al., 2015). Scheel and coworkers showed that BVDV utilizes the cellular miRNAs miR-17 and let-7 and critically depends on the interaction of these miRNAs with the viral 3' UTR for its RNA replication (Scheel et al., 2016). In contrast to canonical repression of cellular mRNAs by miRNA interactions, recruitment of miR-17 and let-7 to the viral 3' UTR of BVDV enhanced pestivirus translation and RNA stability (Scheel et al., 2016). Moreover, sequestration of miR-17 by pestiviruses resulted in functional de-repression of cellular miR-17 targets, thereby altering the host transcriptome (Scheel et al., 2016). Of note, for both viruses the selection of variants with altered or no miRNA dependency was possible suggesting a functional advantage by the recruitment of these cellular miRNAs as essential host factors for these viruses during evolutionary adaptation (Hopcraft et al., 2016; Kokkonos et al., 2020; Yu et al., 2017).

In both viral systems described here, the viral replicase complex is formed by NS proteins NS3 to NS5B, also known as minimal replicase, together with an incompletely defined set of cellular factors (Bartenschlager and Lohmann, 2000; Behrens et al., 1998; Lohmann et al.,

1999; Tautz et al., 2015). Although NS2 is not a constituent of the viral replicase complex, cleavage at the NS2-NS3 junction and the resulting release of NS3 is essential for RNA replication (Behrens et al., 1998; Lackner et al., 2004; Lohmann et al., 1999; Tautz et al., 2015; Welbourn et al., 2005).

3.3.3 Virion morphogenesis

In the case of HCV, RNA genome copies and structural proteins are known to assemble in a temporally and spatially organized manner at cytosolic lipid droplets (cLDs), leading to budding of new HCV particles into the ER (Lindenbach and Rice, 2013). The following sequence of steps is currently proposed for virion morphogenesis: After translation and release from the polyprotein, the core protein is further processed by cellular signal peptidase, leading to release from the ER and recruitment to cLDs (McLauchlan et al., 2002). This separates the mature core proteins from the replicase, presumably to avoid competition for RNA binding. For nucleocapsid formation, the core protein must then be recruited from the surface of cLDs to the newly-synthesized viral RNA at ER-derived membranes (Lindenbach and Rice, 2013). Interaction of the N-terminal RNA-binding domain of the core protein with viral RNA leads to its encapsidation. The formation of the viral envelope occurs via invaginations of ER-derived membranes containing E1-E2 heterodimers and also depends on the interaction of HCV with lipoproteins (André et al., 2002; Gastaminza et al., 2008; Meunier et al., 2008; Nielsen et al., 2006; Paul et al., 2014; Thomssen et al., 1992). Because of their association with hepatocyte-derived lipoproteins to form infectious hybrid particles, HCV virions have been termed lipo-viro particles (LVPs). This interaction to form LVPs is critical for HCV infectivity and evasion of neutralizing antibodies (Wrensch et al., 2018). During transport of virions in export vesicles via the secretory pathway, E1 and E2 are post-translationally modified by glycosylation and rearrangements of disulphide bonds, suggesting transport through the Golgi apparatus (Lindenbach and Rice, 2013).

The process of pestiviral virion morphogenesis is not yet fully understood (Tautz et al., 2015). However, viral particles have been observed in ER structures and small, cytoplasmic vesicles (Bielefeldt Ohmann et al., 1987; Callens et al., 2016; Gray and Nettleton, 1987; Schmeiser et al., 2014). Analysis of purified BVDV viral particles by cryo-electron microscopy revealed nearly spherical viral particles showing an electron dense capsid surrounded by a phospholipid bilayer without visible spikes (Callens et al., 2016). Virion morphogenesis is thought to be initiated by budding of previously formed capsids into the ER lumen at sites where viral glycoproteins have accumulated (Grummer et al., 2001; Schmeiser et al., 2014). Furthermore, the involvement of the Golgi apparatus in virion morphogenesis has been demonstrated (Jordan et al., 2002; Macovei et al., 2006; Schmeiser et al., 2014).

A distinctive feature of the members of the family *Flaviviridae* is that not only the structural proteins but also the nonstructural proteins are essentially involved in virion morphogenesis (Murray et al., 2008a). Whereas in pestiviruses all nonstructural proteins except N^{pro} and NS4B have been shown to be involved in virion morphogenesis (Agapov et al., 2004; Ansari et al., 2004; Harada et al., 2000; Isken et al., 2014; Liang et al., 2009; Moulin et al., 2007), in the case of HCV all NS proteins have been shown to be involved (Dimitrova et al., 2003; Paul et al., 2014). However, it is likely that the pestiviral NS4B is also required, as its HCV homolog is critical for virion morphogenesis (Han et al., 2013; Paul et al., 2011).

3.4 Nonstructural protein 2 (NS2)

The NS2 protein is a critical factor in the life cycle of both HCV and pestiviruses and exerts multiple functions: (i) NS2 cleaves at the NS2-NS3 junction to release NS3, thereby enabling RNA replication, and (ii) NS2 acts as a scaffold for protein-protein interactions between nonstructural and structural proteins that are critical for virion morphogenesis (Lindenbach et al., 2013; Tautz et al., 2015). Although their main functions are similar, HCV and pestiviral NS2 fulfill these tasks differently to some extent. For instance, while free HCV NS2 is functional during virion morphogenesis the uncleaved NS2-3 precursor protein is required for the pestiviral virus assembly process (Lindenbach et al., 2013; Tautz et al., 2015). Another interesting difference refers to the mechanism of their respective protease activation for efficient NS2-NS3 cleavage (see also 3.4.3). Furthermore, both proteins also differ with regard to their respective size: At 453 aa, the pestiviral NS2 is more than twice as large as the 217 aa long HCV NS2. Regardless of their different size, the NS2 proteins of both viruses share an overall similar domain composition: they can be divided into an N-terminal hydrophobic transmembrane domain and a C-terminal cytoplasmic domain containing the protease function that catalyzes cleavage at the junction between NS2 and NS3 (Grakoui et al., 1993; Hijikata et al., 1993b; Lackner et al., 2004).

3.4.1 NS2 protease domain and membrane binding domain

For HCV NS2 it was shown that the C-terminal cytoplasmic domain from aa 94 to 217 is able to mediate NS2-NS3 cleavage (Pallaoro et al., 2001). The crystal structure of the NS2 protease domain showed that the active site is composed of a catalytic triad consisting of His143, Glu163 and Cys184 (Lorenz et al., 2006). Furthermore, the structure revealed a novel protease conformation with a minimal active protease unit consisting of an NS2 dimer that forms two composite active sites (Fig. 4A) (Lorenz et al., 2006). Here, each active site is formed by His143 and Glu163 of one NS2 monomer and the nucleophilic Cys184 of the other NS2 monomer (Fig. 4A). This apparent requirement for dimerization to form the active

protease moiety implies interesting regulatory possibilities for polyprotein processing and suggests a dependence of NS2-NS3 cleavage, and thus RNA replication, on NS2 concentration (Lorenz et al., 2006). An interesting hypothesis is that such a requirement for a critical concentration of NS2-NS3 for subsequent processing could delay the initiation of HCV RNA replication until sufficient amounts of active NS3/4A protease are formed. In this context, it is worth noting that the NS3/4A protease cleaves TRIF and Cardif (also known as MAVS, IPS-1, or VISA), two important adaptor proteins in innate immune defense (Li et al., 2005a, 2005b; Meylan et al., 2005). Thus, a sufficient amount of NS3/4A may be required to antagonize double-stranded RNA-induced type I interferon production in infected cells. In addition, it could be assumed that the NS2 protease remains inactive after cleavage, since the crystal structure showed that the C-terminal residue of NS2 (L217) remains coordinated in the active site by contact with the catalytic triad (Fig. 4A). Accordingly, it was postulated that the NS2 protease is active only *in cis* (Lorenz et al., 2006).

The N-terminal membrane binding domain (MBD) (aa 1-93) of HCV NS2 has also been extensively studied in terms of its structure and function. Detailed structural and functional characterization of the N-terminal MBD of NS2, including determination of the NMR structures of the different transmembrane segments (TMS), led to a model for the membrane association and topology of the HCV NS2 MBD with three transmembrane, mainly helical segments (TMS1: aa 4-23; TMS2: aa 27-49; and TMS3: aa 72-94), connected by a small cytosolic loop (aa 24-26) and by a luminal segment (aa 50-71) containing a short helix proposed to interact with the membrane interface (Fig. 4B) (Jirasko et al., 2008, 2010). Given the dimeric structure of the protease domain (see above) a packed overall NS2 structure is expected with eventually higher-order complexes of NS2 dimers mediated by intermolecular interactions between MBDs.

While structural data are available for HCV NS2 for both the protease domain and the MBD, allowing structure-guided function and interaction studies, such data are so far not available for pestiviral NS2. However, previous mutagenesis studies and analyses of the NS2 protein sequence provided insights into structural elements of pestiviral NS2 cytoplasmic domain. It was hypothesized that the C-terminal domain contains a putative Zn^{2+} binding site consisting of four cysteines that is part of the protease domain of NS2 (Fig. 4C) (Lackner et al., 2004; De Moerlooze et al., 1990). This finding contrasts with findings from HCV, where NS2 protease activity is also dependent on zinc ions, but Zn^{2+} coordination is provided by the NS3 protease domain (Love and Parge, 1996; Schregel et al., 2009; Tedbury and Harris, 2007). Based on mutagenesis studies, the catalytic triad of the BVDV NS2 protease domain is thought to be composed of residues His311, Glu325, and Cys376 (Fig. 4C) (Lackner et al., 2004). For its activity, the NS2 protease relies on interaction with the cellular cofactor DNAJC14, a cellular ER-residing chaperone that is also referred to as Jiv (J-domain protein

interacting with viral protein) (Lackner et al., 2005; Rinck et al., 2001). Interaction with the Jiv cofactor is proposed to occur via two Jiv-binding motifs in the C-terminal cytoplasmic domain of NS2 (Fig. 4C) (Lackner et al., 2006). As with HCV NS2, NS2-3 cleavage is assumed to occur only *in cis* and with the NS2 C terminus remaining in the active site of the protease, because *trans* cleavage of a substrate containing the NS2-NS3 junction was observed only when the NS2 C terminus was truncated by at least four aa (Lackner et al., 2006). Much less is known about the N-terminal hydrophobic domain that mediates membrane association. At the beginning of this work, no structural data or experimentally based membrane topology models were available for this domain. Accordingly, only *in silico* models can be used to propose a model for the membrane association and topology of the pestiviral NS2 MBD (Fig. 4C). Depending on the applied algorithm, up to seven transmembrane segments are predicted.

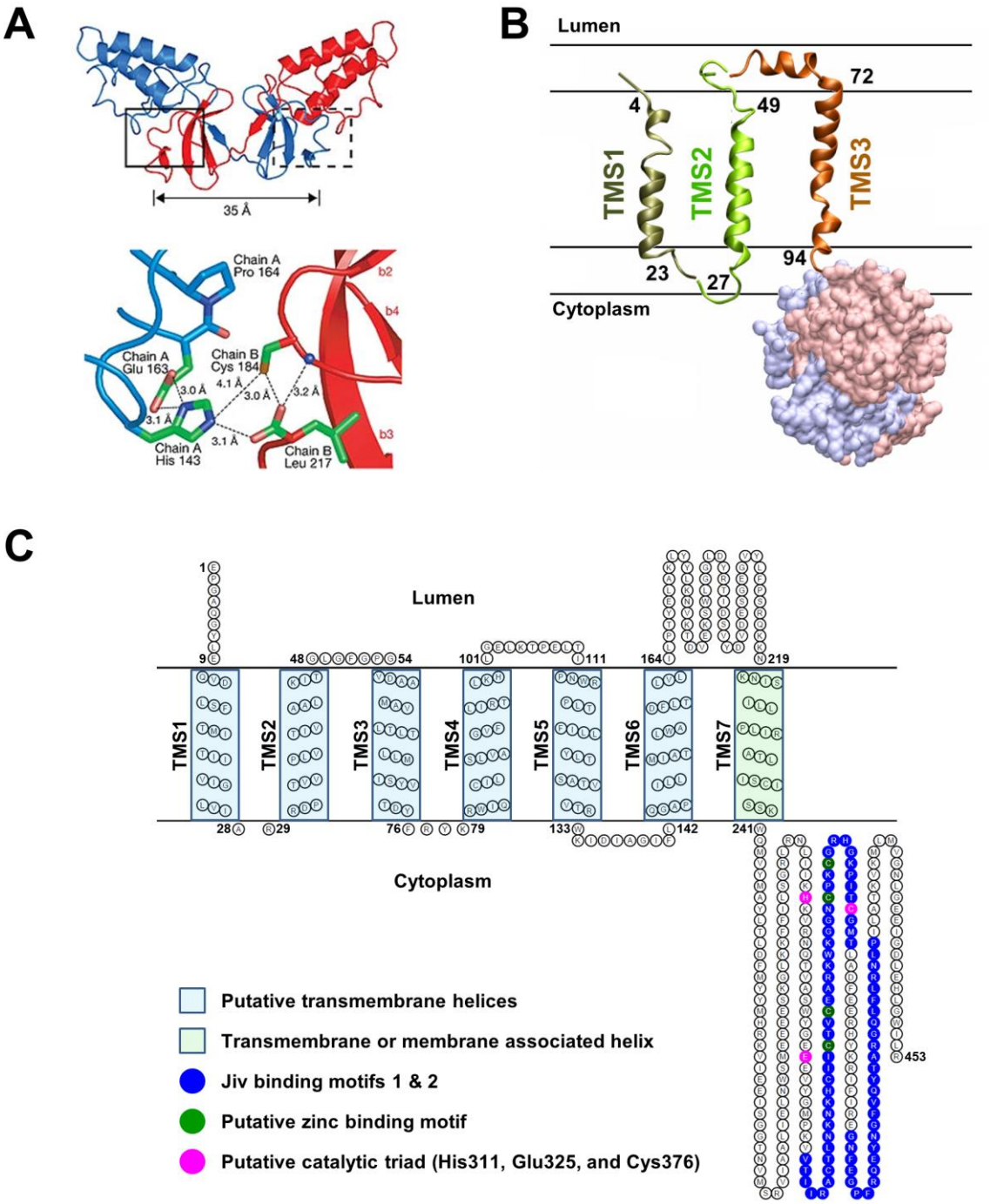

Fig. 4: Structure of NS2 protease domain and topology of membrane binding domain. (**A**) HCV NS2 protease dimer (top) and active site (bottom) (modified according to Lorenz et al., 2006). Location of the two active sites (marked by frames) in the dimer. The solid-lined frame indicates the active site shown below. The residues His143, Glu163 and Cys184 of the catalytic triad as well as the C-terminal residue Leu217 are depicted as stick drawings. (**B**) Membrane topology model of HCV NS2 (modified according to Jirasko et al., 2010). The three transmembrane helices TMS1-3 are shown as a ribbon model and the dimeric protease domain in the sphere representation (PDB: 2HD0). (**C**) *In silico* BVDV NCP7 NS2 membrane topology model (adapted from Klemens, 2014). Shown are the seven predicted transmembrane helices TMS1-7. Furthermore, the two Jiv-binding motifs (blue), the cysteines of the Zn^{2+}- binding motif (green) and the amino acids of the protease catalytic triad (pink) are marked. In addition, the amino acid positions for TMS, luminal and cytoplasmic segments are indicated. (**B+C**) Phospolipid bilayers are schematically marked as black lines.

3.4.2 Role of the NS2-3 region in the viral life cycle

3.4.2.1 Role of NS2-3 cleavage in RNA replication

Cleavage at the junction between NS2 and NS3 has an important function in the lifecycle of both HCV and pestiviruses, as the release of NS3 with its authentic N terminus is critical for the onset of viral RNA replication (Behrens et al., 1998; Lackner et al., 2004; Lamp et al., 2011; Lohmann et al., 1999; Madan et al., 2014; Tautz and Thiel, 2003; Welbourn et al., 2005). In the case of HCV, NS2-NS3 cleavage appears to be a rate-limiting step for RNA replication (Madan et al., 2014). In noncp pestiviruses, however, RNA replication is limited by the DNAJC14-dependent extent of NS2 protease-mediated cleavage between NS2 and NS3 (Lackner et al., 2004). Because NS3, but not uncleaved NS2-3, is an essential component of the viral replicase in both viruses, the liberation of NS3 is a prerequisite for formation of the replicase complex and efficient RNA replication. In the case of HCV, uncleaved NS2-NS3 prevents the formation of replicase complexes (RC), a process that can be experimentally detected by determining the ratio of hypo- and hyperphosphorylated NS5A, which is critical for RC assembly (Isken et al., 2015; Neddermann et al., 1999).

3.4.2.2 NS2 in virion morphogenesis

In addition to its central role in polyprotein processing to enable RNA replication, NS2 also is essentially involved in assembly of viral progeny.

Although the precise role of HCV NS2 in the assembly process is elusive, a multitude of experimental evidence suggests that NS2 is involved not only in early steps of virion assembly like nucleocapsid formation (Jirasko et al., 2008, 2010; Phan et al., 2009; Stapleford and Lindenbach, 2011) but also in late steps like particle assembly and egress (De La Fuente et al., 2013; Yi et al., 2009). HCV NS2 is thought to be a scaffold for virion morphogenesis (Ma et al., 2011), interacting with the structural proteins E1 and E2 as well as with p7, and with nonstructural proteins (Dimitrova et al., 2003; Gouklani et al., 2013; Jirasko et al., 2008, 2010; De La Fuente et al., 2013; Ma et al., 2011; Phan et al., 2009; Popescu et al., 2011; Stapleford and Lindenbach, 2011; Yi et al., 2007, 2009). Apparently, NS2 functions as a key organizer of HCV particle formation by engaging in various protein-protein interactions with viral structural and nonstructural proteins.

A distinctive feature of noncp pestiviruses is that due to the temporal regulation of NS2-3 cleavage, mainly uncleaved NS2-3 is present in infected cells at later time points of infection (Lackner et al., 2004), which is essential for virion morphogenesis and cannot be functionally replaced by free NS2. This was demonstrated via insertion of either a ubiquitin sequence or an EMCV IRES between NS2 and NS3, with both insertions resulting in inhibition of virion

morphogenesis (Agapov et al., 2004; Moulin et al., 2007). However, uncleaved NS2-3 provided by complementation of NS2-3-4A *in trans* is able to restore production of infectious particles (Agapov et al., 2004; Moulin et al., 2007). Furthermore, it was shown that enzymatic activities of NS2 and NS3 are not required for virion formation (Moulin et al., 2007). The regulated cleavage between NS2 and NS3 led to the assumption that NS3 and NS2-3 both in complex with NS4A (NS3/4A or NS2-3/4A) represent essential functional units that support distinct steps in the pestiviral lifecycle (Moulin et al., 2007). In contrast, HCV in cell culture does not rely on uncleaved NS2-NS3 for virus particle production. Insertion of an IRES between NS2 and NS3 sequences in chimeric J6/JFH1 genomes allowed the formation of HCV virions comparable to their respective parental genomes (Jirasko et al., 2008; Jones et al., 2007).

Although noncp pestiviruses are dependent on uncleaved NS2-3 for the generation of infectious particles, cp strains could be isolated that have ubiquitin insertions between NS2 and NS3 and thus no detectable amounts of uncleaved NS2-3 (Meyers et al., 1989; Tautz et al., 1993). The fact that these cp strains exist and that virion formation of the closely related HCV is independent of uncleaved NS2-3 inspired a successful attempt to adapt a noncp BVDV strain to NS2-3-independent virion morphogenesis (Klemens et al., 2015; Lattwein et al., 2012). Interestingly, to restore efficient particle formation in the absence of uncleaved NS2-3, only two amino acid exchanges were required: one C-terminally localized within NS2 (E440V) and the other in the NS3 protease domain (V132A) (Klemens et al., 2015). A crystallographic structure of CSFV NS3/4A allowed the identification of an interaction between the NS4A kink region and residue 132 of NS3 and it was shown that attenuation of this interaction supported a NS2-3-independent virion formation (Dubrau et al., 2017). These observations led to a model that a compact NS3/4A conformation is essential for RNA replication, whereas virion morphogenesis requires a more open conformation of this complex (Dubrau et al., 2017). The lack of structural data on NS2 complicates studies to elucidate the molecular function of the NS2 mutation, that is required for NS2-3-independent virion morphogenesis.

3.4.3 Differences in HCV and pestiviral NS2 protease activation and implications for the life cycle

For efficient NS2-3 cleavage, the NS2 protease of both HCV and pestiviruses requires activation by a cofactor. Interestingly, cofactor utilization is a distinguishing feature of the two closely related viral systems.

The HCV NS2 protease has been shown to be a *bona fide* protease with low intrinsic protease activity. However, the NS3 protease domain acts as a cofactor that greatly

increases the activity of the NS2 protease (Schregel et al., 2009; Tedbury and Harris, 2007). In cell culture, this *cis*-activation of the NS2 protease leads to an efficient cleavage between NS2 and NS3 (Grakoui et al., 1993; Hijikata et al., 1993a; Isken et al., 2015; Schregel et al., 2009). The exact molecular mechanism of NS2 activation by NS3 has not been fully elucidated. Based on the post-cleavage structure of the NS2 protease, it was proposed that an interaction between NS2 and NS3 surfaces contributes to correct positioning of the scissile bond at the NS2-NS3 junction in the active site, therby enabling autoprocessing (Lorenz et al., 2006). The lack of a structure of the NS2-NS3 precursor prevents a more detailed understanding of the conformational changes in the NS2 protease induced by interaction with NS3 prior to NS2-NS3 cleavage. However, recent insights into this activation provided by an alanine scanning mutagenesis approach led to the identification of a conserved hydrophobic NS3 protease surface patch (Isken et al., 2015). It was demonstrated that the conserved hydrophobic NS3 amino acids Y105, P115 and L127 are essential for NS2 activation by NS3 in the context of uncleaved NS2-NS3 (Isken et al., 2015).

The importance of the NS3 N-terminal domain as HCV NS2 protease cofactor via the hydrophobic NS3 protease surface patch was shown by gain/loss of function mutagenesis studies with NS2 from equine, bat, rodent, New and Old World primate hepaciviruses (Boukadida et al., 2018). These studies confirmed that the function of the NS3 protease domain with the respective HCV-like hydrophobic surface residues as cofactor for NS2 protease activiation is conserved among mammalian hepaciviruses (Boukadida et al., 2018).

Interestingly, this NS3 surface was also shown to serve multiple functions, as mutation of L127 also impaired NS5A hyperphosphorylation, replicase assembly and consequently RNA replication (Isken et al., 2015). The defective replicase assembly is most likely due to an incorrect ratio of NS5A hypo- and hyperphosphorylated forms, a known prerequisite for viral replicase assembly and efficient RNA replication (Neddermann et al., 1999; Oliver Koch and Bartenschlager, 1999). At present, functional replicase assembly is proposed to be the result of a sequence of events (Fig. 5): In uncleaved NS2-NS3, the hydrophobic NS3 surface patch surrounding L127 interacts with NS2, promoting NS2 protease stimulation. Upon NS2-NS3 cleavage and release of NS2, this NS3 surface patch becomes available for novel protein-protein interactions supporting NS5A hyperphosphorylation and subsequent replicase assembly (Isken et al., 2015). This model provides an explanation why the release of NS3 by NS2-NS3 cleavage is essential for viral RNA replication (Welbourn et al., 2005).

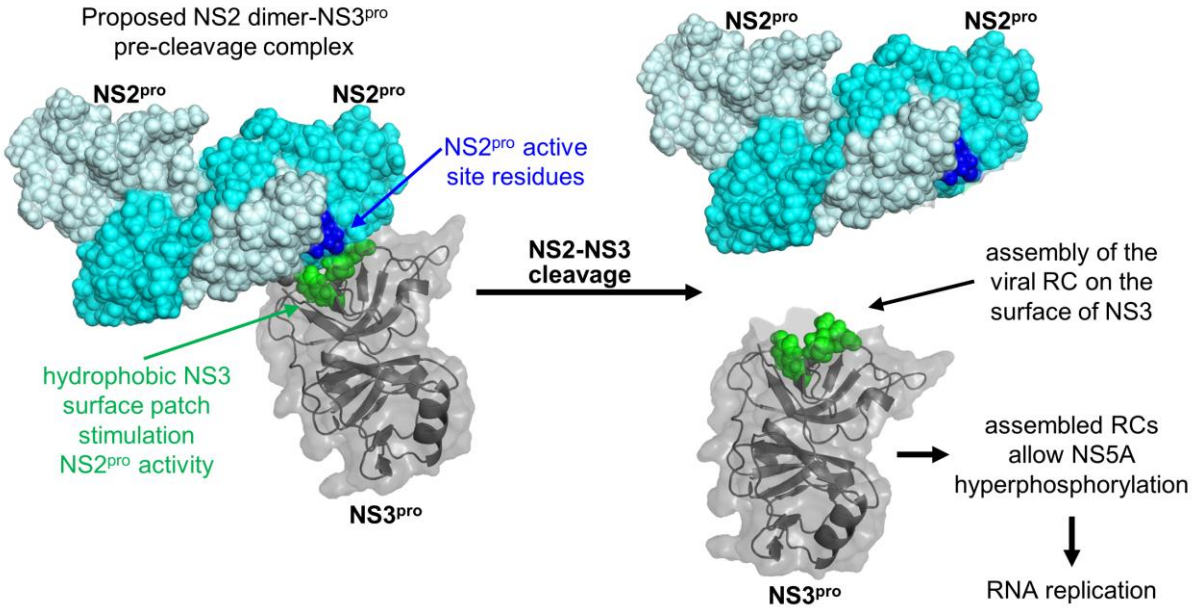

Fig. 5: NS3 surface residues are critical for HCV NS2 protease activation and replicase assembly. The sequence of events shown has been proposed to explain how NS2-NS3 cleavage regulates viral replicase complex (RC) assembly, NS5A hyperphosphorylation and RNA replication in the hepaciviral life cycle (Isken et al., 2015). In uncleaved NS2-NS3, the hydrophobic NS3 surface patch promotes NS2 protease ($NS2^{pro}$) stimulation. After NS2-NS3 processing, the hydrophobic NS3 surface becomes accessible for functional RC assembly and thus NS5A hyperphosphorylation and viral RNA replication can occur. The hypothetical NS2-NS3 pre-cleavage complex was built based on the post-cleavage crystal structures of the $NS2^{pro}$ dimer (light and dark cyan spheres, each showing an $NS2^{pro}$ monomer) (Lorenz et al., 2006) and the NS3 protease domain ($NS3^{pro}$; grey cartoon with surface) (Kim et al., 1996). The $NS2^{pro}$ active site residues His143, Glu163 and Cys184 are shown as blue spheres. The NS3 hydrophobic surface residues Y105, P115, and L127 are shown as green spheres.

In contrast to HCV, which is stimulated by the downstream NS3 protease domain, pestiviral NS2 relies on interaction with the cellular cofactor DNAJC14/Jiv for its stimulation (Lackner et al., 2005). This interaction is mediated via the two Jiv-binding motifs of the NS2 protease domain (Lackner et al., 2006). Due to the lack of structural data of NS2, NS2-3 or the NS2/Jiv complex, molecular details of pestiviral NS2 activation by Jiv are still unknown. Functional characterization has demonstrated that a minimal Jiv fragment of 90 aa (Jiv90) is able to bind NS2 and stimulate NS2 protease activity (Lackner et al., 2005, 2006; Rinck et al., 2001). In addition, a single point mutation of Jiv90 (W39A) has been shown to render it incapable of activating NS2 protease (Lackner et al., 2005). The dependence of the NS2 protease on a cellular cofactor for efficient NS2-3 cleavage is the basis for the temporally regulated switch from RNA replication to virion morphogenesis in the life cycle of noncp pestiviruses (Fig. 6). Free NS3 (regardless of biotype) together with its cofactor NS4A is an essential component of viral replicase and cannot be functionally replaced by uncleaved NS2-3 (Behrens et al., 1998; Lackner et al., 2004). Therefore, NS2-3 cleavage is a prerequisite in the pestiviral life cycle for active RNA replication. On the other hand, uncleaved NS2-3, together with NS4A, has an essential function in virion morphogenesis

(Agapov et al., 2004; Dubrau et al., 2017; Moulin et al., 2007). Accordingly, in the early phase of infection, efficient cleavage of NS2-3 into free NS2 and NS3 occurs in the presence of the cellular cofactor Jiv, which promotes viral RNA replication (Fig. 6) (Lackner et al., 2004). After NS2-3 cleavage, DNAJC14/Jiv remains stably associated with NS2, leading to a local depletion of the available cellular DNAJC14/Jiv pool in infected cells during the course of viral infection (Lackner et al., 2005). This local coactor depletion leads to inefficient NS2-3 cleavage and accumulation of uncleaved NS2-3 at later time points of infection (Lackner et al., 2004), resulting in the switch to virion morphogenesis (Fig. 6).

In cp strains, NS2-3 cleavage is deregulated by RNA recombination-mediated gene insertions, deletions, duplications or mutations (Tautz et al., 2015). The resulting continuous availability of significant amounts of free NS3 leads to a continous support of RNA replication which correlates with the cp phenotype (Agapov et al., 2004; Becher and Tautz, 2011; Moulin et al., 2007). For the cp BVDV strain CP7 used in this work, it was shown that the upregulated NS3 release is caused by an insertion of nine amino acids in NS2 that renders the NS2 autoprotease independent of activation by DNAJC14/Jiv (Isken et al., 2019; Lackner et al., 2004; Tautz et al., 1996).

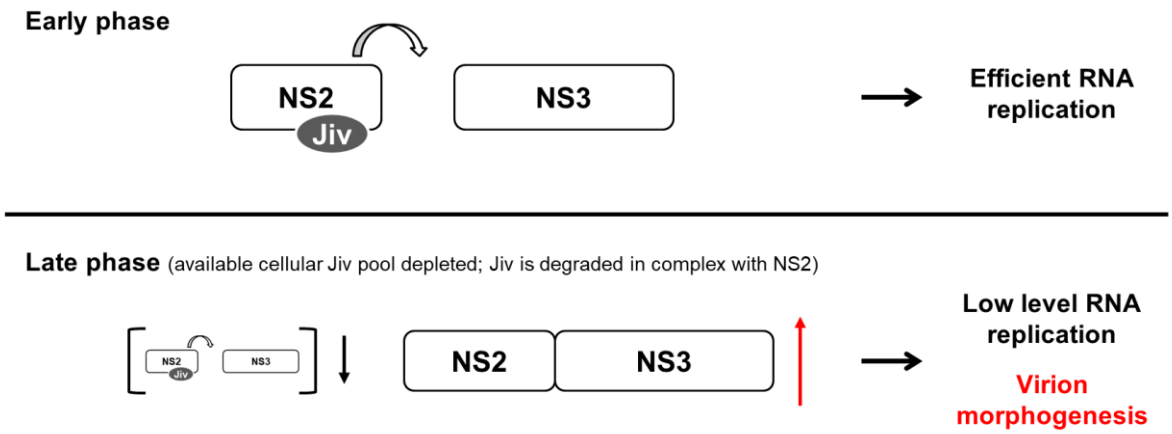

Fig. 6: Temporal regulation of the switch from viral RNA replication to virion morphogenesis through NS2-3 cleavage in noncp pestiviruses. Cleavage of the precursor protein NS2-3 is dependent on the cellular cofactor DNAJC14/Jiv. In the early phase of infection,DNAJC14/Jiv is available for efficient NS2-3 cleavage, allowing free NS3 together with its cofactor NS4A to promote viral replicase assembly. As infection progresses, the locally available cellular DNAJC14/Jiv pool is depleted, leading to inefficient cleavage of NS2-3. Uncleaved NS2-3 cannot functionally compensate for free NS3 in the replicase complex but, together with NS4A, is an essential factor for viral particle assembly. Accordingly, a switch from RNA replication to virion morphogenesis occurs.

3.4.4 Studies on the molecular mechanism of HCV NS2 protease stimulation by NS3

A recent study by Boukadida *et al.* suggested that NS3 is not only a stimulatory cofactor for HCV NS2 protease but also has a regulatory function for NS2-NS3 cleavage (Boukadida et al., 2018). This hypothesis was based on the observations that NS2 followed by a flexible linker (GGGGS) and GFP, i.e. in the absence of any NS3 sequences, showed efficient NS2 protease activity (Boukadida et al., 2018), whereas short N-terminal NS3 sequences missing the hydrophobic surface residues for NS2 activiation reduce NS2 protease activity to its basal level (Boukadida et al., 2018). These findings are supported by previous observations showing that minimally the N-terminal 169 residues of NS3 are required to obtain detectable NS2-NS3 cleavage in NS2-NS3 precursor proteins (Isken et al., 2015) and that truncated precursors such as NS2-NS3$_{(1-40)}$ exhibit only basal cleavage efficiency (Schregel et al., 2009). This suggests that the mechanism of NS2 protease stimulation by NS3 represents some sort of quality and/or kinetic control of translation and/or functional folding of the NS3 protease domain. It is conceivable that the newly translated nascent N-terminal NS3 peptide chains could initially either interfere with the correct positioning of the NS2-NS3 cleavage site relative to the active site of the NS2 protease, thereby interfering with NS2 protease-mediated NS2-NS3 cleavage, or that they could interfere with the optimal formation of the active NS2 site. Only at a certain length can the NS3 moiety adopt a conformation that leads to proper folding and positioning of the hydrophobic NS3 surface patch to allow NS3-mediated NS2 protease stimulation to occur.

The hypothesis that hydrophobic surface contacts between NS2 and NS3 are at the core of the NS3-mediated NS2 protease stimulation implies the existence of corresponding hydrophobic surface residues on the NS2 protease domain. Such potential NS2 surface determinants have not yet been characterized but should allow either an optimization of the active site geometry or assist the efficent positioning of the NS2-NS3 cleavage site relative to the active site.

3.5 Objective

NS2 is a key player in the life cycle of hepaciviruses and pestiviruses. On the one hand, it supports RNA replication by cleavage at the junction between NS2 and NS3, thereby releasing the essential replicase component NS3, and on the other hand, it plays an important role in virion morphogenesis.

Due to the lack of structural data on pestiviral NS2, it has not been possible to elucidate the molecular details of its functions in the pestiviral life cycle. Insights into the domain architecture of pestiviral NS2 would greatly help to design meaningful reverse-genetic experiments to obtain mechanistic information about its functions. The first main objective of the present work was to determine a topology model of the membrane binding domain of BVDV NS2 based on a preliminary data set obtained in my master thesis (Walther, 2017). The resulting experimentally determined membrane topology model will provide the foundation to determine the minimal NS2 protease domain. Together, these information will lead to a better understanding of the domain structure of the pestiviral NS2 and will allow further functional and structural studies on pestiviral NS2.

For HCV, crystallographic and NMR data are available for NS2 and NS3, but not for the NS2-3 precursor. The available structural data already led to detailed insights into molecular functions of NS2 and NS3. Among those, the stimulation of the HCV NS2 protease activity by its activating cofactor NS3 was intensively studied showing that NS2 protease activation by NS3 depends on conserved hydrophobic NS3 surface residues (Y105, P115 and L127). Although much progress has been made in the understanding of NS2/NS3 biology, key questions concerning NS2-NS3 interactions and structural changes leading to efficient NS2-NS3 cleavage, remain poorly understood. This is mainly due to the lack of structural information of the uncleaved NS2-NS3 precursor protein. Importantly, the NS2 determinants interacting with and reacting to interactions with NS3 during NS2 protease activation have not been determined. Accordingly, the second major aim of this work was to indentify and characterize these HCV NS2 determinants by reverse genetics. To verify the critical importance of these surface residues, their functional conservation should also be tested in related mammalian hepaciviruses.

Taken together, these analyses will increase insight into the molecular mechanism of NS2, which can be considered a major control factor for orchestrating RNA replication and virion morphogenesis in pestiviruses and hepaciviruses.

4 Materials and Methods

4.1 Materials

4.1.1 Chemicals

Table 1: List of used chemicals

Name	Supplier
4,6-Diamidin-2-phenylindol (DAPI)	Roche, Mannheim, Germany
5-Bromo-4-Chloro-3-Indolyl-β-D-Galactopyranosid (X-Gal)	ICN, Eschwege, Germany
AccuGENE PBS	Lonza, Hessisch Oldendorf, Germany
Acrylamide (4K solution, 40%)	Applichem, Darmstadt, Germany
Adenosine triphosphate (ATP)	Roche, Mannheim, Germany
Agarose LE Standard	7Bioscience, Hartheim, Germany
Ammonium persulfate (APS)	Roth, Karlsruhe, Germany
Ampicillin (Amp)	Roth, Karlsruhe, Germany
Bromophenol blue	Sigma-Aldrich, Taufkirchen, Germany
Calcium chloride ($CaCl_2$)	Merck, Darmstadt, Germany
Chloroform	Roth, Karlsruhe, Germany
Cutsmart Buffer (10x)	NEB, Frankfurt am Main, Germany
Desoxynucleoside triphosphate (dNTPs)	Life Technologies, Darmstadt, Germany
Digitonin	Sigma-Aldrich, Taufkirchen, Germany
Disodium phosphate (Na_2HPO_4)	Merck, Darmstadt,, Germany
Dithiothreitol (DTT)	Invitrogen, Darmstadt, Germany
Dried skim milk powder	Roth, Karlsruhe, Germany
Dulbecco's Modified Eagle Medium (DMEM)	Fisher Scientific, Schwerte, Germany
Ethanol	Roth, Karlsruhe, Germany
Ethylene diamine tetraacetic acid (EDTA)	Roth, Karlsruhe, Germany
Ethylene glycol-bis(β-aminoethyl ether)-N,N,N',N'-tetraacetic acid (EGTA)	Sigma Aldrich, Taufkirchen, Germany
Fetal calf serum (FCS)	PAA, Cölbe, Germany
G7 Reaction Buffer (10x)	NEB, Frankfurt am Main, Germany
GeneRuler™ 1 kb Plus DNA ladder	Thermo Fisher Scientific, Schwerte, Germany
Geneticin (G418)	Thermo Fisher Scientific, Schwerte, Germany
Glutathione	Sigma Aldrich, Taufkirchen, Germany
Glycerine	Roth, Karlsruhe, Germany

Name	**Supplier**
Glycine	Biomol, Hamburg, Germany
Glycoprotein Denaturing Buffer	NEB, Frankfurt am Main, Germany
Horse serum (HS)	PAA, Cölbe, Germany
Hydrochloric acid (HCl)	Roth, Karlsruhe, Germany
4-(2-hydroxyethyl)-1-piperazinylethanesulfonic acid (HEPES)	Roth, Karlsruhe, Germany
Isopropanol	Roth, Karlsruhe, Germany
Lysogeny broth agar (LB agar)	Roth, Karlsruhe, Germany
Magnesium chloride ($MgCl_2$)	Roth, Karlsruhe,, Germany
Metafectene® Transfection Reagent	Biontex, München, Germany
Methanol	Roth, Karlsruhe, Germany
Methoxypolyethylenglycol(5000)-maleimide (PEG-Mal)	Sigma-Aldrich, Taufkirchen, Germany
Midori Green Xtra	Nippon Genetics, Düren, Germany
Minimum Essential Medium (MEM)	Fisher Scientific, Schwerte, Germany
N-Dodecyl-β-D-maltoside	Thermo Fisher Scientific, Darmstadt, Germany
N-Octylglucopyranoside	Sigma-Aldrich Taufkirchen, Germany
Nonidet P-40 (NP-40) (10%)	NEB, Frankfurt am Main, Germany
N-Tris-(hydroxymethyl)-methyl-glycine (Tricine)	Roth, Karlsruhe, Germany
PageRuler™ Prestained Protein Ladder	Thermo Fisher Scientific, Darmstadt, Germany
Paraformaldehyde	Affymetrix, USB, Cleveland, OH, USA
Penicillin/Streptomycin	Thermo Fisher Scientific, Darmstadt, Germany
Phenol/chloroform/isoamyl alcohol (25:24:1)	Roth, Karlsruhe, Germany
Polyethylenimine (PEI)	Sigma-Aldrich, Taufkirchen, Germany
Ponceau S	Serva, Heidelberg, Germany
Potassium acetate (KAc)	Roth, Karlsruhe, Germany
Potassium chloride (KCl)	Roth, Karlsruhe, Germany
Potassium dihydrogen phosphat (KH_2PO_4)	Merck, Darmstadt,, Germany
Potassium hydroxide (KOH)	Roth, Karlsruhe, Germany
Purple Gel Loading Dye (6x)	NEB, Frankfurt am Main, Germany
Ribonucleosidetriphospate (rNTPs)	Ambion, Austin, TX, USA
Skim milk powder	Roth, Karlsruhe, Germany
Sodium acetate (NAOAc)	Sigma-Aldrich, Taufkirchen, Germany
Sodium chloride (NaCl)	Roth, Karlsruhe, Germany

Name	Supplier
Sodium dodecylsulfate (SDS)	Roth, Karlsruhe, Germany
Sodium hydroxide (NaOH)	Roth, Karlsruhe, Germany
Tetramethylethylenediamine (TEMED)	Roth, Karlsruhe, Germany
Trichloromethane (Chloroform)	Roth, Karlsruhe, Germany
Tris(hydroxymethyl)aminomethane (Tris)	Roth, Karlsruhe, Germany
Triton X-100	Sigma-Aldrich, Taufkirchen, Germany
Trypsin/EDTA	Sigma-Aldrich, Taufkirchen, Germany
Tween20	Invitrogen, Darmstadt, Germany
VectaShield®	Vector Laboratories, Burlingame, CA, USA
Water, double distilled (ddH_2O)	Roth, Karlsruhe, Germany
β-Mercaptoethanol	Roth, Karlsruhe, Germany

4.1.2 Consumables

Table 2: List of used consumables

Name	Supplier
Baffled flasks	Schott, Mainz, Germany
Cell culture dishes (Ø 10 cm)	BD Falcon, Heidelberg, Germany
Cell culture plates (6 well, 12 well, 96 well)	BD Falcon, Heidelberg, Germany / TPP, Trasadingen, Switzerland
Cell scrapers	TPP, Trasadingen, Switzerland
Centrifuge tubes (15 ml, 50 ml)	Sarstedt, Nümbrecht, Germany / TPP, Trasadingen, Switzerland
Disposable pipettes (5 ml, 10 ml, 25 ml, 50 ml)	Greiner Bio-One, Frickenhausen, Germany
Disposable scalpels	Feather, Osaka, Japan
Electroporation cuvettes (2 mm, 4 mm gap)	Sigma-Aldrich, Taufkirchen, Germany
Filter papers (for Western blotting)	Whatman, Solingen, Germany
Glass pipettes	Schott, Mainz, Germany
Nitrocellulose membranes	Pall Life Sciences, Port Washington, USA
PCR tubes (0.1 ml)	Biozym, Hessisch Oldendorf(D)
Petri dishes	Greiner Bio-One, Frickenhausen, Germany
Pipette tips (10 - 1000 µl)	Sarstedt, Nümbrecht, Germany
Reaction tubes (1,5 und 2 ml)	Eppendorf, Hamburg, Germany
Sterile filters (0.2 µm)	Sartorius, Göttingen, Germany
Vynil gloves (Meditrade)	Medita, Düsseldorf, Germany

4.1.3 Devices

Table 3: List of used devices

Name	Supplier
Balances	Sartorius, Göttingen, Germany
CCD camera AxioCam MRm	Zeiss, Jena, Germany
CCD camera FUculus	New Electronic Technology, Finning, Germany
Centrifuge (Avanti J-25, J-35)	Beckman, Krefeld, Germany
Clean benches (MCS Advance / BSC-EN-2-6 120)	Thermo Fisher Scientific, Schwerte, Germany / Zapf, Ferarra, Italy
Electroporation module (GenePulser Xcell™)	Biorad, München, Germany
Fluorescence microscope (Axio Observer.Z1)	Zeiss, Jena, Germany
Gelelectrophoresis chamber for agarose gels	Werkstatt des MZI, JLU Gießen, Germany
Gelelectrophoresis chamber for SDS-PAGE (Mini-PROTEAN Tetra Cell)	Biorad, München, Germany
Glassware	Schott, Mainz, Germany
Heating block	Liebisch Labortechnik, Bielefeld, Germany
Incubator for bacterial cultures	Bachofer, Reutlingen, Germany
Incubator shaker for bacterial cultures (Multitron Standard)	Infors HT, Bottmingen, Switzerland
Incubator with CO_2 supply (C200)	Labotec, Rosdorf, Germany
Light microscope Axiovert 25	Zeiss, Jena, Germany
Luminometer (Junior LB9505)	Berthold Technologies, Bad Wildbad, germany
Magnetic stirrer (Magnetomix)	IKA-Werke, Staufen, Germany
Minishaker (Vibrax VXR)	IKA-Werke, Staufen, Germany
Nanodrop 2000c	Thermo Fisher Scientific, Schwerte, Germany
pH meter (763 Multi-Calimatic)	Mettler Toledo, Gießen, Germany
Pipettes	Eppendorf, Hamburg, Germany; Gilson, Middleton, WI, USA
Pipettor (PipetBoy Acu)	Integra Biosciences, Fernwald, Germany
Platform shaker (Polymax 1040)	Heidolph Instruments, Schwalbach, Germany
Power supply (PowerPac Basic; SDS-PAGE & Western Blot)	Biorad, München, Germany

Name	Supplier
Power supply (Standard Power Pack P25; Agarosegele)	Biometra, Göttingen, Germany
Spinning wheel	NeoLab, Heidelberg, Germany
Tabletop centrifuge (1,5 und 2 ml) (5424)	Eppendorf, Hamburg, Germany
Tabletop centrifuge (1,5 und 2 ml), coolable (5415R)	Eppendorf, Hamburg, Germany
Tabletop centrifuge (15 und 50 ml) (5804R)	Eppendorf, Hamburg, Germany
Tankblot module (Mini Trans-Blot®)	Biorad, München, Germany
Thermomixer Comfort (1,5 und 2 ml)	Eppendorf, Hamburg, Germany
Thermoycler (Piko 24)	Thermo Fisher Scientific, Schwerte, Germany
Transilluminator for agarose gels (FastGene Blue/Green)	Nippon Genetics, Düren, Germany
Vortexer	IKA-Werke, Staufen, Germany
Water bath	Memmert, Büchenbach, Germany
Western Blot Image Analyzer LAS-4000 mini	Fujifilm, Düsseldorf, Germany
Western Blot Imaging System Odyssey® Classic	LI-COR Biosciences, Lincoln, Nebraska, USA

4.1.4 Kits

Table 4: List of used kits

Kit	Supplier
Luciferase Assay system	p.j.k, Kleinblittersdorf, Germany
MAXIScript™ SP6/T7 Kit	Ambion, Austin, TX, USA
Millipore Montage™ Gel Extraction Kit	Merck Millipore, Darmstadt, Germany
Nucleobond® PC 100 Kit	Macherey-Nagel, Düren, German
pGEM®-T Vector Kit	Promega, Madison, WI, USA
Western Lightning™ Chemiluminescence Reagent Plus	Perkin Elmer, Boston, USA

4.1.5 Enzymes

Table 5: List of used enzymes

Enzyme	Supplier
DNaseI	Ambion, Austin, TX, USA
Peptide-N-glycosidase F (PNGase F)	NEB, Frankfurt am Main, Germany
Pfu-X DNA polymerase	Jena Bioscience, Jena, Germany

Enzyme	Supplier
Restriction endonucleases	NEB, Frankfurt am Main, Germany
Ribonuclease A (RNase A)	Roth, Karlsruhe, Germany
SP6 RNA polymerase	Ambion, Austin, TX, USA
T4 DNA ligase	NEB, Frankfurt am Main, Germany
T7 RNA polymerase	Ambion, Austin, TX, USA
Taq DNA polymerase	NatuTec, Frankfurt am Main, Germany
Trypsin	Sigma-Aldrich, Taufkirchen, Germany

4.1.6 Buffers, solutions and media

Table 6: List of used buffers, solutions and media

Name	Composition
Acrylamide separation gel (10%) according to Laemmli (Laemmli, 1970)	3,6 ml ddH_2O, 2,5 ml 1,5 M Tris-HCl (pH 8,8), 100 µl SDS (10%), 2,5 ml Acrylamide (40%; 29:1), 100 µl APS (10%), 10 µl TEMED
Acrylamide separation gel (10%) according to Schägger/von Jagow (Schägger and von Jagow, 1987)	3,6 ml ddH_2O, 3,3 ml Jagow gel buffer, 0,5 ml Glycerin, 2,5 ml Acrylamide (40%; 29:1), 100 µl APS (10%), 10 µl TEMED
Acrylamide separation gel (8%) nach according to Schägger/von Jagow (Schägger and von Jagow, 1987)	4,1 ml ddH_2O, 3,3 ml Jagow gel buffer, 0,5 ml Glycerin, 2 ml Acrylamide (40%; 29:1), 100 µl APS (10%), 10 µl TEMED
Acrylamide stacking gel (4%) according to Laemmli (Laemmli, 1970)	3,15 ml ddH_2O, 1,25 ml 0,5 M Tris-HCl (pH 6,8), 50 µl SDS (10%), 0,5 ml Acrylamide (40%; 29:1), 50 µl APS (10%), 5 µl TEMED
Acrylamide stacking gel (4%) according to Schägger/von Jagow (Schägger and von Jagow, 1987)	3,2 ml ddH_2O, 1,25 ml Jagow gel buffer, 0,5 ml Acrylamide (40%; 29:1), 50 µl APS (10%), 5 µl TEMED
Agarose gel solution (0,8%)	4 g Agarose in 500 ml 1x TAE buffer
Anode buffer (10x)	2 M Tris in ddH_2O (pH 8.9 with HCl)
APS solution (10%)	1 g APS in 10 ml ddH_2O
Blocking solution (Western blot)	5% (w/v) dried skim milk powder in PBS-T
Cathode buffer (10x)	1 M Tris, 1 M Tricin, 1% SDS in ddH_2O; pH 8.25 with HCl
Cytomix	120 mM KCl, 0.15 mM $CaCl_2$, 10 mM K_2HPO_4/KH_2PO_4 (pH 7.6), 25 mM HEPES, 2 mM EGTA, 5 mM $MgCl_2$, 2 mM ATP and 5 mM Glutathione (added just before use),

Name	Composition
	adjusted to pH 7.6 with KOH, sterile filtered
DAPI solution	2 mg/ml DAPI in ddH_2O
Digitonin solution (5%)	5 mg Digitonin in 1 ml PBS
dNTP mix	10 mM dATP, dCTP, dGTP, dTTP each in ddH_2O
DTT solution	0,5 M DTT in ddH_2O
Elution buffer (N5)	100 mM Tris, 15% Ethanol, 1 M KCl; pH 8.5 with H_3PO_4
Equilibration buffer (N2)	100 mM Tris, 15% Ethanol, 900 mM KCl, 0,15% Triton X-100; pH 6.3 with H_3PO_4
HCN buffer	50 mM HEPES, 150 mM NaCl, 2 mM $CaCl_2$; pH 7.3 at 4 °C
Huh7-T7 complete medium	DMEM with 10% (v/v) FKS, 100.000 U/l Penicillin, 0,1 g/l Streptomycin, 125 µg/ml G418
Infection medium	MEM or DMEM without additives
Jagow gel buffer	3 M Tris, 0,3% SDS in ddH_2O; pH 8.45 with HCl
Laemmli running buffer (10x)	0,25 M Tris, 1,92 M Glycin, 1% (v/v) SDS in ddH_2O
LB medium	1% (w/v) Bacto-Trypton, 0,5% (w/v) yeast extract, 1% (w/v) NaCl
Lysis buffer (S2, P2)	200 mM NaOH; 1% (w/v) SDS
Maltoside lysis buffer	0,5% n-Dodecyl-β-D-maltoside, 100 mM NaCl, 20 mM Tris, pH 7.5
MDBK complete medium	DMEM with 10% (v/v) FKS, 100.000 U/l Penicillin, 0,1 g/l Streptomycin
Neutralisation buffer (S3, P3)	2,8 M $K(CH_3COO)$; pH 5.1 with CH_3COOH
PBS-Tween (PBS-T)	0,05% (v/v) Tween20 in PBS
PEG-Mal solution	40 mM PEG-Mal in HCN buffer
Phosphate buffered saline (PBS) (1x)	137 mM NaCl, 2,7 mM KCl, 4,3 mM Na_2HPO_4, 1,47 mM KH_2PO_4; pH 7.4 with HCl
Resuspension buffer (S1, P1)	50 mM Tris-HCl, 10 mM EDTA, 100 mg/l RNase A; pH 8.0
SDS sample buffer	3,55 ml ddH_2O, 1,25 ml 0,5 M Tris-HCl (pH 6,8), 2,5 ml Glycerin, 2,0 ml 10% SDS, 0,2 ml 0,5% Bromphenol blue, 5% (v/v) β-Mercaptoethanol
SK6 complete medium	MEM mit 10% FCS, 100.000 U/l Penicillin, 0,1g/l Streptomycin
Sodium acetate (NaOAc) solution	3 M NaOAc in ddH_2O, pH 5.2
T4 ligase buffer	50 mM Tris, 10 mM $MgCl_2$ 1 mM ATP, 10 mM DTT; pH 7.5
TAE buffer (1x)	2% (w/v) TAE buffer concentrate (50 x Modified Tris-Acetate EDTA buffer, Merck Millipore, Darmstadt) in ddH_2O
Transfer buffer (1x)	10% Tris-Glycin (10x), 20% Methanol in ddH_2O
Tris-Glycin (10x)	0,25 M Tris, 1,92 M Glycin in ddH_2O

Name	Composition
Washing buffer (N3)	100 mM Tris, 15% EtOH, 1,15 M KCl; pH 6.3 with H_3PO_4
X-Gal solution	40 mg/ml X-Gal in Dimethylformamide

4.1.7 *E. coli* strains

Table 7: List of used *E. coli* strains

E. coli K12 strain	Description
DH5α	F^- endA1 glnV44 thi-1 recA1 relA1 gyrA96 deoR nupG Φ80dlacZΔM15 Δ (lacZYA-argF) U169, hsdR17(rK^- mK^+), λ^-; for pGEM®-T vector cloning, blue/white selection
HB101	F^- mcrB mrr hsdS20 (rB^- mB^-) recA13 leuB6 ara-14 proA2 lacY1 galK2 xyl-5 mtl-1 rpsL20(Sm^R) glnV44 λ^-; for routine cloning

4.1.8 Eukaryotic cell lines

Table 8: List of used eukaryotic cell lines

Cell line	Description
Huh7 Lunet	Human hepatoma cell line highly permissive for HCV (Oliver Koch and Bartenschlager, 1999), received from Ralf Bartenschlager, University Heidelberg, Germany.
Huh7-T7	Human hepatoma cell line stably expressing T7 RNA polymerase (Schultz et al., 1996); obtained from Dr. Stanley Lemon, UNC, Chapel Hill, NC, USA
MDBK	Madin-Darby Bovine Kidney cell line, obtained from the American Type Culture Collection (ATCC), Rockville, MD, USA
SK6	Swine Kidney cells (Kasza et al., 1972), obtained from the ATCC, Rockville, MD, USA
SK6 DNAJC14-KO (SK6 KO)	SK6 cells with CRISPR-Cas-mediated knockout of DNAJC14 expression, which renders cells deficient for the pestiviral NS2 protease-activating cofactor DNAJC14/Jiv (Isken et al., 2019)
SK6 DNAJC14-KO GST-JIV90(WT) (SK6 KO GST-Jiv90)	Functional rescue of the ability to activate pestiviral NS2 protease by overexpression of the minimal cofactor domain Jiv90 C-terminally fused to GST in SK6 KO cells (Isken et al., 2019)

4.1.9 Viruses

Table 9: List of used viruses

Virus	Description
CP7	Cytopathogenic (cp) BVDV-1 strain CP7 (Meyers et al., 1996; Pankraz et al., 2005)
CP7 2/H-F	Based on BVDV-1 CP7; the NS2 contains and N-terminal HA-Flag (H-F) epitope (Klemens, 2014)
NCP7	cDNA clone of noncp BVDV-1 strain CP7 (Meyers et al., 1996; Pankraz et al., 2005)
NCP7 2/H-F	Based on BVDV-1 NCP7; the NS2 contains and N-terminal HA/Flag (H-F) epitope (Klemens, 2014)
MVA-T7^{pol}	Recombinant Modified Vaccinia Virus Ankara (MVA)-T7^{pol} (Sutter et al., 1995), obtained from G. Sutter, LMU, München (D)

4.1.10 Antibodies

Table 10: List of used primary and secondary antibodies

Antibody	Description
IRDye® 800CW α-mouse	polyclonal donkey IgG against mouse IgG, conjugated with IRDye® 800CW; LI-COR Biosciences, Lincoln, NE, USA
α-FLAG M2	monoclonal mouse IgG against Flag® epitope; Sigma-Aldrich, Taufkirchen, Germany
α-GST (26H1)	monoclonal mouse IgG against Glutathion-S-Transferase (GST); Cell Signaling Technology, NEB, Frankfurt/Main, Germany
α-HA (C29F4)	monoclonal rabbit IgG against hemagglutinin (HA) epitope; Cell Signaling Technology, NEB, Frankfurt/Main, Germany
α-HA.11 (16B12)	monoclonal mouse IgG against HA epitope; Covance, Münster, Germany
α-rabbit-AlexaFluor®488	monoclonal goat IgG against rabbit IgG, conjugated with AlexaFluor®488; Thermo Fisher Scientific, Darmstadt, Germany
α-rabbit-PO	monoclonal goat IgG against rabbit IgG, conjugated with horseradish peroxidase (PO); Dianova, Hamburg, Germany
α-mouse-Cy3®	monoclonal goat IgG against mouse IgG, conjugated with Cyanine 3 (Cy3®); Dianova, Hamburg, Germany
α-mouse-PO	monoclonal goat IgG against mouse IgG, conjugated with horseradish peroxidase (PO); Dianova, Hamburg, Germany

Antibody	Description
α-BVDV NS3 8.12.7 (Code 4)	monoclonal mouse IgG directed against an epitope of NS3 of all species analyzed within the genus *Pestivirus*, detects NS2-3 and NS3 (Corapi et al., 1990); obtained from E. J. Dubovi (New York State College of Veterinary Medicine, Cornell University, Ithaka, New York, USA).

4.1.11 Oligo nucleotides

The primers listed were used for polymerase chain reactions (PCR), sequencing, and site-directed mutagenesis. All oligonucleotides were purchased from Sigma-Aldrich, Taufkirchen, Germany. Restriction sites are marked in bold, nucleotides deviating from the template are shown in capital letters.

Table 11: Primers used for site-directed mutagenesis (QuikChange® PCR) within BVDV NS2. Only primers for mutants generated in this work are listed here. The primers for the initial set mutant can be found in my master thesis and in bachelor thesis of J. Fellenberg (Fellenberg, 2017; Walther, 2017).

Primer	Sequence (5‘-3‘)
BVDV NS2 Y75C se	ctgatgattagttatgtgacagactGcttcaggtataaaaggtgg
BVDV NS2 Y75C ase	ccacctttatacctgaagCagtctgtcacataactaatcatcag
BVDV NS2 F76C se	ctgatgattagttatgtgacagactactGcaggtataaaaggtggatacaatc
BVDV NS2 F76C ase	gattgtatccacctttatacctgCagtagtctgtcacataactaatcatcag
BVDV NS2 T73C se	cctactgatgattagttatgtgTGCgactacttcaggtataaaagg
BVDV NS2 T73C ase	ccttttatacctgaagtagtcGCAcacataactaatcatcagtagg
BVDV NS2 L86C se	ggtataaaaggtggatacaatctatcTGcagcttagtagccggggtgttcc
BVDV NS2 L86C ase	ggaacaccccggctactaagctgCAgatagattgtatccacctttatacc
BVDV NS2 R96C se	gcttagtagccggggtgttccttatcTGCaccctcaaacatctaggtgaactc
BVDV NS2 R96C ase	gagttcacctagatgtttgagggtGCAgataaggaacaccccggctactaagc
BVDV NS2 E108C se	ctaggtgaactcaaaacccctTGCctgaccataccaaactggagg
BVDV NS2 E108C ase	cctccagtttggtatggtcagGCAaggggttttgagttcacctag
BVDV NS2 L109C se	ggtgaactcaaaacccctgagTGCaccataccaaactggaggccac
BVDV NS2 L109C ase	gtggcctccagtttggtatggtGCActcaggggttttgagttcacc
BVDV NS2 W114C se	cctgagctgaccataccaaactgCaggccactaaccttcatactattatacc
BVDV NS2 W114C ase	ggtataatagtatgaaggttagtggcctGcagtttggtatggtcagctcagg

Table 12: Primers used to generate NCP7 and CP7 NS2$_{(x\text{-}453)}$-3$_{(1\text{-}10)}$-SUMO-HA-V5 reporter constructs

Primer	Sequence (5‘-3‘)
NcoI-Met-Gly-NS2_1 se	**ccatgGG**Agaaccaggtgcccaggggtacc
NheI-NcoI-Met-Gly-BVDV NS2_78 se	**gctagc**A**ccatgGG**Atataaaaggtggatacaatgtatcctcagc

Primer	Sequence (5‘-3‘)
NheI-NcoI-Met-Gly-BVDV NS2_136 se	**gctagc**A**ccatgg**gggcccctatccttttgatgatcg
BsrGI-NS2 BVDV ase	tgtat**tgtaca**aacccattgtattcctgc
NcoI-MG-BVDV NS2_99 se	gggtgttccttatccgga**ccAtGG**GAaaacatctaggtgaactcaaaacc
NcoI-MG-BVDV NS2_99 ase	ggttttgagttcacctagatgtttTC**CCaTgg**tccggataaggaacaccc
NcoI-MG-BVDV NS2_112 se	ctcaaaacccctgagctga**ccatGG**GAccaaattggaggccactaacc
NcoI-MG-BVDV NS2_112 ase	ggttagtggcctccaatttggTC**CCatgg**tcagctcaggggttttgag
NcoI-MG-BVDV NS2_169 se	ctgatcctacccacctac**CCATGG**GAgaattagccaagctgtactacc
NcoI-MG-BVDV NS2_169 ase	ggtagtacagcttggctaattcTC**CCATGG**gtaggtgggtaggatcag
pCITE SacII-HA-V5-SbfI se	**CCGCGG**CTTACCCGTACGATGTTCCGGATTATGCTGG GTCCGGAGGTAAGCCTATCCCTAACCCTCTCCTCGGT CTCGATTCTACGTGA**cctgcagg**catgcaagcttttgttcc
pCITE SacII-HA-V5-SbfI ase	GTACGGGTAAG**CCGCGG**tcgatcgactctagaggatcggagatctc
BamHI-3(1-10)-SUMOdGG-SacII se	**GGATCC**TAAGGGGACCTGCCGTGTGCAAGAAAATAAC TGAGgggtcggactcagaagtcaatcaag
BamHI-3(1-10)-SUMOdGG-SacII ase	**CCGCGG**Caatctgttcgcggtgagcctc
BVDV NS2 C376A se	ccacgggaagcccatcACCGCGgggatgactctagcggattttg
BVDV NS2 C376A ase	caaaatccgctagagtcatcccCGCGGTgatgggcttcccgtgg

Table 13: Primers used to generate reporter constructs for hepaciviral NS2-APIT, NS2-NS or NS2-4GS cleavage

Primer	Sequence (5‘-3‘)
NotI-JFH1 NS2 rec se	g**gcggccgc**gacggaattgcctgggccgtgacc
BsmBI-4GS-JFH1 NS2 ase	**CGTCTC**GCCGCCGCCGCCcagcagcttccagcccttgctggtgtag ccatcgg
BsmBI-4GS-eGFP se	**CGTCTC**ggcggcagcGTGAGCAAGGGCGAGGAGCTGTT CACCGGGGTGGTGC
SphI-NotI-Stop-eYFP ase	**gcatgcgcggccgc**tttacttgtacagctcgtccatgccgagagtgatcccgg
APIT-BK-AgeI se	gctccttgctcccatc**acCgGt**tatgcccagcaaacacgag
APIT-BK-AgeI ase	ctcgtgtttgctgggcata**aCcGgt**gatgggagcaaggagc
APIT-JFH1-AgeI se	gactcctcgcgcccatc**acCgGT**cctactcccaacagacgcgg
APIT-JFH1-AgeI ase	ccgcgtctgttgggagtagg**ACcGgt**gatgggcgcgaggagtc
GHV-NS2-XmaI se	**CCCGGG**agaagcgccgtgggctttgacgacctgggctac
GHV-NS2-BsaI se	**GGTCTCT**cagcatggaccatcccactggcagatcgcccac
GHV-NS3-BsaI se	**GGTCTC**gaacccattctctgtgcaccgggtgtatag
GHV-NS3-AgeI ase	**ACCGGT**cttagttgacttcccacttccagtaggagccacc

Table 14: Primers used for site-directed mutagenesis (QuikChange PCR) within hepaciviral NS2 and NS3

Primer	Sequence (5‘-3‘)
BK NS2 L90A se	ctaattgccatactcggtccgGCcatggtgctccaagctggcataac
BK NS2 L90A ase	gttatgccagcttggagcaccatgGCcggaccgagtatggcaattag
BK NS2 I97A se	catggtgctccaagctggcGCaaccagagtgccgtacttcgtg
BK NS2 I97A ase	cacgaagtacggcactctggttGCgccagcttggagcaccatg
BK NS2 V104A se	ccagagtgccgtacttcgCgcgcgctcaagggctcattc
BK NS2 V104A ase	gaatgagcccttgagcgcgcGcgaagtacggcactctgg
BK NS2 L115A se	gctcattcatgcatgcatgGCagtgcggaaggtcgctggggg
BK NS2 L115A ase	cccccagcgaccttccgcactGCcatgcatgcatgaatgagc
BK NS2 V119A se	gcatgcatgttagtgcggaaggCcgctgggggtcattatgtcc
BK NS2 V119A ase	ggacataatgacccccagcgGccttccgcactaacatgcatgc
BK NS2 L135A se	cttcatgaagctgggcgcgGCgacaggcacgtacatttacaac
BK NS2 L135A ase	gttgtaaatgtacgtgcctgtcGCcgcgcccagcttcatgaag
BK NS2 Y141A se	gctgacaggcacgtacattGCcaaccatcttaccccgctacg
BK NS2 Y141A ase	cgtagcggggtaagatggttgGCaatgtacgtgcctgtcagc
BK NS2 N142A se	gacaggcacgtacatttacGCccatcttaccccgctacggg
BK NS2 N142A ase	cccgtagcggggtaagatggGCgtaaatgtacgtgcctgtc
BK NS2 T145A se	cacgtacatttacaaccatcttGccccgctacgggattgggcc
BK NS2 T145A ase	ggcccaatcccgtagcggggCaagatggttgtaaatgtacgtg
BK NS2 P146A se	gtacatttacaaccatcttaccGcgctacgggattgggcccacg
BK NS2 P146A ase	cgtgggcccaatcccgtagcgCggtaagatggttgtaaatgtac
BK NS2 L147A se	gtacatttacaaccatcttaccccgGCacgggattgggcccacgcgg
BK NS2 L147A ase	ccgcgtgggcccaatcccgtGCcggggtaagatggttgtaaatgtac
BK NS2 V160A se	gcctacgagaccttgcggCggcagtggagcccgttgtcttc
BK NS2 V160A ase	gaagacaacgggctccactgccGccgcaaggtctcgtaggc
BK NS2 F103A se	ggcataaccagagtgccgtacGCcgtgcgcgctcaagggctc
BK NS2 F103A ase	gagcccttgagcgcgcacgGCgtacggcactctggttatgcc
BK NS2 F103D se	ggcataaccagagtgccgtacGAcgtgcgcgctcaagggctc
BK NS2 F103D ase	gagcccttgagcgcgcacgTCgtacggcactctggttatgcc
BK NS2 F103G se	ggcataaccagagtgccgtacGGcgtgcgcgctcaagggctc
BK NS2 F103G ase	gagcccttgagcgcgcacgCCgtacggcactctggttatgcc
BK NS2 F103M se	ggcataaccagagtgccgtacATGgtgcgcgctcaagggctc
BK NS2 F103M ase	gagcccttgagcgcgcacCATgtacggcactctggttatgcc
BK NS2 F103I se	ggcataaccagagtgccgtacAtcgtgcgcgctcaagggctc
BK NS2 F103I ase	gagcccttgagcgcgcacgaTgtacggcactctggttatgcc
BK NS2 F103N se	ggcataaccagagtgccgtacAAcgtgcgcgctcaagggctc

Primer	Sequence (5‘-3‘)
BK NS2 F103N ase	gagcccttgagcgcgcacgTTgtacggcactctggttatgcc
BK NS2 F103P se	ggcataaccagagtgccgtacCCcgtgcgcgctcaagggctc
BK NS2 F103P ase	gagcccttgagcgcgcacgGGgtacggcactctggttatgcc
BK NS2 F103Q se	ggcataaccagagtgccgtacCAAgtgcgcgctcaagggctc
BK NS2 F103Q ase	gagcccttgagcgcgcacTTGgtacggcactctggttatgcc
BK NS2 F103V se	ggcataaccagagtgccgtacGtcgtgcgcgctcaagggctc
BK NS2 F103V ase	gagcccttgagcgcgcacgaCgtacggcactctggttatgcc
BK NS2 F103W se	ggcataaccagagtgccgtactGGgtgcgcgctcaagggctc
BK NS2 F103W ase	gagcccttgagcgcgcacCCagtacggcactctggttatgcc
BK NS2 L144A se	ggcacgtacatttacaaccatGCtaccccgctacgggattgg
BK NS2 L144A ase	ccaatcccgtagcggggtaGCatggttgtaaatgtacgtgcc
BK NS2 L144D se	ggcacgtacatttacaaccatGAtaccccgctacgggattgg
BK NS2 L144D ase	ccaatcccgtagcggggtaTCatggttgtaaatgtacgtgcc
BK NS2 L144G se	ggcacgtacatttacaaccatGGtaccccgctacgggattgggcc
BK NS2 L144G ase	ggcccaatcccgtagcggggtaCCatggttgtaaatgtacgtgcc
BK NS2 L144M se	ggcacgtacatttacaaccatATGaccccgctacgggattgggcc
BK NS2 L144M ase	ggcccaatcccgtagcggggtCATatggttgtaaatgtacgtgcc
BK NS2 L144I se	ggcacgtacatttacaaccatATCaccccgctacgggattgggcc
BK NS2 L144I ase	ggcccaatcccgtagcggggtGATatggttgtaaatgtacgtgcc
BK NS2 L144N se	ggcacgtacatttacaaccatAACaccccgctacgggattgggcc
BK NS2 L144N ase	ggcccaatcccgtagcggggtGTTatggttgtaaatgtacgtgcc
BK NS2 L144P se	ggcacgtacatttacaaccatCCtaccccgctacgggattgggcc
BK NS2 L144P ase	ggcccaatcccgtagcggggtaGGatggttgtaaatgtacgtgcc
BK NS2 L144Q se	ggcacgtacatttacaaccatcAAaccccgctacgggattgggcc
BK NS2 L144Q ase	ggcccaatcccgtagcggggtTTgatggttgtaaatgtacgtgcc
BK NS2 L144V se	ggcacgtacatttacaaccatGttaccccgctacgggattgggcc
BK NS2 L144V ase	ggcccaatcccgtagcggggtaaCatggttgtaaatgtacgtgcc
BK NS2 L144W se	ggcacgtacatttacaaccatTGGaccccgctacgggattgggcc
BK NS2 L144W ase	ggcccaatcccgtagcggggtCCAatggttgtaaatgtacgtgcc
JFH1 NS2 F103A se	gctttgacacatgtgccgtacGCcgtcagagctcacgctctg
JFH1 NS2 F103A ase	cagagcgtgagctctgacgGCgtacggcacatgtgtcaaagc
JFH1 NS2 F103R se	gctttgacacatgtgccgtacCGcgtcagagctcacgctctg
JFH1 NS2 F103R ase	cagagcgtgagctctgacgCGgtacggcacatgtgtcaaagc
JFH1 NS2 L144I se	cacctacatctatgaccacAtcacacctatgtcggactgggc
JFH1 NS2 L144I ase	gcccagtccgacataggtgtgaTgtggtcatagatgtaggtg
JFH1 NS3 P115E se	gaacgctgatgtcatcGAggctcggagacgcggggacaag
JFH1 NS3 P115E ase	cttgtccccgcgtctccgagccTCgatgacatcagcgttc

Primer	Sequence (5‘-3‘)
JFH1 NS2rec-4GS-eYFP F103A se	ccgctctgacccacgtgccctacGCcgtgagagcccacgccctgattcg
JFH1 NS2rec-4GS-eYFP F103A ase	cgaatcagggcgtgggctctcacgGCgtagggcacgtgggtcagagcgg
JFH1 NS2rec-4GS-eYFP L144I se	cggcacctacatctacgaccacAtTactcctatgagcgattgggctg
JFH1 NS2rec-4GS-eYFP L144I ase	cagcccaatcgctcataggagtAaTgtggtcgtagatgtaggtgccg

Table 15: Sequencing primers

Primer	Sequence (5‘-3‘)
BVDV 1 se	gtatacgaggttaggcaagttc
BVDV 1000 ase	ccactatcgtagcatctggcgg
BVDV 11000 se	aagtaactagtagagatctacg
BVDV 3500 se	cttcgctgagtccctgttggtg
BVDV 4000 ase	cctgaagtagtctgtcacataac
BVDV 4000 se	tatgtgacagactacttcagg
BVDV 4500 ase	ggcaagagtatgctgatattc
BVDV 4500 se	gaatatcagcatactcttgcc
BVDV 5000 ase	gaagggtccttcaaagttaccttc
BVDV 5000 se	aaggtaactttgaaggacccttc
BVDV 5500 ase	ccgtcttgacaccatattctg
Cite 440 se	ggggacgtggttttcctttg
M13 rev	ggaaacagctatgaccat

4.1.12 Plasmids

Table 16: List of commercially available plasmids

Plasmid	Description
pGEM®-T	Linearized vector with a single 3’-terminal thymidine at both ends for ligation of PCR products generated by Taq DNA polymerase; Promega, Madison, WI, USA
pCITE-2A	Vector used for subcloning and expression vector for $T7^{pol}$-mediated gene expression; Novagen, Merck, Darmstadt, Germany

Table 17: List of used BVDV-1 full-length clones (viral cDNAs)

Plasmid	Description
pCP7-388	Infectious cDNA clone of BVDV-1 strain CP7 (Corapi et al., 1988; Meyers et al., 1996)
pCP7 2/H-F	derivative of pCP7-388 with encoded NS2 being N-terminally HA/Flag-labeled (Klemens, 2014)
pNCP7-388	Infectious cDNA clone of BVDV-1 strain NCP7 (Corapi et al., 1988; Meyers et al., 1996)
pNCP7 2/H-F	derivative of pNCP7-388 with encoded NS2 being N-terminally HA/Flag-labeled (Klemens, 2014)

Table 18: Expression constructs encoding subgenomic sequences of BVDV-1 NCP7 or CP7

Plasmid	Description
pCITE CP7 E2-4A 2/H-F	Encodes the subgenomic E2 to NS4A region of BVDV-1 strain CP7; NS2 is N-terminally HA/Flag-labeled (Klemens, 2014)
pCITE NCP7 E2-4A 2/H-F	Encodes the subgenomic E2 to NS4A region of BVDV-1 strain NCP7; NS2 is N-terminally HA/Flag-labeled (Klemens, 2014)
pCITE p7-H-F-$NS2_{(1-290)}$-SUMO C84S C236S (CS)	Encodes the subgenomic region p7 to NS2 of BVDV-1 NCP7, NS2 is N-terminally HA/Flag-labeled, NS2 cysteines C84 and C236 are mutated to serines (Fellenberg, 2017)
pCITE p7-H-F-$NS2_{(1-290)}$-SUMO G6C / D31C / F51C / Y75C / F76C / Y78C / L86C / R96C / T106C / E108C / L109C / W114C / K 134C / I137C / I140C / L173C / L191C/ Y210C	Derivatives of pCITE p7-H-F-$NS2_{(1-290)}$-SUMO CS with cysteine subtitutions in NS2 at indicated positions
pCITE p7-H-F-$NS2_{(1-290)}$-SUMO SUMO-G98C	Derivative of pCITE p7-H-F-$NS2_{(1-290)}$-SUMO CS with C-terminal glycine of SUMO mutated to cysteine
pCITE NCP7/CP7 $NS2_{(x-453)}$-$NS3_{-(1-10)}$-SUMO-HA-V5	Reporter constructs encoding N-terminally truncated BVDV-1 NCP7 or CP7 NS2 variants of various lengths ($NS2_{(x-453)}$, where the x indicates the position of the N-terminal NS2 aa), followed by the first 10 aa of NS3 (NS3(1-10), SUMO and and HA-V5 double tag
pCITE NCP7/CP7 $NS2_{(x-453)}$-$NS3_{-(1-10)}$-SUMO-HA-V5 CA	Derivatives of pCITE NCP7/CP7 $NS2_{(x-453)}$-$NS3_{-(1-10)}$-SUMO-HA-V5 with active site cysteine of NS2 mutated to alanine (CA)

Table 19: Expression constructs encoding subgenomic sequences of *Hepacivirus* species

Plasmid	Description
pCITE Flag-NS2-NS3$_{(1-172)}$-GST/BK	Encodes the subgenomic NS2 to NS3(1-172) of the HCV strain BK with a Flag epitope tag fused N-terminally to NS2 and GST fused C-terminally to the NS3 moiety (Isken et al., 2015)
pCITE Flag-NS2-NS3$_{(1-172)}$-GST/BK C184A	Derivatives of pCITE Flag-NS2-NS3$_{(1-172)}$-GST/BK with active site cysteine of NS2 mutated to alanine (CA) (Isken et al., 2015)
pCITE Flag-NS2-NS3$_{(1-172)}$-GST/BK L90A / I97A / F103A / V104A / L115A / V119A / L135A / Y141A / N142A / L144A / T145A / P146A / L147A / V160A	Derivatives of pCITE Flag-NS2-NS3$_{(1-172)}$-GST/BK with alanine subtitutions in NS2 at indicated positions
pCITE Flag-NS2-NS3$_{(1-172)}$-GST/BK NS3/YPL-AAA	Derivative of pCITE Flag-NS2-NS3$_{(1-172)}$-GST/BK with NS3 protease domain mutations Y105A, P115A and L127A (Isken et al., 2015)
pCITE Flag-NS2-NS3$_{(1-172)}$-GST/JFH1 (F103 / P115)	Encodes the subgenomic NS2 to NS3(1-172) of the HCV strain JFH1 with a Flag epitope tag fused N-terminally to NS2 and GST fused C-terminally to the NS3 moiety (Isken et al., 2015); HCV-HCV situation (NS2 F103 / NS3 P115)
pCITE Flag-NS2-NS3$_{(1-172)}$-GST/JFH1 C184	Derivative of pCITE Flag-NS2-NS3$_{(1-172)}$-GST/JFH1 F103 / P115 with active site cysteine of NS2 (C184) mutated to alanine (Isken et al., 2015)
pCITE Flag-NS2-NS3$_{(1-172)}$-GST/JFH1 F103R / P115	Derivative of pCITE Flag-NS2-NS3$_{(1-172)}$-GST/JFH1 F103 / P115 with F103 mutated to R; GHV-HCV situation (NS2 F103R / NS3 P115)
pCITE Flag-NS2-NS3$_{(1-172)}$-GST/JFH1 F103 / P115E	Derivative of pCITE Flag-NS2-NS3$_{(1-172)}$-GST/JFH1 F103 / P115 with P115 mutated to E; HCV-GHV situation (NS2 F103 / NS3 P115E)
pCITE Flag-NS2-NS3$_{(1-172)}$-GST/JFH1 F103R / P115E	Derivative of pCITE Flag-NS2-NS3$_{(1-172)}$-GST/JFH1 F103 / P115 with mutations F103R and P115E; GHV-GHV situation (NS2 F103R / NS3 P115E)
pCITE Flag-NS2-APIT-GST/BK	Derivative of pCITE Flag-NS2-NS3$_{(1-172)}$-GST/BK where NS2 is followed by the four authentic N-terminal residues of NS3
pCITE Flag-NS2-APIT-GST/BK C184A	Derivatives of pCITE Flag-NS2-APIT-GST/BK with active site cysteine of NS2 mutated to alanine (CA)
pCITE Flag-NS2- APIT-GST/BK L90A / I97A / F103A / V104A / L115A / V119A / L135A / Y141A / N142A / L144A / T145A / P146A / L147A / V160A	Derivatives of pCITE Flag-NS2-APIT-GST/BK with alanine subtitutions in NS2 at indicated positions

Plasmid	Description
pCITE Flag-NS2- APIT-GST/BK F103-A/D/G/M/I/N/P/Q/V/W	Derivatives of pCITE Flag-NS2-APIT-GST/BK with indicated permutations NS2 at position F103
pCITE Flag-NS2- APIT-GST/BK L144-A/D/G/M/I/N/P/Q/V/W	Derivatives of pCITE Flag-NS2-APIT-GST/BK with indicated permutations NS2 at position L144
pCITE Flag-NS2- APIT-GST/BK F103A/L144I	Derivative of pCITE Flag-NS2-APIT-GST/BK with combined NS2 mutations F103A and L144I
pCITE Flag-NS2-APIT-GST/JFH1	Derivative of pCITE Flag-NS2-$NS3_{(1-172)}$-GST/JFH1 where NS2 is followed by the four authentic N-terminal residues of NS3
pCITE Flag-NS2-APIT-GST/JFH1 C184A	Derivatives of pCITE Flag-NS2-APIT-GST/JFH1 with active site cysteine of NS2 mutated to alanine (CA)
pCITE Flag-NS2- APIT-GST/JFH1 F103A/L144I	Derivative of pCITE Flag-NS2-APIT-GST/JFH1 with combined NS2 mutations F103A and L144I
pCITE Flag-$NS2_{hepaci}$-4GS-GFP	Encode the NS2 of the Hepacivirus species RHV, NPHV or HCV JFH1 with a Flag epitope tag fused N-terminally to NS2 and NS2 being followed by a flexibile linker (GGGGS; 4GS) and eYFP
pCITE Flag-$NS2_{hepaci}$-4GS-GFP L144I	Derivatives of NPHV or HCV JFH1-derived pCITE Flag-$NS2_{hepaci}$-4GS-GFP with NS2 mutation L144I
pCITE Flag-$NS2_{RHV}$-4GS-GFP L144I	Derivatives of RHV-derived pCITE Flag-$NS2_{hepaci}$-4GS-GFP with NS2 mutation L132I
pCITE Flag-$NS2_{JFH1}$-4GS-eYFP	Encodes the NS2 of the HCV JFH1 with a Flag epitope tag fused N-terminally to NS2 and NS2 being followed by a flexibile linker (GGGGS; 4GS) and eYFP
pCITE Flag-$NS2_{JFH1}$-4GS-eYFP C184A	Derivative of pCITE Flag-$NS2_{JFH1}$-4GS-eYFP with active site cysteine of NS2 (C184) mutated to alanine
pCITE Flag-$NS2_{JFH1}$-4GS-eYFP F103A	Derivative of pCITE Flag-$NS2_{JFH1}$-4GS-eYFP with NS2 mutation F103A
pCITE Flag-$NS2_{JFH1}$-4GS-eYFP L144I	Derivative of pCITE Flag-$NS2_{JFH1}$-4GS-eYFP with NS2 mutation L144I
pCITE Flag-$NS2_{JFH1}$-4GS-eYFP F103A/L144I	Derivative of pCITE Flag-$NS2_{JFH1}$-4GS-eYFP with combined NS2 mutations F103A and L144I
pCITE Flag-$NS2_{JFH1}$-$NS3_{GHV(1-216)}$-GST F103 / E116	Chimeric NS2-NS3 expression construct encoding NS2 from HCV strain JFH1 and NS3(1-216) from GHV strain BWC08; a Flag epitope tag is fused N-terminally to NS2 and GST is fused C-terminally to the NS3 moiety; HCV-GHV situation (NS2 F103 / NS3 E116)
pCITE Flag-$NS2_{JFH1}$-$NS3_{GHV(1-216)}$-GST C184A	Derivative of pCITE Flag-$NS2_{JFH1}$-$NS3_{GHV(1-216)}$-GST F103 / E116 with active site cysteine of NS2 (C184) mutated to alanine

Plasmid	Description
pCITE Flag-NS2$_{JFH1}$-NS3$_{GHV(1-216)}$-GST F103R / E116	Derivative of pCITE Flag-NS2$_{JFH1}$-NS3$_{GHV(1-216)}$-GST F103 / E116 with F103 mutated to R; GHV-GHV situation (NS2 F103R / NS3 E116)
pCITE Flag-NS2$_{JFH1}$-NS3$_{GHV(1-216)}$-GST F103 / E116P	Derivative of pCITE Flag-NS2$_{JFH1}$-NS3$_{GHV(1-216)}$-GST F103 / E116 with E116 mutated to P; HCV-HCV situation (NS2 F103 / NS3 E116P)
pCITE Flag-NS2$_{JFH1}$-NS3$_{GHV(1-216)}$-GST F103R / E116P	Derivative of pCITE Flag-NS2$_{JFH1}$-NS3$_{GHV(1-216)}$-GST F103 / E116 with mutations F103R and E116P; GHV-HCV situation (NS2 F103R / NS3 E116P)

Table 20: List of used HCV JFH1-derived replicons

Plasmid	Description
pFKI-389 FLuc NS2-3'/JFH1	bicistronic HCV JFH1-derived reporter gene replicon encoding Firefly luciferase in the first and NS3-5B in the second ORF (Isken et al., 2015)
pFKI-389 FLuc NS2-3'/JFH1 C184A	Derivative of pFKI-389 FLuc NS2-3'/JFH1 with active site cysteine of NS2 (C184) mutated to alanine
pFKI-389 FLuc NS2-3'/JFH1 F103A	Derivative of pFKI-389 FLuc NS2-3'/JFH1 with NS2 mutation F103A
pFKI-389 FLuc NS2-3'/JFH1 L144I	Derivative of pFKI-389 FLuc NS2-3'/JFH1 with NS2 mutation L144I
pFKI-389 FLuc NS2-3'/JFH1 F103A/L114I	Derivative of pFKI-389 FLuc NS2-3'/JFH1 with combined NS2 mutations F103A and L144I

4.2 Methods

4.2.1 Working with nucleic acids

4.2.1.1 Mini preparation of plasmid DNA

The isolation plasmid DNA from a 2 ml overnight bacterial culture was performed by alkaline lysis. The bacterial suspension was transferred to a 2 ml reaction tube and centrifuged at 15,700 g for 1 min. The supernatant was discarded and the pellet was resuspended in 100 µl of ice-cold buffer P1. For the lysis 200 µl of buffer P2 was added and the suspension was mixed by inverting twice. After incubation for 5 min at RT, 150 µl of buffer P3 was added and the suspension was inverted twice. After incubation for 5 min on ice, centrifugation was performed for 10 min at 15,700 g and 4 °C. The clear supernatant was transferred to a new 1.5 ml reaction tube containing 400 µl of 100% isopropanol. The DNA-isopropanol mixture was mixed by inversion and then centrifuged at 15,700 g and 4 °C for 30 min. The supernatant was discarded and the pellet was washed with 200 µl of 70% (v/v) ethanol followed by centrifugation at 15,700 g and 4 °C for 5 min. The ethanol was thoroughly removed and the pellet was left to dry at 37 °C. Finally, the plasmid DNA was resuspended in 30 – 50 µl of ddH_2O.

4.2.1.2 Midi preparation of plasmid DNA

To isolate plasmid DNA bacterial cultures up to 200 ml, the Nucleobond® PC100 kit (Macherey-Nagel, Düren, Germany) was used. An overnight bacterial culture was centrifuged in 50 ml tubes at 3.836 g and 4 °C for 10 min. The supernatant was discarded and the pellet was resuspended in 4 ml of ice-cold buffer S1. For the lysis 4 ml of buffer S2 was added and the suspension was mixed by inverting six times. After incubation for 5 min at RT, 4 ml of ice-cold buffer S3 was added and the suspension was inverted six times. After incubation for 5 min on ice, the crude lysate was passed through a filter onto the AX100 column, which was beforehand equilibrated with 2.5 ml of N2 buffer. After complete passage of the lysate, the column was washed once with 10 ml of N3 buffer. Subsequently, the plasmid DNA was eluted with 3 ml of N5 buffer into a 15 ml centrifuge tube already containing 2.1 ml of 100% isopropanol. The eluate was divided among three 2 ml reaction tubes and centrifuged for 20 min at 15,700 g and 4 °C. The clear supernatant was discarded, and the pellets were washed with a total of 600 µl of 70% (v/v) ethanol and combined onto one reaction tube at this step. After centrifugation at 15,700 g and 4 °C for 5 min, the ethanol was thoroughly removed and the DNA pellet was let to dry at 37 °C. The DNA was resuspended in 100 µl ddH_2O at 4 °C and DNA concentration was determined by measuring

absorbance at 260 nm on the Nanodrop spectrophotometer (Thermo Fisher Scientific, Schwerte, Germany).

4.2.1.3 DNA restriction (analytical, preparative and linearization)

DNA restrictions were used to verify exisiting plasmid DNA (analytical), to generate new DNA constructs (preparative) or to linearize plasmid DNA in preparation for *in vitro* transcription. All restriction enzymes were obtained from New England Biolabs® Inc. (NEB, Frankfurt am Main, Germany). For analytical or preparative purpose, depending on DNA amount, enzyme activity and purpose of the generated DNA fragments, DNA restrictions were performed using 0.5 – 3 µg plasmid DNA, 10% (v/v) corresponding NEB buffer (10x) and 0.3 - 2 µl per restriction enzyme in 20 – 30 µl total volume. The restriction digest was incubated for 1 up to 2 hours depending on DNA amount and at enzyme-specfic temperature. For linearization 6 – 10 µg plasmid DNA was incubated with 10% (v/v) NEB Cutsmart buffer (10x) and 3 µl SmaI in a total volume of 200 µl at 25 °C for 3 h. DNA linearizations were further processed by phenol/chloroform extraction. All restrictions were analyzed by agarose gel electrophoresis.

4.2.1.4 Polymerase chain reaction (PCR)

To amplify specific DNA fragments, the polymerase chain reaction (PCR) was used. For this purpose, appropriate sense/antisense primer pairs were first designed using the Serial Cloner program and ordered from Sigma-Aldrich (Taufkirchen, Germany). The lyophilized primers were resuspended in ddH_2O to produce 100 µM stock solutions. From these, 1:10 diluted working solutions were prepared. A PCR reaction contained 40 µl ddH_2O, 5 µl 10x Taq DNA polymerase buffer, 1 µl dNTP mix (dATP, dCTP, dGTP, dTTP; 10 mM each; Invitrogen, Darmstadt, Germany), 1 µl 10 µM sense primer, 1 µl 10 µM antisense primer, 1 µl 50 ng/µl template DNA and 1 µl Taq DNA polymerase. After initial denaturation for 2 min at 94 °C, 20 - 30 cycles were run as follows: 45 sec denaturation at 94 °C, 45 sec annealing at 50 - 55 °C (depending on the primers) and 1 min/kb elongation at 72 °C. After a final elongation step for 2 min/kb at 72 °C, the PCR products were kept at 10 °C until they were further analyzed by agarose gel electrophoresis and subsequently purified from the gel.

4.2.1.5 Site-directed mutagenesis (QuikChange® PCR)

Site-directed mutagenesis by QuikChange® PCR (Strategene, Heidelberg, Germany) was used to introduce point mutations or shorter DNA sequences in gene segments on plasmids. First, sense/antisense primer pairs carrying flanking sections (≥ 19 nt) of the template around the mutated positions were designed using the Serial Cloner program and ordered from Sigma-Aldrich (Taufkirchen, Germany). The lyophilized primers were resuspended in ddH_2O to produce 100 µM stock solutions. From these, 1:6.25 diluted working solutions were

prepared. A QuikChange® PCR reaction contained of 39.5 µl ddH_2O, 5 µl 10x Pfu DNA polymerase buffer, 1 µl dNTP mix (dATP, dCTP, dGTP, dTTP; 10 mM each; Invitrogen, Darmstadt, Germany), 1.25 µl 16 µM sense primer, 1.25 µl 16 µM antisense primer, 1 µl 50 ng/µl template DNA, and 1 µl Pfu DNA polymerase. As a negative control, a reaction per template containing ddH_2O instead of the primers was used. After initial denaturation for 2 min at 94 °C, 20 cycles were run as follows: 45 sec denaturation at 94 °C, 45 sec annealing at 50 - 55 °C (depending on the primers) and 2 min/kb elongation at 72 °C. After a final elongation step for 2 min/kb at 72 °C, the PCR products were kept at 10 °C until further processing.

6 µl of the PCR reaction were taken and stored at 4 °C (-*Dpn*I sample). To destroy the template DNA, 5 µl 10x NEB Cutsmart buffer and 1 µl *Dpn*I were added to the remaining 44 µl of the PCR product. The restriction was incubated for 2 h at 37 °C. From the restriction mixture, 6 µl were taken (+*Dpn*I sample) and analyzed together with the -*Dpn*I sample by agarose gel electrophoresis. Subsequently, 2 - 5 µl of the restriction were transformed into competent *E. coli* HB101.

4.2.1.6 Agarose gel electrophoresis and DNA extraction

For the analysis or separation of DNA fragments of a restriction digest, 0.8% agarose gels were used. For this, 0.8% (w/v) agarose was dissolved in 1x Tris-acetate-EDTA (TAE) buffer by boiling. The solution cooled to 56 °C was poured into a gel slide and a comb was inserted. For subsequent detection of DNA, 0.5 - 1.5 µl of Midori Green Xtra was added to the still liquid gel. Samples from a restriction digest were mixed with one part 6x DNA sample buffer and separated on the agarose gel together with a DNA size standard (GeneRuler 1kb Plus DNA Ladder). Separation of the DNA fragments was performed at 120 V for 20 – 30 min.

In case of analytical restriction digestion, 12 µl per sample were separated and the gel was subsequently evaluated on a blue/green LED transilluminator and documented with a camera. Samples of a preparative restriction digest were applied completely to the gel and the desired fragment was excised with a scalpel while the gel was placed on a blue/green LED transilluminator. The DNA fragment was then isolated from the gel by centrifugation at 5,000 g for 3 min in a gel extraction column (Montage Gel Extraction Kit).

4.2.1.7 DNA ligation

DNA ligation reactions were performed in a total volume of 20 µl, generally containing 2 µl of vector DNA, 15 µl of insert DNA, 2 µl of 10x T4 DNA ligase buffer and 1 µl of T4 DNA ligase were added to the batch. In parallel, a control preparation was made for each vector DNA

using ddH_2O instead of insert DNA. The ligation reactions were incubated for 2 h at 16 °C and the ligation products were transformed into competent *E. coli* HB101.

4.2.1.8 pGEM®-T-vector cloning

Promega's pGEM®-T vectors are linearized vectors with a 3'-thymidine overhang at both ends that allow efficient ligation of PCR fragments generated with a *Taq* DNA polymerase. Ligation reactions contained 5 µl of 2x Rapid Ligation buffer, 3 µl of purified PCR fragment, 1 µl of 50 ng/µl pGEM®-T vector, and 1 µl of Promega T4 DNA ligase. The mixture was incubated for 1 h at 16 °C and completely transformed into competent *E. coli* DH5α. For blue/white selection, 20 µl of 40 mg/ml X-Gal was added to the transformation mixture.

4.2.1.9 Transformation of E. coli

For transformation of plasmid DNA from mini preparations, midi preparation or QuikChange® PCR products, 20 µl of competent *E. coli* HB101 were used. DNA ligations or pGEM®-T vector clonings were transformed into 50 µl of competent *E. coli* HB101 or DH5α, respectively. Appropriate aliquots of the competent bacteria were slowly thawed on ice. The appropriate amount of bacteria was then added to the DNA to be transformed (50 – 100 ng of mini/midi preparation, 2 µl of the *Dpn*I restriction of QuikChange® PCRs, or complete amounts of DNA ligations or pGEM®-T vector clonings) and incubated on ice for 20 min. A heat shock at 42 °C was carried out for 2 min, followed by cooling the bacteria-DNA mixture on ice for 2 min. 200 µl of cold LB medium without antibiotics was added to the bacteria, followed by incubation 30 – 60 min at 37 °C and 550 rpm. In the case of transformations into *E. coli* DH5α, 20 µl of 40 mg/ml X-Gal was added to enable blue/white selection. Transformations of QuikChange® PCRs, DNA ligations, and pGEM®-T vector clonings were completely plated on prewarmed LB agar plates containing appropriate antibiotic (usually 100 µg/ml ampicillin). For transformations of mini or midi preparations, 50 µl of the transformation mixtures were plated. Agar plates were incubated at 37 °C overnight.

4.2.1.10 DNA sequencing

Sanger sequencing of plasmid DNA was performed by LGC Genomics (Berlin, Germany). Sequencing samples contained at least 1 µg of plasmid DNA and 4 µl of 10 mM sequencing primer in a total volume of 14 µl. The obtained sequencing reads were analyzed using the program Serial Cloner.

4.2.1.11 Phenol/chloroform extraction

Since the DNA was to be used in RNA works, filtered tips and RNA grade reagents were used for the following steps. For purification of linearized plasmid DNA an equal volume of phenol-chloroform-isoamylalcohol (25:24:1) was added to the restriction reaction. The sample was mixed thoroughly for 30 sec and centrifuged for 3 min at 15,700 g. The aqueous phase was transferred to a new reaction tube, which already contained one volume of chloroform. After thoroughly mixing for 30 sec, another centrifugation step was performed at 15,700 g for 5 min. Again, the aqueous phase was transferred to another new reaction tube, which already contained 0.1 M sodium acetate (pH 5.2) in three volumes of 100% ethanol. The DNA was precipitated by incubation at -80 °C for at least 1 h or overnight. The samples were then centrifuged at 15,700 g and 4 °C for 30 min. The supernatant was discarded and the pellet was washed with 500 µl of 70% (v/v) ethanol. After centrifugation at 15,700 g and 4 °C for 5 min, the supernatant was discarded. The DNA pellet was let to dry for 10 min at 37 °C and was resuspended in 55 µl RNase-free ddH_2O. From this, 2 µl were taken and analyzed by agarose gel electrophoresis.

4.2.1.12 In vitro trancription

In vitro transcriptions were performed using the MAXIscript™ SP6 or T7 kit (Ambion, Austin, TX, USA). For transcription, 2 µg of linearized, phenol/chloroform-extracted template DNA were used in a 20 µl reaction with 2 µl of 10x transcription buffer, 4 µl rNTP mix (2.5 µM each), and 1 µl of SP6 or T7 RNA polymerase enzyme mix. The amounts in the reaction were doubled if larger amounts of RNA were needed (e.g. positive or negative controls).The mixture was incubated for 2 h at 37 °C. Then, the template DNA was destroyed by adding 1 µl DNaseI (Turbo DNase) and incubation for another 20 min at 37 °C. To verify the quality of the transcription and estimate the amount of RNA, 2 µl of the transcription reaction were analyzed after addition of 6 µl RNase-free ddH_2O and 2 µl formamide sample buffer by agarose gel electrophoresis. The transcripts were stored at -80 °C until further use.

4.2.2 Working with proteins

4.2.2.1 SDS-PAGE

Proteins were separated according to their molecular weight by SDS-PAGE on 8 and 10% polyacrylamide gels according to Schägger and von Jagow (Schägger and von Jagow, 1987) or Laemmli (Laemmli, 1970), depending on the application. The gel run was performed in Mini-PROTEAN® Tetra Cell electrophoresis chambers (BioRad, Munich, Germany). Unless otherwise indicated, cells cultured in 6-well cell culture plates (Ø 3.5 cm) were lysed and

denatured in 80 – 160 µl SDS sample buffer containing 5% β-mercaptoethanol, depending on the cell pellet size, and incubated for 10 min at 95 °C. Polyacrylamide gels were then loaded with 20 µl of each sample. As a size standard, 5 µl of PageRuler™ Prestained Protein Ladder (Thermo Scientific, Schwerte, Germany) was applied. For the gels according to Schägger and von Jagow, the gels were first run at 80 V for 10 min and then at 120 V for 90 – 180 min. In case of gels according to Laemmli, gels were run at 200 V for 45 – 90 min.

4.2.2.2 Western blot

Proteins separated by SDS-PAGE were transferred to nitrocellulose membranes (Pall, Pensacola, FL, USA) by tank blotting. Transfer was performed in Mini-PROTEAN® Tetra Cell electrophoresis chambers with Mini Trans-Blot® module (BioRad, Munich, Germany) for 1 h at 100 V. The success of the transfer was checked by staining the membrane with Ponceau S solution. Subsequently, the membrane was rinsed with ddH_2O and the Ponceau S staining was removed by washing with PBS/0.05% Tween 20 (PBS-T). After blocking of nonspecific antibody binding sites with a blocking solution of 5% skim milk powder in PBS-T for 1 h at RT or overnight at 4 °C, the membrane was incubated with appropriate primary antibodies diluted in blocking solution for 1 h at RT. In the present work, the following primary antibodies were used at the indicated dilutions: anti-Flag M2 (1:1000), anti-GST (1:2,500), anti-HA.11 (16B12) (1:1,000); anti-HA (C29F4) (1:1,000), anti-HCV NS3 (JFH1: 4D11 or Con1: 2E3) (1:1000), anti-BVDV NS3/NS2-3 (mAk 8.12.7) (1:10).

After incubation, the membrane was washed three times with PBS-T for 10 min each. This was followed by incubation with secondary antibody diluted in blocking solution for 1 h at RT. Depending on the species of the primary antibody and application, the appropriate secondary antibody was used. In general, horseradish peroxidase-conjugated secondary antibodies (anti-mouse-PO or anti-Rabbit-PO) were used at a 1:4,000 dilution (both from goat; Dianova, Hamburg, Germany), and detection was performed on the LAS-4000 mini (Fujifilm, Düsseldorf, Germany) using WesternLightning® Chemiluminescence Reagent Plus (PerkinElmer, Boston, MA, USA). For quantitative analyses using the Odyssey infrared imaging system (LI-COR©), the IRDye® 800CW donkey anti-Mouse secondary antibody was used at a dilution of 1:10,000. Incubation with the secondary antibody was generally followed by three washes with PBS-T prior to detection. Quantification of signals on western blot membranes that were incubated with a peroxidase-coupled secondary antibody (quantification of HCV NS2 cleavage efficiency) was carried out using ImageJ 1.47t.

4.2.2.3 Substituted Cysteine Accessibility Method (SCAM)

For the SCAM assay, Huh7-T7 cells cultured in 6-well cell culture plates (Ø 3.5 cm) were transfected with 4 µg of plasmid DNA encoding hemagglutinin (HA)-labeled BVDV NS2 cysteine derivatives under the control of the T7 promoter. After 8 h, cells were harvested into the culture medium using a cell scraper and transferred to a 1.5 ml reaction tube. The cells were centrifuged at 400 g for 4 min, the supernatant was discarded, and the pellet was washed with 1 ml PBS. After another centrifugation for 4 min at 400 g, the supernatant was discarded and the pellet resuspended in 40 µl of cold HCN buffer. For selective membrane permeabilization or full solubilization of cellular membranes, the cell suspension was incubated with either 10 µg/ml digitonin or 1% Triton X-100 for 10 min at 4 °C. Polyethylene glycol (5000)-maleimide (PEG-Mal, 5 kDa) was then added at a final concentration of 2 mM and the mixture was incubated for an additional 10 min at 4 °C. To stop the reaction, dithiothreitol (DTT) was added at a final concentration of 50 mM and the samples were incubated for 10 min at 4 °C. Proteins were precipitated using the methanol-chloroform procedure described previously (Wessel and Flügge, 1984). Briefly, 4 volumes of methanol were added, the sample was mixed vigorously and centrifuged at 9000 g for 10 s. Then 1 volume of chloroform was added and the sample was again vigorously mixed and centrifuged for 10 s at 9000 g. After addition of 3 volumes of ddH_2O, the sample was mixed thoroughly for at least 30 s and centrifuged at 9000 g for 1 min. The upper phase was discarded carefully without disturbing the interphase. Finally, 3 volumes of methanol were added, the sample was mixed, and then centrifuged at 9000 g for 2 min. The supernatant was completely removed and the protein pellet was dried at room temperature for a maximum of 30 min. The proteins were dissolved in 120 µl of SDS sample buffer and separated on 10% polyacrylamide gels according to Lammli and detected with anti-HA (C29F4) (1:1,000) after transfer to a nitrocellulose membrane. The α-rabbit-PO (1:4,000) was used as a secondary antibody.

4.2.2.4 Construction of a NS2-NS3 precursor model

To construct the NS2-NS3 model, the software SybylX 1.2, the information from the NS2 protease domain crystal structure (residues 94–217, PDB ID 2HD0, Lorenz et al., 2006) and the crystal structure of the NS3 protease domain complexed with a synthetic NS4A cofactor peptide (PDB ID 1A1R, Kim et al., 1996) representing protein sequences from HCV genotype 1a (isolate H77) were used. The model was constructed as follows: the number of molecules in the asymmetric unit was reduced to the smallest functional unit. Subsequently, hydrogen atoms were added by software and the B-factors were replaced by charges according to the Gasteiger-Huckel model. Refinement was achieved by undertaking independent energetic minimizations of both proteins (Powell, 1977).

The following constraints were integrated into the model: The activating NS3 hydrophobic region is formed by the amino acids I3, T105, P115 and I127 (Isken et al., 2015). The NS2 and the NS3 proteins are covalently linked with a minimal interaction radius between both proteins. The NS2-NS3 cleavage site should be less than 4 Å away from the active site sulfur atom of Cys184. The structures of NS2 and NS3 are assumed to be identical to the determined post-cleavage crystal structure, e.g. the NS2 is present as an active dimer, the NS3 protein as an active monomer.

The NS2-NS3 model was constructed in several stages: (i) analysis of the NS2 hydrophobic regions near the C-terminus and placement of the activating hydrophobic region of the NS3 protein into proximity of the identified NS2 regions, (ii) change of the binding angles of the NS2 C-terminus and the NS3 N-terminus to optimize the distance between both atoms to establish the covalent bond of the NS2-NS3 precursor protein and (iii) energetic minimization of the NS2-NS3 precursor protein.

4.2.2.5 Bioinformatics applications for analysis of membrane topology, secondary protein structures and for sequence alignments

For the prediction of membrane topology models several methods were used, including CCTOP (http://cctop.enzim.ttk.mta.hu/), HMMTOP (http://www.enzim.hu/hmmtop/), MEMSAT2 (http://www.sacs.ucsf.edu/cgi-bin/memsat.py), MEMSAT3 (http://bioinf.cs.ucl.ac.uk/psipred/), MEMSAT SVM (http://bioinf.cs.ucl.ac.uk/psipred/), OCTOPUS (http://octopus.cbr.su.se/), TMHMM (http://www.cbs.dtu.dk/services/TMHMM-2.0/), TMPRED (https://embnet.vital-it.ch/software/TMPRED_form.html) and Phobius (http://phobius.sbc.su.se/), the latter one allowing the usage of constraints determined by experimental results. Membrane topology models were visualized using TOPO2 (http://www.sacs.ucsf.edu/cgi-bin/open-topo2.py). To predict secondary protein structures the program PSIPRED was used (http://bioinf.cs.ucl.ac.uk/psipred/). Putative helical protein elements were analyzed concerning their hydrophobicity and hydrophobic moments using HeliQuest (https://heliquest.ipmc.cnrs.fr/). For multiple protein sequence and structure alignments PROMALS3D was used (http://prodata.swmed.edu/promals3d/promals3d.php).

4.2.3 Working with cells

4.2.3.1 General cell culture

All cell culture work was performed in laminar flow cabinets (MSC-Advantage, Thermo Scientific; BSC-EN, Zapf). The cell lines used were cultured in Ø10 cm cell culture dishes at 37 °C, 5% CO_2 and 95% humidity. Depending on the experiment, cells were beforehand seeded into the appropriate 6-, 12-, 24-, 48-, or 96-well format.

Huh7 Lunet and Huh7-T7 cells were cultured in Dulbecco's Modified Eagles Medium (DMEM; Gibco, Thermo Fisher Scientific, Darmstadt, Germany) with addition of 10% (v/v) fetal calf serum (FCS, Thermo Fisher Scientific GmbH, Schwerte, Germany), 100 U/ml penicillin and 100 µg/ml streptomycin. Huh7-T7 cells were maintained in the prescence of 125 µg/ml G418 (Gibco, Thermo Fisher Scientific, Darmstadt, Germany).

SK6 cells (American Type Culture Collection (ATCC), Rockville, MD, USA) were cultured in Minimal Essential Medium (MEM; Gibco, Thermo Fisher Scientific, Darmstadt, Germany) with the addition of 10% (v/v) FCS (Thermo Fisher Scientific GmbH, Schwerte, Germany), 100 U/ml penicillin, and 100 µg/ml streptomycin. To study NS2-3 cleavage of BVDV NS2 derivatives the recently described SK6 cell lines DNAJC14-KO (referred to as SK6 KO in this study) and DNAJC14-KO GST-Jiv90(WT) (referred to as SK6 KO GST-Jiv90 in this study) were used (Isken et al., 2019). CRISPR-Cas9-mediated knockout of DNAJC14 expression renders SK6 KO cells deficient for the NS2 protease-activating cofactor DNAJC14/Jiv. In SK6 KO GST-Jiv90 cells, the ability to activate NS2 protease was functionally rescued by overexpression of the minimal cofactor domain Jiv90. For culturing SK6 KO cells, 5 µg/ml puromycin (Thermo Fisher Scientific GmbH, Schwerte, Germany) was added to the medium and for SK6 GST-Jiv90 cells, 5 µg/ml puromycin and 125 µg/ml G418 (Thermo Fisher Scientific GmbH, Schwerte, Germany) were added to the medium.

MDBK cells (American Type Culture Collection (ATCC), Rockville, MD, USA) were cultured in DMEM (Gibco, Thermo Fisher Scientific, Darmstadt, Germany) with the addition of 10% (v/v) horse serum (HS) (Thermo Fisher Scientific GmbH, Schwerte, Germany), 100 U/ml penicillin and 100 µg/ml streptomycin.

The term "full medium" refers to the respective culture medium in which all additives (see above) were contained.

4.2.3.2 MVA-T7^{pol} infection and DNA transfection

Replication-indpendent expression of viral genes was carried out T7 RNA polymerase (T7^{pol})-mediated in Huh7-T7 cells or SK6 cell lines (also referred to as vaccinia experiment). For this

purpose, the respective cells were first infected with the recombinant Modified Vaccinia Virus Ankara (MVA) encoding T7^{pol} (MVA-T7^{pol}) (Sutter et al., 1995). This step was followed by transfection of plasmid DNA, with transcription under the control of the T7 promoter.

As preparation, 1/12 - 1/15, depending on the required cell density, of a confluent-grown Ø10 cm cell culture dish was seeded per well of a 6-well cell culture plate on the day before the experiment. Prior to infection with MVA-T7^{pol}, cells were washed once with 1 ml PBS. Infection was performed with 5 µl of MVA-T7^{pol} viral stock solution in 1 ml of infection medium (cell culture medium without additives) per well for 1 h at 37 °C. Subsequently, the supernatant was discarded and replaced by 1 ml of the respective complete medium.

Transfection of 4-8 µg plasmid DNA per well was performed either with Metafectene® Transfection Reagent (Biontex, Munich, Germany) (SK6 cell lines) or polyethylenimine (PEI MAX 40,000, Polysciences, Hirschberg, an der Bergstraße, Germany) (Huh7-T7), depending on the cell line. For transfection with Metafectene®, plasmid DNA was added to 70 µl medium without additives. In a separate reaction tube, 10 µl Metafectene® was added to 70 µl medium without additives. For transfection with PEI, plasmid DNA was added to 100 µl medium without additives. In a separate reaction tube, 3 µl of PEI stock solution (1 mg/ml) per µg of DNA was added to 100 µl of medium without additives.

The transfection reagent solution and the DNA solution were mixed together. After incubation for 10 min at RT, the transfection mixture was applied dropwise into the respective well and the cells were incubated at 37 °C for 8-24 h, depending on the experiment.

4.2.3.3 Electroporation of MDBK and SK6 cells

Electroporation of *in vitro* transcribed RNAs into MDBK and SK6 cells was carried out as described previously (Tautz et al., 1999).

On the day before the experiment, a confluent 10 cm dish of MDBK or SK6 cells was transferred to new 10 cm dishes at a ratio of 1:2. In preparation for electroporation, the cells were first washed with PBS, detached from the cell culture dish using trypsin/EDTA, taken up in 10 ml of complete medium, and transferred to a 50 ml tube. Cells were then centrifuged for 2 min at 300 g and RT and washed twice with 50 ml PBS. Cells from a 10 cm dish were taken up in 1.2 ml of AccuGENE-PBS.

For electroporation, 400 µl of the cell suspension was transferred to a fresh 1.5 ml Eppendorf reaction tube. Subsequently, 1 µg of *in vitro* transcribed RNA was added to the cell suspension, mixed gently, and the suspension was transferred to an electroporation cuvette with 2 mm gap. Electroporation was performed using the BioRad GenePulser II Xcell at the following conditions: 180 V and 950 µF. Subsequently, the cells were first rinsed with 800 µl

of medium from the cuvette, transferred to a 15 ml tube containing an appropriate amount of medium and then seeded into 6-well-plates containing 2 ml of complete medium per well. Cells electroporated without RNA served as negative control (Mock). Depending on the experimental approach, different proportions of the electroporated cells were seeded in the wells of a 6-well plate.

For luciferase measurements, cells of one electroporation were seeded as follows: 300 µl for 2 and 24 h, 200 µl for 48 and 72 h. For qualitative studies on RNA replication of full-length genomes post electroporation (pe), electroporated cells were seeded evenly in four wells of a 6-well plate. Depending on the experiment, cell culture supernatant was used for infection experiments or for determination of the virus titer before fixing the cells.

4.2.3.4 Electroporation of Huh7-Lunet cells

Electroporation of *in vitro* transcribed RNAs into Huh7-Lunet cells was carried out as described for Huh7.5 cells (Jirasko et al., 2008).

A confluent 10 cm dish of Huh7-Lunet cells was split 1:2 one day prior to the experiment. In preparation for electroporation, the cells were harvested and washed as described above (see 4.2.3.3). Cells from one 10 cm dish were resuspended in 1.2 ml of Cytomix.

For electroporation, 400 µl of the cell suspension was transferred to a fresh 1.5 ml Eppendorf reaction tube. Subsequently, 1.5 µg of *in vitro* transcribed RNA was added to the cell suspension, mixed gently, and the suspension was transferred into an 4 mm gap electroporation cuvette. Electroporation was performed using the BioRad GenePulser II Xcell at the following conditions: 270 V and 975 µF. Subsequently, the cells were rinsed with 600 µl of complete medium from the cuvette and then seeded into 6-well-plates containing 2 ml of complete medium per well. Cells electroporated without RNA served as negative control (Mock). For luciferase measurements, cells of one electroporation were seeded as follows: 300 µl for 4 and 24 h, 150 µl for 48 and 72 h.

4.2.3.5 Luciferase assay

Cells electroporated with *Firefly* or *Renilla* luciferase encoding replicon or full-length genome RNA were harvested 2, 24, 48, 72 h pe, washed once with 1 ml of PBS per well and then scraped into 1 ml of PBS. The suspensions were transerred into 1.5 ml reaction tubes, centrifuged for 2 min at 15,700 g and the supernatant was removed. Afterwards, cell pellets were frozen at -80 °C for at least 1 h.

To quantify luciferase activity in cell lysates the p.j.k Luciferase Assay system was used. The pelleted cells of one sample were lysed in 40 µl 1x lysis buffer on the shaker for 20 min at 1200 rpm and RT. For measurement, 20 µl of the lysate was added to either 100 µl *Renilla*-

GLOW-Juice containing 2 µl coelenterazine (*Renilla* luciferase) or 100 µl Beetle-Juice containing D-luciferin and ATP (*Firefly* luciferase) in a 5 ml round-bottomed tube, depending on the luciferase used. Luciferase activity was determined immediately afterwards on the Junior LB9509 luminometer (Berthold, Bad Wildbad, Germany).

4.2.3.6 Infection of MDBK cells

The detection of infectious viruses in cell culture supernatants was performed by reinfection of naïve MDBK cells.

For reinfection for qualitative detection of viruses in cell culture supernatants, 1/30 of a confluent 10 cm dish with MDBK cells was seeded onto a well of a 6-well plate in 2 ml medium. After 2-4 h, 300-500 µl of medium was removed, depending on the amount of assay time points required, and replaced with the same amount of cell culture supernatant to be assayed. Subsequently, the cells were incubated at 37 °C for 72 h unless otherwise indicated. This was followed by the detection of infected cells by anti-NS3 immunofluorescence analysis and virus titer determination, if necessary.

For infection with defined multiplicity of infection (MOI), 4 x 10^5 MDBK cells were seeded into a well of a 6-well plate in 2 ml medium. After 2-4 h, the supernatant was replaced with 2 ml of fresh medium. Cells were then infected with cell culture supernatant with an MOI 0.1 in 2 ml total volume. At 1 h after infection, the infectious supernatant was discarded, the cells were washed 3 times with 1 ml of PBS, and 2 ml of medium was added to the cells. Then, the cells were incubated at 37 °C for 12, 24, 48, and 72 h unless otherwise indicated. The cell culture supernatant was then removed, filtered through a 0.22 µm sterile filter (Minisart, Sartorius, Göttingen, Germany), and stored at -80 °C. To analyze for success of reinfection, virus titer was determined or, alternatively, luciferase activity was determined for virus genomes encoding a *Renilla* luciferase. In addition, infected cells were detected by anti-NS3 immunofluorescence analysis, if necessary.

4.2.3.7 Determination of virus titers in cell culture supernatant (titration)

Determination of viral titer of cell culture supernatants from electroporation or infection experiments was performed using an endpoint dilution. 100 µl of medium was pipetted into the wells of a 96-well plate. Depending on the expected viral titer the supernatant to be titrated was used directly or a dilution of 1:10 or 1:100 of the supernatant was generated. 50 µl of the supernatant or dilution was added to the first well of a row of the 96-well microtiter plate. By default, a 4-fold determination was performed per supernatant or dilution. Using an 8-well multichannel pipette, serial dilutions were made from row to row in 50 µl steps (1:3 each). Subsequently, MDBK cells from a confluent 10 cm dish were harvested and

taken up in a total of 12 ml medium. 2 ml of this suspension was mixed with 8 ml of medium. Then, 100 µl of this cell suspension was added per well of the 96-well microtiter plate in which the cell culture supernatant had been serially diluted. Subsequently, the cells were incubated for 72 h at 37 °C. This was followed by immunofluorescence analysis using anti-NS3 antibody and determination of infected wells using the microscope.

Titer calculations in endpoint dilution procedures are always performed using statistical estimation procedures. In the present work, the formula according to Spaermann and Kärber was used to calculate virus titers as tissue culture infectieous dose 50 per ml ($TCID_{50}$/ml) (Kärber, 1931).

$$m = x_i \frac{d}{2} - d \sum R_i$$

m negative decadic logarithm of the titer in relation to the test volume, i.e. the titer of the test volume results from 10^{-m}. Since 50 µl was used as the test volume, this value must be multiplied by 20 to obtain the number of infectious viruses per ml ($TCID_{50}$/ml)

x_i logarithm of the smallest dilution that leads to the infection of all four replicates of a dilution level (e.g., in level 6, xi = lg (1/72,900) = -4.86)

d logarithm of the dilution factor

ΣR_i Sum of reaction rates; this sum includes all positive reactions starting from the highest dilution level in which all replicates are positive and divides by the number of replicates (i.e., if 3 out of 4 replicates still react positively in the next dilution level: $\Sigma R_i = 1 + ¾ = 1{,}75$)

4.2.3.8 Indirect immunofluorescence analysis

Detection of BVDV-positive cells at the indicated time points as well as localization of H-F-NS2 derivatives was performed by indirect immunofluorescence analysis (IF). For this, cells were washed with PBS and fixed with 2% (w/v) paraformaldehyde (Thermo Fisher Scientific GmbH, Schwerte, Germany) in PBS for 20 min at 4 °C. Cell permeabilization was achieved by incubation with 0.5% (w/v) N-octyl-β-D-glycopyranoside (Sigma-Aldrich, Taufkirchen, Germany) in PBS for 10 min at 4 °C. Cells were washed with PBS and incubated for 30 min at 37 °C with blocking solution containing 2% (w/v) bovine serum albumin (BSA, Carl Roth, Karlsruhe, Germany) in PBS with 0.05% (v/v) Tween 20 (Thermo Fisher Scientific, Schwerte, Germany) (PBS-T).

For detection of BVDV-positive cells, NS3/NS2-3 was detected using mAb 8.12.7 in a dilution of 1:40 in blocking solution. After 1 h, cells were washed with blocking solution and incubated

with mouse-specific Cy3-labeled secondary antibody in a dilution of 1:2.000 in blocking solution for 1 h.

For H-F-NS2-specific localization studies, the HA-specific mAb C29F4 was used in a dilution of 1:1000 in blocking solution. After 1 h, cells were washed in blocking solution and incubated with rabbit-specific Alexa 488-labeled secondary antibody in a 1:2000 dilution in blocking solution for 1 h.

In parallel to secondary antibody incubation, cellular nuclei were stained with DAPI. After staining procedure, cells were washed with PBS-T and images were obtained with a Zeiss Axio Observer.Z1 fluorescence microscope (Zeiss, Goettingen, Germany).

5 Results

5.1 Characterization of structural organization of BVDV NS2

NS2 is a key player in the pestiviral life cycle, as temporally regulated NS2-3 cleavage is critical for the switch from pestiviral RNA replication to virion morphogenesis. This regulation is dependent on the cellular cofactor DNAJC14/Jiv and is important for the maintenance of the noncp biotype (Tautz et al., 2015). Several previous mutagenesis studies provided insights into functional elements of the pestiviral NS2 protease domain, such as the putative catalytic triad, the Zn^{2+}-binding motif and the two JBDs, as well as into the functional relationship with its cofactor Jiv (Lackner et al., 2004, 2005, 2006; Rinck et al., 2001). Moreover, functional studies have provided a detailed knowledge on the involvement of NS2, as uncleaved NS2-3, in pestiviral virion morphogenesis (Agapov et al., 2004; Dubrau et al., 2017; Moulin et al., 2007). Until now, structural data on pestiviral NS2 are missing and the topology of its N-terminal MBD has not been determined. Accordingly, the precise molecular mechanisms of the NS2 protease activation as well as details of functional protein-protein interactions involved in virion morphogenesis remain unknown. The first aim of the present work was to gain deeper insights into the structural organization of BVDV NS2. First, the membrane topology of the N-terminal section was determined based on a preliminary, incomplete data set from my master's thesis (Walther, 2017) using a Substituted Cysteine Accessibility Method (SCAM) assay. Based on the experimentally defined membrane topology, the minimal C-terminal NS2 portion resembling an active protease was elucidated by an NS2-3 cleavage assay.

5.1.1 Establishment of a functional N-terminally HA-Flag epitope-labeled BVDV NS2

Studies concerning the structural organization of pestiviral NS2 require suitable BVDV NS2-specific antibodies for protein detection. Since no such antibodies were available, BVDV-1 NCP7 and CP7 full-length cDNA genomes that encode an N-terminally HA-Flag epitope-tagged NS2 protein (H-F-NS2) were previously generated (Klemens, 2014; Fig. 7A). Analogous to a successful strategy applied to HCV NS2 (Jirasko et al., 2010), the composition of the inserted amino acid sequence between p7 and NS2 is as follows: 5 N-terminal aa of NS2 (EPGAQ), SG-linker, HA epitope tag (YPYDVPDYA), GSG-linker, Flag epitope tag (DYKDDDDK), GSG linker (Fig. 7A).

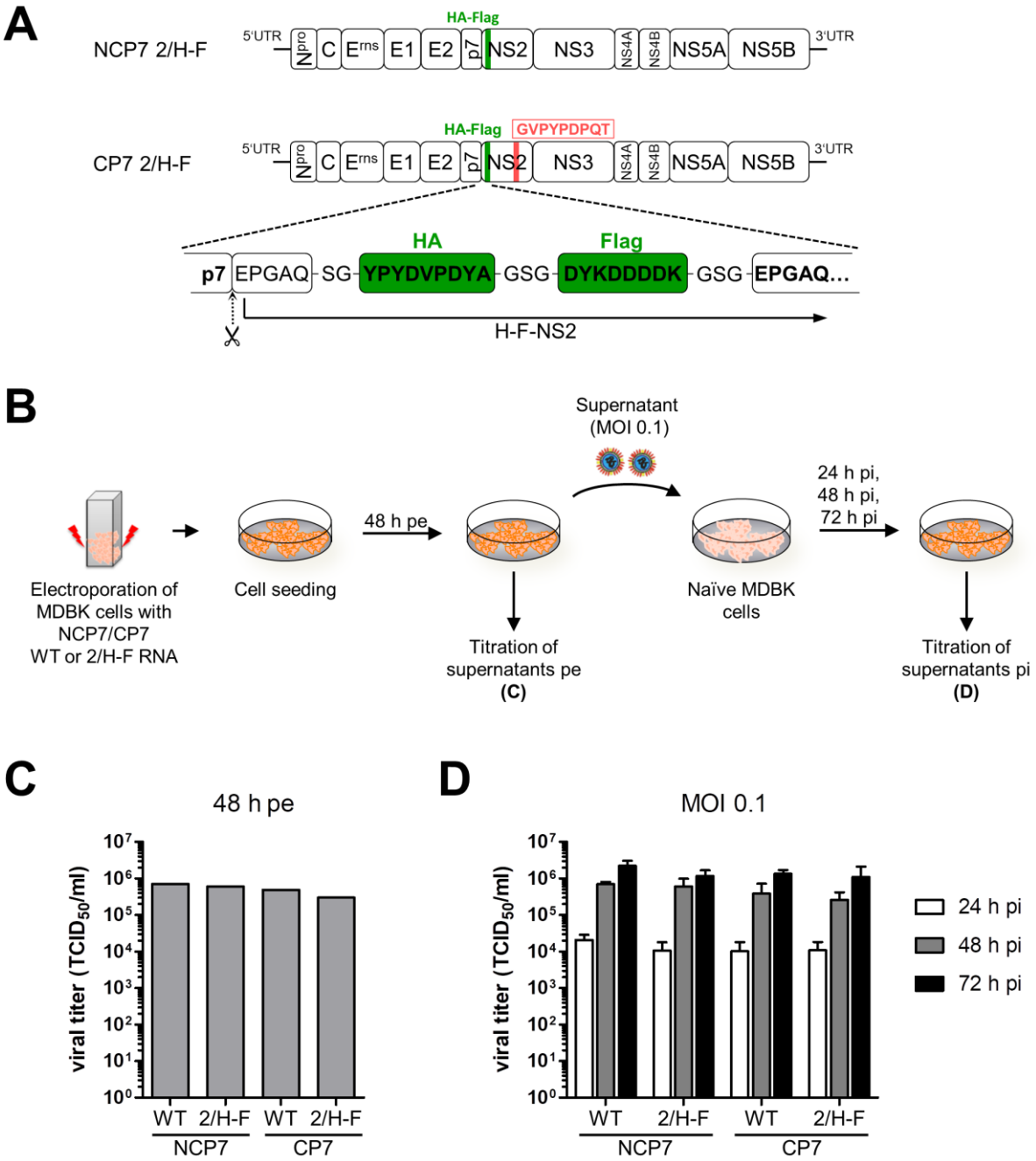

Fig. 7: Functional characterization of BVDV-1 genomes encoding an N-terminally tagged NS2 protein (modified according to Walther et al., 2021). (**A**) Schematic genome representation of BVDV-1 strains NCP7 2/H-F and CP7 2/H-F. The exact composition of the HA-Flag tag (H-F) in NS2 is depicted below. The 9 aa insertion in NS2 present in strain CP7 is displayed in a red box (Tautz et al., 1996); the cleavage site between p7 and NS2 as well as the Gly-Ser linker sequences are indicated. The HA and Flag epitope sequences are shown as green boxes. (**B**) Schematic depiction of the experimental setup. (**C**) Analysis of viral titers as $TCID_{50}$/ml in cell culture supernatants derived 48 h after RNA electroporation (pe) of the respective viral RNAs into MDBK cells. The values of one experiment are shown. (**D**) Growth curve analysis of NCP7 WT, CP7 WT and their respective NCP7 2/H-F and CP7 2/H-F derivatives. MDBK cells were infected with the virus supernatants depicted in (C) at an MOI of 0.1 and viral growth was analyzed for the indicated time points. Supernatants were collected and viral titers were determined as $TCID_{50}$/ml. Mean values and standard deviations of three independent experiments are depicted.

To verify the functionality of the tagged virus variants NCP7 2/H-F and CP7 2/H-F, their replication capacity and the kinetics of virus production were determined and compared to the respective NCP7 and CP7 wildtype (WT) cDNA clones (Fig. 7B). *In vitro* transcribed genomic RNAs of NCP7 WT, CP7 WT, NCP7 2/H-F and CP7 2/H-F were electroporated into MDBK cells and viral titers of cell culture supernatants 48 h post electroporation (pe) were determined as tissue culture infectious dose 50 per ml ($TCID_{50}$/ml) (Fig. 7B). Comparable titers were determined 48 h pe for all four viruses tested: for NCP7 WT and its 2/H-F derivative, titers were 7.1 x 10^5 $TCID_{50}$/ml and 6.0 x 10^5 $TCID_{50}$/ml, respectively, and titers of CP7 WT and 2/H-F were 4.9 x 10^5 $TCID_{50}$/ml and 3.0 x 10^5 $TCID_{50}$/ml, respectively (Fig. 7C). These supernatants were used to infect naïve MDBK cells at a multiplicity of infection (MOI) of 0.1 and viral titers in cell culture supernatants were determined 24, 48 and 72 h post infection (pi) (Fig. 7B). NCP7 2/H-F as well as CP7 2/H-F showed viral titers comparable to their corresponding parental WT virus at all analyzed time points (Fig. 7D).

Next, it was tested if the H-F tag is suited for the detection of NS2 in western blotting and to directly determine the influence of the epitope-tag sequence on NS2-3 cleavage. In addition, the H-F tag was tested concerning its suitability for immunoprecipitation, which would be a prerequisite for studying protein-protein interactions involving NS2. Accordingly, pCITE expression constructs encoding the BVDV-1 NCP7 or CP7 polyprotein region E2 to NS4A with N-terminally H-F-tagged NS2 were generated (pCITE NCP7 E2-4A 2/H-F; pCITE CP7 E2-4A 2/H-F) (Fig. 8A). To test the detectability of H-F-NS2 and verify support for NS2-3 cleavage, porcine cell lines SK6 KO (deficient of pestiviral NS2 protease cofactor DNAJC14; Isken et al., 2019) or SK6 KO GST-Jiv90 (overexpression of minimal pestiviral NS2 protease cofactor domain Jiv90 in SK6 KO cells; Isken et al., 2019) were used. Porcine cell lines were used since DNA plasmid transfection is not sufficiently efficient in the available bovine cell lines. For transient $T7^{pol}$-mediated gene expression, SK6 KO and SK6 KO GST-Jiv90 cells were first infected with the vaccinia virus MVA-$T7^{pol}$, to express T7 RNA polymerase in the cytoplasm, and then transfected with the pCITE NCP7 E2-4A 2/H-F plasmid (Fig. 8B). Western blot analyses with an HA-specific antibody showed that H-F-NS2 and its uncleaved precursors (E2-NS3 2/H-F, H-F-NS2-3) could be detected confirming that the N-terminally tagged NS2 is capable of catalyzing the NS2-3 cleavage (Fig. 8C). This observation was verified by a NS3/NS2-3-specific western blot (Fig. 8C). Furthermore, the NCP7 2/H-F derived NS2 protease displayed the characteristic DNAJC14/Jiv-dependent regulation for efficient NS2-3 cleavage (Fig. 8C, compare lane 2 and 4).

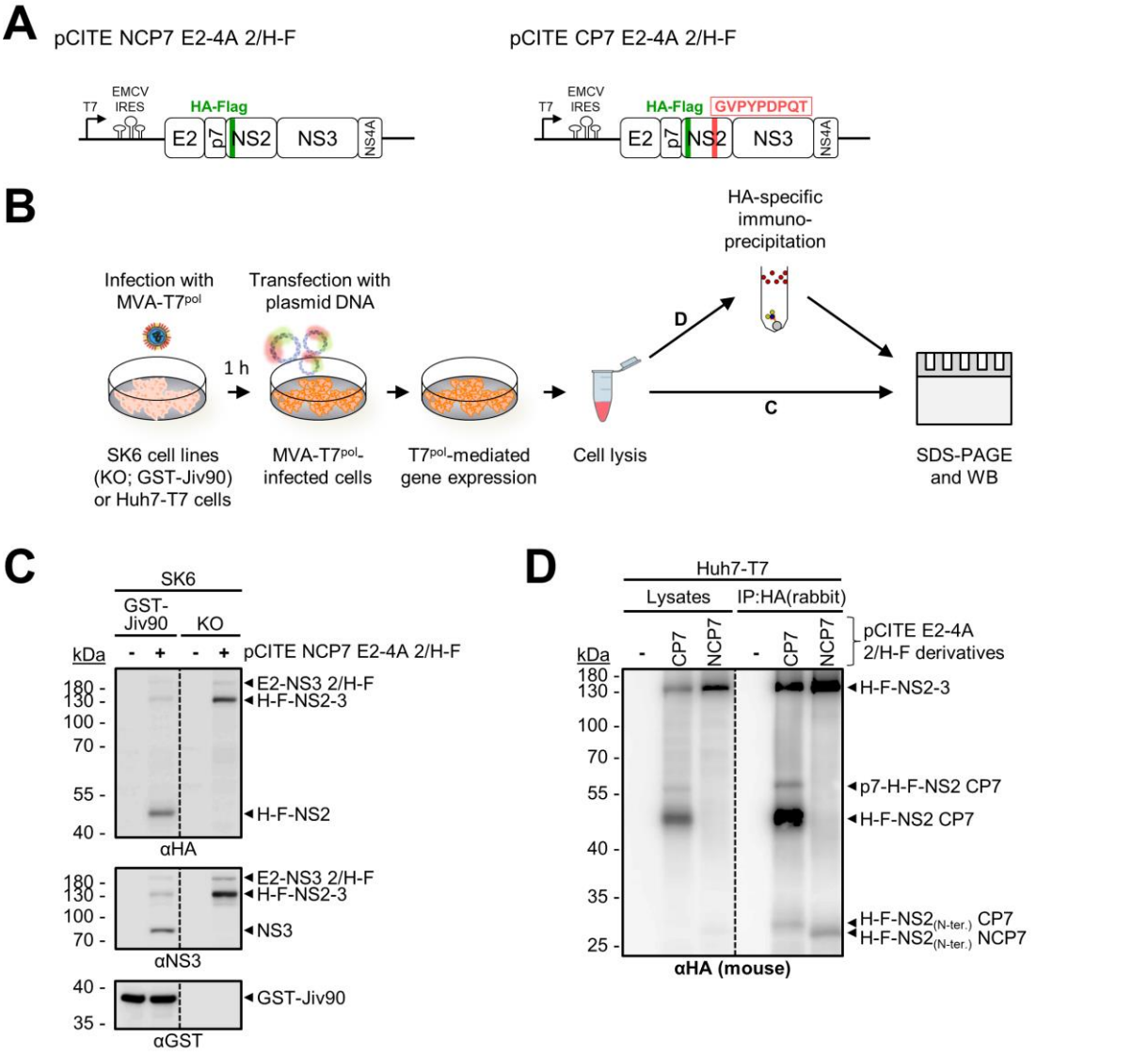

Fig. 8: Functional characterization of N-terminally tagged NS2 in a replication-independent subgenomic context (modified according to Walther et al., 2021). (**A**) Schemes of the pCITE NCP7 or CP7 E2-4A 2/H-F expression constructs coding for the BVDV-1 NCP7 E2 to NS4A region with an N-terminally HA-Flag-tagged NS2 as shown in Fig. 7. (**B**) Schematic depiction of the experimental setup. (**C**) Western Blot analysis of pCITE NCP7 E2-4A 2/H-F expression, polyprotein processing and H-F-NS2 detection. SK6 KO or SK6 GST-Jiv90 cells transfected with pCITE NCP7 E2-4A 2/H-F were lysed 18 h pt and analyzed by western blot using the indicated primary antibodies. (**D**) HA-specific immunoprecipitation of H-F-NS2. Huh7-T7 cells transfected with pCITE NCP7 or CP7 E2-4A 2/H-F were lysed 24 h pt. After HA-specific immunoprecipitation, lysates and precipitated proteins were analyzed by western blot using the indicated primary antibodies. (**C+D**) Western blots of one representative experiment are shown. The molecular mass standard in kilodalton (kDa) is given on the left. Positions of the protein products are indicated on the right. Dashed lines indicate splitting of gels.

Another important application for the H-F-NS2 epitope tag would be its suitability for immunoprecipitation. Huh7-T7 cells, which already express T7^{pol}, were infected with MVA-T7^{pol} to increase T7^{pol} expression and transfected with the pCITE NCP7 or CP7 E2-4A 2/H-F plasmid (Fig. 8B). Cell lysates were subjected to HA-specific immunoprecipitation using αHA antibodies (rabbit IgG) conjugated to sepharose beads (Fig. 8B). Western blot analysis with an αHA antibody (mouse IgG) confirmed that H-F epitope tag containing protein products

(NCP7 or CP7 H-F-NS2-3, p7-H-F-NS2 CP7 and H-F-NS2 CP7) can be precipitated (Fig. 8D, IP:HA). Furthermore, the CP7 2/H-F showed the characteristic cofactor independence for NS2-3 cleavage (Fig. 8D, compare CP7 and NCP7 H-F-NS2). Interestingly, after immunoprecipitation an additional HA-specific protein product of about 25-27 kDa was enriched that was difficult to detect in lysates (Fig. 8D, compare lysates to IP:HA). Due to its apparently smaller size compared to full-length H-F-NS2 it was termed H-F-NS2$_{(N\text{-}ter.)}$ (Fig. 8D). The difference in size between the NCP7 and CP7 variants of the fragment (Fig. 8D, compare CP7 to NCP7) suggests a cleavage within NS2 that occurs after the CP7-specific 9 aa insertion (Tautz et al., 1996). However, this internal cleavage was not further characterized in the present work.

5.1.2 Studies on the membrane topology of BVDV NS2

The BVDV NS2 membrane topology was studied using a Substituted Cysteine Accessibility Method (SCAM) assay, which is based on the chemical modification of cytoplasmic cysteines in the analyzed protein by membrane-impermeable reagents such as PEG-maleimide (PEG-Mal; referred to as PEGylation) after selective plasma membrane permeabilization (Bogdanov et al., 2005; Van Geest and Lolkema, 2000; Zhu and Casey, 2007).

5.1.2.1 Generation of an in silico membrane topology model of BVDV NS2 and a SCAM assay compatible NS2 derivative

As a basis for the analysis of BVDV-1 NS2 membrane topology, an *in silico* model had to be generated using established topology prediction programs. In a previous work (Fellenberg, 2017), the following freely available transmembrane segment prediction programs were used for this purpose: MEMSAT3, MEMSAT-SVM, HMMTOP, TMHMM, SACS MEMSAT, CCTOP, OCTOPUS, PHOBIUS, and TMPRED. The following topological constraints are required for authentic processing of the viral polyprotein: (i) the NS2 N terminus is localized in the ER lumen to allow cleavage at the p7-NS2 junction by cellular ER-resident signal peptidase and (ii) the C terminus of NS2 is located in the cytoplasm for the NS2-3 cleavage by the C-terminal NS2 autoprotease domain. When applying these constraints to the membrane topology prediction of BVDV-1 NS2 by different programs, several predictions (CCTOP, HMMTOP, OCTOPUS, TMPRED and TMHMM) that did not meet one or both of these criteria where immediately ignored (data not shown; Fellenberg, 2017). The MEMSAT SVM program predicted a NS2 topology model with two very large (~30 aa) transmembrane segments (TMs) as well as two unlikely short TM-connecting loop sequences (3 aa) (data not shown) and was therefore not further considered. The calculation with Phobius also gave rise to a NS2 membrane topology model matching the polyprotein processing prerequisites. It

predicted a short (aa 1-6) luminal N-terminal sequence, seven TMs and a C-terminal, cytoplasmic domain spanning aa 252-453 (containing the active site, the Zn^{2+}-coordinating cysteines and the two Jiv-binding domains (JBDs)) (Fig. 9A; Fellenberg, 2017). MEMSAT2 also delivered a similar model (data not shown; Fellenberg, 2017) with just minor differences with respect to TM localization/length and connecting loop sequences. Since the Phobius webserver allows defining constraints for the prediction resulting from experimental approaches, this program was subsequently used and its topology prediction (Fig. 9A) served as starting point to decide where to introduce cysteine mutations for the SCAM assay approach.

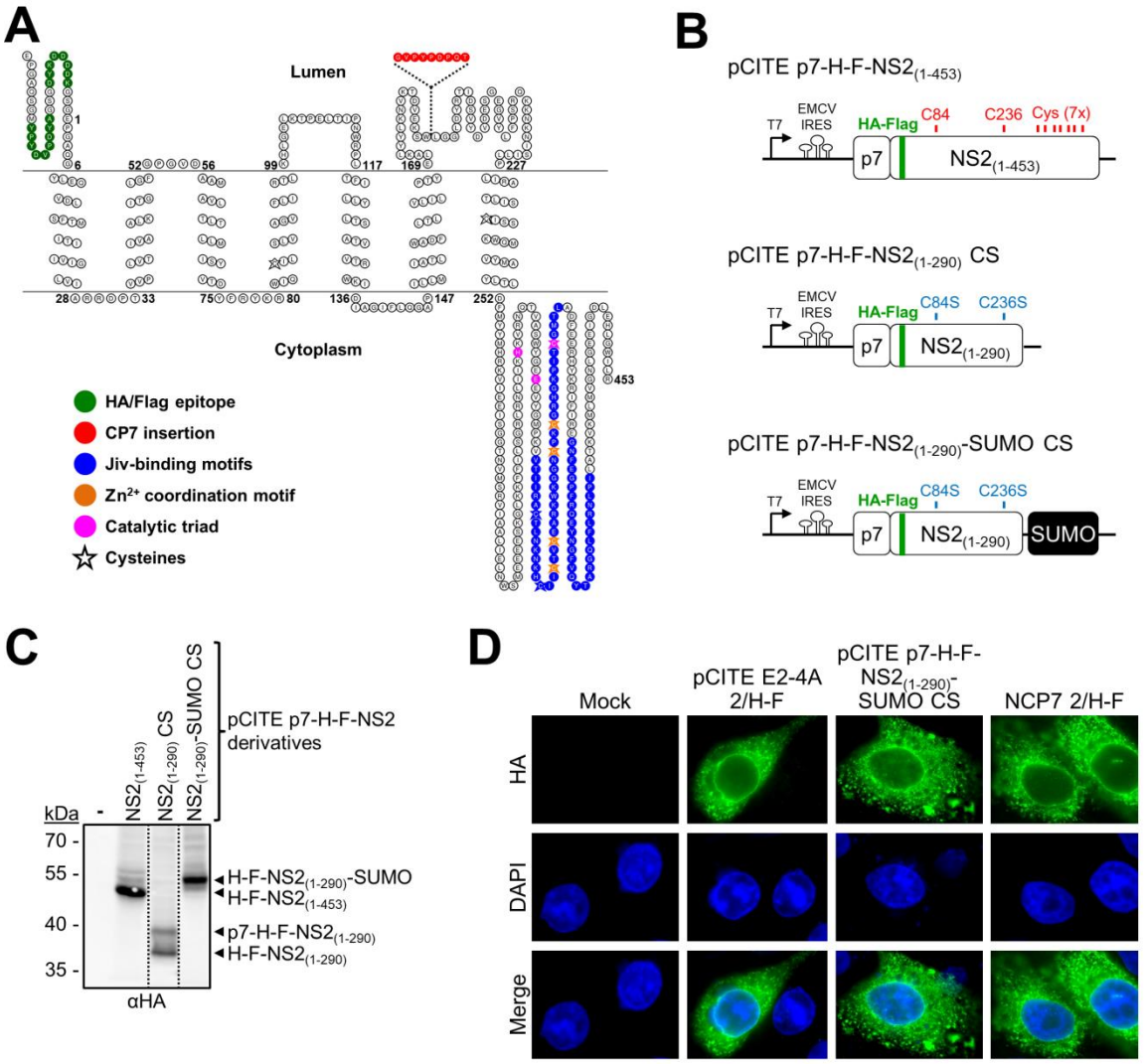

Fig. 9: Cysteine-free BVDV-1 NS2(1-290)-SUMO fusion protein allows NS2 membrane topology determination by Substituted Cysteine Accessibility Method (SCAM) assay (adapted from Walther et al., 2021). (**A**) Membrane topology prediction based on the aa sequence of BVDV-1 NCP7 NS2 with N-terminal HA-Flag epitope (modified according to Fellenberg, 2017). The model was generated using the Phobius software and visualized with the TOPO2 program. Amino acids are depicted as circles; cysteines are indicated as stars. The HA-Flag epitope (green sequences), the two Jiv binding motifs (blue), the residues of the putative Zn^{2+} coordination motif (orange) and the putative catalytic triad of the protease (pink) are highlighted and indicated in the legend. The CP7-specific 9 aa insertion (red) is shown with its insertion site indicated by a dashed line. Numbers indicate the first and last aa of NS2 as well as amino acid positions of luminal or cytoplasmic sections of

NS2. The intracellular membrane is displayed as black double line. Lumen, luminal side of the membrane; Cytoplasm, cytoplasmic side of the membrane. (**B**) Top: Scheme of the pCITE p7-H-F-NS2$_{(1-453)}$ expression construct coding for p7 and full-length BVDV-1 NCP7 NS2. The two cysteines (C84 and C236) in the hydrophobic N-terminal part as well as the seven cysteines in the putative cytoplasmic domain are indicated. Middle: Scheme of the pCITE p7-H-F-NS2$_{(1-290)}$ CS expression construct coding for p7 and the N-terminal part of NS2 from aa 1 to 290 (NS2$_{(1-290)}$). The two cysteine-to-serine mutations (C84S and C236S) are indicated. Bottom: Scheme of the pCITE p7-H-F-NS2$_{(1-290)}$-SUMO CS expression construct coding for p7 and NS2$_{(1-290)}$ fused to SUMO protein. C84S and C236S are indicated. (according to Fellenberg, 2017) (**C**) Expression of p7-H-F-NS2 derivatives (modified according to Fellenberg, 2017). MVA-T7^{pol} infected Huh7-T7 cells were transfected with the pCITE p7-H-F-NS2 plasmid derivatives and 18 h pt cells were processed by western blot analysis using an αHA primary antibody. The molecular mass standard in kDa and detected protein products are indicated. Dotted lines indicate splitting of gels. (**D**) Comparison of intracellular location of N-terminally HA-Flag-tagged NS2 derivatives (modified according to Walther, 2017). The intracellular localization of N-terminally HA-Flag-tagged NS2 derivatives expressed from pCITE E2-4A 2/H-F and pCITE p7-H-F-NS2$_{(1-290)}$-SUMO CS plasmid DNAs in MVA-T7^{pol}-infected SK6 cells were compared to H-F-NS2 produced by replication of full-length NCP7 2/H-F in SK6 cells. All SK6 cells were incubated for 24 h at 37 °C. Localization of NS2 derivatives was detected by HA-specific immunofluorescence (IF) after cell fixation with paraformaldehyde (PFA) and permeabilization with n-Octyl-β-D-Glukopyranosid. Nuclei were visualized by DAPI staining.

The application of the SCAM approach to determine the membrane topology requires that only one single cysteine is present at a defined position in the examined protein (Van Geest and Lolkema, 2000; Zhu and Casey, 2007). BVDV-1 NCP7 NS2 contains 9 native cysteines: two cysteines located in the predicted TM4 (C84) and TM7 (C236) and the remaining 7 cysteines present in the C-terminal cytoplasmic domain (Fig. 9A, cysteines are indicated by stars; Fig. 9B, top). Therefore, in the bachelor thesis of J. Fellenberg a p7-H-F-NS2$_{(1-290)}$ derivative was generated encoding a C-terminal truncated NS2 variant (NS2 aa 1 to 290) that included all of the predicted TMs and a short part of the C-terminal cytoplasmic domain to eliminate the 7 cysteines of the cytoplasmic domain (Fig. 9A+B; Fellenberg, 2017). A cysteine-free version of p7-H-F-NS2$_{(1-290)}$ was obtained by exchanging the remaining two cysteines in TM4 (C84) and in TM7 (C236) with serine (C84S and C236S, respectively, termed CS; Fig. 9B, middle; Fellenberg, 2017). In addition, the globular cysteine-free SUMO protein was fused to the C-terminally truncated NS2 downstream of amino acid 290, resulting in a NS2$_{(1-290)}$-SUMO fusion protein (pCITE p7-H-F-NS2$_{(1-290)}$-SUMO CS) to improve protein folding and stability (Fig. 9B, bottom; Fellenberg, 2017). Importantly, SUMO is a globular cysteine-free protein and is well established as a solubility tag to prevent insolubility of the protein of interest (Kuo et al., 2014). Therefore, SUMO is a well suited replacement for the deleted C-terminal NS2 part to create a stable, SCAM assay-compatible fusion protein. p7 was retained in both constructs to support authentic p7-NS2 processing and correct localization of NS2 to ER membranes. To test stability and detectability of the H-F-NS2 derivatives, the respective pCITE p7-H-F-NS2 constructs were transfected into MVA-T7^{pol} infected Huh7-T7 cells to express p7-H-F-NS2$_{(1-453)}$, p7-H-F-NS2$_{(1-290)}$ CS and p7-H-F-NS2$_{(1-290)}$-SUMO CS (Fellenberg, 2017). Huh7-T7 cells were used for expression, because they yielded higher amounts of protein products compared with SK6 cells. Western blot

analysis using an HA-specific antibody showed protein stability and detectability of both cysteine-free H-F-NS2 derivatives comparable to full-length H-F-NS2 (Fig. 9C; Fellenberg, 2017). The expression from pCITE p7-H-F-NS2$_{(1-453)}$ and pCITE p7-H-F-NS2$_{(1-290)}$-SUMO CS resulted in single prominent bands of the expected size for either H-F-NS2$_{(1-453)}$ or H-F-NS2$_{(1-290)}$-SUMO, respectively (Fig. 9C; Fellenberg, 2017). This observation is indicating efficient co-translational p7-NS2 processing for both proteins. In contrast, the expression from pCITE p7-H-F-NS2$_{(1-290)}$ CS showed an additional higher molecular band with the size of unprocessed p7-H-F-NS2$_{(1-290)}$ precursor protein most likely derived from incomplete p7-NS2 processing (Fig. 9C, compare pCITE p7-H-F-NS2$_{(1-290)}$-SUMO CS with pCITE p7-H-F-NS2$_{(1-290)}$ CS). Based on these findings, pCITE p7-H-F-NS2$_{(1-290)}$-SUMO CS was used for further experiments.

Furthermore, my master's thesis compared the intracellular localization of H-F-NS2$_{(1-290)}$-SUMO CS with that of full-length H-F-NS2 (Walther, 2017). To this end, full-length H-F-NS2 was expressed either in the context of an E2-NS4A polyprotein fragment (pCITE E2-4A 2/H-F) or in the context of an infectious clone (NCP7 2/H-F). For the replication-independent expression, SK6 cells were infected with MVA-T7^{pol} and then transfected with either pCITE p7-H-F-NS2$_{(1-290)}$-SUMO CS or with pCITE E2-4A 2/H-F, respectively (Walther, 2017). In addition, *in vitro* transcribed NCP7 2/H-F RNA was electroporated into SK6 cells to include full-length H-F-NS2 expression in the context of viral infection (Walther, 2017). The intracellular localization of the H-F-NS2 derivatives was compared by HA-specific immunofluorescence (IF), showing a reticular as well as perinuclear localization for all H-F-NS2 derivatives (Fig. 9D; Walther, 2017). This confirmed that the H-F-NS2$_{(1-290)}$-SUMO fusion protein has an intracellular localization comparable to full-length H-F-NS2 during viral replication.

5.1.2.2 Elucidation of the BVDV NS2 membrane topology using a Substituted Cysteine Accessibility Method (SCAM) assay

The creation of the cysteine-free pCITE p7-H-F-NS2$_{(1-290)}$-SUMO CS and the validation of its authentic NS2 localization and efficient p7-NS2 polyprotein processing provided the basis to experimentally determine the NS2 membrane topology. To this end, a series of pCITE p7-H-F-NS2$_{(1-290)}$-SUMO CS variants were generated, each containing a single cysteine residue at a defined position. Positions for these cysteine mutations were chosen based on the predicted H-F-NS2$_{(1-453)}$ membrane topology (Fig. 9A). The single cysteines were introduced in putative cytoplasmic regions, which would allow PEG-Mal modification (PEGylation) after selective plasma membrane (PM) permeabilization, or in putatively luminal sequences, where the selective PEGylation should not be possible. As a positive control, a derivative was created in which the C-terminal glycine of the cytoplasmic SUMO protein was mutated to

cysteine (SUMO-G98C), assuming that SUMO-G98C should always be accessible for PEGylation. A subset of the analyzed derivatives was created in previous works (Fellenberg, 2017; Walther, 2017). In addition, general experimental conditions of the SCAM assay procedure for application on BVDV NS2 have already been established in master's thesis (Walther, 2017), which were further optimized in the present work to allow the establishment of an NS2 membrane topology. For the SCAM assay, MVA-T7^{pol} infected Huh7-T7 cells were transfected with the mutated pCITE p7-H-F-NS2$_{(1-290)}$-SUMO CS derivatives, using the pCITE p7-H-F-NS2$_{(1-290)}$-SUMO CS SUMO-G98C and the cysteine-free pCITE p7-H-F-NS2$_{(1-290)}$-SUMO CS construct as positive and negative controls for PEGylation, respectively (Fig. 10A and B). 8 h pt cells were harvested and permeabilized by either Triton X-100 to test all cysteine mutants for general accessibility for PEG-Mal modification or with Digitonin to determine selective accessibility for PEGylation, respectively (Fig. 10A). After treatment with PEG-Mal the reaction was stopped by addition of DTT and the proteins were precipitated with methanol/chloroform (Fig. 10A), which proved to be most efficient in recovery of the proteins while maintaining a low background compared to the initially used precipitation by acetone or phenol/chloroform (data not shown). The precipitated proteins were resuspended in SDS sample buffer and the samples were heated at 37 °C, which allowed better detectability of the protein products compared with the previously used incubation at 95 °C (data not shown), probably due to prevention of aggregation of the denatured H-F-NS2$_{(1-290)}$-SUMO. Proteins were analyzed via SDS-PAGE and HA-specific western blot to detect H-F-NS2$_{(1-290)}$-SUMO variants (Fig. 10A).

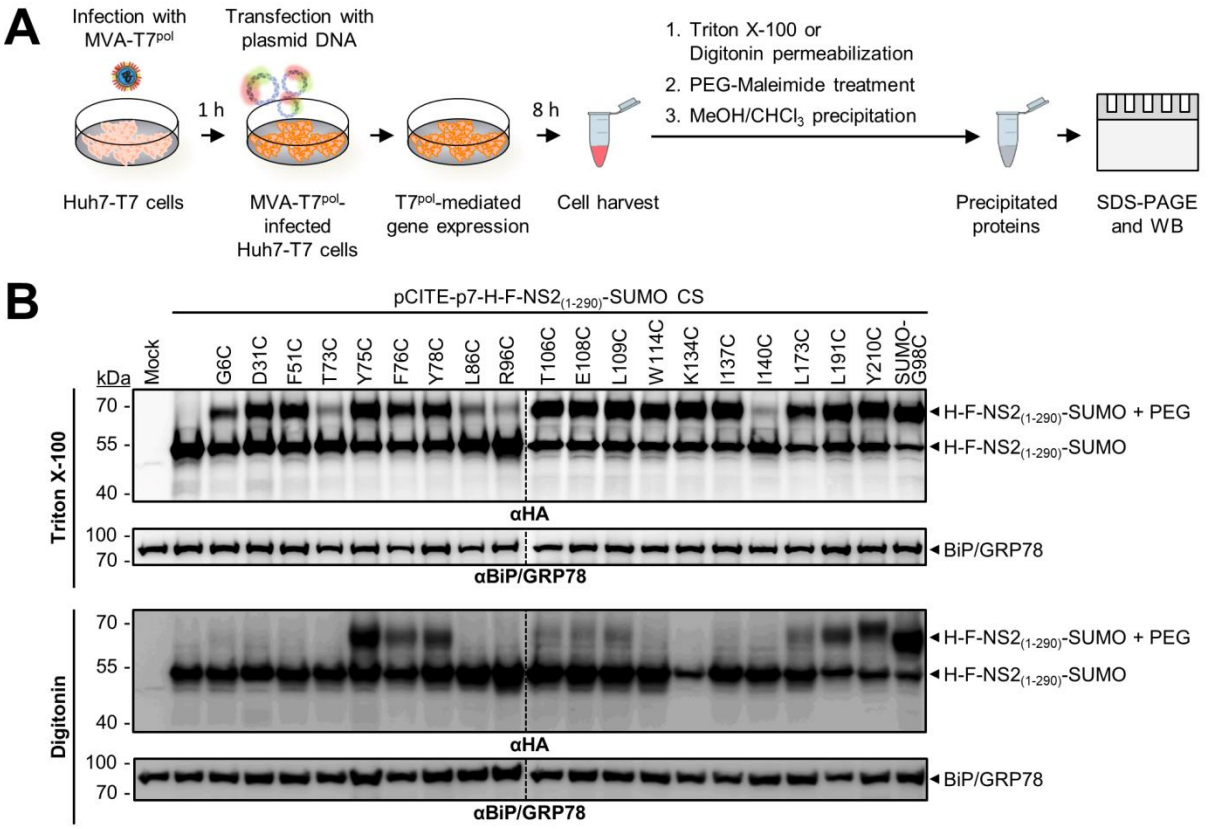

Fig. 10: Experimental determination of a BVDV-1 NS2 membrane topology model using a SCAM assay (adapted from Walther et al., 2021). (**A**) Schematic depiction of the experimental setup. (**B**) Analysis of polyethylene glycol modification (PEGylation) of H-F-NS2$_{(1-290)}$-SUMO CS derivatives after treatment with Triton X-100 (top; general accessibility for PEG-Mal modification) or Digitonin (bottom; accessibility for PEG-Mal modification after selective plasma membrane (PM) permeabilization). Protein samples were separated by SDS-PAGE followed by western blot analyses using an αHA primary antibody. The cysteine-free NS2 derivative and the SUMO-G98C variant served as negative or positive control, respectively. Mock refers to cell lysates without transfected plasmid DNA. Positions of the PEGylated (H-F-NS2$_{(1-290)}$-SUMO + PEG) and the unmodified (H-F-NS2$_{(1-290)}$-SUMO) protein products are indicated on the right. The detection of BiP/GRP78 served as loading control. The molecular mass standards in kDa are given on the left. One representative western blot for each treatment with Triton X-100 or Digitonin is shown. Dashed lines indicate separate western blots.

Western blot analysis of Triton X-100 treated cells showed for all cysteine mutants two HA-reactive proteins: the unmodified protein product H-F-NS2$_{(1-290)}$-SUMO and a PEGylated form (H-F-NS2$_{(1-290)}$-SUMO + PEG) (Fig. 10B, top). As expected, the cysteine-free variant (CS) did not show any detectable PEG-Mal-modified form, while the positive control (SUMO-G98C) was efficiently modified (Fig. 10B, top). All introduced cysteines were generally accessible to modification by PEG-Mal (Fig. 10B, top). However, some of the cysteine mutations (T73C, L86C, R96C and I140C) showed weaker PEG-Mal modification indicating they were less accessible for PEGylation (Fig. 10B, top).

After selective permeabilization with Digitonin, a PEGylated form of H-F-NS2$_{(1-290)}$-SUMO was detected for cysteine mutants Y75C, F76C, Y78C, T106C, E108C, L109C, L173C, L191C and Y210 as well as for the positive control SUMO-G98C (Fig. 10B, bottom),

indicating a cytoplasmic localization of these cysteine mutations. The derivatives G6C, D31C, F51C, W114C, K134C and I137C did not display detectable amounts of the PEGylated form after Digitonin treatment (Fig. 10B, bottom). This observation suggests either a luminal localization or inaccessibility of these cysteines due to close proximity to the ER membrane. In the displayed western blot the K134C derivative showed a lower protein amount after selective PM permeabilization compared to the other constructs (Fig. 10B, bottom), which made detection of the PEGylated form difficult. However, in several other experiments no PEGylated form was detected for the K134C derivative, while the protein amounts were comparable to the other NS2 variants (Fig. S 1). As mentioned above, due to the general lower accessibility of the T73C, L86C, R96C and I140C mutations for PEG-Mal modification, no definitive statement concerning their localization can be made (Fig. 10B, compare top and bottom panel).

These experimental data on the localization of the analyzed amino acid positions were subsequently used as constraints (Y75, F76, Y78, T106, E108, L109, L173, L191, Y210 = cytoplasmic and G6, D31, F51, W114, K134, I137 = non-cytoplasmic) to determine an updated membrane topology model for BVDV NS2 (Fig. 11). Since the SCAM assay results were obtained using H-F-NS2$_{(1-290)}$-SUMO, the prediction with the Phobius program was done using the sequence of this NS2 derivative. Also the initial model without experimental constraints was re-calculated applying H-F-NS2$_{(1-290)}$-SUMO sequence instead of H-F-NS2$_{(1-453)}$, leading to a highly similar topology with a few minor changes in the TMs 3, 4 and 5 and therefore also in the loop sequences connecting these TMs (compare Fig. 11C, left and Fig. 9A). The experimental data-based model predicts 3 TMs instead of 7 TMs for the *in silico* generated model (compare Fig. 11, left and right).

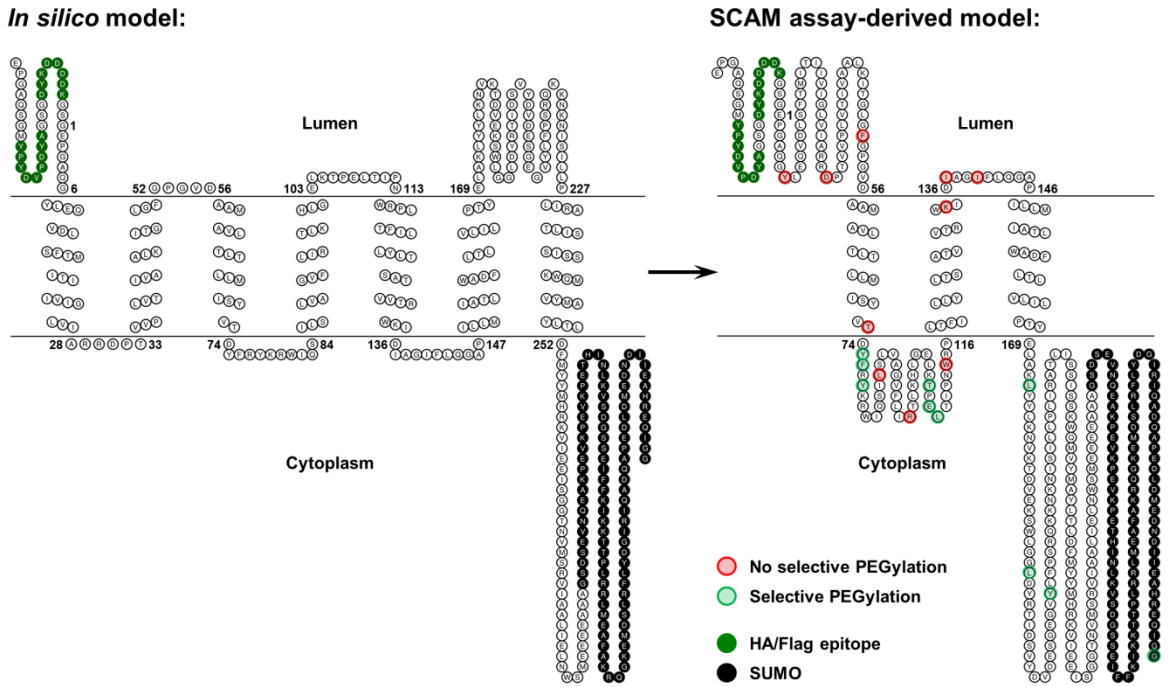

Fig. 11: Experimentally confirmed BVDV NS2 membrane topology model based on SCAM results using p7-H-F-NS2$_{(1-290)}$-SUMO derivatives (modified according to Walther et al., 2021). Left, *In silico* membrane topology model of H-F-NS2$_{(1-290)}$-SUMO CS determined without constraints using the Phobius program. Right, modified BVDV NS2 membrane topology model based on experimental data from the SCAM assay (Fig. 10). Positions of cysteine mutations that were accessible (light green) and that were not accessible (light red) for PEG modification after selective PM permeabilization are highlighted. In both models, the HA-Flag epitope (dark green) and the SUMO moiety (black) are indicated. The first aa of NS2 as well as aa positions of luminal or cytoplasmic sections are numbered. The intracellular membrane is displayed as black double line. Lumen, luminal side of the membrane; Cytoplasm, cytoplasmic side of the membrane.

Due to their length, it can be assumed that these areas might form defined secondary structures. Supporting this hypothesis, the Psipred program predicted two distinct helical regions (aa 12-28 and aa 35-46) for the N-terminal luminal sequence (Fig. 12A, top), with a high confidence value for both regions (7-10 and 7-9, respectively). Further analysis with HeliQuest revealed strong hydrophobicity (0.937 and 0.911, respectively) for both predicted helical elements (Fig. 12A, bottom). Secondary structure analysis of the TMS1-2 sequence using Psipred also predicted a helical structural element in the first two-thirds of this region (aa 75-101) (Fig. 12B, top). A more detailed analysis of the central part of this putative helix, where prediction with Psipred showed high confidence values, revealed a hydrophobicity of 0.974 and a hydrophobic moment of 0.44 with HeliQuest (Fig. 12B, bottom).

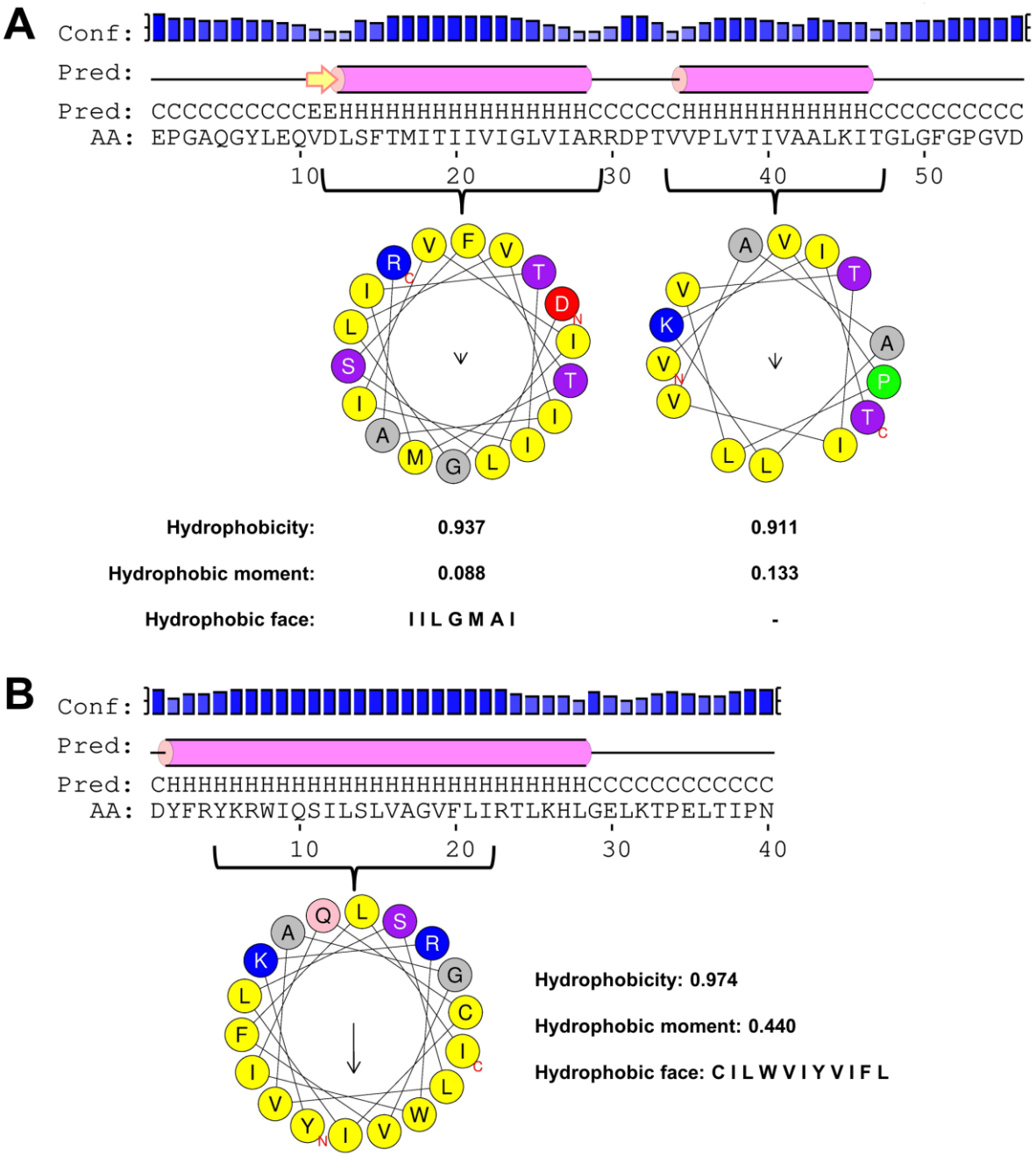

Fig. 12: Analysis of BVDV NS2 luminal N terminus (A) and TMS1-2 sequence (B) using Psipred and HeliQuest programs (modified according to Walther et al., 2021). The secondary structure analysis of the two regions with Psipred is given first. Secondary structure predicitions (Pred) are displayed both graphically and as letter codes (coil: line, C; strand: arrow, E; helix: barrel, H). The confidence of the prediction (Conf) is given above and the analyzed amino acid sequence (AA) is given below the prediction. Further analysis of putative helical regions with HeliQuest is indicated below the Psipred analysis in each case, and the selected regions are indicated by brackets. Hydrophobicity, hydrophobic moment as wells as the hydrophobic face for each putative helix are given. Amino acids are color-coded concerning to their character: hydrophobic residues are depicted in yellow; positively and negatively charged aa are shown in blue or red, respectively; uncharged, polar residues are colored in pink or purple; proline is depicted in green and glycin and alanine in grey.

5.1.3 Determination of the minimal BVDV NS2 protease domain based on the membrane topology model

Until now, no protein structures of pestiviral NS2 are available. In part due to its high hydrophobicity, it has not yet been possible to express functional pestiviral NS2 in bacteria (Lackner et al., 2004). Previous attempts to reduce its hydrophobicity by generating N-terminal truncations led to either strongly reduced or fully abolished NS2-3 processing, suggesting the importance of the hydrophobic N-terminal part of NS2 for the NS2 autoprotease activity (Lackner et al., 2004). However, without detailed knowledge about the NS2 topological organization NS2 truncations were set at random positions (Lackner et al., 2004). With the established NS2 membrane topology model, it was now possible to make another attempt to define the minimally active NS2 protease moiety. To this end, reporter constructs encoding N-terminally truncated NS2 variants of various lengths were generated ($NS2_{(x\text{-}453)}$, where the x indicates the position of the N-terminal NS2 aa), followed by the first 10 aa of NS3, which were described to be sufficient for efficient NS2-3 cleavage (Lackner et al., 2004) (Fig. 13A). The SUMO protein, followed by a combined HA-V5 epitope tag, was fused to the NS3 moiety to allow detection of the $NS3_{(1\text{-}10)}$-SUMO-HA-V5 cleavage product (Fig. 13A). Since the activity of the noncp pestiviral NS2 protease is dependent on its cofactor DNAJC14/Jiv, the NS2 truncations were examined in the DNAJC14-dependent NCP7 context as well as in the cofactor-independent context of cp BVDV CP7 (Fig. 13A). To enable efficient NS2-3 cleavage, SK6 KO GST-Jiv90 cells over-expressing the minimal activating Jiv90 domain were used (Isken et al., 2019). Accordingly, the reporter constructs with N-terminally truncated NCP7 NS2 derivatives were expressed in these SK6 KO GST-Jiv90 cells using the MVA-$T7^{pol}$ expression system (Fig. 13B). Western blot analysis with an HA-specific antibody showed that NS2-3 cleavage with the release of the $NS3_{(1\text{-}10)}$-SUMO-HA-V5 reporter moiety was detected not only for full-length NS2 ($NS2_{(1\text{-}453)}$) but also for its N-terminally truncated versions starting at NS2 amino acid positions 78, 99 or 112 (Fig. 13C). These observations indicate the formation of a functional NS2 protease in the absence of the luminal N-terminal part of NS2, TM1 or almost the complete TM1-2 sequence, respectively (compare Fig. 13C). An NS2 protease active site mutant (NS2/C376A, CA; Lackner et al., 2004) verified that cleavage between NS2 and $NS3_{(1\text{-}10)}$ is NS2-specific (Fig. 13C).

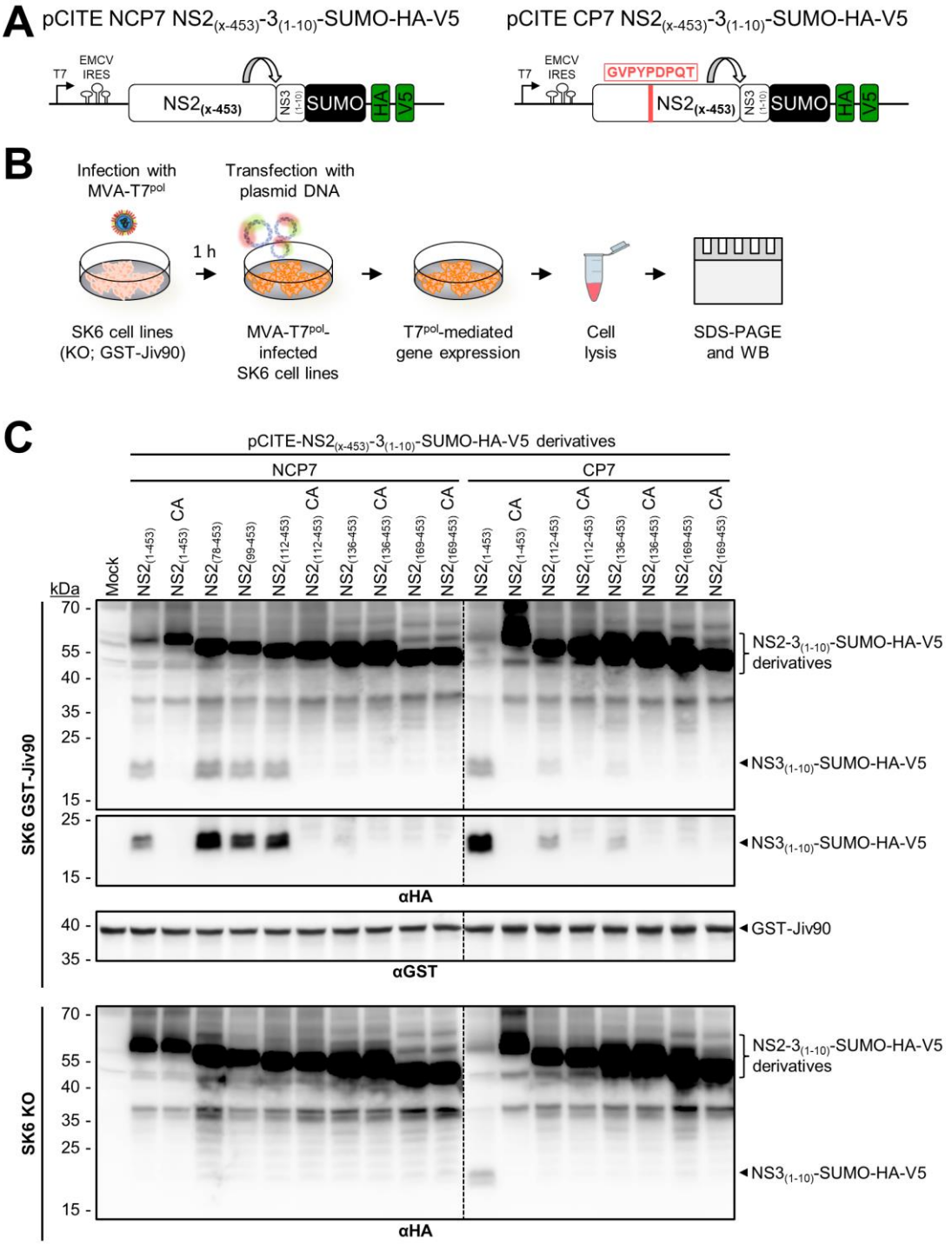

Fig. 13: Determination of an active minimal BVDV-1 NS2 protease domain (adapted from Walther et al., 2021). (**A**) Scheme of the pCITE NCP7 or CP7 NS2$_{(x-453)}$-3$_{(1-10)}$-SUMO-HA-V5 expression constructs. The NS2 fragment is C-terminally fused to the first 10 aa of NS3 followed by SUMO and a combined HA-V5 epitope tag. The 9 aa insertion of the strain CP7 is shown in red. (**B**) Schematic depiction of the experimental setup. (**C**) Analysis of NS2-3 cleavage of different N-terminal NS2$_{(x-453)}$-3$_{(1-10)}$-SUMO-HA-V5 truncations. MVA-T7^{pol}-infected SK6 KO or SK6 KO GST-Jiv90 cells were transfected with pCITE NCP7 or CP7 NS2$_{(x-453)}$-3$_{(1-10)}$-SUMO-HA-V5 derivatives. Transfected cells were processed 18 h pt for western blot analyses with an αHA primary antibody. The respective full-length constructs (NCP7 and CP7 NS2$_{(1-453)}$) served as positive controls and the NS2 active site mutant versions (NCP7 and CP7 NS2/C376A, CA) as negative controls, respectively. For HA-specific analysis of the cell lysates shown in the lower panel after expression in SK6 KO GST-Jiv90 cells, cells were lysed in one-third of the usually used lysis buffer. To detect GST-Jiv90 expression in the SK6 KO GST-Jiv90 cells an αGST primary antibody was used. Mock refers to cell lysates infected with MVA-T7^{pol} and transfected without

plasmid DNA. Positions of protein products are indicated on the right. The molecular mass standards in kDa are given on the left. Dashed lines indicate separate western blots.

Analysis of cofactor-independent CP7 NS2, confirmed these observations and additionally showed a weak NS2 protease activity for a truncated NS2 starting at aa 136 (Fig. 13C), indicating that the TM2 is dispensable for residual CP7 NS2 protease activity (Fig. 13C, compare NCP7 and CP7 $NS2_{(136-453)}$). For better detection of the $NS3_{(1-10)}$-SUMO-HA-V5 cleavage product, cell lysates were resuspended in one-third of the normally used volume of lysis buffer and re-analyzed (Fig. 13C, SK6 KO GST-Jiv90, αHA, lower panel). To determine whether the minimal protease domain functions independently of its cofactor DNAJC14/Jiv, the panel of NS2 truncations was re-analyzed in SK6 KO cells. In the absence of its DNAJC14/Jiv cofactor, none of the analyzed NCP7-derived NS2 variants showed any detectable NS2-3 cleavage activity, as expected (Fig. 13C, bottom panel). For the different CP7 NS2 variants, NS2-3 cleavage could only be detected for full-length NS2 ($NS2_{(1-453)}$) in SK6 KO cells, i.e., in the absence of the DNAJC14/Jiv cofactor (Fig. 13C, bottom panel).

5.2 Molecular characterization of stimulating HCV NS2 protease determinants

The HCV NS2 cysteine protease catalyzes the cleavage at the NS2-NS3 junction (Lorenz et al., 2006). To do this efficiently, the intrinsic proteolytic activity of NS2 is stimulated by the NS3 protease domain, which acts as its activating cofactor (Boukadida et al., 2018; Santolini et al., 1995; Schregel et al., 2009). Recently, this activation was shown to rely on a conserved hydrophobic NS3 surface patch consisting of Y105, P115, and L127 as major determinants of NS3-dependent NS2 protease stimulation and that activation is a shared mode of NS2 protease regulation among different mammalian hepaciviruses (Boukadida et al., 2018; Isken et al., 2015). However, the determinants on the NS2 surface putatively involved in this process have been poorly characterized until now. Accordingly, the second part of this work aimed at the identification and characterization of NS2 surface determinants involved in the NS2 protease stimulation by NS3. To this end, two functional assays were used, both based on the observation of NS2-NS3 cleavage. In the first experimental approach, the effect of mutations of NS2 surface residues potentially located towards the NS3 protease domain on NS2-NS3 cleavage in presence of the NS3 cofactor (NS2-$NS3_{(1\text{-}172)}$) was determined. In the second assay, the effect of these mutations was investigated only in the presence of the four N-terminal NS3 amino acids (NS2-$NS3_{APIT}$), i.e. in absence of the NS3 cofactor. The latter approach allowed the study of the effect on intrinsic NS2 protease activity. Discovered potential determinants on the NS2 surface were further investigated by permutating and combining them as well as examining their effect in a replicative context. In addition, these residues were further investigated in the context of other mammalian hepaciviruses.

5.2.1 Hypothetical HCV NS2-NS3 precursor model

It has been suggested that hydrophobic NS2-NS3 surface interactions are salient features for NS2 activation by NS3 (Isken et al., 2015). Critical for a better understanding of the process is the identification of the NS2 determinants required for this NS2 protease activation. While structural information of the NS2 protease domain and the NS3 protease are available (Kim et al., 1996; Lorenz et al., 2006), similar information for the uncleaved NS2-NS3 is still missing. To overcome this lack of information, a NS2-NS3 precursor model was generated in collaboration with D. Rehders and L. Redecke (University of Luebeck, Luebeck, Germany) based on post-cleavage structures of the NS2 and NS3 protease domains ($NS2^{pro}$: PDB 2HD0 and $NS3^{pro}$: PDB 1A1R; Fig. 14). It was hypothesized that the stimulating hydrophobic NS3 surface residues Y105, P115 and L127 most likely interact with NS2 surface residues in close proximity to the NS2 active site to allow NS2 protease activation by NS3. Accordingly,

the following constraints were incoporated into the model: The activating NS3 hydrophobic region is formed by the amino acids I3, Y105, P115 and L127 (Isken et al., 2015) and should face the NS2 surface in close proximity of the NS2 active site. The NS2 and the NS3 proteins are covalently linked with a reduced interaction radius between both proteins. To allow cleavage, the NS2-NS3 cleavage site should be less than 4 Å away from the active site sulfur atom of C184. The structures of $NS2^{pro}$ and $NS3^{pro}$ are assumed to be identical to their determined post-cleavage crystal structures, e.g. the NS2 is present as an active dimer, the NS3 protein as an active monomer. The $NS2^{pro}$-$NS3^{pro}$ precursor model (Fig. 14) was constructed in several stages (see also Materials and Methods).

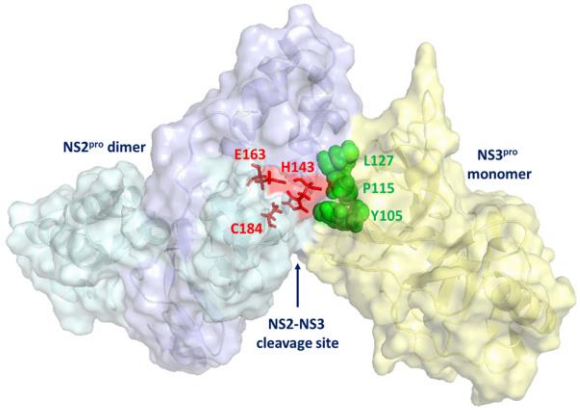

Fig. 14: Hypothetical model of $NS2^{pro}$-$NS3^{pro}$ precursor prior to NS2-NS3 cleavage. Ribbon structural representation of a hypothetical $NS2^{pro}$-$NS3^{pro}$ precursor model consisting of two $NS2^{pro}$ (light yellow and light purple, respectively) and one $NS3^{pro}$ molecule (grey ribbon). Post-cleavage structures of $NS2^{pro}$ (PDB: 2HD0; Lorenz et al., 2006) and $NS3^{pro}$ (PDB: 1A1R; Kim et al., 1996) have been used to generate this model. One $NS2^{pro}$ composite active is shown with H143, E163 and C184 in red. The $NS2^{pro}$-activating NS3 surface residues Y105, P115 and L127 are shown as green spheres. NS2-NS3 cleavage site is indicated.

5.2.2 Identification of NS2 surface determinants for NS3-mediated NS2 protease activation by alanine mutagenesis

Based on the $NS2^{pro}$-$NS3^{pro}$ precursor model (Fig. 14), surface residues in close proximity to H143 of the NS2 active site could potentially form interactions with the activating NS3 surface residues Y105, P115 and L127 during NS2 protease stimulation (Fig. 15A). The result of the energetic minimization suggested that NS2 residues F103, L110, L144, T145 and W150 could be able to undergo such interactions (Fig. 15A). It is noteworthy that F103, which is very exposed, would be able to form potential interactions with any of the three activating NS3 surface residues. Furthermore, NS2 L144 could potentially interact with NS3 Y105 and/or P115, while NS2 L110 and W150 could communicate with NS3 L127.

To test the importance of these hydrophobic NS2 residues for NS3-mediated NS2 stimulation, the NS2 residues F103, L144, T145 and W150 were mutated to alanine. The mutagenesis analysis was performed using the pCITE Flag-NS2-NS3$_{(1-172)}$-GST/BK (HCV genotype 1B) construct previously used to study HCV NS2-NS3 cleavage (Fig. 15B; Isken et al., 2015). In addition, several other conserved residues, that are either in close proximity to the NS2 active site (Y141, N142 and P146) or are more distantly located from the active site residues (L90, I97, V104A, L115, V119 and L135), were exchanged with alanine.

The NS2/C184A mutant with an inactive NS2 protease served as negative control. The NS3/YPL-AAA mutant (NS3/Y105A-P115A-L127A) that is unable to support NS3-mediated NS2 protease stimulation was also included to show the extent of NS2-NS3 cleavage without NS2 protease activation by NS3 (Isken et al., 2015). Accordingly, WT-like NS2-NS3 cleavage efficiencies would mark residues not critical for the NS2 protease activation, while mutations with an impact on NS2-NS3 cleavage comparable to the NS3/YPL-AAA mutant would identify NS2 amino acids potentially involved in the NS3-mediated NS2 protease activation process. NS2-NS3 cleavage was analyzed in a replication-independent cell-based cleavage assay based on Huh7-T7 cells and T7^{pol}-mediated expression from pCITE Flag-NS2-NS3$_{(1-172)}$-GST/BK derivatives (Fig. 15C). The uncleaved Flag-NS2-NS3$_{(1-172)}$-GST polyprotein fragment and the products of NS2-mediated cleavage (Flag-NS2 and NS3$_{(1-172)}$-GST) were separated by SDS-PAGE and analyzed by western blot using Flag- and GST-specific antibodies, respectively (Fig. 15D). Western blot signal intensities of uncleaved Flag-NS2-NS3$_{(1-172)}$-GST and cleaved Flag-NS2 were determined using the ImageJ software to calculate the individual NS2-NS3 cleavage rates (Fig. 15E). As expected, Flag-NS2-NS3$_{(1-172)}$-GST/BK WT exhibited efficient NS2-NS3 cleavage, while the C184A mutant did not show detectable cleavage (Fig. 15D+E). In the case of NS3/YPL-AAA only residual NS2 protease activity was detected marking the intrinsic NS2 protease activity in the absence of NS3 activation (Fig. 15D+E; Isken et al., 2015). The alanine scanning mutagenesis revealed that most of the tested NS2 mutations had no (L90A, I97A, F103A, V104A, L115A, V119A) or moderate negative (L135A, N142A, T145A, V160A) effects on NS2-NS3 cleavage (Fig. 15D+E). In contrast, Y141A and P146A inhibited NS2-NS3 cleavage similar to the active site mutant C184A, indicating that either the active site configuration or NS2 protein conformation is affected. Interestingly, the NS2 L144A and L147A mutations did show a very low level of NS2-NS3 cleavage, comparable to the NS3/YPL-AAA mutant and thus appear to block NS3-mediated NS2 stimulation in a manner similar to the NS3/YPL-AAA mutant (Fig. 15D+E).

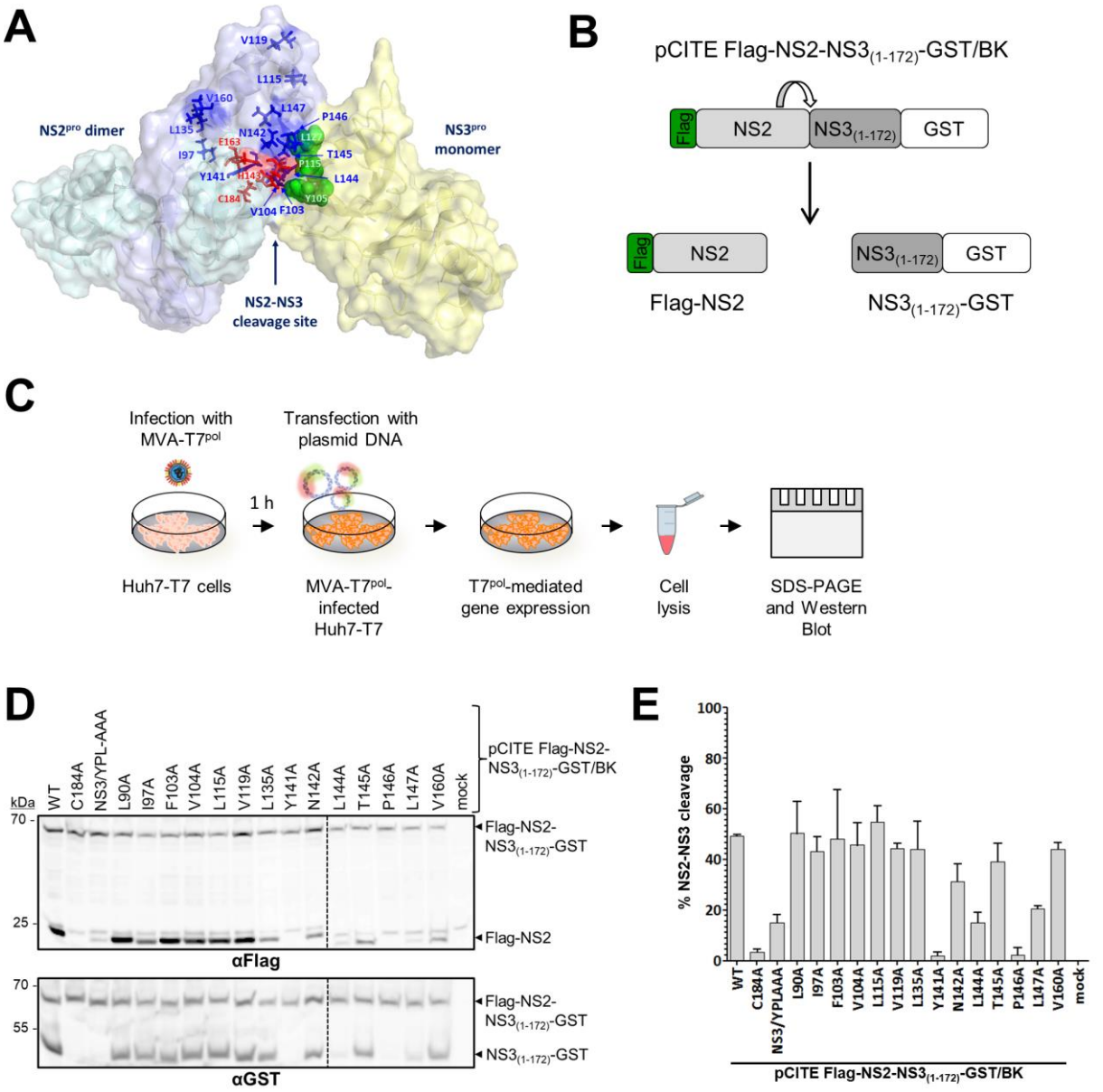

Fig. 15: Mapping of NS2 determinants important for NS3-mediated NS2 protease activation by alanine scanning mutagenesis. (**A**) Selection of NS2 protease surface residues for alanine scanning mutagenesis based on hypothetical NS2^{pro}-NS3^{pro} precursor model (also see Fig. 14). One NS2^{pro} composite active site is shown with H143, E163 and C184 in red. The NS2 protease-activating NS3 surface residues Y105, P115 and L127 are shown as green spheres. The NS2-NS3 cleavage site is indicated. The analyzed NS2 protease surface residues are depicted as blue stick drawings. (**B**) Scheme of NS2-NS3 cleavage analysis using the pCITE Flag-NS2-NS3$_{(1-172)}$-GST/BK expression construct. (**C**) Schematic depiction of the experimental setup. (**D**) Western blot analysis of NS2-NS3 cleavage after expression of Flag-NS2-NS3$_{(1-172)}$-GST polyprotein fragments in MVA-T7^{pol}-infected Huh7-T7 cells and harvest 20 h pt. One representative blot from three independent experiments is shown. Molecular mass standards in kDa are shown on the left. Positions of the uncleaved precursor Flag-NS2-NS3$_{(1-172)}$-GST and cleavage products Flag-NS2 or NS3$_{(1-172)}$-GST are indicated on the right. Dashed lines indicate separate western blots. (**E**) NS2 protease cleavage efficiencies. Signals of uncleaved Flag-NS2-NS3$_{(1-172)}$-GST and the cleavage products Flag-NS2 and NS3$_{(1-172)}$-GST were quantified by ImageJ software from western blots to calculate the percentage of NS2-NS3 cleavage. Mean and standard deviations of NS2 cleavage efficiencies from three independent experiments are presented. WT: wild-type; mock: transfection control without plasmid DNA.

5.2.3 Analysis of NS2 surface mutations with respect to NS2-NS3 cleavage in the absence of the NS3 cofactor revealed that the F103A mutation stimulates intrinsic NS2 autoprotease activity

The observed interference of the L144A or L147A mutations with the NS3-mediated NS2 stimulation during NS2-NS3 cleavage (Fig. 15D+E) indicates that these mutations might block crucial interactions between activating NS2 and NS3 surface residues critical for this process. However, the inefficient cleavage between NS2-NS3 could also result from disruption of the NS2 active site configuration due to the close proximity of the mutated NS2 residues to the NS2 active site H143. Accordingly, the set of NS2 mutations was analyzed for their effect on intrinsic NS2 protease activity in the absence of the NS3 cofactor to exclude direct effects on the NS2 protease unrelated to NS2 activation by NS3. For this purpose, the pCITE Flag-NS2-APIT-GST/BK construct was used, in which C-terminal to Flag-NS2 the first four NS3 amino acids (APIT) are fused to obtain the authentic NS2-NS3 cleavage site, followed by GST to allow monitoring of NS2 cleavage activity (Fig. 16A). Cleavage of Flag-NS2-APIT-GST is mediated by the intrinsic NS2 protease activity. All NS2 mutations analyzed before were introduced in this construct, generating the respective pCITE Flag-NS2-APIT-GST/BK derivatives. Again, $T7^{pol}$-mediated gene expression in Huh7-T7 cells was used to produce WT and mutant Flag-NS2-APIT-GST proteins to monitor NS2 cleavage efficiencies by western blotting with Flag-specific antibodies (Fig. 16B). As a reference for efficient NS2-NS3 cleavage Flag-NS2-$NS3_{(1-172)}$-GST/BK WT was employed. To determine cleavage rates of the individual variants, intensities of western blot signals for uncleaved Flag-NS2-APIT-GST and cleaved Flag-NS2 were determined using the ImageJ software (Fig. 16C).

As expected, Flag-NS2-APIT-GST WT showed only the weak cleavage characteristic of intrinsic NS2 protease activity (Fig. 16B+C). No intrinsic activity was detected for the Flag-NS2-APIT-GST C184A negative control mutant (Fig. 16B+C), confirming the specificity of this assay. The NS2 mutations L90A, I97A, V104A, L115A, N124A, L144A T145A and V160A showed slightly reduced intrinsic NS2 protease activities in the absence of NS3 compared to WT (Fig. 16B+C). Furthermore, the Y141A, P146A and L147A mutations either fully abolished (Y141A and P146A) or strongly reduced (L147A) intrinsic NS2 protease activity in Flag-NS2-APIT-GST context (Fig. 16B+C) suggesting a rather defective NS2 protease. The observation that the L144A exchange supports intrinsic NS2 protease activity is indicating that (i) the NS2 protease is functional and (ii) the strong reduction of NS2-NS3 cleavage in the NS2-$NS3_{(1-172)}$ context (Fig. 15D+E) is likely the consequence of the L144A-mediated interference with the NS2 protease activation by NS3. Together these results

suggest that L144 represents a NS2 surface residue important for the NS3-mediated NS2 activation.

Another interesting observation from this analysis was that mutation F103A led to an increased NS2 protease activity in the absence of the NS3 cofactor compared to WT Flag-NS2-APIT-GST (Fig. 16B+C).

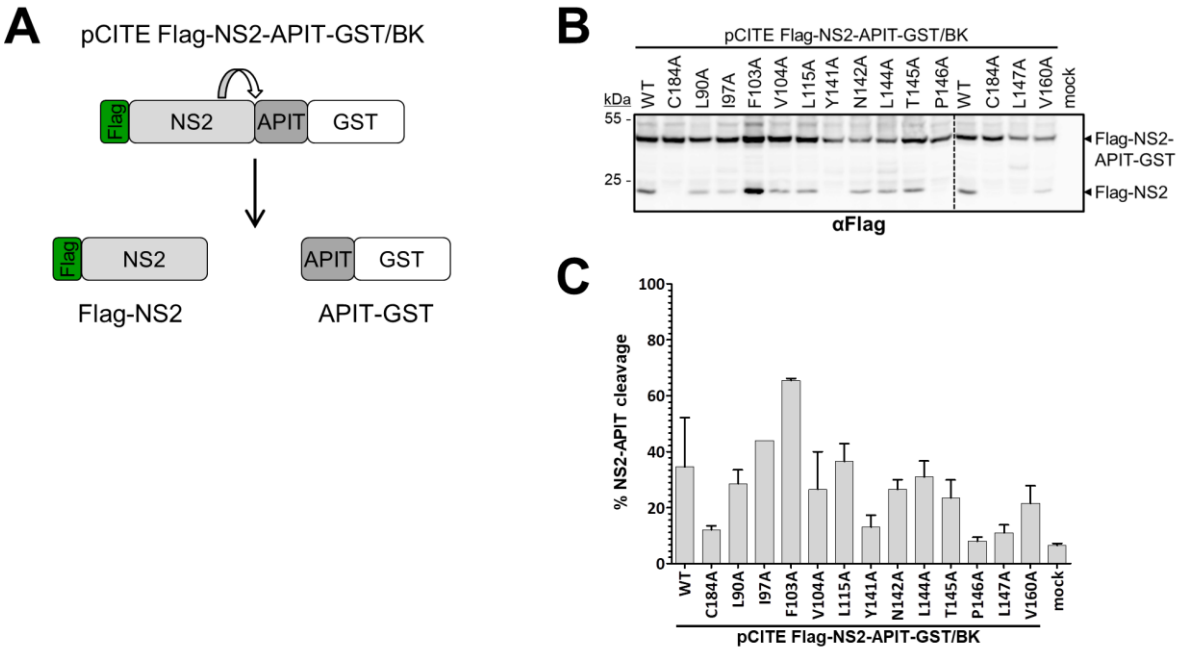

Fig. 16: Re-analysis of NS2 protease surface residues in the absence of the NS3 cofactor revealed F103A as a stimulating determinant for the intrinsic NS2 protease activity. (**A**) Schematic representation of the pCITE Flag-NS2-APIT-GST/BK expression construct used to analyze the intrinsic NS2 protease activity in the absence of its cofactor NS3. Cleavage of Flag-NS2-APIT-GST results in generation of Flag-NS2 and APIT-GST. (**B**) Indicated pCITE Flag-NS2-APIT-GST plasmids were transfected into MVA-T7^{pol}-infected Huh7-T7 cells and harvested 20 h pt. One representative western blot from three independent experiments is shown. Molecular mass standards in kDa are shown on the left. Positions of the Flag-NS2-APIT-GST and the cleavage product APIT-GST are indicated on the right. WT: wild-type; mock: transfection control without DNA. Dashed lines indicate separate western blots. (**C**) NS2 protease cleavage efficiencies. Western blot signals of uncleaved Flag-NS2-APIT-GST and cleavage product Flag-NS2 were quantified using the ImageJ software to calculate the percentage of Flag-NS2-APIT-GST cleavage. Mean and standard deviations of NS2 cleavage efficiencies from three independent experiments are presented.

5.2.4 Permutation analysis of NS2 L144 in the absence of the NS3 cofactor showed that L144I stimulates intrinsic NS2 protease activity

The surprising finding that the F103A mutation increases the intrinsic NS2 protease activity suggests that certain NS2 mutations may have the ability to either induce optimizations of the cleavage site positioning and/or active site conformation in the absence of the NS3 cofactor. Mechanistically, such mutations might mimic NS2 alterations induced by NS3 in the NS2-NS3 precursor resulting in efficient NS2 activity. Considering the importance of the L144A

exchange for NS2 activation by NS3 (Fig. 15D+E), the NS2 position 144 was further investigated to determine whether amino acid exchanges could also increase intrinsic NS2 protease activity. Accordingly, a panel of NS2 L144 permutations in the context of Flag-NS2-APIT-GST/BK was analyzed for their impact on the intrinsic NS2 protease activity in the absence of the NS3 cofactor (Fig. 17). The Flag-NS2-APIT-GST L144 derivatives were expressed in MVA-T7^{pol}-infected Huh7-T7 cells and NS2 protease activity was analyzed by western blotting. The expression of Flag-NS2-APIT-GST WT and Flag-NS2-APIT-GST C184A served as positive and negative control for intrinsic NS2 protease activity, respectively.

Whereas most of the L144 permutations analyzed (L144A, L144D, L144G, L144M and L144N, L144Q, L144P and L144W) impaired intrinsic NS2 protease activity in the Flag-NS2-APIT-GST context to varying degrees (Fig. 17), the exchange of L144 to isoleucine (L144I) massively stimulated the intrinsic NS2 protease activity compared to WT (Fig. 17). L144V also allowed moderate stimulation of intrinsic NS2 protease activity (Fig. 17).

Accordingly, two amino acid exchanges in the NS2 protease domain (F103A and L144I) were identified that have the ability to stimulate the intrinsic NS2 protease activity.

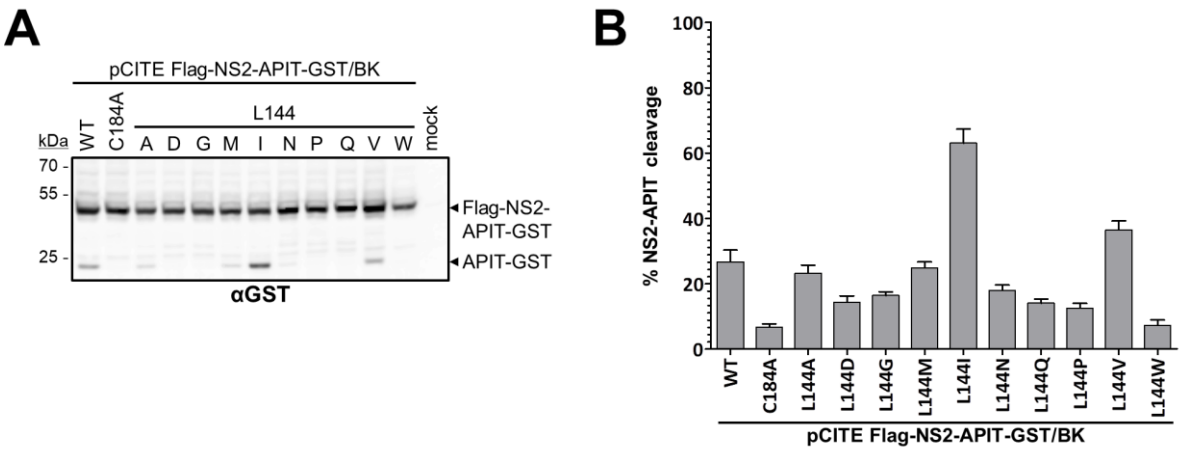

Fig. 17: The amino acid exchange L144I is stimulating the intrinsic NS2 protease cleavage efficiency in the absence of the NS3 cofactor. (**A**) Analysis of the intrinsic NS2 protease activity in the MVA-T7^{pol} expression system in Huh7-T7 cells. NS2-mediated cleavage of Flag-NS2-APIT-GST derivatives was analyzed by western blotting using GST-specific antibodies. One representative blot from three independent experiments is shown. Molecular mass standards in kDa are shown on the left. Positions of the uncleaved precursor Flag-NS2-APIT-GST and the cleavage product APIT-GST are indicated on the right. (**B**) NS2 protease cleavage efficiencies. Signals of uncleaved Flag-NS2-APIT-GST and the cleavage product APIT-GST were quantified using the ImageJ software from western blots to calculate the percentage of NS2-APIT-GST cleavage. Mean and standard deviations of NS2 cleavage efficiencies from three independent experiments are presented. WT: wild-type; mock: transfection control without plasmid DNA.

5.2.5 Comparison of NS2 F103 and L144 mutations revealed different requirements for intrinsic NS2 protease activity at these positions

The finding that two different NS2 mutations can stimulate the intrinsic NS2 protease activity is intriguing since it may provide insight into the NS2 protease stimulation process. To also determine the amino acid characteristics at NS2 position 103 critical for efficient intrinsic NS2 protease activity, F103 permutations were introduced into pCITE Flag-NS2-APIT-GST/BK. The Flag-NS2-APIT-GST F103 derivatives were expressed in MVA-T7^{pol}-infected Huh7-T7 cells and NS2 protease activity was analyzed by western blotting. Flag-NS2-APIT-GST WT and C184A served as positive and negative control, respectively.

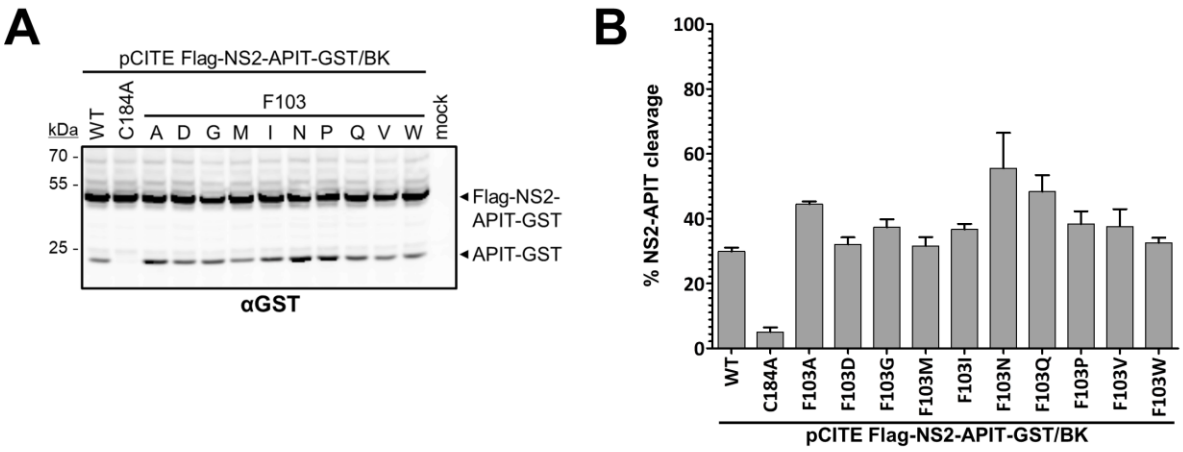

C

Hepacivirus species (host)	NS2 position	
HCV (human)	F103	L144
NPHV (equine)	L103	L144
BHV (bat)	N103	L144
GHV (old world primate)	R100	L141
RHV (rodent)	K92	L132
GBV-B (new world primate)	D97	L139

Fig. 18: Permutation analysis of HCV NS2 F103 revealed a broad spectrum of amino acids that enable intrinsic NS2 protease cleavage. (**A**) Analysis of the intrinsic NS2 protease activity in the MVA-T7^{pol} expression system in Huh7-T7 cells. NS2-mediated cleavage of Flag-NS2-APIT-GST was analyzed by western blotting using GST-specific antibodies. Molecular mass standards in kDa are shown on the left. Positions of the uncleaved precursors Flag-NS2-APIT-GST and the cleavage product APIT-GST are indicated on the right. WT: wild-type; mock: transfection control without plasmid DNA. (**B**) NS2 protease cleavage efficiencies. Signals of uncleaved Flag-NS2-APIT-GST and the cleavage product APIT-GST were quantified using the ImageJ from western blots to calculate the percentage of NS2-APIT-GST cleavage. Mean and standard deviations of NS2 cleavage efficiencies from three independent experiments are presented. (**C**) Conservation of residues corresponding to HCV NS2 F103 and L144 in indicated mammalian hepacivirus species (according to Boukadida et al., 2018).

In contrast to the strict requirement for branched aliphatic amino acids observed for NS2 position 144 (Fig. 17), all analyzed F103 permutations showed a similar (F103D, F103G, F103M, F103I, F103P, F103V, F103W) or slightly higher (F103A, F103N, F103Q) intrinsic NS2 protease activity when compared to WT (Fig. 18A+B). Accordingly, there is a broad

functional flexibility for NS2 position 103 to allow intrinsic NS2 protease activity. Thus, these results demonstrate striking differences regarding the required amino acid characteristics at these two positions concerning NS2 protease functionality.

These observations are supported by the comparison of HCV NS2 ($NS2_{HCV}$) with NS2 sequences of different hepaciviruses ($NS2_{hepaci}$) showing a strong conservation for leucine at positions corresponding to $NS2_{HCV}$ L144 while at positions corresponding to $NS2_{HCV}$ F103 amino acids with different side-chain characteristics can be found in different $NS2_{hepaci}$ sequences (Fig. 18C; Boukadida et al., 2018).

5.2.6 Combination of F103A and L144I exchanges increases the stimulation of intrinsic NS2 protease activity in two HCV genotypes

The next step was to analyze whether the stimulation of the intrinsic NS2 protease activity by the F103A and L144I mutations is conserved among different HCV genotypes and if a combination of both exchanges would further increase the intrinsic NS2 protease activity. To this end, these mutations were introduced individually and in combination into Flag-NS2-APIT-GST/JFH1 (genotype 2a; gt.2a) and their effect on intrinsic NS2 protease activity was determined side-by-side with their respective BK strain (genotype 1b; gt.1b) derivatives (Fig. 19). The Flag-NS2-APIT-GST/BK or JFH1 derivatives were expressed in MVA-$T7^{pol}$-infected in Huh7-T7 cells. The respective Flag-NS2-$NS3_{(1-172)}$-GST variants were used as references for efficient NS2-NS3 cleavage. NS2 protease cleavage rates were determined from lysates subjected to immunoblotting using infrared fluorescence-labeled secondary antibodies and quantified using the LI-COR Odyssey SA imaging system.

The comparison of the NS2 protease activities of the two genotypes showed that the NS2 protease of the JFH1 strain in the presence of the NS3 cofactor (Flag-NS2-$NS3_{(1-172)}$-GST/JFH1-WT) achieved almost complete NS2-$NS3_{(1-172)}$ cleavage with no detectable Flag-NS2-$NS3_{(1-172)}$-GST precursor protein. In contrast, NS2 protease of the BK strain cleaved only approximately 80% of the Flag-NS2-$NS3_{(1-172)}$-GST precursor protein (Fig. 19; compare Flag-NS2-$NS3_{(1-172)}$-GST/JFH1 WT with Flag-NS2-$NS3_{(1-172)}$-GST/BK WT). This difference can be partly attributed to more efficient intrinsic NS2 protease activity of JFH1 in contrast to BK (Fig. 19; compare Flag-NS2-APIT-GST/JFH1 WT with Flag-NS2-APIT-GST/BK WT). As expected, the NS2 C184A mutant is deficient in supporting NS2-APIT cleavage in both genotypes (Fig. 19). The introduction of either NS2 F103A or NS2 L144I mutations resulted in an increased NS2 intrinsic protease activity relative to Flag-NS2-APIT-GST WT of both genotypes (Fig. 19; see Flag-NS2-APIT-GST/JFH1 F103A and L144I as well as Flag-NS2-APIT-GST/BK F103A and L144I).

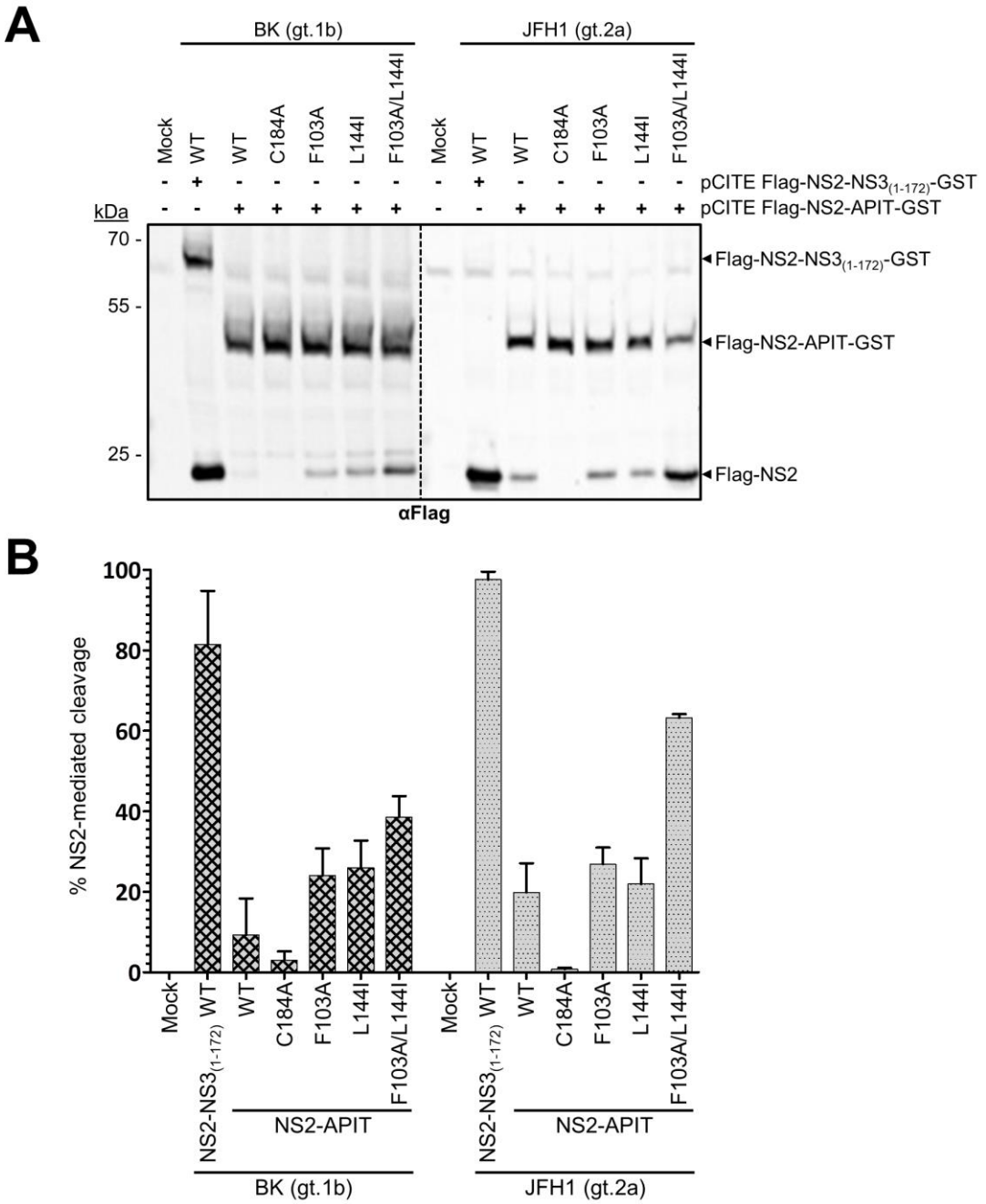

Fig. 19: The amino acid exchanges F103A and L144I lead to stimulation of the intrinsic NS2 protease cleavage efficiency in the absence of the NS3 cofactor in two different HCV genotypes. (**A**) Analysis of the intrinsic NS2 protease activity using the MVA-T7^{pol} expression system in Huh7-T7 cells. NS2-mediated cleavage of Flag-NS2-NS3$_{(1-172)}$-GST or Flag-NS2-APIT-GST polyprotein fragments was analyzed by western blotting using Flag-specific antibodies. One representative western blot from three independent experiments is shown. Molecular mass standards in kDa are shown on the left. Positions of the uncleaved precursors Flag-NS2-NS3$_{(1-172)}$-GST or Flag-NS2-APIT-GST and cleavage product Flag-NS2 are indicated by arrows on the right. Dashed lines indicate separate western blots. (**B**) Quantification of efficiencies of NS2 protease-mediated cleavage (percentage of NS2-mediated cleavage, calculated as percentage of cleavage product to the sum of uncleaved precursor and cleavage product) from lysates subjected to immunoblotting using infrared fluorescent-labeled secondary antibodies and the LI-COR Odyssey SA imaging system. Background was subtracted from Flag-specific signals of uncleaved precursors and cleavage product using the corresponding signal of the mock sample. Mean and standard deviation of NS2 cleavage efficiencies from three independent experiments are presented. WT: wild-type; mock: transfection control without plasmid DNA.

Interestingly, the combination of both NS2 mutations (F103A/L144I) resulted in an approximately 3- to 4-fold increase in NS2-APIT cleavage efficiency when compared to the WT (Fig. 19B). In the context of genotype 2a, the F103A/L144I combination resulted in a remarkably efficient NS2-APIT cleavage of approx. 65% (Fig. 19B). Taken together, these observations demonstrate that the stimulating effect of F103A/L144I amino acid exchanges on the intrinsic NS2 protease activity is conserved between different HCV genotypes (Fig. 19). The ability of the double mutation F103A/L144I to strongly increase the intrinsic NS2 protease activity suggests that the functional roles of F103 and L144 might be mechanistically linked.

5.2.7 The stimulating NS2 protease mutations F103A and L144I enhance the intrinsic proteolytic NS2 activity in absence of any NS3 sequence

It has been previously reported that HCV NS2 exhibits efficient intrinsic activity in the absence of any NS3 sequence and that NS3-specific amino acids immediately downstream of NS2 (NS3/APITA) reduce NS2 protease function to basal levels that require NS3 cofactor-mediated stimulation for efficient NS2-NS3 cleavage (Boukadida et al., 2018). Based on these observations, it has been proposed that the N-terminal sequence of NS3 has a modulatory effect on NS2-NS3 cleavage that is compensated by specific hydrophobic surface residues in the NS3 protease domain, resulting in stimulation of the NS2 protease by NS3 (Boukadida et al., 2018; Isken et al., 2015). To determine whether the stimulatory effect of the F103A and L144I mutations on NS2 protease activity in the Flag-NS2-APIT-GST context compensates for the negative influence of the NS3 N-terminal APIT sequence, the influence of the F103A and L144 mutations on the stimulation of NS2 protease activity in the absence of any NS3-derived sequence was analyzed. Both mutations were inserted either separately or in combination into the pCITE Flag-$NS2_{JFH1}$-4GS-eYFP construct (Fig. 20A). In this construct Flag-$NS2_{JFH1}$ is followed by the amino acid linker sequence GGGGS (4GS) and eYFP so that the NS2-NS3 cleavage site is replaced by a cleavage site with no similarity to the authentic NS2-NS3 cleavage site, which allows evaluation of the intrinsic basal NS2 protease activity in the absence of any NS3 moiety. The Flag-$NS2_{JFH1}$-4GS-eYFP derivatives were expressed in MVA-$T7^{pol}$-infected Huh7-T7 cells. The effect of the amino acid exchanges F103A, L144I or F103A/L144I was determined from lysates subjected to immunoblotting using infrared fluorescence-labeled secondary antibodies and quantified using the LI-COR Odyssey SA imaging system (Fig. 20). The WT construct and the C184A mutant served as positive and negative control, respectively.

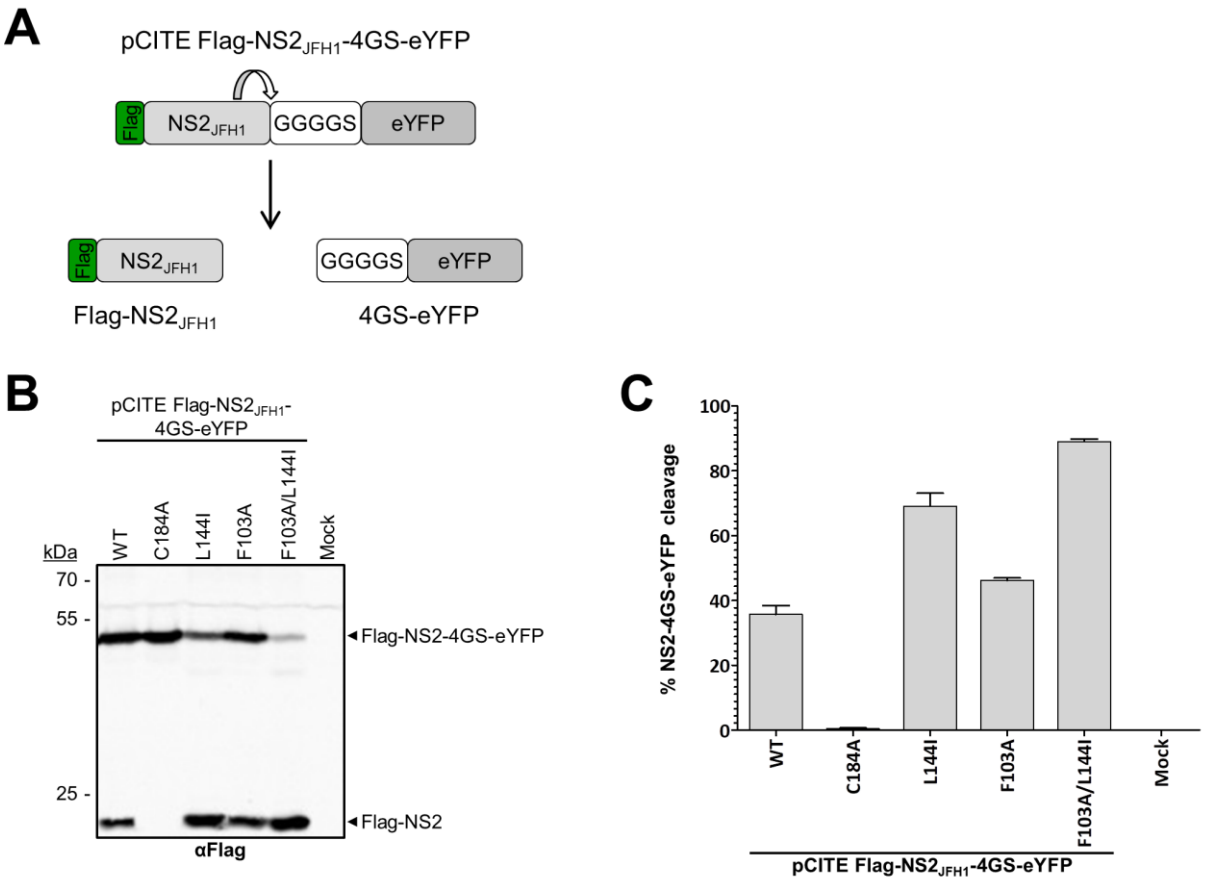

Fig. 20: HCV NS2 protease activity in the absence of any NS3 sequence is stimulated by NS2 mutations F103A and L144I. (**A**) Scheme of pCITE Flag-NS2$_{JFH1}$-4GS-eYFP reporter construct to analyze NS2 protease activity in the absence of any NS3 sequence using a flexible linker (GGGGS). (**B**) The indicated plasmids were transfected into MVA-T7^{pol}-infected Huh7-T7 cells. Transfected cells were harvested 20h pt and NS2 protease activity was analyzed by western blotting using Flag-specific primary antibodies. One representative blot from three independent experiments is shown. Molecular mass standards in kDa are shown on the left. The positions of the uncleaved precursor Flag-NS2-4GS-eYFP and the cleavage product Flag-NS2 are indicated by arrows on the right. (**C**) NS2 protease cleavage efficiencies. Western blot signals generated by using Flag-specific primary and infrared fluorescent-labeled secondary antibodies were quantified using the LI-COR Odyssey SA imaging system. Mean and standard deviations of NS2 cleavage efficiencies from three independent experiments are presented. WT: wild-type; mock: transfection control without DNA.

Robust NS2 cleavage activity (approx. 35%) could be detected with the Flag-NS2$_{JFH1}$-4GS-eYFP WT construct (Fig. 20B+C) confirming earlier observations (Boukadida et al., 2018). Furthermore, the stimulating character of the individual NS2 F103A or L144I amino acid exchanges was also observed in absence of any NS3 sequence (Fig. 20B+C). Interestingly, the F103A mutation increased NS2 protease cleavage efficiency in the NS2$_{JFH1}$-4GS-eYFP context only slightly from 35% to approx. 50%, while the introduction of the L144I amino acid exchange resulted in a stronger improvement (to approx. 70%) of the intrinsic NS2 protease activity (Fig. 20B+C). Importantly, the combination of both mutations (F103A/L144I) led to approximately 90% NS2 cleavage efficiency (Fig. 20B+C).

5.2.8 The L144I mutation is activating the intrinsic NS2 protease activity in other mammalian hepaciviruses

Comparative studies of several mammalian hepaciviruses have been useful to identify conserved or divergent features of NS2 protein function(s) (Boukadida et al., 2014, 2018). Alignment of different mammalian hepaciviruses revealed that residues corresponding to HCV L144 are conserved among these viruses suggesting a functional importance for this residue (Fig. 18C; Boukadida et al., 2018). Therefore, the next step was to investigate whether the ability of the L144I exchange to activate the intrinsic NS2 protease activity is also conserved in related mammalian hepaciviruses. To this end, hepaciviral NS2 proteins from the equine hepacivirus (NPHV) strain H3-011, which is more closely related to HCV, and from the rodent hepacivirus (RHV) strain NLR07-oct70, which is more distantly related to HCV (Fig. 21A), were examined. The Leucine-to-isoleucine mutation was introduced into pCITE Flag-$NS2_{RHV}$-4GS-eGFP and pCITE Flag-$NS2_{NPHV}$-4GS-eGFP constructs at positions corresponding to HCV NS2 L144 ($NS2_{NPHV}$ L144I and $NS2_{RHV}$ L132I) (Fig. 21B). The autoproteolytic properties of $NS2_{NPHV}$-4GS-eGFP L144I or $NS2_{RHV}$-4GS-eGFP L132I were compared with their respective WT derivatives after transient expression in MVA-$T7^{pol}$-infected Huh7-T7 cells. Flag-$NS2_{JFH1}$-4GS-eGFP WT and L144I were used as references. The respective NS2 protease activities were analyzed by western blotting using a Flag-specific antibody. Interestingly, the intrinsic activity of both RHV and NPHV NS2 proteases could be stimulated by a factor of 2 by $NS2_{NPHV}$ L144I and $NS2_{RHV}$ L132I exchanges similarly to $NS2_{JFH1}$ L144I (Fig. 21B+C). Accordingly, these observations suggest that $NS2_{JFH1}$ L144 and corresponding residues in other mammalian hepaciviruses ($NS2_{NPHV}$ L144 and $NS2_{RHV}$ L132) represent a conserved functional determinant for the activation of the intrinsic NS2 protease activity.

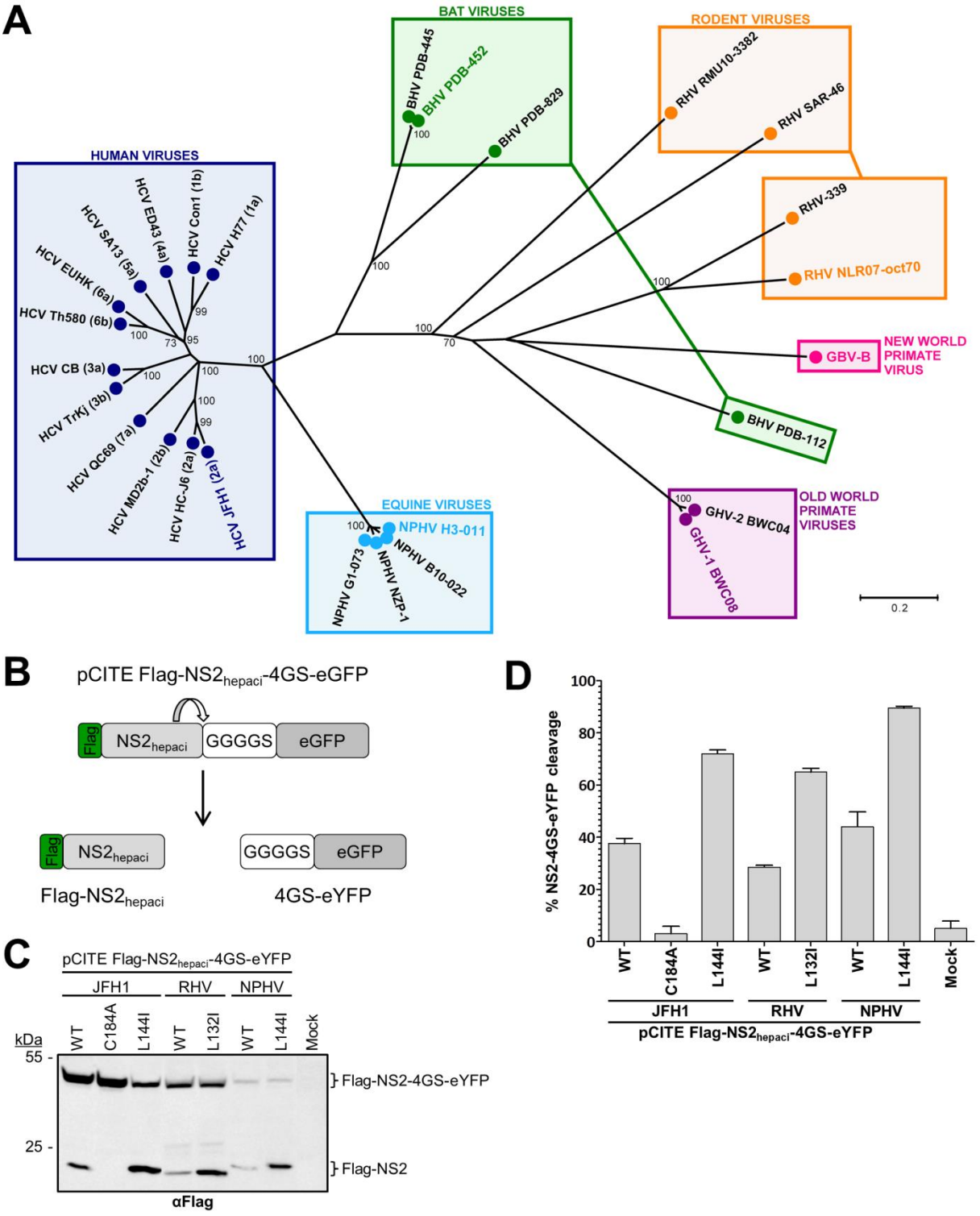

Fig. 21: The L144I exchange is activating the intrinsic NS2 protease activity in different related mammalian hepaciviruses. (**A**) Phylogenetic tree representation of phylogenetic analysis of NS2 and NS3 N-terminal domain ($NS3_N$) of selected *Hepacivirus* members (adapted from Boukadida et al., 2018). Clustering of viruses according to their hosts is represented by colored boxes. The strains HCV JFH1 (gt.2a), NPHV H3-011, and RHV NLR07-oct70 used in this section are highlighted in dark blue, light blue, and orange, respectively, according to their cluster. (**B**) Scheme of pCITE Flag-$NS2_{hepaci}$-4GS-eGFP reporter construct to analyze the intrinsic NS2 protease activity in related mammalian hepaciviruses. (**C**) Indicated pCITE Flag-$NS2_{hepaci}$-4GS-eGFP derivatives were transfected into MVA-$T7^{pol}$-infected Huh7-T7 cells. 20 h pt, transfected cells were harvested into lysis buffer and NS2 protease activity was analyzed by western blot analysis using Flag-specific antibodies. One representative blot from three independent experiments is shown. Molecular mass standards in

kDa are shown on the left. The positions of the uncleaved precursor Flag-NS2$_{hepaci}$-4GS-eGFP and cleavage product Flag-NS2 are indicated by arrows on the right. (**D**) NS2 protease cleavage efficiencies (percentage of NS2-4GS-eYFP cleavage, calculated as percentage of cleavage product to the sum of uncleaved precursor and cleavage product) determined from lysates subjected to immunoblotting using infrared fluorescence-labeled secondary antibodies and the LI-COR Odyssey SA imaging system. Background was subtracted from Flag-specific signals of uncleaved precursors and cleavage products using the corresponding signal of the mock sample. Mean and standard deviations of NS2 cleavage efficiencies from three independent experiments are presented. WT: wild-type; mock: transfection control without DNA.

5.2.9 Mutations stimulating NS2 autoprotease modulate viral RNA replication of an NS2-3' replicon

The observation that the NS2 protease has efficient intrinsic proteolytic activity in the absence of the NS3 cofactor suggests that the NS3 protease domain acts as a regulatory rather than essential cofactor for NS2 to kinetically control NS2-NS3 cleavage (Boukadida et al., 2018; Fig. 20). To determine whether the presence of the activating NS2 mutations F103A and L144I stimulates polyprotein processing and thereby influences RNA replication, their effect was analyzed in the pFKI-389 FLuc NS2-3'/JFH1 replicon context (Fig. 22).

Accordingly, the FKI-389 FLuc NS2-3'/JFH1 replicon derivatives F103A, L144A, L144I and F103A/L144I were generated (Fig. 22A). The WT and the NS2/C184A variant served as positive and negative control, respectively. *In vitro* transcribed replicon RNAs were electroporated into Huh7 Lunet cells, and the NS2-NS3 cleavage efficiency and RNA replication capacities were determined by western blotting and luciferase assay, respectively (Fig. 22A). As expected, the western blot analysis showed that WT NS2 supported efficient NS2-NS3 cleavage, while the NS2 active site mutation C184A completely blocked NS2-NS3 cleavage (Fig. 22B+C). The NS2 exchanges F103A and L144I exhibited NS2 -NS3 cleavage efficiencies comparable to WT while the NS2 L144A mutation reduced NS2-NS3 cleavage to a degree allowing the detection of uncleaved NS2-NS3 (Fig. 22B), which is in line with earlier results (Fig. 15B). Interestingly, the combination of both activating NS2 exchanges (F103A/L144I) in the context of the NS2-5B polyprotein resulted in an inefficient NS2-NS3 cleavage with detectable levels of NS2-NS3 precursor protein (Fig. 22B+C).

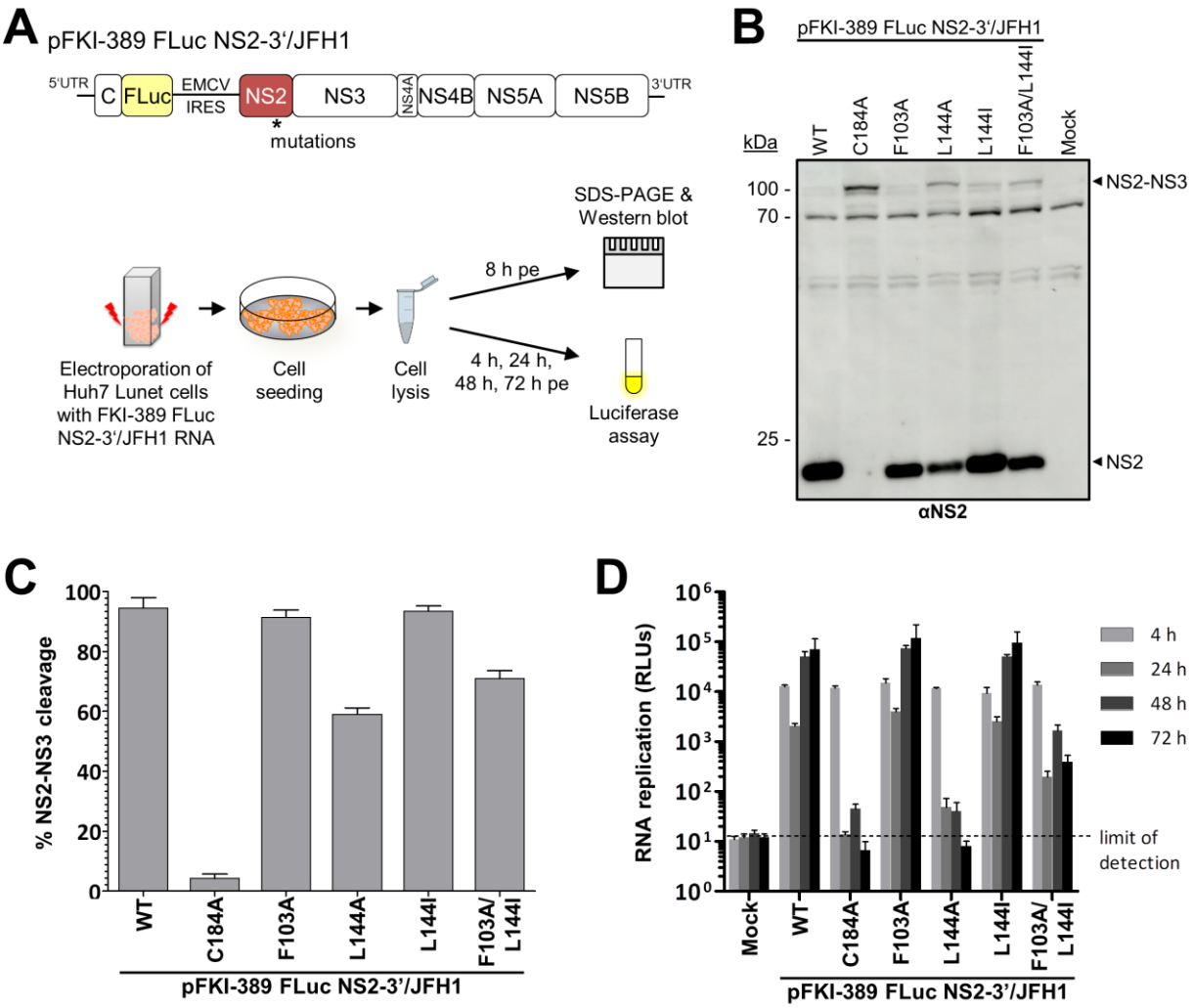

Fig. 22: The NS2 F103A/L144I double mutation reduces NS2-NS3 cleavage efficiency in the NS2-NS5B context and inhibits robust RNA replication of a NS2-3'/JFH1 replicon. (**A**) Scheme of experimental setup. Huh7 Lunet cells were electroporated with 10 µg of respective FKi-389 FLuc-NS2-3'/JFH1 RNAs. Cells were harvested at indicated time points pe either into SDS sample buffer for analysis by SDS-PAGE and western blot or into passive lysis buffer for luciferase assay. (**B**) NS2-NS3 cleavage was monitored by western blotting using an NS2-specific antibody detecting HCV NS2-NS3 and NS2. One representative blot from three independent experiments is shown. Molecular mass standards in kDa are indicated on the left. The positions of the uncleaved precursor NS2-NS3 and cleavage product NS2 are indicated by arrows on the right. (**C**) Quantification of cleavage rates (% NS2-NS3 cleavage) were performed on 3 independent experiments subjected to infrared fluorescent immunoblot imaging. Mean and standard deviations of NS2-NS3 cleavage efficiencies are presented. (**D**) Determination of viral replication. HCV RNA replication kinetics were quantified 4, 24, 48 and 72 hours pe by measuring firefly luciferase activity (relative light units, RLU). Graphs are representative results of three independent experiments with standard deviations. WT: wild-type; mock: electroporation control without RNA.

RNA replication of the bicistronic FKI-389 FLuc NS2-3'/JFH1 F103A and L144I replicon derivatives was similar to WT in agreement with their observed efficient NS2-NS3 cleavage (Fig. 22D). In contrast, replication of the FKI-389 FLuc NS2-3'/JFH1 L144A replicon was blocked correlating with its inefficient NS2-NS3 cleavage (Fig. 22D). Interestingly, replication of FKI-389 FLuc NS2-3'/JFH1 F103A/L144I was approximately 50- to 150-fold lower compared with WT, F103A, or L144I replicon at 48 h and 72 h pe (Fig. 22D).

5.2.10 Evidence for a functional cooperation of NS2 and NS3 surface residues during NS3-mediated NS2 protease stimulation

$NS2_{HCV}$-mediated NS2-NS3 cleavage has been shown to be stimulated by heterologous hepaciviral NS3 protease domains ($NS3_N$) from NPHV, BHV, and RHV, but only very weakly by $NS3_N$ from GHV or GBV-B, suggesting that specific requirements exist for activating residues within the hydrophobic NS3 surface patch (Boukadida et al., 2018). Interestingly, $NS3_{HCV}$ residue P115 is conserved in the activating NS3 protease domains of NPHV, BHV and RHV, whereas it aligns with a negatively charged glutamic acid residue in NS3 of GHV (E116) and GBV-B (E115) (Fig. 23A). A substantial gain-of-function of the $NS3_{GHV}$ protease domain as stimulating cofactor for HCV NS2 in a chimeric $NS2_{HCV}$-$NS3_{GHV}$ precursor could be achieved by substituting the GHV-specific E116 with an HCV-equivalent proline (E116P) supporting the importance for hydrophobic surface interactions between the NS3 surface patch and NS2 protease during NS2 stimulation by NS3 (Boukadida et al., 2018). Accordingly, this $NS2_{HCV}$-$NS3_{GHV}$ chimera represents an excellent tool to further dissect potential NS2-NS3 surface interactions during NS3-mediated NS2 stimulation.

Therefore, this chimera was used to investigate the functional interaction between NS2 and NS3 surface residues. Based on two observations, it was hypothesized that $NS2_{HCV}$ F103 might interact with the $NS3_{GHV}$ residue corresponding to $NS3_{HCV}$ P115 to form a functional interaction pair at the NS2-NS3 surface interface that supports NS3-mediated NS2 protease stimulation: (i) in the hypothetical NS2-NS3 precursor model, $NS2_{HCV}$ F103 has the potential to interact with $NS3_{HCV}$ P115 (Fig. 15A) and (ii) in GHV the residues corresponding to $NS2_{HCV}$ F103 and $NS3_{HCV}$ P115 are charged residues ($NS2_{GHV}$ R100 and $NS3_{GHV}$ E116) that could potentially form a salt bridge (Fig. 23A). To test whether the surface residues at $NS2_{HCV}$ position 103 and $NS3_{GHV}$ position 116 could functionally interact with each other in support of efficient NS2-NS3 processing, NS2-NS3 cleavage of chimeric Flag-$NS2_{JFH1}$-$NS3_{GHV}$-GST precursor variants (Fig. 23B), with different NS2-NS3 interaction pair combinations at these positions, was determined. NS2 protease activity of these mutant chimeric precursors was examined following to transient expression in MVA-$T7^{pol}$-infected Huh7-T7 cells. The respective NS2 and/or NS3 residues were mutated to create potential NS2-NS3 surface interaction pairs representing the GHV-GHV (F103R / E116), the HCV-HCV (F103 / E116P) as well as the chimeric GHV-HCV (F103R / E116P) and the HCV-GHV (F103 / E116) situations (Fig. 23C). As a negative control an NS2 active site mutation ($NS2_{JFH1}$/C184A) was introduced in the chimeric NS2-NS3 precursor (Fig. 23C).

A

Hepacivirus species (host)	HCV residues activating NS2 protease		HCV NS3 hydrophobic surface patch residues		
HCV (human)	F103	L144	Y105	P115	L127
Aligned residues in other hepaciviruses					
NPHV (equine)	L103	L144	F105	P115	I127
BHV (bat)	N103	L144	Y105	P115	T128
GHV (old world primate)	R100	L141	Y106	E116	I128
RHV (rodent)	K92	L132	F105	P115	T127
GBV-B (new world primate)	D97	L139	Y105	E115	C127

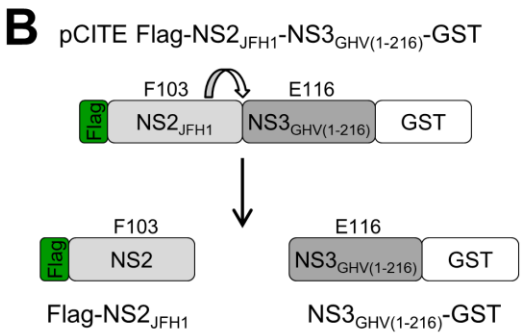

C

Flag-NS2$_{JFH1}$-NS3$_{GHV(1-216)}$-GST derivative			
NS2	**/**	**NS3**	**Situation**
F103R	/	E116	GHV - GHV
C184A			
F103R	/	E116P	GHV - HCV
F103	/	E116	HCV - GHV
F103	/	E116P	HCV - HCV

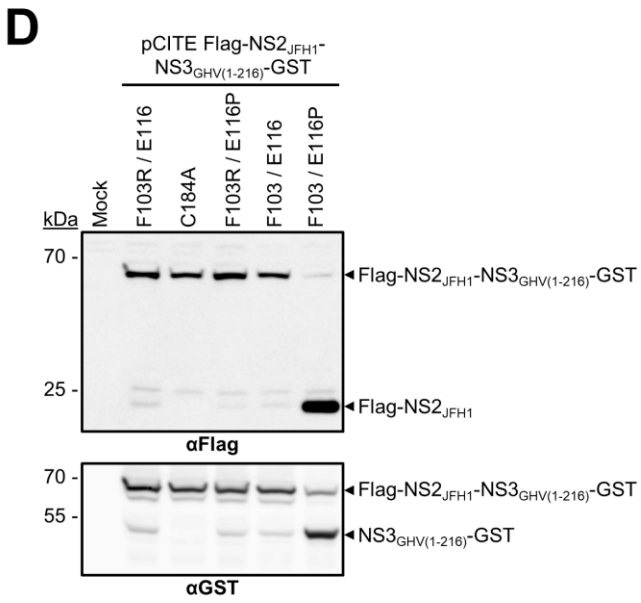

Fig. 23: HCV-specific surface residues at the proposed NS2-NS3 interaction interface of a chimeric NS2$_{HCV}$-NS3$_{GHV}$ precursor are required for efficient NS2-NS3 cleavage. (**A**) Alignment of residues corresponding to HCV NS2 protease activating F103 and L144 and hydrophobic HCV NS3 surface patch residues (Y105, P115 and L127) in indicated mammalian hepacivirus species (according to Boukadida et al., 2018) (**B**) Scheme of pCITE Flag-NS2$_{JFH1}$-NS3$_{GHV(1-216)}$-GST reporter construct to dissect NS2-NS3 surface interactions. (**C**) Generated pCITE Flag-NS2$_{JFH1}$-NS3$_{GHV(1-216)}$-GST derivatives and indication of the situation considered in each case with respect to the NS2$_{JFH1}$ 103 and NS3$_{GHV}$ 116 surface residues. (**D**) Indicated pCITE Flag-NS2$_{JFH1}$-NS3$_{GHV(1-216)}$-GST derivatives were transfected into MVA-T7^{pol}-infected Huh7-T7 cells. 20 h pt, cells were harvested in lysis buffer and NS2 protease activity was analyzed by western blot analysis using Flag- and GST-specific antibodies. One representative western blot from three independent experiments is shown. Molecular mass standards in kDa are depicted on the left. The positions of the uncleaved precursor Flag-NS2$_{JFH1}$-NS3$_{GHV(1-216)}$-GST and cleavage products Flag-NS2$_{JFH1}$ or NS3$_{GHV(1-216)}$-GST are indicated by arrows on the right. Mock: transfection control without DNA.

As reported previously, weak NS2$_{JFH1}$-NS3$_{GHV}$ cleavage and thus inefficient NS2$_{JFH1}$ protease stimulation by the heterologous NS3$_{GHV}$ (F103 / E116) was observed (Fig. 23D; Boukadida et al., 2018). Furthermore, the dramatic enhancement of this stimulation by introduction of the HCV-specific proline residue in GHV NS3 at position 116 (E116P) in Flag-NS2$_{JFH1}$-NS3$_{GHV}$-GST (F103 / E116P) could be confirmed (Fig. 23D). Interestingly, this gain-of-function was blocked by the combination of a GHV-equivalent charged NS2 F103R substitution with an

HCV-analogous hydrophobic NS3 E116P exchange in Flag-$NS2_{JFH1}$-$NS3_{GHV}$-GST (F103R / E116P). This variant showed very weak NS2 protease activity similar to the parental chimeric derivative (F103 / E116) (Fig. 23D), indicating a strong decrease in NS2 protease stimulation by NS3 most likely due to de-optimization of NS2-NS3 surface contacts by the $NS2_{JFH1}$ F103R exchange. The complementation of GHV-specific NS2 F103R substitution with a charged NS3 residue at the proposed NS2-NS3 interaction interface (E116) in Flag-$NS2_{JFH1}$-$NS3_{GHV}$-GST (F103R / E116) could not rescue this weak NS2-NS3 cleavage (Fig. 23D). Together, the results suggest that NS2 F103 is indeed an important determinant of the NS2 stimulation by NS3. Furthermore, these data indicate that an optimal communication between both surface areas (surrounding F103/L144 in $NS2_{HCV}$ and E116 in $NS3_{GHV}$) is pivotal for efficient NS3-mediated NS2 protease stimulation in this $NS2_{JFH1}$-$NS3_{GHV}$ chimera.

To further verify the hypothesis that an optimal communication of NS2 and NS3 surface residues in the proposed NS2-NS3 surface interface is required for efficient NS2-NS3 cleavage, HCV and GHV-equivalent NS2 103/NS3 115 interaction pairs were analyzed in a JFH1-derived NS2-NS3 precursor (Flag-NS2-$NS3_{(1-172)}$-GST/JFH1) (Fig. 24A). Accordingly, pCITE Flag-NS2-$NS3_{(1-172)}$-GST/JFH1 derivatives encoding HCV and/or GHV-specific residues at NS2 position 103 and/or NS3 position 115 were generated and NS2 protease activity of the Flag-NS2-$NS3_{(1-172)}$-GST/JFH1 precursors after transient expression in MVA-$T7^{pol}$-infected Huh7-T7 cells was examined. In addition to the HCV-specific interaction pair (F103 / P115), NS2 and/or NS3 residues were mutated to create derivatives with an NS2-NS3 interaction pair representing the GHV-GHV (F103R / P115R) as well as the chimeric GHV-HCV (F103R / P115) and HCV-GHV (F103 / P115E) situations, respectively (Fig. 24B). The Flag-NS2-$NS3_{(1-172)}$-GST/JFH1 NS2 active site mutant (NS2/C184A) was used as negative control (Fig. 24B).

As expected, the native HCV-specific interaction pair (F103 / P115) allowed for efficient NS2-NS3 cleavage and thus strong stimulation of NS2 protease, whereas mutation in the NS2 protease active site (C184A) completely blocked cleavage (Fig. 24C). Interestingly, the NS2 phenylalanine-to-arginine exchange (F103R) in Flag-NS2-$NS3_{(1-172)}$-GST/JFH1 creating the GHV-HCV-specific interaction pair (NS2 F103R/NS3 P115) also allowed for efficient NS2-NS3 cleavage (Fig. 24C). Consistent with the previous report by Boukadida et al. and observations in this work, the combination of NS2 F103 and NS3 P115E (HCV-GHV-specific interaction pair) in Flag-NS2-$NS3_{(1-172)}$-GST/JFH1 reduced NS2-NS3 cleavage and thus permitted only inefficient NS2 protease stimulation (compare Fig. 24C, F103 / P115E and Fig. 23D, F103 / E116; Boukadida et al., 2018). Electrostatic complementation of this negative charge in NS3 (P115E) with the NS2 F103R exchange creating the proposed GHV-GHV-specific NS2-NS3 interaction pair resulted in a slight increase of the NS2-NS3 cleavage efficiency compared to the Flag-NS2-$NS3_{(1-172)}$-GST/JFH1 (NS2 F103/NS3 P115E) variant

comprising a HCV-GHV-specific interaction pair (Fig. 24C). Taken together, these results also point to a critical role of optimized surface contacts mediated by NS2 position 103 and NS3 position 115 for efficient NS2-NS3 cleavage.

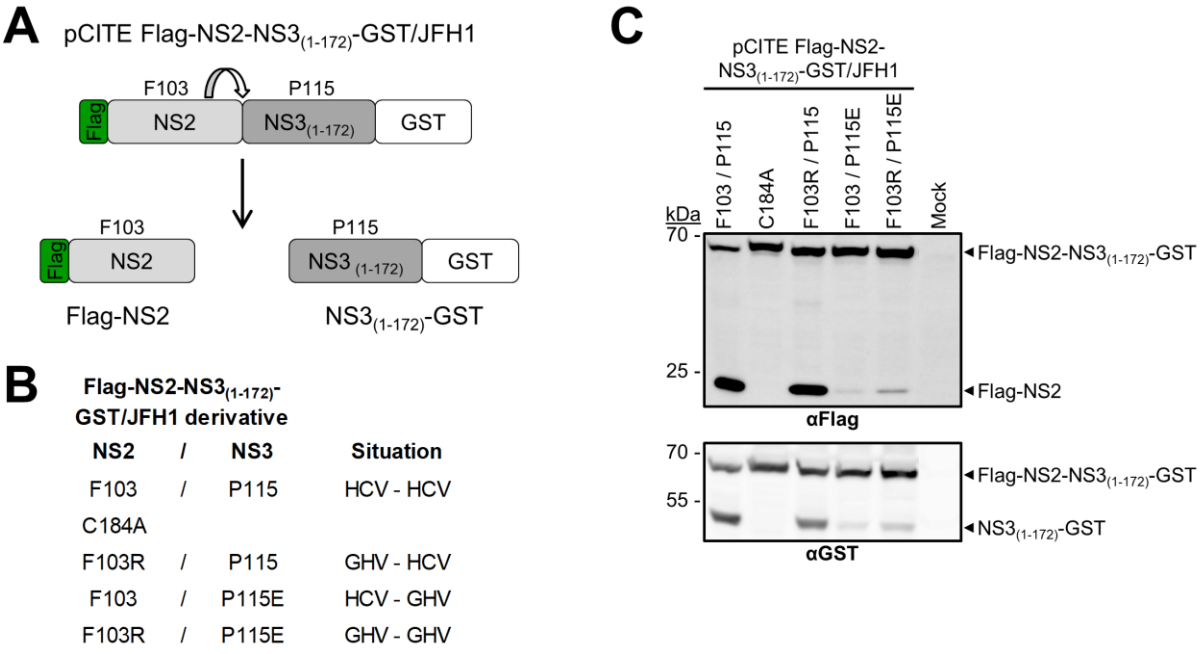

Fig. 24: Verification of the need for HCV-specific surface residues at the proposed NS2-NS3 interaction interface for efficient NS2-NS3 cleavage in an HCV JFH1-derived NS2-NS3 precursor. (**A**) Scheme of pCITE Flag-NS2-NS3$_{(1-172)}$-GST/JFH1 reporter construct. (**B**) Generated pCITE Flag-NS2-NS3$_{(1-172)}$-GST/JFH1 derivatives and indication of the situation considered in each case with respect to the NS2 103 and NS3 115 surface residues. (**C**) Western blot analysis of pCITE Flag-NS2-NS3$_{(1-172)}$-GST/JFH1 derivatives transfected into MVA-T7^{pol}-infected Huh7-T7 cells and harvested 20 h pt, in lysis buffer. NS2 protease activity was analyzed by using Flag- and GST-specific antibodies. One representative western blot from three independent experiments is shown. Molecular mass standards in kDa are depicted on the left. The positions of the uncleaved precursor Flag-NS2-NS3$_{(1-172)}$-GST and cleavage products Flag-NS2 or NS3$_{(1-172)}$-GST are indicated by arrows on the right. Mock: transfection control without DNA.

6 Discussion

Due to their small genome size, plus-strand RNA viruses encode only a very limited number of proteins. In order to efficiently support the complex processes of the viral life cycle, such as replication of the RNA genome and assembly of viral particles, many of the viral proteins perform multiple functions (Lindenbach and Rice, 2013). A distinctive feature of the *Flaviviridae*, such as HCV and pestiviruses, is the involvement of nonstructural proteins in both RNA replication and virion morphogenesis (Murray et al., 2008b). To support these spatially and temporally separated processes by a limited repertoire of viral proteins, the regulated assembly of viral proteins is thought to lead to formation of distinct protein complexes and the specific recruitment of additional cellular or viral interaction partners to perform essential functions in RNA replication or virion morphogenesis (Bartenschlager et al., 2010; Dubrau et al., 2017; Lindenbach and Rice, 2013; Tautz et al., 2015). Controlled processing of viral polyprotein by cellular and viral proteases is another regulatory element in the life cycle of plus-strand RNA viruses to prevent assembly of non-functional protein complexes and to control protein functions temporally and spatially (Tautz et al., 2015; Yost and Marcotrigiano, 2013). In the life cycle of the closely related HCV and pestiviruses, NS2 plays a central role. First, it allows RNA replication by releasing NS3 through cleavage at the NS2-NS3 junction, and second, it is essentially involved in the formation of viral particles (Lindenbach et al., 2013; Tautz et al., 2015). While the availability of structural data from HCV NS2 has enabled intensive studies of the molecular details of its functions, the lack of structural information from pestiviral NS2 prevents such deeper insights.

6.1 Structural organization of BVDV NS2

Studies on molecular details of NS2 functions within the pestiviral life cycle and deciphering of NS2 protein-protein interactions require insights into its domain organization. Therefore, the aim of this part of the present work was to generate an experimentally determined topology model of the N-terminal membrane binding domain of BVDV-1 NS2 and to define the minimal functional NS2 protease domain.

An N-terminal HA-Flag epitope-tagged BVDV-1 NS2 (H-F-NS2) derivative was used for specific detection of pestiviral NS2. The analysis of growth kinectics of BVDV-1 NCP7 and CP7 full-length cDNA clones encoding H-F-NS2 (Fig. 7) demonstrated that the insertion of the combined HA-Flag (H-F) antibody epitope into NS2 has no detectable influence on viral RNA replication and virion production. This also indirectly indicates that the inserted heterologous sequence has no negative influence on NS2-3 cleavage as the liberation of NS3 by the NS2 autoprotease is a prerequisite for pestiviral RNA replication (Grassmann et

al., 1999). This assumption as well as the detectability of the H-F epitope and its applicability for downstream analyses such as immunoprecipitation were confirmed after replication-independent expression of the BVDV-1 NCP7 E2 to NS4A polyprotein region (Fig. 8) Taken together, these observations are in line with the knowledge from studies on a H-F-labeled HCV NS2 (Jirasko et al., 2010), which served as a template for generation of BVDV-1 H-F-NS2. Moreover, these results demonstrate the ability of N-terminally H-F-tagged NS2 to fully support the BVDV lifecycle in cell culture and show that this epitope tag is applicable for the detection of BVDV NS2 in western blots.

6.1.1 SCAM assay results suggest the existence of three transmembrane segments in BVDV NS2

To elucidate the membrane topology of pestiviral NS2, the SCAM assay was chosen from a variety of possible approaches. Approaches involving N- or C-terminal fusion of reporter molecules, such as alkaline phosphatase PhoA or beta-galactosidase LacZ, to differentially truncated variants of the investigated protein were directly excluded because truncation of membrane proteins and fusion with reporter molecules could very likely affect native topology (Van Geest and Lolkema, 2000). Other approaches that exploit compartmentalization of the cell by membranes, such as the SCAM assay (Bogdanov et al., 2005; Zhu and Casey, 2007) used in this work or the exploitation of N-glycosylation (Lundin et al., 2003, 2006; Welply et al., 1983), require less harsh alterations of the protein under study than reporter fusions. However, the use of the SCAM assay to study membrane topology needs the presence of defined single cysteines, which may require first generating a cysteine-free variant of the analyzed protein (Van Geest and Lolkema, 2000), as in the case of the pestiviral NS2 studied here (Fig. 9). On the other hand, the application of N-glycosylation to asses membrane topology requires the introduction of a glycosylation consensus sequence (Welply et al., 1983). This again carries a high risk of compromising membrane topology, as it has been shown that for efficient N-glycosylation, the loop containing the consensus must be greater than 25 residues, with the glycosylation acceptor being 12-14 aa away from the preceding and following transmembrane segments (Nilsson and von Heijne, 1993; Popov et al., 1997). The SCAM assay has a major advantage over the glycosylation assay and other approaches in that the introduction of defined cysteines represents point mutations that are usually very well tolerated. In this assay, the modifiability of these individual cysteine residues, e.g. by PEG-Mal, after selective PM permeabilization is determined to identify regions in membrane proteins with a cytoplasmic localization.

In silico generated membrane topology models of BVDV-1 NCP7 NS2 served as templates to define positions for these cysteine substitutions (Fig. 4C and Fig. 9A). Some striking

characteristics in these hypothetical models made alternative topologies seem possible. For example, the connection sequence between TM1 and TM2 in the theoretical model according to the thesis of O. Klemens (Fig. 4C; Klemens, 2014) is improbably short with two amino acids (one of which is an alanine with a very small methyl side chain). Furthermore, according to this model and according to the model calculated on the basis of H-F-NS2 (Fig. 9A), the 9 aa long CP7 insertion would be placed between the putative TM6 and TM7 and thus has a luminal localization. Because this insertion allows Jiv-independent deregulated NS2-3 cleavage in the cytoplasm, this NS2 region is more likely to be localized in the cytoplasm. Compared to the established membrane topology of HCV NS2 with 3 TMs and a cytoplasmic domain (aa 94-217) (Fig. 4B, Jirasko et al., 2010), the higher number of 7 TMs and the two relatively long luminal loop sequences connecting TM4 and 5 (aa 99-117) or TM6 and 7 (aa 169-227), respectively (Fig. 9A), were especially noteworthy. Thus, it was essential to determine an experimentally validated topology model. To apply the SCAM assay for membrane topology elucidation, a cysteine-free variant of the investigated protein is mandatory. For this reason, the cysteine-free pCITE p7-H-F-NS2$_{(1-290)}$-SUMO CS expression construct (Fig. 9B) established in the bachelor thesis of J. Fellenberg was used as a test system to determine the membrane topology of BVDV NS2 (Fellenberg, 2017). To test the applicability of this construct, the expression and detectability (Fig. 9C) of the encoded p7-H-F-NS2$_{(1-290)}$-SUMO CS and its intracellular localization (Fig. 9D) have been investigated in previous works (Fellenberg, 2017; Walther, 2017). The detection of a single prominent band that can be assigned to H-F-NS2$_{(1-290)}$-SUMO indicates that this fusion protein is stably produced and that co-translational p7-NS2 processing occurs efficiently. The latter is an important prerequisite for the SCAM assay, as an unprocessed p7-H-F-NS2$_{(1-290)}$-SUMO precursor protein would very likely interfere with SCAM assay results, as the modification of accessible cysteine residues with PEG-Mal is increasing the apparent protein size by 5 kDa, proposedly leading to a very similar size shift. Examination of the intracellular localization of H-F-NS2$_{(1-290)}$-SUMO with H-F-NS2 authentically expressed in the infectious full-length context NCP7 2/H-F and in the context of a subgenomic polyprotein fragment E2-4A 2/H-F, showed comparable reticular as well as perinuclear localization of all H-F-NS2 variants, confirming the correct membrane insertion of the N-terminal NS2 portion H-F-NS2$_{(1-290)}$-SUMO fusion protein. Taken together, validation of p7-H-F-NS2$_{(1-290)}$-SUMO CS in terms of expression, p7-NS2 processing, and localization demonstrates its suitability for determining NS2 membrane topology by SCAM assay.

Based on the results of the SCAM assay (Fig. 10), an experimentally supported BVDV NS2 membrane topology model could be generated using the program Phobius (Fig. 11, right). Compared to purely *in silico* calculated models, the experimental SCAM data based model, shows some clear differences. First, only three TMs (hypothetical models: 7 TMs) are found

in the new model (compare Fig. 11, right to Fig. 11,left, Fig. 9A and Fig. 4C). The luminal N-terminal part (NS2 aa 1-56) as well as the cytoplasmic C-terminal region (NS2 aa 169-290) are considerably longer in the SCAM-assay derived model (Fig. 11). Furthermore, the existence of a large cytoplasmic loop sequence connecting TMs 1 and 2 (NS2 aa 74-116) is also remarkable (Fig. 11, right). Interestingly, this experimentally determined membrane topology suggests a shared overall membrane topology between BVDV and HCV NS2 with an N-terminal luminal region, three TMs and a C-terminal cytoplasmic domain (compare Fig. 4B and Fig. 11, right). But the NS2 membrane topologies of these two closely related viruses also show striking differences: (i) the N-terminal luminal region preceding TM1 is with 56 aa 52 residues longer in the case of BVDV and (ii) the cytoplasmic loop region connecting TMs 1 and 2 (TM1-2) is also much longer compared to HCV NS2 (compare Fig. 4B and Fig. 11, right). This prediction and further analyses of the two deviating regions regarding secondary structure and hydrophobicity (Fig. 12) suggest that these sequences mediate additional association with the luminal membrane interface for BVDV NS2. N-terminal, hydrophobic helices are not unusual structural elements for anchoring viral proteins to cellular membranes. For example, amphipathic helical structures have been described for pestiviral as well as hepaciviral NS4B and NS5A (Gouttenoire et al., 2014; Tellinghuisen et al., 2004, 2006). These structures can be important for viral RNA replication (HCV NS5A: Biswas et al., 2016) and in some cases even serve dual function in RNA replication and virion morphogenesis (Gouttenoire et al., 2014).

This new model of NS2 membrane topology now provides the opportunity of topology-guided functional studies. Uncleaved NS2-3 is known to be essentially involved in virion morphogenesis together with NS4A (Agapov et al., 2004; Dubrau et al., 2017; Moulin et al., 2007). However, due to a lack of structural information regarding NS2 or the NS2-3 precursor, more focused studies on interactions with other viral or cellular proteins have not been possible so far. For HCV NS2, on the other hand, based on the available structural data of the N-terminal MBD, structural and functional sections could be defined with respect to protein-protein interactions in this region (Jirasko et al., 2008, 2010). Additionally, the MBD served as crossover region to construct viable intra- and intergenotypic HCV chimeras, which underlines that the N-terminal part of the MBD interacts mainly with the structural proteins while the C-terminal part of the MBD and the cytoplasmic domain are critical for the interaction with the nonstructural proteins (Pietschmann et al., 2006). Moreover, a multitude of studies suggest the mediating role of HCV NS2 between structural and nonstructural proteins (see 3.4.2.2). Such interactions can also be assumed for BVDV NS2 (in the uncleaved NS2-3 context) with other viral proteins and possibly also with host factors. For example, it has been shown that NS2-3 must interact with NS4A to enable the production of infectious virus particles (Moulin et al., 2007). The larger N-terminal sequence as well as the

TM1-2 sequence in case of BVDV NS2 may indicate that there are additional pestivirus-specific interaction sites for viral and/or cellular proteins compared to HCV NS2. By identifying the putative TM regions (TM1, TM2, TM3), there is now the opportunity to perform topology-guided reverse-genetic analyses aiming at the identification of protein regions involved in protein-protein interactions with critical functions for the pestiviral life cycle.

6.1.2 BVDV-1 NS2 truncated by the first 135 amino acids is an active protease

The experimentally established membrane topology model of BVDV NS2 was further used in the present work to characterize the NS2 protease in more detail. Although its protease activity is well characterized (Lackner et al., 2004, 2005, 2006), the minimal functional protease domain of BVDV NS2 has not yet been defined. While for HCV NS2 the C-terminal, cytoplasmic portion of the protein (amino acids 94-217) is known to be sufficient for protease activity (Pallaoro et al., 2001), for BVDV NS2 it is only known that a deletion of the first 73 N-terminal amino acids leads to a significant attenuation of protease activity (Lackner et al., 2004). The availability of the BVDV NS2 MBD topology now enabled a structured approach to define the minimal functional BVDV NS2 protease domain, in which topology-guided N-terminal truncations of NS2 were examined for their protease activity in a NS2-$NS3_{(1-10)}$-SUMO-HA-V5 reporter construct (Fig. 13A). Accordingly, a minimal active protease domain of NCP7 NS2 (aa 112-453) or CP7 NS2 (aa 136-453), respectively, could be defined (Fig. 13C). These data extend the knowledge of the minimal pestiviral NS2 protease (Fig. 13C and Fig. 25; Lackner et al., 2004). The observation that only CP7 $NS2_{(136-453)}$ but not NCP7 $NS2_{(136-453)}$ shows residual protease activity is probably due to a stronger cleavage activity of CP7 NS2 compared to NCP7 NS2 in the chosen experimental setup in SK6 GST-Jiv90 cells (Fig. 13C, compare NCP7 WT and CP7 WT; Isken et al., 2019). This might suggest that also NCP7 $NS2_{(136-453)}$ exhibits residual protease activity which, however, is undetectable in this setting. This study on the minimal protease domain of the BVDV NS2 indicates that a membrane anchoring via at least one transmembrane segment is necessary for BVDV NS2 to catalyze the NS2-3 cleavage. It seems likely that membrane association is a requirement for correct folding of NS2-3 prior to cleavage. The knowledge of the minimal active NS2 protease domain might also be helpful for structural studies since hydrophobic regions are often problematic for crystallographic approaches. The requirement of at least one TM for proteolytic activity contrasts data on HCV NS2, where the cytoplasmic domain alone showed residual protease activity (Pallaoro et al., 2001) and its structure could be successfully determined (Lorenz et al., 2006). However, the protease domain of HCV NS2 still requires membrane association independently from the N-terminal MBD via additional determinants

for NS2 protein stability and efficient protease activity (Lange et al., 2014; Wu et al., 2019). Nevertheless, for certain other members of the genus Hepacivirus, like bat hepacivirus (BHV), rodent hepacivirus (RHV) and GB virus B (GBV-B), it was shown that their NS2 protease requires its N-terminal membrane binding domain for catalytic activity (Boukadida et al., 2018).

Taken together, this detailed mapping of the structural organization of BVDV NS2 will support further studies aiming at a better understanding of the complex functions of NS2 in the pestiviral life cycle.

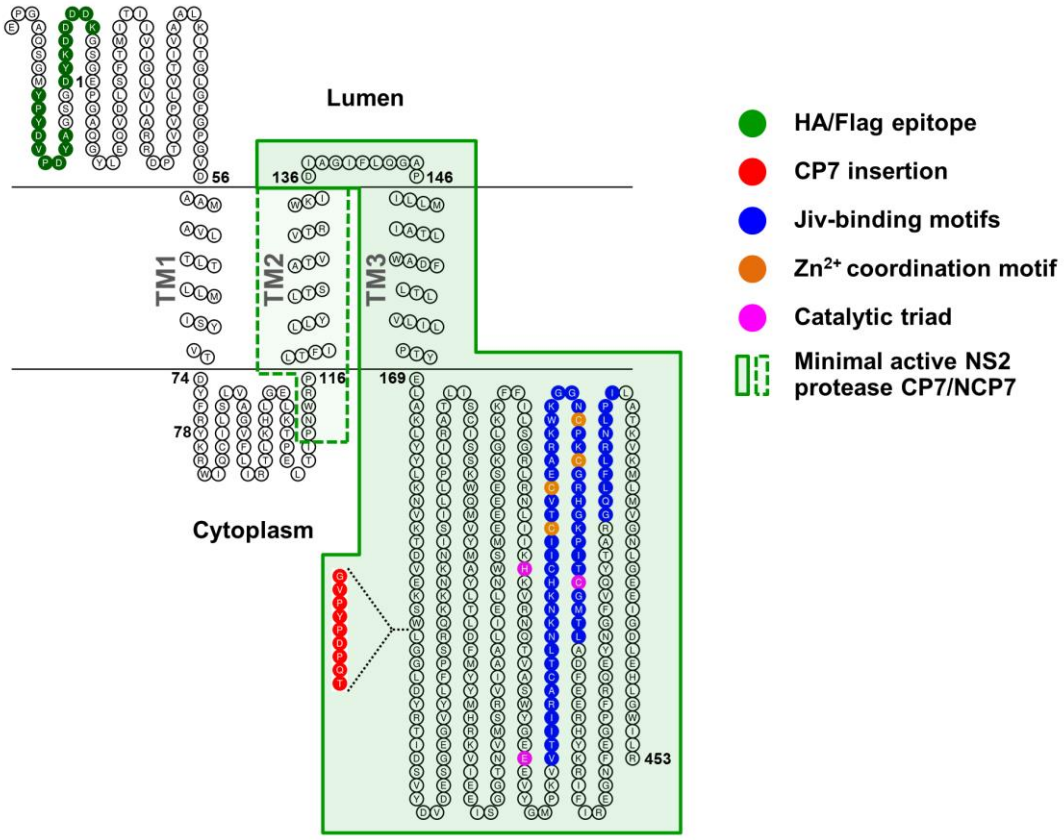

Fig. 25: Experimentally determined BVDV-1 NS2 membrane topology model and minimal active protease domain. Membrane topology model of H-F-NS2(1-453) based on experimental results of SCAM assay visualized with TOPO2. Amino acids are depicted as circles. The HA-Flag tag (green), the two Jiv binding motifs (blue), the residues of the putative Zn2+ coordination motif (orange) and the putative catalytic triad of the protease (pink) are highlighted. The position of the 9 aa insertion in the CP7 strain (red) is indicated by a dashed line. The portion of NS2 that represents the minimal active protease is framed by a green box (solid line: minimal requirement for CP7 NS2; dashed line: additional requirement for NCP7 NS2). The numbers indicate first and last aa of NS2 as well as aa positions of luminal or cytoplasmic sections. The intracellular membrane is displayed as black double line. Lumen, luminal side of the ER membrane; Cytoplasm, cytoplasmic side of the ER membrane.

6.2 Stimulating HCV NS2 protease determinants

Protein-protein interactions between NS2 and NS3 are thought to play an essential role during HCV NS2 stimulation by NS3 to enable efficient NS2-NS3 cleavage. This hypothesis is based on the observation that the NS3 protease domain acts as cofactor for NS2 protease stimulation (Isken et al., 2015; Schregel et al., 2009). A conserved hydrophobic surface region within the NS3 protease domain has been shown to provide critical NS3 determinants for NS2 protease stimulation by NS3, a feature conserved among several related mammalian hepaciviruses (Boukadida et al., 2018; Isken et al., 2015). However, the NS2 determinants, which are thought to be involved in this process of NS2 protease stimulation, have not been characterized. These determinants have to receive a signal via hydrophobic surface interactions from NS3 and transform it into structural changes leading to enhanced NS2-3 autocleavage.

An alanine scanning mutagenesis of a selected set of NS2 residues identified surface residues L144 and L147 as potential recipients for NS2 protease stimulation by NS3 (Fig. 15D and E). These residues, when mutated to alanine, showed a strong decrease in NS2-NS3 cleavage efficiency comparable to mutations in the recently identified hydrophobic NS3 surface patch (Fig. 15D and E, compare NS3/YPLAAA with L144A and L147A; Isken et al., 2015). Other NS2 alanine mutations (Y141A and P146A) completely abolished NS2-NS3 cleavage, suggesting destruction of the NS2 protease function rather than interfering with its stimulation by NS3 (Fig. 15D and E). Support for these conclusions was provided by re-analysis of the respective alanine mutations in the Flag-NS2-APIT-GST context in the absence of the NS3 cofactor domain, as the Y141A and P146A mutations blocked intrinsic NS2 protease activity (Fig. 16). The deleterious effect of these mutations is indicative for a more global effect on NS2 architecture and that these residues are important for active site geometry, similar to the unusual *cis*-proline residue P164 (Lorenz et al., 2006). For Y141A, these observations are consistent with previous experiments showing that the mutation Y141A also strongly impairs RNA accumulation, likely by impairing NS2-3 processing (Dentzer et al., 2009). The L144 and L147 residues are highly conserved amino acids close to the protease active site. In the case of L144, previous work by Dentzer and coworkers already suggested its functional importance for NS2-NS3 cleavage and RNA replication (Dentzer et al., 2009). They demonstrated that replacement with phenylalanine allowed detectable NS2-NS3 processing and RNA replication, whereas a lysine at this position disrupted these processes, suggesting that L144 supports the formation of the correct active site architecture (Dentzer et al., 2009). The involvement of L144 in the correct active site architecture is further strengthened by the observations that only the NS2 variant L144A, but not L147A, showed intrinsic NS2 protease activity similar to the WT variant in the

NS2-APIT context (Fig. 16). These results suggest that L144 is one of the NS2 determinants critical for NS2 protease stimulation by NS3.

6.2.1 The NS2 amino acid exchanges F103A and L144I stimulate the intrinsic NS2 protease activity in a phylogentically conserved fashion by potentially distinct mechanisms

Analysis of NS2 mutations for their influence on intrinsic NS2 protease activity revealed that NS2 F103A was able to stimulate this activity (Fig. 16B and C). In addition, NS2 L144 permutation analysis showed that L144I exchange also increased intrinsic NS2 protease activity (Fig. 17). Interestingly, the combination of both exchanges further improved the intrinsic NS2 protease activity (Fig. 19). This effect appears to be additive in the case BK (gt.1b) and synergistic in the case of JFH1 (gt.2a) (Fig. 19).

Side-by-side analysis of these two NS2 exchanges in two different HCV genotypes confirmed that the ability to stimulate NS2 protease activity in absence of the NS3 cofactor (i) is conserved in different HCV genotypes and (ii) is independent of genotype-specific increases in Flag-NS2-APIT-GST/JFH1 cleavage (gt.2a) compared to Flag-NS2-APIT-GST/BK cleavage (gt.1b) (Fig. 19). These observations not only highlight the functional importance of these findings, but are also imply that the stimulatory NS2 exchanges F103A and L144I influence NS2 protease function and/or protein folding in a conserved fashion. The observed genotype-specific differences in Flag-NS2-APIT-GST cleavage efficiencies could either be due to more efficient translation of the Flag-NS2-APIT-GST/JFH1 reporter construct or indicate that the Flag-NS2-APIT-GST/JFH1 precursor protein folds more efficiently into its active conformation. An attractive hypothesis for intrinsic NS2 protease stimulation by NS2 exchanges F103A and L144I in the Flag-NS2-APIT-GST context would be that the effects of these mutations mimic the molecular events of NS2 protease stimulation by NS3 and thus provide mechanistic insights into this process. Mechanistically, NS2 protease stimulation by the NS3 cofactor could involve optimization of the active site geometry by compensating for the modulatory influence of the NS3 protease domain and/or an improved positioning of the NS2-NS3 cleavage site relative to the nucleophilic active site cysteine.

An important finding emerging from the F103 and L144 permutation experiments is that both positions may stimulate intrinsic NS2 protease activity possibly by different mechanisms (Fig. 17 and Fig. 18). This hypothesis is based on the observation that a very wide range of F103 exchanges either did not affect intrinsic NS2 protease activity or resulted in an increase (Fig. 18). In the case of L144 permutations, however, only a leucine-to-isoleucine exchange massively increased Flag-NS2-APIT-GST cleavage while several other mutations reduced cleavage activity (Fig. 17). Consistent with the striking differences in amino acid

requirements at NS2 positions 103 and 144 to stimulate intrinsic NS2 protease activity in the absence of NS3 (Fig. 17 and Fig. 18), leucine is conserved at L144-equivalent positions in several mammalian hepaciviral NS2 sequences, whereas a wide range of amino acids is found at the positions equivalent to HCV F103 (Fig. 18C). These differences in their conservation strengthen the hypothesis that the identified stimulatory NS2 determinants may use different modes to stimulate NS2 protease activity.

The observation that only isoleucine (and to a lesser extent valine) at position 144 is able to stimulate intrinsic NS2 protease activity (Fig. 17) beyond the WT level suggests that isoleucine may adopt an orientation adjacent to the neighboring catalytic histidine 143 that may optimize its positioning with respect to the other two catalytic residues of the NS2 protease active site (E163 and C184). In support of this hypothesis, H143 makes many hydrogen bond contacts relative to C184 (Lorenz et al., 2006) and therefore the NS2 protease may benefit from the L144I exchange to create an optimized active site by enhancing essential hydrogen bond formation. The importance of these hydrogen bond contacts is emphasized by the observation that an H143A but not a C184A mutation in the active site results in a global loss of NS2 secondary structure properties (Foster et al., 2010). Moreover, the strict conservation of leucine at NS2 position 144 in different HCV genotypes or at an equivalent position in mammalian hepaciviruses (Fig. 17 and Fig. 18C) argues for a central role of this leucine adjacent to the active site histidine in the process of NS3-mediated NS2 protease stimulation. This assumption was supported by leucine-to-isoleucine exchanges at HCV NS2 L144-equivalent positions in NS2 proteins from either distantly (RHV; rodents) or closely related (NPHV; horses) hepaciviruses: both enhanced the intrinsic NS2 protease activities of these NS2 proteases relative to their respective WT protein (Fig. 21).

The observed increase in the intrinsic protease activity by NS2 F103A and other F103 permutations (Fig. 18) could be the result of changes in the local protein folding that lead to a stimulation of the NS2 activity by optimizing interactions near the composite active site. Alternatively, these permutations could allow a better accommodation of the NS2 C-terminus in the context of NS2-APIT construct. Taken together, it appears that the stimulatory NS2 determinants F103A and L144I might use distinct functional modes that may cooperate in stimulating the intrinsic protease activity of NS2 in absence of NS3.

As mentioned above, F103A and L144I might also exert their stimulatory influence on intrinsic NS2 protease activity by compensating for the postulated inhibitory influence of N-terminal amino acids of NS3 (e.g. NS3 APIT) (Boukadida et al., 2018). However, the observation that the F103A/L144I combination in particular retains its ability to stimulate the intrinsic NS2 protease activity not only in the presence (NS2-APIT) but also in the absence

(NS2-4GS) of inhibitory NS3 amino acids (Fig. 19 and Fig. 20) suggests that the beneficial effect of these mutations is mediated mainly within NS2 and not via diminishing the negative effect of the NS3 APIT sequence on intrinsic NS2 protease activity.

In the HCV polyprotein context the NS3 protease domain was shown to mediate a stimulatory effect on NS2-NS3 cleavage with a critical role of NS3 surface residues (Isken et al., 2015), a functional feature shared among mammalian hepaciviruses (Boukadida et al., 2018). In theory, the stimulatory NS2 determinants could function in concert with the NS3 surface patch to further increase NS2-NS3 cleavage. However, the functional analysis of the NS2 exchanges in a NS2-NS5B replicon system revealed that the double mutant F103A/L144I reduced NS2-NS3 cleavage relative to WT, or single mutants F103A and L144I (Fig. 22B and C) and attenuated RNA replication in a bicistronic NS2-3'/JFH1 replicon (Fig. 22D). These results suggest that the stimulatory NS2 mutations mainly act on the intrinsic NS2 protease activity, most likely by optimizing NS2 protease geometry, possibly in a mode similar to the NS3 protease domain. The latter hypothesis is supported by the finding that the two mutations interfere with NS2 protease activation by the NS3 cofactor (Fig. 22). Possibly F103A and L144I address the same interaction partners in NS2 which in the wildtype situation are stimulated by NS3. However, this model awaits final proof by crystallographic analyses.

6.2.2 Optimal surface interactions between NS2 and NS3 are required to promote NS2 protease stimulation and efficient NS2-NS3 cleavage

The observation that NS2-NS3 cleavage efficiency is attenuated compared to WT when the NS2 F103A/L144I exchanges are introduced into the NS2-NS5B polyprotein context suggests that NS3-mediated NS2 protease stimulation is negatively affected by these NS2 exchanges (Fig. 22). One explanation is that the ability of the stimulatory hydrophobic NS3 surface patch to interact with the mutant NS2 surface residues F103A and L144I is reduced, supporting the hypothesis that the NS2 determinants F103 and L144 may play a role during NS3-mediated NS2 protease stimulation in the uncleaved NS2-NS3 precursor protein.

Accordingly, specific interactions between NS2 and NS3 protease domain surfaces are assumed to be important for NS3-mediated NS2 protease stimulation. Experimental support for this hypothesis comes from the work by Boukadida and coworkers, showing that the NS3 protease domains of some hepaciviruses are able to activate the HCV NS2 protease in chimeric NS2-NS3 precursors and that this heterologous stimulation is dependent on the nature of specific residues within heterologous NS3 surface patch sequences (Boukadida et al., 2018). Especially, a substantial gain-of-function of the $NS3_{GHV}$ protease domain as HCV NS2 stimulating cofactor was achieved by the creation of a more HCV-like NS3 surface

patch via converting E116 to proline, as found at equivalent NS3 position 115 in HCV and NPHV (Boukadida et al., 2018). In the present work, an analogous analysis of different amino acid pairs residing on the NS2 and NS3 protease domain surfaces were investigated in the context of a $NS2_{JFH1}$-$NS3_{GHV}$ chimeric precursor. Here, it was possible to reproduce the impressive positive effect of mutation E116P in the $NS3_{GHV}$ protease domain on $NS2_{JFH1}$ protease stimulation (compare Fig. 23 with Boukadida et al., 2018). Most importantly, the increased activation potential of the $NS3_{GHV}$ E116P mutant was lost when residue F103 in the $NS2_{JFH1}$ protease domain was replaced by arginine (Fig. 23, F103R / E116P), mimicking the situation of the GHV NS2 protease. These data demonstrate that residue 103 in NS2 and 115 or in NS3 (both positions refer to HCV) are absolutely critical for NS3 dependent activation of the NS2 protease. This loss of response to activation of NS2 mutant F103R would even be consistent with a working model in which NS2 residue 103 receives the activation signal from NS3 residue 115. Within a fully HCV JFH1-derived NS2-NS3 precursor, the NS2 exchange F103R allowed efficient NS2-NS3 cleavage compared to the native HCV-specific situation (F103 / P115), whereas an F103R/P115E exchange resulted in only a very moderate increase of NS2-NS3 cleavage compared to the very weak cleavage detected with the F103/P115E variant (Fig. 24). This allows the assumption that electrostatic interactions at the HCV interface are not essential for efficient NS2 protease stimulation. Taken together, these experiments suggest that in addition to NS2 F103 and L144 further NS2 determinants are involved in the surface interaction with the NS3 surface patch to promote NS3 mediated NS2 protease activation. Still, structural data will be required to finally clarify the mechanism of NS2 protease activation by its NS3 cofactor.

6.3 Outlook

The experimentally determined membrane topology of BVDV NS2 obtained in the first part of this work will allow topology-guided identification of potential protein-protein interactions of the N-terminal MBD that are likely to be relevant to virion morphogenesis. Interestingly, the differences of the membrane topology of BVDV NS2 compared to HCV NS2 (larger luminal N-terminal sequence and longer TM1-2 sequence) argue for the existence of pestivirus-specific interactions. The established fully functional tagged NS2 represents an ideal tool to study these interactions. Moreover, the fine mapping of the minimal active NS2 protease domain, and thus the identification of a functional NS2 protease moiety with reduced hydrophobicity will support future structural studies of the pestiviral NS2 protease domain. However, the need for membrane association via at least one TM to maintain detectable protease activity has to be kept in mind for future structure elucidation approaches. The HCV NS2 protease domain also requires membrane association, mainly mediated by the N-terminal membrane domain of NS2 but also by determinants independent of this region (Jirasko et al., 2010; Lange et al., 2014; Lorenz et al., 2006). One of these determinants is an N-terminal helix-turn-helix motif (Fig. 26A; Lange et al., 2014). Sequence and structural alignment of the C-terminal cytoplasmic domain of several pestivirus strains proposes the presence of several putative helical elements in its N-terminal portion (Fig. 26B), which might suggest that these also harbor determinants for membrane association. These potential membrane-association determinants could be mutated in a way to decrease their hydrophobicity while still retaining their structural integrity and NS2 protease activity. Another approach to identify an active NS2 protease domain deprived of the entire MBD might be to switch to a more efficient NS2 protease. As observed, CP7 NS2, which contains a 9 aa insertion that renders this protease protein DNAJC14/Jiv-independent with regard to NS2-3 cleavage, still benefits from the presence of the NS2 protease cofactor Jiv90 in SK6-KO-GSTJiv90 cells (Fig. 13). Along these lines, it is worth mentioning that NS2 of the BVDV-1 strain NADL naturally encompasses a Jiv90 insertion. Accordingly this NS2 variant could present an even more active NS2 protease and could support the identification of a functional NS2 protease without the transmembrane region.

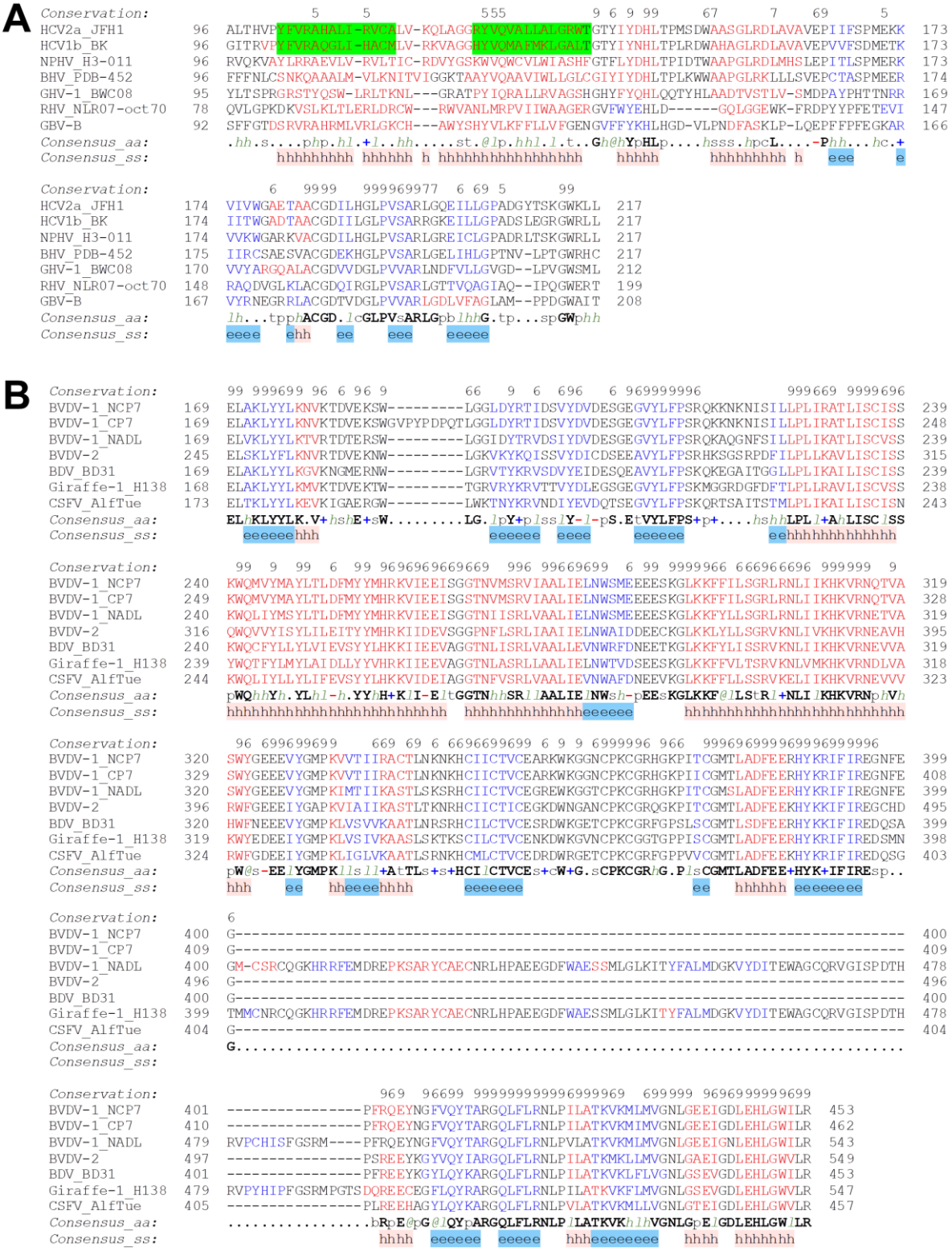

Fig. 26: Multiple protein sequence and structure alignments of the C-terminal cytoplasmic domains of NS2 of various Hepacivirus strains (A) and Pestivirus strains (B) using PROMALS3D webserver. The numbering of the analyzed amino acid sequences is in relation to the respective total NS2 protein. Predictions of secondary structure elements are indicated as red (α-helix) or blue (β-sheet) letters in the respective sequences or as "h" or "e", respectively, in secondary structure consensus (Consensus_ss). For details concerning sequence consensus (Consensus_aa) and Conservation see PROMALS3D documentation. The described helices of the helix-turn-helix motif mediating membrane association of HCV NS2 (Lange et al., 2014) are marked as green boxes (A).

The HCV NS2 surface determinants F103 and L144 identified and characterized in the second part of this work provide an exciting basis for further dissection of the molecular mechanism of NS3-mediated activation of the HCV NS2 protease. The suggested structural mimicries by the mutations F103A and L144I may represent the transition state of the NS2 protease domain during activation by its cofactor NS3. Accordingly, a crystal structure of these mutants would provide interesting further insights into molecular details of the process of NS2 protease activation and NS2-NS3 cleavage which is critical for the HCV life cycle. Moreover, further experimental consolidation of the hypothesized NS2-NS3 surface interactions should be the goal of future investigations. Furthermore, direct evidence for the interaction of these surface determinants with each other or with additional interaction partners of the respective opposite protein surface could further strengthen this theory. Since it can be assumed that these interactions are very short-lived, a method should be applied that can resolve these temporally existing contacts. Here, the so-called bio-orthogonal labeling would be an ideal approach, where photo-activatable non-canonical amino acids inserted at defined positions in the investigated protein by alternative usage of amber stop codons can be used to identify protein-protein interaction by photo-crosslinks coupled to subsequent mass-spectrometry analysis (Chin, 2017; He et al., 2017).

The insights obtained in this work expand the knowledge of NS2 proteins of the closely related pestiviruses and hepaciviruses and will help future studies to understand complex functions of NS2 in the life cycle of these viruses.

7 Bibliography

Agapov, E. V, Murray, C.L., Frolov, I., Qu, L., Myers, T.M., and Rice, C.M. (2004). Uncleaved NS2-3 Is Required for Production of Infectious Bovine Viral Diarrhea Virus. J. Virol. *78*, 2414–2425.

Agnello, V., Ábel, G., Elfahal, M., Knight, G.B., and Zhang, Q.X. (1999). Hepatitis C virus and other flaviviridae viruses enter cells via low density lipoprotein receptor. Proc. Natl. Acad. Sci. U. S. A. *96*, 12766–12771.

Ali, N., Tardif, K.D., and Siddiqui, A. (2002). Cell-Free Replication of the Hepatitis C Virus Subgenomic Replicon. J. Virol. *76*, 12001–12007.

Aligeti, M., Roder, A., and Horner, S.M. (2015). Cooperation between the Hepatitis C Virus p7 and NS5B Proteins Enhances Virion Infectivity. J. Virol. *89*, 11523–11533.

Alter, M.J. (2007). Epidemiology of hepatitis C virus infection. World J. Gastroenterol. *13*, 2436–2441.

André, P., Komurian-Pradel, F., Deforges, S., Perret, M., Berland, J.L., Sodoyer, M., Pol, S., Bréchot, C., Paranhos-Baccalà, G., and Lotteau, V. (2002). Characterization of Low- and Very-Low-Density Hepatitis C Virus RNA-Containing Particles. J. Virol. *76*, 6919–6928.

Ansari, I.H., Chen, L.-M., Liang, D., Gil, L.H., Zhong, W., and Donis, R.O. (2004). Involvement of a Bovine Viral Diarrhea Virus NS5B Locus in Virion Assembly. J. Virol. *78*, 9612–9623.

Appel, N., Pietschmann, T., and Bartenschlager, R. (2005). Mutational Analysis of Hepatitis C Virus Nonstructural Protein 5A: Potential Role of Differential Phosphorylation in RNA Replication and Identification of a Genetically Flexible Domain. J. Virol. *79*, 3187–3194.

Baigent, S.J., Zhang, G., Fray, M.D., Flick-Smith, H., Goodbourn, S., and McCauley, J.W. (2002). Inhibition of Beta Interferon Transcription by Noncytopathogenic Bovine Viral Diarrhea Virus Is through an Interferon Regulatory Factor 3-Dependent Mechanism. J. Virol. *76*, 8979–8988.

Baker, J.C. (1987). Bovine viral diarrhea virus: a review. J. Am. Vet. Med. Assoc. *190*, 1449–1458.

Bankwitz, D., Steinmann, E., Bitzegeio, J., Ciesek, S., Friesland, M., Herrmann, E., Zeisel, M.B., Baumert, T.F., Keck, Z., Foung, S.K.H., et al. (2010). Hepatitis C Virus Hypervariable Region 1 Modulates Receptor Interactions, Conceals the CD81 Binding Site, and Protects Conserved Neutralizing Epitopes. J. Virol. *84*, 5751–5763.

Bartenschlager, R., and Lohmann, V. (2000). Replication of hepatitis C virus. J. Gen. Virol. *81*, 1631–1648.

Bartenschlager, R., Ahlborn-Laake, L., Mous, J., and Jacobsen, H. (1994). Kinetic and structural analyses of hepatitis C virus polyprotein processing. J. Virol. *68*, 5045–5055.

Bartenschlager, R., Frese, M., and Pietschmann, T. (2004). Novel Insights into Hepatitis C Virus Replication and Persistence. Adv. Virus Res. *63*, 71–180.

Bartenschlager, R., Cosset, F.-L., and Lohmann, V. (2010). Hepatitis C virus replication cycle. J. Hepatol. *53*, 583–585.

Becher, P., and Tautz, N. (2011). RNA recombination in pestiviruses: Cellular RNA sequences in viral genomes highlight the role of host factors for viral persistence and lethal disease. RNA Biol. *8*, 216–224.

Becher, P., Orlich, M., König, M., and Thiel, H.-J. (1999). Nonhomologous RNA Recombination in Bovine Viral Diarrhea Virus: Molecular Characterization of a Variety of Subgenomic RNAs Isolated during an Outbreak of Fatal Mucosal Disease. J. Virol. *73*, 5646–5653.

Behrens, S.-E., Grassmann, C.W., Thiel, H.-J., Meyers, G., and Tautz, N. (1998). Characterization of an Autonomous Subgenomic Pestivirus RNA Replicon. J. Virol. *72*, 2364–2372.

Behrens, S.E., Tomei, L., and De Francesco, R. (1996). Identification and properties of the RNA-dependent RNA polymerase of hepatitis C virus. EMBO J. *15*, 12–22.

Bertaux, C., and Dragic, T. (2006). Different Domains of CD81 Mediate Distinct Stages of Hepatitis C Virus Pseudoparticle Entry. J. Virol. *80*, 4940–4948.

Bielefeldt Ohmann, H., Ronsholt, L., and Bloch, B. (1987). Demonstration of Bovine Viral Diarrhoea Virus in Peripheral Blood Mononuclear Cells of Persistently Infected, Clinically Normal Cattle. J. Gen. Virol. *68*, 1971–1982.

Binder, F. (2016). Molecular biological investigation of intracellular membrane association of pestiviral protein NS4B. Universität zu Lübeck.

Biswas, A., Treadaway, J., and Tellinghuisen, T.L. (2016). Interaction between Nonstructural Proteins NS4B and NS5A Is Essential for Proper NS5A Localization and Hepatitis C Virus RNA Replication. J. Virol. *90*, 7205–7218.

Bogdanov, M., Zhang, W., Xie, J., and Dowhan, W. (2005). Transmembrane protein topology mapping by the substituted cysteine accessibility method (SCAM^{TM}): Application to lipid-specific membrane protein topogenesis. Methods *36*, 148–171.

Bolin, S.R., McClurkin, A.W., Cutlip, R.C., and Coria, M.F. (1985). Severe clinical disease induced in cattle persistently infected with noncytopathic bovine viral diarrhea virus by superinfection with cytopathic bovine viral diarrhea virus. Am. J. Vet. Res. *46*, 573–576.

Boson, B., Granio, O., Bartenschlager, R., and Cosset, F.-L. (2011). A Concerted Action of Hepatitis C Virus P7 and Nonstructural Protein 2 Regulates Core Localization at the Endoplasmic Reticulum and Virus Assembly. PLoS Pathog. *7*, e1002144.

Boukadida, C., Marnata, C., Montserret, R., Cohen, L., Blumen, B., Gouttenoire, J., Moradpour, D., Penin, F., and Martin, A. (2014). NS2 Proteins of GB Virus B and Hepatitis C Virus Share Common Protease Activities and Membrane Topologies. J. Virol. *88*, 7426–7444.

Boukadida, C., Fritz, M., Blumen, B., Fogeron, M.-L., Penin, F., and Martin, A. (2018). NS2 proteases from hepatitis C virus and related hepaciviruses share composite active sites and previously unrecognized intrinsic proteolytic activities. PLoS Pathog. *14*, e1006863.

Brass, V., Pal, Z., Sapay, N., Deléage, G., Blum, H.E., Penin, F., and Moradpour, D. (2007). Conserved Determinants for Membrane Association of Nonstructural Protein 5A from Hepatitis C Virus and Related Viruses. J. Virol. *81*, 2745–2757.

Brazzoli, M., Bianchi, A., Filippini, S., Weiner, A., Zhu, Q., Pizza, M., and Crotta, S. (2008). CD81 Is a Central Regulator of Cellular Events Required for Hepatitis C Virus Infection of Human Hepatocytes. J. Virol. *82*, 8316–8329.

Brownlie, J., Clarke, M.C., and Howard, C.J. (1989). Experimental infection of cattle in early pregnancy with a cytopathic strain of bovine virus diarrhoea virus. Res. Vet. Sci. *46*, 307–311.

Bukh, J., Miller, R., and Purcell, R. (1995). Genetic Heterogeneity of Hepatitis C Virus: Quasispecies and Genotypes. Semin. Liver Dis. *15*, 41–63.

Callens, N., Brügger, B., Bonnafous, P., Drobecq, H., Gerl, M.J., Krey, T., Roman-Sosa, G., Rümenapf, T., Lambert, O., Dubuisson, J., et al. (2016). Morphology and Molecular Composition of Purified Bovine Viral Diarrhea Virus Envelope. PLoS Pathog. *12*, e1005476.

Caruthers, J.M., and McKay, D.B. (2002). Helicase structure and mechanism. Curr. Opin. Struct. Biol. *12*, 123–133.

Chen, Z., Rijnbrand, R., Jangra, R.K., Devaraj, S.G., Qu, L., Ma, Y., Lemon, S.M., and Li, K. (2007). Ubiquitination and Proteasomal Degradation of Interferon Regulatory Factor-3

induced by Npro from a Cytopathic Bovine Viral Diarrhea Virus. Virology *366*, 277–292.

Chin, J.W. (2017). Expanding and reprogramming the genetic code. Nature *550*, 53–60.

Chon, S.K., Perez, D.R., and Donis, R.O. (1998). Genetic Analysis of the Internal Ribosome Entry Segment of Bovine Viral Diarrhea Virus. Virology *251*, 370–382.

Choo, Q., Kuo, G., Weiner, A., Overby, L., Bradley, D., and Houghton, M. (1989). Isolation of a cDNA clone derived from a blood-borne non-A, non-B viral hepatitis genome. Science (80-.). *244*, 359–362.

Choo, Q.L., Richman, K.H., Han, J.H., Berger, K., Lee, C., Dong, C., Gallegos, C., Coit, D., Medina-Selby, A., Barr, P.J., et al. (1991). Genetic organization and diversity of the hepatitis C virus. Proc. Natl. Acad. Sci. U. S. A. *88*, 2451–2455.

Chung, R.T., and Baumert, T.F. (2014). Curing Chronic Hepatitis C — The Arc of a Medical Triumph. N. Engl. J. Med. *370*, 1576–1578.

Collett, M.S., Larson, R., Gold, C., Strick, D., Anderson, D.K., and Purchio, A.F. (1988a). Molecular Cloning and Nucleotide Sequence of the Pestivirus Bovine Viral Diarrhea Virus. Virology *165*, 191–199.

Collett, M.S., Larson, R., Belzer, S.K., and Retzelt, E. (1988b). Proteins Encoded by Bovine Viral Diarrhea Virus: The Genomic Organization of a Pestivirus. Virology *165*, 200–208.

Collett, M.S., Wiskerchen, M.A., Welniak, E., and Belzer, S.K. (1991). Bovine viral diarrhea virus genomic organization. In Archives of Virology, (Springer, Vienna), pp. 19–27.

Corapi, W. V, Donis, R.O., and Dubovi, E.J. (1988). Monoclonal Antibody Analyses of Cytopathic and Noncytopathic Viruses from Fatal Bovine Viral Diarrhea Virus Infections. J. Virol. *62*, 2823–2827.

Corapi, W. V, Donis, R.O., and Dubovi, E.J. (1990). Characterization of a panel of monoclonal antibodies and their use in the study of the antigenic diversity of bovine viral diarrhea virus. Am. J. Vet. Res. *51*, 1388–1394.

Deleersnyder, V., Pillez, A., Wychowski, C., Blight, K., Xu, J., Hahn, Y.S., Rice, C.M., and Dubuisson, J. (1997). Formation of native hepatitis C virus glycoprotein complexes. J. Virol. *71*, 697–704.

Deng, R., and Brock, K. V (1993). 5’ and 3’ untranslated regions of pestivirus genome: primary and secondary structure analyses. Nucleic Acids Res. *21*, 1949–1957.

Dentzer, T.G., Lorenz, I.C., Evans, M.J., and Rice, C.M. (2009). Determinants of the Hepatitis C Virus Nonstructural Protein 2 Protease Domain Required for Production of Infectious Virus. J. Virol. *83*, 12702–12713.

Dimitrova, M., Imbert, I., Kieny, M.P., and Schuster, C. (2003). Protein-Protein Interactions between Hepatitis C Virus Nonstructural Proteins. J. Virol. *77*, 5401–5414.

Dorner, M., Horwitz, J.A., Robbins, J.B., Barry, W.T., Feng, Q., Mu, K., Jones, C.T., Schoggins, J.W., Catanese, M.T., Burton, D.R., et al. (2011). A genetically humanized mouse model for hepatitis C virus infection. Nature *474*, 208–211.

Dorner, M., Horwitz, J.A., Donovan, B.M., Labitt, R.N., Budell, W.C., Friling, T., Vogt, A., Catanese, M.T., Satoh, T., Kawai, T., et al. (2013). Completion of the entire hepatitis C virus life cycle in genetically humanized mice. Nature *501*, 237–241.

Dubrau, D., Tortorici, M.A., Rey, F.A., and Tautz, N. (2017). A positive-strand RNA virus uses alternative protein-protein interactions within a viral protease/cofactor complex to switch between RNA replication and virion morphogenesis. PLoS Pathog. *13*, 1–30.

Dubuisson, J., Hsu, H.H., Cheung, R.C., Greenberg, H.B., Russell, D.G., and Rice, C.M. (1994). Formation and intracellular localization of hepatitis C virus envelope glycoprotein complexes expressed by recombinant vaccinia and Sindbis viruses. J. Virol. *68*, 6147–6160.

Egger, D., Wölk, B., Gosert, R., Bianchi, L., Blum, H.E., Moradpour, D., and Bienz, K. (2002).

Expression of Hepatitis C Virus Proteins Induces Distinct Membrane Alterations Including a Candidate Viral Replication Complex. J. Virol. *76*, 5974–5984.

Elbers, K., Tautz, N., Becher, P., Stoll, D., Rümenapf, T., and Thiel, H.-J. (1996). Processing in the Pestivirus E2-NS2 Region: Identification of Proteins p7 and E2p7. J. Virol. *70*, 4131–4135.

Evans, M.J., Von Hahn, T., Tscherne, D.M., Syder, A.J., Panis, M., Wölk, B., Hatziioannou, T., McKeating, J.A., Bieniasz, P.D., and Rice, C.M. (2007). Claudin-1 is a hepatitis C virus co-receptor required for a late step in entry. Nature *446*, 801–805.

Failla, C., Tomei, L., and De Francesco, R. (1994). Both NS3 and NS4A are required for proteolytic processing of hepatitis C virus nonstructural proteins. J. Virol. *68*, 3753–3760.

Fellenberg, J. (2017). Etablierung experimenteller Testsysteme zur Ermittlung der Membrantopologie von BVDV NS2. Universität zu Lübeck.

Ferraris, P., Blanchard, E., and Roingeard, P. (2010). Ultrastructural and biochemical analyses of hepatitis C virus-associated host cell membranes. J. Gen. Virol. *91*, 2230–2237.

Foster, T.L., Tedbury, P.R., Pearson, A.R., and Harris, M. (2010). A comparative analysis of the fluorescence properties of the wild-type and active site mutants of the hepatitis C virus autoprotease NS2-3. Biochim. Biophys. Acta - Proteins Proteomics *1804*, 212–222.

Friebe, P., and Bartenschlager, R. (2002). Genetic Analysis of Sequences in the 3′ Nontranslated Region of Hepatitis C Virus That Are Important for RNA Replication. J. Virol. *76*, 5326–5338.

Friebe, P., Lohmann, V., Krieger, N., and Bartenschlager, R. (2001). Sequences in the 5′ Nontranslated Region of Hepatitis C Virus Required for RNA Replication. J. Virol. *75*, 12047–12057.

Gagné, B., Tremblay, N., Park, A.Y., Baril, M., and Lamarre, D. (2017). Importin β1 targeting by hepatitis C virus NS3/4A protein restricts IRF3 and NF-κB signaling of IFNB1 antiviral response. Traffic *18*, 362–377.

Gastaminza, P., Cheng, G., Wieland, S., Zhong, J., Liao, W., and Chisari, F. V. (2008). Cellular Determinants of Hepatitis C Virus Assembly, Maturation, Degradation, and Secretion. J. Virol. *82*, 2120–2129.

Van Geest, M., and Lolkema, J.S. (2000). Membrane Topology and Insertion of Membrane Proteins: Search for Topogenic Signals. Microbiol. Mol. Biol. Rev. *64*, 13–33.

Geller, R., Estada, Ú., Peris, J.B., Andreu, I., Bou, J.-V., Garijo, R., Cuevas, J.M., Sabariegos, R., Mas, A., and Sanjuán, R. (2016). Highly heterogeneous mutation rates in the hepatitis C virus genome. Nat. Microbiol. *1*, 16045.

Germi, R., Crance, J.M., Garin, D., Guimet, J., Lortat-Jacob, H., Ruigrok, R.W.H., Zarski, J.P., and Drouet, E. (2002). Cellular glycosaminoglycans and low density lipoprotein receptor are involved in hepatitis C virus adsorption. J. Med. Virol. *68*, 206–215.

Gomez, J., Martell, M., Quer, J., Cabot, B., and Esteban, J.I. (1999). Hepatitis C viral quasispecies. J. Viral Hepat. *6*, 3–16.

Gong, Y., Trowbridge, R., Macnaughton, T.B., Westaway, E.G., Shannon, A.D., and Gowans, E.J. (1996). Characterization of RNA synthesis during a one-step growth curve and of the replication mechanism of bovine viral diarrhoea virus. J. Gen. Virol. *77*, 2729–2736.

Gong, Y., Shannon, A., Westaway, E.G., and Gowans, E.J. (1998). The replicative intermediate molecule of bovine viral diarrhoea virus contains multiple nascent strands. Arch. Virol. *143*, 399–404.

Gorbalenya, A.E., Koonin, E. V, Donchenko, A.P., and Blinov, V.M. (1989). Two related superfamilies of putative helicases involved in replication, recombination, repair and expression of DNA and RNA genomes. Nucleic Acids Res. *17*, 4713–4730.

Gosert, R., Egger, D., Lohmann, V., Bartenschlager, R., Blum, H.E., Bienz, K., and

Moradpour, D. (2003). Identification of the Hepatitis C Virus RNA Replication Complex in Huh-7 Cells Harboring Subgenomic Replicons. J. Virol. *77*, 5487–5492.

Gottipati, K., Marcelo, L., Holthauzen, F., Ruggli, N., and Choi, K.H. (2016). Pestivirus Npro Directly Interacts with Interferon Regulatory Factor 3 Monomer and Dimer. J. Virol. *90*, 7740–7747.

Gouklani, H., Bull, R.A., Beyer, C., Coulibaly, F., Gowans, E.J., Drummer, H.E., Netter, H.J., White, P.A., and Haqshenas, G. (2012). Hepatitis C Virus Nonstructural Protein 5B Is Involved in Virus Morphogenesis. J. Virol. *86*, 5080–5088.

Gouklani, H., Beyer, C., Drummer, H., Gowans, E.J., Netter, H.J., and Haqshenas, G. (2013). Identification of specific regions in hepatitis C virus core, NS2 and NS5A that genetically interact with p7 and co-ordinate infectious virus production. J. Viral Hepat. *20*, e66–e71.

Gouttenoire, J., Montserret, R., Paul, D., Castillo, R., Meister, S., Bartenschlager, R., Penin, F., Moradpour, D., and Randall, G. (2014). Aminoterminal Amphipathic a-Helix AH1 of Hepatitis C Virus Nonstructural Protein 4B Possesses a Dual Role in RNA Replication and Virus Production. PLoS Pathog. *10*, e1004501.

Grakoui, A., Wychowski, C., Lin, C., Feinstone, S.M., and Rice, C.M. (1993). Expression and identification of hepatitis C virus polyprotein cleavage products. J. Virol. *67*, 1385–1395.

Grassmann, C.W., Isken, O., and Behrens, S.-E. (1999). Assignment of the Multifunctional NS3 Protein of Bovine Viral Diarrhea Virus during RNA Replication: an In Vivo and In Vitro Study. J. Virol. *73*, 9196–9205.

Grassmann, C.W., Isken, O., Tautz, N., and Behrens, S.-E. (2001). Genetic Analysis of the Pestivirus Nonstructural Coding Region: Defects in the NS5A Unit Can Be Complemented in trans. J. Virol. *75*, 7791–7802.

Grassmann, C.W., Yu, H., Isken, O., and Behrens, S.-E. (2005). Hepatitis C virus and the related bovine viral diarrhea virus considerably differ in the functional organization of the 5' non-translated region: Implications for the viral life cycle. Virology *333*, 349–366.

Gray, E.W., and Nettleton, P.F. (1987). The Ultrastructure of Cell Cultures Infected with Border Disease and Bovine Virus Diarrhoea Viruses. J. Gen. Virol. *68*, 2339–2346.

Griffin, S.D.C., Beales, L.P., Clarke, D.S., Worsfold, O., Evans, S.D., Jaeger, J., Harris, M.P.G., and Rowlands, D.J. (2003). The p7 protein of hepatitis C virus forms an ion channel that is blocked by the antiviral drug, Amantadine. FEBS Lett. *535*, 34–38.

Grummer, B., Beer, M., Liebler-Tenorio, E., and Greiser-Wilke, I. (2001). Localization of viral proteins in cells infected with bovine viral diarrhoea virus. J. Gen. Virol. *82*, 2597–2605.

Grummer, B., Grotha, S., and Greiser-Wilke, I. (2004). Bovine Viral Diarrhoea Virus is Internalized by Clathrin-dependent Receptor-mediated Endocytosis. J. Vet. Med. B, Infect. Dis. Vet. Public Heal. *51*, 427–432.

Gu, M., and Rice, C.M. (2013). Structures of hepatitis C virus nonstructural proteins required for replicase assembly and function. Curr. Opin. Virol. *3*, 129–136.

Han, Q., Manna, D., Belton, K., Cole, R., and Konan, K. V. (2013). Modulation of Hepatitis C Virus Genome Encapsidation by Nonstructural Protein 4B. J. Virol. *87*, 7409–7422.

Harada, T., Tautz, N., and Thiel, H.-J. (2000). E2-p7 Region of the Bovine Viral Diarrhea Virus Polyprotein: Processing and Functional Studies. J. Virol. *74*, 9498–9506.

Harris, H.J., Davis, C., Mullins, J.G.L., Hu, K., Goodall, M., Farquhar, M.J., Mee, C.J., McCaffrey, K., Young, S., Drummer, H., et al. (2010). Claudin association with CD81 defines hepatitis C virus entry. J. Biol. Chem. *285*, 21092–21102.

Hausmann, Y., Roman-Sosa, G., Thiel, H.-J., and Rümenapf, T. (2004). Classical Swine Fever Virus Glycoprotein Erns Is an Endoribonuclease with an Unusual Base Specificity. J. Virol. *78*, 5507–5512.

He, D., Xie, X., Yang, F., Zhang, H., Su, H., Ge, Y., Song, H., and Chen, P.R. (2017). Quantitative and Comparative Profiling of Protease Substrates through a Genetically Encoded Multifunctional Photocrosslinker. Angew. Chemie Int. Ed. *56*, 14521–14525.

Heimann, M., Roman-Sosa, G., Martoglio, B., Thiel, H.-J., and Rümenapf, T. (2006). Core Protein of Pestiviruses Is Processed at the C Terminus by Signal Peptide Peptidase. J. Virol. *80*, 1915–1921.

Hijikata, M., Kato, N., Ootsuyama, Y., Nakagawa, M., and Shimotohno, K. (1991). Gene mapping of the putative structural region of the hepatitis C virus genome by in vitro processing analysis. Proc. Natl. Acad. Sci. U. S. A. *88*, 5547–5551.

Hijikata, M., Mizushima, H., Tanji, Y., Komoda, Y., Hirowatari, Y., Akagi, T., Kato, N., Kimura, K., and Shimotohno, K. (1993a). Proteolytic processing and membrane association of putative nonstructural proteins of hepatitis C virus. Proc. Natl. Acad. Sci. U. S. A. *90*, 10773–10777.

Hijikata, M., Mizushima, H., Akagi, T., Mori, S., Kakiuchi, N., Kato, N., Tanaka, T., Kimura, K., and Shimotohno, K. (1993b). Two distinct proteinase activities required for the processing of a putative nonstructural precursor protein of hepatitis C virus. J. Virol. *67*, 4665–4675.

Hilton, L., Moganeradj, K., Zhang, G., Chen, Y.-H., Randall, R.E., Mccauley, J.W., and Goodbourn, S. (2006). The Npro Product of Bovine Viral Diarrhea Virus Inhibits DNA Binding by Interferon Regulatory Factor 3 and Targets It for Proteasomal Degradation. J. Virol. *80*, 11723–11732.

Hoff, H.S., and Donis, R.O. (1997). Induction of apoptosis and cleavage of poly(ADP-ribose) polymerase by cytopathic bovine vital diarrhea virus infection. Virus Res. *49*, 101–113.

Honda, M., Ping, L.-H., Rijnbrand, R.C.A., Amphlett, E., Clarke, B., Rowlands, D., and Lemon, S.M. (1996). Structural Requirements for Initiation of Translation by Internal Ribosome Entry within Genome-Length Hepatitis C Virus RNA. Virology *222*, 31–42.

Hopcraft, S.E., Azarm, K.D., Israelow, B., Lévêque, N., Schwarz, M.C., Hsu, T.-H., Chambers, M.T., Sourisseau, M., Semler, B.L., and Evans, M.J. (2016). Viral Determinants of miR-122-Independent Hepatitis C Virus Replication. MSphere *1*.

Horner, S.M., Liu, H.M., Park, H.S., Briley, J., and Gale, M. (2011). Mitochondrial-associated endoplasmic reticulum membranes (MAM) form innate immune synapses and are targeted by hepatitis C virus. Proc. Natl. Acad. Sci. U. S. A. *108*, 14590–14595.

Huang, C.F., Yeh, M.L., Huang, C.I., Lin, Y.J., Tsai, P.C., Lin, Z.Y., Chan, S.Y., Chen, S.C., Yang, H.I., Huang, J.F., et al. (2017). Risk of hepatitis C virus related hepatocellular carcinoma between subjects with spontaneous and treatment-induced viral clearance. Oncotarget *8*, 43925–43933.

Hügle, T., Fehrmann, F., Bieck, E., Kohara, M., Kräusslich, H.G., Rice, C.M., Blum, H.E., and Moradpour, D. (2001). The hepatitis C virus nonstructural protein 4B is an integral endoplasmic reticulum membrane protein. Virology *284*, 70–81.

Iqbal, M., and McCauley, J.W. (2002). Identification of the glycosaminoglycan-binding site on the glycoprotein Erns of bovine viral diarrhoea virus by site-directed mutagenesis. J. Gen. Virol. *83*, 2153–2159.

Iqbal, M., Flick-Smith, H., and McCauley, J.W. (2000). Interactions of bovine viral diarrhoea virus glycoprotein Erns with cell surface glycosaminoglycans. J. Gen. Virol. *81*, 451–459.

Iqbal, M., Poole, E., Goodbourn, S., and McCauley, J.W. (2004). Role for Bovine Viral Diarrhea Virus Erns Glycoprotein in the Control of Activation of Beta Interferon by Double-Stranded RNA. J. Virol. *78*, 136–145.

Isken, O., Grassmann, C.W., Sarisky, R.T., Kann, M., Zhang, S., Grosse, F., Kao, P.N., and Behrens, S.-E. (2003). Members of the NF90/NFAR protein group are involved in the life cycle of a positive-strand RNA virus. EMBO J. *22*, 5655–5665.

Isken, O., Grassmann, C.W., Yu, H., and Behrens, S.-E. (2004). Complex signals in the genomic 3' nontranslated region of bovine viral diarrhea virus coordinate translation and replication of the viral RNA. RNA *10*, 1637–1652.

Isken, O., Langerwisch, U., Schönherr, R., Lamp, B., Schröder, K., Duden, R., Rümenapf, T.H., and Tautz, N. (2014). Functional Characterization of Bovine Viral Diarrhea Virus Nonstructural Protein 5A by Reverse Genetic Analysis and Live Cell Imaging. J. Virol. *88*, 82–98.

Isken, O., Langerwisch, U., Jirasko, V., Rehders, D., Redecke, L., Ramanathan, H., Lindenbach, B.D., Bartenschlager, R., and Tautz, N. (2015). A Conserved NS3 Surface Patch Orchestrates NS2 Protease Stimulation, NS5A Hyperphosphorylation and HCV Genome Replication. PLoS Pathog. *11*, e1004736.

Isken, O., Postel, A., Bruhn, B., Lattwein, E., Becher, P., and Tautz, N. (2019). CRISPR/Cas9-Mediated Knockout of DNAJC14 Verifies This Chaperone as a Pivotal Host Factor for RNA Replication of Pestiviruses. J. Virol. *93*, e01714-18.

Ivanyi-Nagy, R., Lavergne, J.-P., Gabus, C., Ficheux, D., and Darlix, J.-L. (2008). RNA chaperoning and intrinsic disorder in the core proteins of Flaviviridae. Nucleic Acids Res. *36*, 712–725.

Jangra, R.K., Yi, M., and Lemon, S.M. (2010). Regulation of Hepatitis C Virus Translation and Infectious Virus Production by the MicroRNA miR-122. J. Virol. *84*, 6615–6625.

Jirasko, V., Montserret, R., Appel, N., Janvier, A., Eustachi, L., Brohm, C., Steinmann, E., Pietschmann, T., Penin, F., and Bartenschlager, R. (2008). Structural and Functional Characterization of Nonstructural Protein 2 for Its Role in Hepatitis C Virus Assembly. J. Biol. Chem. *283*, 28546–28562.

Jirasko, V., Montserret, R., Lee, J.Y., Gouttenoire, J., Moradpour, D., Penin, F., and Bartenschlager, R. (2010). Structural and Functional Studies of Nonstructural Protein 2 of the Hepatitis C Virus Reveal Its Key Role as Organizer of Virion Assembly. PLoS Pathog. *6*, e1001233.

Jones, C.T., Murray, C.L., Eastman, D.K., Tassello, J., and Rice, C.M. (2007). Hepatitis C Virus p7 and NS2 Proteins Are Essential for Production of Infectious Virus. J. Virol. *81*, 8374–8383.

Jopling, C.L., Yi, M.K., Lancaster, A.M., Lemon, S.M., and Sarnow, P. (2005). Molecular biology: Modulation of hepatitis C virus RNA abundance by a liver-specific MicroRNA. Science (80-.). *309*, 1577–1581.

Jordan, R., Wang, L., Graczyk, T.M., Block, T.M., and Romano, P.R. (2002). Replication of a Cytopathic Strain of Bovine Viral Diarrhea Virus Activates PERK and Induces Endoplasmic Reticulum Stress-Mediated Apoptosis of MDBK Cells. J. Virol. *76*, 9588–9599.

Kaneko, T., Tanji, Y., Satoh, S., Hijikata, M., Asabe, S., Kimura, K., and Shimotohno, K. (1994). Production of Two Phosphoproteins from the NS5A Region of the Hepatitis C Viral Genome. Biochem. Biophys. Res. Commun. *205*, 320–326.

Kao, C.C., Del Vecchio, A.M., and Zhong, W. (1999). De novo initiation of RNA synthesis by a recombinant flaviridae RNA- dependent RNA polymerase. Virology *253*, 1–7.

Kärber, G. (1931). Beitrag zur kollektiven Behandlung pharmakologischer Reihenversuche. Naunyn. Schmiedebergs. Arch. Exp. Pathol. Pharmakol. *162*, 480–483.

Kasza, L., Shadduck, J., and Christofinis, G. (1972). Establishment, viral susceptibility and biological characteristics of a swine kidney cell line SK-6. Res. Vet. Sci. *13*, 46–51.

Kato, N. (2000). Genome of human hepatitis C virus (HCV): Gene organization, sequence diversity, and variation. Microb. Comp. Genomics *5*, 129–151.

Kim, J.L., Morgenstern, K.A., Lin, C., Fox, T., Dwyer, M.D., Landro, J.A., Chambers, S.P., Markland, W., Lepre, C.A., O'Malley, E.T., et al. (1996). Crystal structure of the hepatitis C

virus NS3 protease domain complexed with a synthetic NS4A cofactor peptide. Cell *87*, 343–355.

Klemens, O. (2014). Charakterisierung der Determinanten für die NS2-3-unabhängige Virionmorphogenese bei Pestiviren. Universität zu Lübeck.

Klemens, O., Dubrau, D., and Tautz, N. (2015). Characterization of the Determinants of NS2-3-Independent Virion Morphogenesis of Pestiviruses. J. Virol. *89*, 11668–11680.

Kohlway, A., Pirakitikulr, N., Barrera, F.N., Potapova, O., Engelman, D.M., Pyle, A.M., and Lindenbach, B.D. (2014). Hepatitis C Virus RNA Replication and Virus Particle Assembly Require Specific Dimerization of the NS4A Protein Transmembrane Domain. J. Virol. *88*, 628–642.

Kokkonos, K.G., Fossat, N., Nielsen, L., Holm, C., Hepkema, W.M., Bukh, J., and Scheel, T.K.H. (2020). Evolutionary selection of pestivirus variants with altered or no microRNA dependency. Nucleic Acids Res. *48*, 5555–5571.

Kolykhalov, A.A., Agapov, E. V, and Rice, C.M. (1994). Specificity of the hepatitis C virus NS3 serine protease: effects of substitutions at the 3/4A, 4A/4B, 4B/5A, and 5A/5B cleavage sites on polyprotein processing. J. Virol. *68*, 7525–7533.

Kolykhalov, A.A., Feinstone, S.M., and Rice, C.M. (1996). Identification of a highly conserved sequence element at the 3' terminus of hepatitis C virus genome RNA. J. Virol. *70*.

Krey, T., Thiel, H.-J., and Rümenapf, T. (2005). Acid-Resistant Bovine Pestivirus Requires Activation for pH-Triggered Fusion during Entry. J. Virol. *79*, 4191–4200.

Kuo, D., Nie, M., and Courey, A.J. (2014). Sumo as a solubility tag and in vivo cleavage of SUMO fusion proteins with Ulp1. Methods Mol. Biol. *1177*, 71–80.

De La Fuente, C., Goodman, Z., and Rice, C.M. (2013). Genetic and Functional Characterization of the N-Terminal Region of the Hepatitis C Virus NS2 Protein. J. Virol. *87*, 4130–4145.

Lackner, T., Müller, A., Pankraz, A., Becher, P., Thiel, H.-J., Gorbalenya, A.E., and Tautz, N. (2004). Temporal Modulation of an Autoprotease Is Crucial for Replication and Pathogenicity of an RNA Virus. J. Virol. *78*, 10765–10775.

Lackner, T., Müller, A., König, M., Thiel, H.-J., and Tautz, N. (2005). Persistence of Bovine Viral Diarrhea Virus Is Determined by a Cellular Cofactor of a Viral Autoprotease. J. Virol. *79*, 9746–9755.

Lackner, T., Thiel, H.-J., and Tautz, N. (2006). Dissection of a viral autoprotease elucidates a function of a cellular chaperone in proteolysis. Proc. Natl. Acad. Sci. U. S. A. *103*, 1510–1515.

Laemmli, U.K. (1970). Cleavage of Structural Proteins during the Assembly of the Head of Bacteriophage T4. Nature *227*, 680–685.

Lai, V.C.H., Cheng Kao, C., Ferrari, E., Park, J., Uss, A.S., Wright-Minogue, J., Hong, Z., and Lau, J.Y.N. (1999). Mutational Analysis of Bovine Viral Diarrhea Virus RNA-Dependent RNA Polymerase. J. Virol. *73*, 10129–10136.

Lamp, B., Riedel, C., Roman-Sosa, G., Heimann, M., Jacobi, S., Becher, P., Thiel, H.-J., and Rümenapf, T. (2011). Biosynthesis of Classical Swine Fever Virus Nonstructural Proteins. J. Virol. *85*, 3607–3620.

Lange, C.M., Bellecave, P., Dao Thi, V.L., Tran, H.T.L., Penin, F., Moradpour, D., and Gouttenoire, J. (2014). Determinants for Membrane Association of the Hepatitis C Virus NS2 Protease Domain. J. Virol. *88*, 6519–6523.

Langerwisch, U. (2015). Characterization of the non-structural proteins 4B and 5A of the bovine viral diarrhea virus. Universität zu Luebeck.

Largo, E., Gladue, D.P., Huarte, N., Borca, M. V, and Nieva, J.L. (2014). Pore-forming activity of pestivirus p7 in a minimal model system supports genus-specific viroporin function.

Antiviral Res. *101*, 30–36.

Lattwein, E., Klemens, O., Schwindt, S., Becher, P., and Tautz, N. (2012). Pestivirus Virion Morphogenesis in the Absence of Uncleaved Nonstructural Protein 2-3. J. Virol. *86*, 427–437.

Li, K., Foy, E., Ferreon, J.C., Nakamura, M., Ferreon, A.C.M., Ikeda, M., Ray, S.C., Gale, M., and Lemon, S.M. (2005a). Immune evasion by hepatitis C virus NS3/4A protease-mediated cleavage of the Toll-like receptor 3 adaptor protein TRIF. Proc. Natl. Acad. Sci. U. S. A. *102*, 2992–2997.

Li, X.D., Sun, L., Seth, R.B., Pineda, G., and Chen, Z.J. (2005b). Hepatitis C virus protease NS3/4A cleaves mitochondrial antiviral signaling protein off the mitochondria to evade innate immunity. Proc. Natl. Acad. Sci. U. S. A. *102*, 17717–17722.

Liang, D., Chen, L., Ansari, I.H., Gil, L.H.V.G., Topliff, C.L., Kelling, C.L., and Donis, R.O. (2009). A replicon trans-packaging system reveals the requirement of nonstructural proteins for the assembly of bovine viral diarrhea virus (BVDV) virion. Virology *387*, 331–340.

Lin, C., Lindenbach, B.D., Prágai, B.M., McCourt, D.W., and Rice, C.M. (1994). Processing in the hepatitis C virus E2-NS2 region: identification of p7 and two distinct E2-specific products with different C termini. J. Virol. *68*, 5063–5073.

Lin, C., Thomson, J.A., and Rice, C.M. (1995). A central region in the hepatitis C virus NS4A protein allows formation of an active NS3-NS4A serine proteinase complex in vivo and in vitro. J. Virol. *69*, 4373–4380.

Lindenbach, B.D., and Rice, C.M. (2013). The ins and outs of hepatitis C virus entry and assembly. Nat. Rev. Microbiol. *11*, 688–700.

Lindenbach, B.D., Evans, M.J., Syder, A.J., Wölk, B., Tellinghuisen, T.L., Liu, C.C., Maruyama, T., Hynes, R.O., Burton, D.R., McKeating, J.A., et al. (2005). Complete Replication of Hepatitis C Virus in Cell Culture. Science (80-.). *309*, 623–626.

Lindenbach, B.D., Thiel, H.-J., and Rice, C.M. (2007a). Flaviviridae: The Viruses and Their Replication. In Fields Virology, D.M. Knipe, and P.M. Howley, eds. (Philadelphia: Lippincott-Raven Publishers), pp. 1101–1152.

Lindenbach, B.D., Prágai, B.M., Montserret, R., Beran, R.K.F., Pyle, A.M., Penin, F., and Rice, C.M. (2007b). The C Terminus of Hepatitis C Virus NS4A Encodes an Electrostatic Switch That Regulates NS5A Hyperphosphorylation and Viral Replication. J. Virol. *81*, 8905–8918.

Lindenbach, B.D., Murray, C.L., Thiel, H.J., and Rice, C.M. (2013). Flaviviridae. In Fields Virology, D.M. Knipe, and P.M. Howley, eds. (Philadelphia: Lippincott Williams & Wilkin), pp. 712–746.

Liu, Q., Tackney, C., Bhat, R.A., Prince, A.M., and Zhang, P. (1997). Regulated processing of hepatitis C virus core protein is linked to subcellular localization. J. Virol. *71*, 657–662.

Liu, S., Yang, W., Shen, L., Turner, J.R., Coyne, C.B., and Wang, T. (2009). Tight Junction Proteins Claudin-1 and Occludin Control Hepatitis C Virus Entry and Are Downregulated during Infection To Prevent Superinfection. J. Virol. *83*, 2011–2014.

Lohmann, V., Körner, F., Koch, J.O., Herian, U., Theilmann, L., and Bartenschlager, R. (1999). Replication of subgenomic hepatitis C virus RNAs in a hepatoma cell line. Science (80-.). *285*, 110–113.

Lorenz, I.C., Marcotrigiano, J., Dentzer, T.G., and Rice, C.M. (2006). Structure of the catalytic domain of the hepatitis C virus NS2-3 protease. Nature *442*, 831–835.

Love, R.A., and Parge, H.E. (1996). The Crystal Structure of Hepatitis C Virus NS3 Proteinase Reveals a Trypsin-like Fold and a Structural Zinc Binding Site. Cell *87*, 331–342.

Luna, J.M., Scheel, T.K.H., Danino, T., Shaw, K.S., Mele, A., Fak, J.J., Nishiuchi, E., Takacs, C.N., Catanese, M.T., De Jong, Y.P., et al. (2015). Hepatitis C virus RNA functionally

sequesters miR-122. Cell *160*, 1099–1110.

Lundin, M., Monné, M., Widell, A., Von, G., Persson, M.A.A., Monne, M., and Heijne, G. Von (2003). Topology of the Membrane-Associated Hepatitis C Virus Protein NS4B Topology of the Membrane-Associated Hepatitis C Virus Protein NS4B. J. Virol. *77*, 5428–5438.

Lundin, M., Lindström, H., Grönwall, C., and Persson, M.A.A. (2006). Dual topology of the processed hepatitis C virus protein NS4B is influenced by the NS5A protein. J. Gen. Virol. *87*, 3263–3272.

Lupberger, J., Zeisel, M.B., Xiao, F., Thumann, C., Fofana, I., Zona, L., Davis, C., Mee, C.J., Turek, M., Gorke, S., et al. (2011). EGFR and EphA2 are host factors for hepatitis C virus entry and possible targets for antiviral therapy. Nat. Med. *17*, 589–595.

Ma, Y., Anantpadma, M., Timpe, J.M., Shanmugam, S., Singh, S.M., Lemon, S.M., and Yi, M. (2011). Hepatitis C Virus NS2 Protein Serves as a Scaffold for Virus Assembly by Interacting with both Structural and Nonstructural Proteins. J. Virol. *85*, 86–97.

Macovei, A., Zitzmann, N., Lazar, C., Dwek, R.A., and Branza-Nichita, N. (2006). Brefeldin A inhibits pestivirus release from infected cells, without affecting its assembly and infectivity. Biochem. Biophys. Res. Commun. *346*, 1083–1090.

Madan, V., Paul, D., Lohmann, V., and Bartenschlager, R. (2014). Inhibition of HCV Replication by Cyclophilin Antagonists Is Linked to Replication Fitness and Occurs by Inhibition of Membranous Web Formation. Gasroenterology *146*, 1361–1372.

Magkouras, I., Mätzener, P., Rümenapf, T., Peterhans, E., and Schweizer, M. (2008). RNase-dependent inhibition of extracellular, but not intracellular, dsRNA-induced interferon synthesis by Erns of pestiviruses. J. Gen. Virol. *89*, 2501–2506.

Martell, M., Esteban, J.I., Quer, J., Genescà, J., Weiner, A., Esteban, R., Guardia, J., and Gómez, J. (1992). Hepatitis C virus (HCV) circulates as a population of different but closely related genomes: quasispecies nature of HCV genome distribution. J. Virol. *66*, 3225–3229.

Martin, D.N., and Uprichard, S.L. (2013). Identification of transferrin receptor 1 as a hepatitis C virus entry factor. Proc. Natl. Acad. Sci. U. S. A. *110*, 10777–10782.

Masaki, T., Arend, K.C., Moorman, N.J., Lemon Correspondence, S.M., Li, Y., Yamane, D., Mcgivern, D.R., Kato, T., Wakita, T., and Lemon, S.M. (2015). miR-122 Stimulates Hepatitis C Virus RNA Synthesis by Altering the Balance of Viral RNAs Engaged in Replication versus Translation. Cell Host Microbe *17*, 217–228.

Mathapati, B.S., Mishra, N., Rajukumar, K., Nema, R.K., Behera, S.P., and Dubey, S.C. (2010). Entry of bovine viral diarrhea virus into ovine cells occurs through clathrin-dependent endocytosis and low pH-dependent fusion. Vitr. Cell. Dev. Biol. - Anim. *46*, 403–407.

Mätzener, P., Magkouras, I., Rümenapf, T., Peterhans, E., and Schweizer, M. (2009). The viral RNase Erns prevents IFN type-I triggering by pestiviral single-and double-stranded RNAs. Virus Res. *140*, 15–23.

Maurer, K., Krey, T., Moennig, V., Thiel, H.-J., and Rümenapf, T. (2004). CD46 Is a Cellular Receptor for Bovine Viral Diarrhea Virus. J. Virol. *78*, 1792–1799.

McLauchlan, J., Lemberg, M.K., Hope, G., and Martoglio, B. (2002). Intramembrane proteolysis promotes trafficking of hepatitis C virus core protein to lipid droplets. EMBO J. *21*, 3980–3988.

Mendez, E., Ruggli, N., Collett, M.S., and Rice, C.M. (1998). Infectious Bovine Viral Diarrhea Virus (Strain NADL) RNA from Stable cDNA Clones: a Cellular Insert Determines NS3 Production and Viral Cytopathogenicity. J. Virol. *72*, 4737–4745.

Meunier, J.-C., Russell, R.S., Engle, R.E., Faulk, K.N., Purcell, R.H., and Emerson, S.U. (2008). Apolipoprotein C1 Association with Hepatitis C Virus. J. Virol. *82*, 9647–9656.

Meyers, G., Rümenapf, T., and Thiel, H.-J. (1989). Ubiquitin in a togavirus. Nature *341*, 491.

Meyers, G., Tautz, N., Stark, R., Brownlie, J., Dubovi, E.J., Collelt, M.S., and Thiel, H.-J.

(1992). Rearrangement of Viral Sequences in Cytopathogenic Pestiviruses. Virology *191*, 368–386.

Meyers, G., Tautz, N., Becher, P., Thiel, H.-J., and Kümmerer, B.M. (1996). Recovery of Cytopathogenic and Noncytopathogenic Bovine Viral Diarrhea Viruses from cDNA Constructs. J. Virol. *70*, 8606–8613.

Meylan, E., Curran, J., Hofmann, K., Moradpour, D., Binder, M., Bartenschlager, R., and Tschopp, J. (2005). Cardif is an adaptor protein in the RIG-I antiviral pathway and is targeted by hepatitis C virus. Nature *437*, 1167–1172.

Miyanari, Y., Atsuzawa, K., Usuda, N., Watashi, K., Hishiki, T., Zayas, M., Bartenschlager, R., Wakita, T., Hijikata, M., and Shimotohno, K. (2007). The lipid droplet is an important organelle for hepatitis C virus production. Nat. Cell Biol. *9*, 1089–1097.

De Moerlooze, L., Desport, M., Renard, A., Lecomte, C., Brownlie, J., and Martial, J.A. (1990). The Coding Region for the 54-kDa Protein of Several Pestiviruses Lacks Host Insertions but Reveals a “Zinc Finger-Like” Domain. Virology *177*, 812–815.

Monazahian, M., Böhme, I., Bonk, S., Koch, A., Scholz, C., Grethe, S., and Thomssen, R. (1999). Low density lipoprotein receptor as a candidate receptor for hepatitis C virus. J. Med. Virol. *57*, 223–229.

Moradpour, D., Englert, C., Wakita, T., and Wands, J.R. (1996). Characterization of cell lines allowing tightly regulated expression of hepatitis C virus core protein. Virology *222*, 51–63.

Moradpour, D., Evans, M.J., Gosert, R., Yuan, Z., Blum, H.E., Goff, S.P., Lindenbach, B.D., and Rice, C.M. (2004). Insertion of Green Fluorescent Protein into Nonstructural Protein 5A Allows Direct Visualization of Functional Hepatitis C Virus Replication Complexes. J. Virol. *78*, 7400–7409.

Morikawa, K., Lange, C.M., Gouttenoire, J., Meylan, E., Brass, V., Penin, F., and Moradpour, D. (2011). Nonstructural protein 3-4A: The Swiss army knife of hepatitis C virus. J. Viral Hepat. *18*, 305–315.

Moulin, H.R., Seuberlich, T., Bauhofer, O., Bennett, L.C., Tratschin, J.-D., Hofmann, M.A., and Ruggli, N. (2007). Nonstructural proteins NS2-3 and NS4A of classical swine fever virus: Essential features for infectious particle formation. Virology *365*, 376–389.

Murray, C.L., Marcotrigiano, J., and Rice, C.M. (2008a). Bovine Viral Diarrhea Virus Core Is an Intrinsically Disordered Protein That Binds RNA. J. Virol. *82*, 1294–1304.

Murray, C.L., Jones, C.T., and Rice, C.M. (2008b). Architects of assembly: roles of Flaviviridae non-structural proteins in virion morphogenesis. Nat. Rev. Microbiol. *6*, 699–708.

Neddermann, P., Clementi, A., and De Francesco, R. (1999). Hyperphosphorylation of the Hepatitis C Virus NS5A Protein Requires an Active NS3 Protease, NS4A, NS4B, and NS5A Encoded on the Same Polyprotein. J. Virol. *73*, 9984–9991.

Neufeldt, C.J., Cortese, M., Acosta, E.G., and Bartenschlager, R. (2018). Rewiring cellular networks by members of the Flaviviridae family. Nat. Rev. Microbiol. *16*, 125–142.

Nielsen, S.U., Bassendine, M.F., Burt, A.D., Martin, C., Pumeechockchai, W., and Toms, G.L. (2006). Association between Hepatitis C Virus and Very-Low-Density Lipoprotein (VLDL)/LDL Analyzed in Iodixanol Density Gradients. J. Virol. *80*, 2418–2428.

Niepmann, M. (2013). Hepatitis C virus RNA translation. Curr. Top. Microbiol. Immunol. *369*, 143–166.

Nieva, J.L., Madan, V., and Carrasco, L. (2012). Viroporins: Structure and biological functions. Nat. Rev. Microbiol. *10*, 563–574.

Nilsson, I.M., and von Heijne, G. (1993). Determination of the distance between the oligosaccharyltransferase active site and the endoplasmic reticulum membrane. J. Biol. Chem. *268*, 5798–5801.

Oliver Koch, J., and Bartenschlager, R. (1999). Modulation of Hepatitis C Virus NS5A

Hyperphosphorylation by Nonstructural Proteins NS3, NS4A, and NS4B. J. Virol. *73*, 7138–7146.

Pallaoro, M., Lahm, A., Biasiol, G., Brunetti, M., Nardella, C., Orsatti, L., Bonelli, F., Orr, S., Narjes, F., and Steinkühler, C. (2001). Characterization of the Hepatitis C Virus NS2/3 Processing Reaction by Using a Purified Precursor Protein. J. Virol. *75*, 9939–9946.

Pankraz, A., Thiel, H.-J., and Becher, P. (2005). Essential and Nonessential Elements in the 3' Nontranslated Region of Bovine Viral Diarrhea Virus. J. Virol. *79*, 9119–9127.

Paul, D., and Bartenschlager, R. (2015). Flaviviridae Replication Organelles: Oh, What a Tangled Web We Weave. Annu. Rev. Virol. *2*, 289–310.

Paul, D., Romero-Brey, I., Gouttenoire, J., Stoitsova, S., Krijnse-Locker, J., Moradpour, D., and Bartenschlager, R. (2011). NS4B Self-Interaction through Conserved C-Terminal Elements Is Required for the Establishment of Functional Hepatitis C Virus Replication Complexes. J. Virol. *85*, 6963–6976.

Paul, D., Madan, V., and Bartenschlager, R. (2014). Hepatitis C Virus RNA Replication and Assembly: Living on the Fat of the Land. Cell Host Microbe *16*, 569–579.

Pavlovic, D., Neville, D.C.A., Argaud, O., Blumberg, B., Dwek, R.A., Fischer, W.B., and Zitzmann, N. (2003). The hepatitis C virus p7 protein forms an ion channel that is inhibited by long-alkyl-chain iminosugar derivatives. Proc. Natl. Acad. Sci. U. S. A. *100*, 6104–6108.

Penin, F., Brass, V., Appel, N., Ramboarina, S., Montserret, R., Ficheux, D., Blum, H.E., Bartenschlager, R., and Moradpour, D. (2004). Structure and function of the membrane anchor domain of hepatitis C virus nonstructural protein 5A. J. Biol. Chem. *279*, 40835–40843.

Petracca, R., Falugi, F., Galli, G., Norais, N., Rosa, D., Campagnoli, S., Burgio, V., Di Stasio, E., Giardina, B., Houghton, M., et al. (2000). Structure-Function Analysis of Hepatitis C Virus Envelope-CD81 Binding. J. Virol. *74*, 4824–4830.

Petta, S., and Craxì, A. (2015). Current and future HCV therapy: Do we still need other anti-HCV drugs? Liver Int. *35*, 4–10.

Phan, T., Beran, R.K.F., Peters, C., Lorenz, I.C., and Lindenbach, B.D. (2009). Hepatitis C Virus NS2 Protein Contributes to Virus Particle Assembly via Opposing Epistatic Interactions with the E1-E2 Glycoprotein and NS3-NS4A Enzyme Complexes. J. Virol. *83*, 8379–8395.

Phan, T., Kohlway, A., Dimberu, P., Pyle, A.M., and Lindenbach, B.D. (2011). The Acidic Domain of Hepatitis C Virus NS4A Contributes to RNA Replication and Virus Particle Assembly. J. Virol. *85*, 1193–1204.

Pietschmann, T., Lohmann, V., Kaul, A., Krieger, N., Rinck, G., Rutter, G., Strand, D., and Bartenschlager, R. (2002). Persistent and Transient Replication of Full-Length Hepatitis C Virus Genomes in Cell Culture. J. Virol. *76*, 4008–4021.

Pietschmann, T., Kaul, A., Koutsoudakis, G., Shavinskaya, A., Kallis, S., Steinmann, E., Abid, K., Negro, F., Dreux, M., Cosset, F.-L., et al. (2006). Construction and characterization of infectious intragenotypic and intergenotypic hepatitis C virus chimeras. Proc. Natl. Acad. Sci. U. S. A. *103*, 7408–7413.

Pileri, P., Uematsu, Y., Campagnoli, S., Galli, G., Falugi, F., Petracca, R., Weiner, A.J., Houghton, M., Rosa, D., Grandi, G., et al. (1998). Binding of hepatitis C virus to CD81. Science (80-.). *282*, 938–941.

Piñeiro, D., and Martinez-Salas, E. (2012). RNA Structural Elements of Hepatitis C Virus Controlling Viral RNA Translation and the Implications for Viral Pathogenesis. Viruses *4*, 2233–2250.

Ploss, A., Evans, M.J., Gaysinskaya, V.A., Panis, M., You, H., De Jong, Y.P., and Rice, C.M. (2009). Human occludin is a hepatitis C virus entry factor required for infection of mouse cells. Nature *457*, 882–886.

Poole, T.L., Wang, C., Popp, R.A., Potgieter, L.N.D., Siddiqui, A., and Collett, M.S. (1995). Pestivirus Translation Initiation Occurs by Internal Ribosome Entry. Virology *206*, 750–754.

Popescu, C.-I., Callens, N., Trinel, D., Roingeard, P., Moradpour, D., Descamps, V.R., Duverlie, G., Penin, F., Hé Liot, L., Rouillé, Y., et al. (2011). NS2 Protein of Hepatitis C Virus Interacts with Structural and Non-Structural Proteins towards Virus Assembly. PLoS Pathog. *7*, e1001278.

Popov, M., Tam, L.Y., Li, J., and Reithmeier, R.A.F. (1997). Mapping the ends of transmembrane segments in a polytopic membrane protein. Scanning N-glycosylation mutagenesis of extracytosolic loops in the anion exchanger, band 3. J Biol Chem *272*, 18325–18332.

Powell, M.J.D. (1977). Restart procedures for the conjugate gradient method. Math. Program. *12*, 241–254.

Premkumar, A., Wilson, L., Ewart, G.., and Gage, P.. (2004). Cation-selective ion channels formed by p7 of hepatitis C virus are blocked by hexamethylene amiloride. FEBS Lett. *557*, 99–103.

Quinkert, D., Bartenschlager, R., and Lohmann, V. (2005). Quantitative Analysis of the Hepatitis C Virus Replication Complex. J. Virol. *79*, 13594–13605.

Reed, K.E., Xu, J., and Rice, C.M. (1997). Phosphorylation of the hepatitis C virus NS5A protein in vitro and in vivo: properties of the NS5A-associated kinase. J. Virol. *71*, 7187–7197.

Reed, K.E., Gorbalenya, A.E., and Rice, C.M. (1998). The NS5A/NS5 Proteins of Viruses from Three Genera of the Family Flaviviridae Are Phosphorylated by Associated Serine/Threonine Kinases. J. Virol. *72*, 6199–6206.

Rijnbrand, R., Van Der Straaten, T., Van Rijn, P.A., Spaan, W.J.M., and Bredenbeek, P.J. (1997). Internal Entry of Ribosomes Is Directed by the 5' Noncoding Region of Classical Swine Fever Virus and Is Dependent on the Presence of an RNA Pseudoknot Upstream of the Initiation Codon. J. Virol. *71*, 451–457.

Rinck, G., Birghan, C., Harada, T., Meyers, G., Thiel, H.-J., and Tautz, N. (2001). A Cellular J-Domain Protein Modulates Polyprotein Processing and Cytopathogenicity of a Pestivirus. J. Virol. *75*, 9470–9482.

Romero-Brey, I., and Bartenschlager, R. (2014). Membranous Replication Factories Induced by Plus-Strand RNA Viruses. Viruses *6*, 2826–2857.

Romero-Brey, I., Merz, A., Chiramel, A., Lee, J.-Y., Chlanda, P., Haselman, U., Santarella-Mellwig, R., Habermann, A., Hoppe, S., Kallis, S., et al. (2012). Three-Dimensional Architecture and Biogenesis of Membrane Structures Associated with Hepatitis C Virus Replication. PLoS Pathog. *8*, e1003056.

Ronecker, S., Zimmer, G., Herrler, G., Greiser-Wilke, I., and Grummer, B. (2008). Formation of bovine viral diarrhea virus E1–E2 heterodimers is essential for virus entry and depends on charged residues in the transmembrane domains. J. Gen. Virol. *89*, 2114–2121.

Ruggli, N., Tratschin, J.-D., Schweizer, M., McCullough, K.C., Hofmann, M.A., and Summerfield, A. (2003). Classical Swine Fever Virus Interferes with Cellular Antiviral Defense: Evidence for a Novel Function of Npro. J. Virol. *77*, 7645–7654.

Rümenapf, T., Unger, G., Strauss, J.H., and Thiel2, H.-J. (1993). Processing of the Envelope Glycoproteins of Pestiviruses. J. Virol. *67*, 3288–3294.

Sainz, B., Barretto, N., Martin, D.N., Hiraga, N., Imamura, M., Hussain, S., Marsh, K.A., Yu, X., Chayama, K., Alrefai, W.A., et al. (2012). Identification of the Niemann-Pick C1-like 1 cholesterol absorption receptor as a new hepatitis C virus entry factor. Nat. Med. *18*, 281–285.

Sakai, A., St. Claire, M., Faulk, K., Govindarajan, S., Emerson, S.U., Purcell, R.H., and Bukh,

J. (2003). The p7 polypeptide of hepatitis C virus is critical for infectivity and contains functionally important genotype-specific sequences. Proc. Natl. Acad. Sci. U. S. A. *100*, 11646–11651.

Santolini, E., Pacini, L., Fipaldini, C., Migliaccio, G., and Monica, N. La (1995). The NS2 Protein of Hepatitis C Virus Is a Transmembrane Polypeptide. J. Virol. *69*, 7461–7471.

Scarselli, E., Ansuini, H., Cerino, R., Roccasecca, R.M., Acali, S., Filocamo, G., Traboni, C., Nicosia, A., Cortese, R., and Vitelli, A. (2002). The human scavenger receptor class B type I is a novel candidate receptor for the hepatitis C virus. EMBO J. *21*, 5017–5025.

Schägger, H., and von Jagow, G. (1987). Tricine-Sodium Dodecyl Sulfate-Polyacrylamide Gel Electrophoresis for the Separation of Proteins in the Range from 1 to 100 kDa. Anal. Biochem. *166*, 368–379.

Scheel, T.K.H., Luna, J.M., Liniger, M., Nishiuchi, E., Rozen-Gagnon, K., Shlomai, A., Auray, G., Gerber, M., Fak, J., Keller, I., et al. (2016). A Broad RNA Virus Survey Reveals Both miRNA Dependence and Functional Sequestration. Cell Host Microbe *19*, 409–423.

Schmeiser, S., Mast, J., Thiel, H.-J., and König, M. (2014). Morphogenesis of Pestiviruses: New Insights from Ultrastructural Studies of Strain Giraffe-1. J. Virol. *88*, 2717–2724.

Schregel, V., Jacobi, S., Penin, F., and Tautz, N. (2009). Hepatitis C virus NS2 is a protease stimulated by cofactor domains in NS3. Proc. Natl. Acad. Sci. *106*, 5342–5347.

Schult, P., Roth, H., Adams, R.L., Mas, C., Imbert, L., Orlik, C., Ruggieri, A., Pyle, A.M., and Lohmann, V. (2018). microRNA-122 amplifies hepatitis C virus translation by shaping the structure of the internal ribosomal entry site. Nat. Commun. *9*, 2613.

Schultz, D.E., Honda, M., Whetter, L.E., Mcknight, K.L., and Lemon, S.M. (1996). Mutations within the 5' Nontranslated RNA of Cell Culture-Adapted Hepatitis A Virus Which Enhance Cap-Independent Translation in Cultured African Green Monkey Kidney Cells. J. Virol. *70*, 1041–1049.

Sedano, C.D., and Sarnow, P. (2014). Hepatitis C virus subverts liver-specific miR-122 to protect the viral genome from exoribonuclease Xrn2. Cell Host Microbe *16*, 257–264.

Selby, M.J., Glazer, E., Masiarz, F., and Houghton, M. (1994). Complex Processing and Protein:Protein Interactions in the E2:NS2 Region of HCV. Virology *204*, 114–122.

Shi, S.T., Polyak, S.J., Tu, H., Taylor, D.R., Gretch, D.R., and Lai, M.M.C. (2002). Hepatitis C virus NS5A colocalizes with the core protein on lipid droplets and interacts with apolipoproteins. Virology *292*, 198–210.

Simmonds, P., Becher, P., Bukh, J., Gould, E.A., Meyers, G., Monath, T., Muerhoff, S., Pletnev, A., Rico-Hesse, R., Smith, D.B., et al. (2017). ICTV Virus Taxonomy Profile: Flaviviridae. J. Gen. Virol. *98*, 2–3.

Smith, D.B., Bukh, J., Kuiken, C., Muerhoff, A.S., Rice, C.M., Stapleton, J.T., and Simmonds, P. (2014). Expanded classification of hepatitis C virus into 7 genotypes and 67 subtypes: Updated criteria and genotype assignment web resource. Hepatology *59*, 318–327.

Smith, D.B., Becher, P., Bukh, J., Gould, E.A., Meyers, G., Monath, T., Muerhoff, A.S., Pletnev, A., Rico-Hesse, R., Stapleton, J.T., et al. (2016). Proposed update to the taxonomy of the genera Hepacivirus and Pegivirus within the Flaviviridae family. J. Gen. Virol. *97*, 2894–2907.

Smith, D.B., Meyers, G., Bukh, J., Gould, E.A., Monath, T., Muerhoff, A.S., Pletnev, A., Rico-Hesse, R., Stapleton, J.T., Simmonds, P., et al. (2017). Proposed revision to the taxonomy of the genus Pestivirus, family Flaviviridae. J. Gen. Virol. *98*, 2106–2112.

Stapleford, K.A., and Lindenbach, B.D. (2011). Hepatitis C Virus NS2 Coordinates Virus Particle Assembly through Physical Interactions with the E1-E2 Glycoprotein and NS3-NS4A Enzyme Complexes. J. Virol. *85*, 1706–1717.

Stapleton, J.T., Foung, S., Muerhoff, A.S., Bukh, J., Simmonds, P., and Jack Stapleton, C.T.

(2011). The GB viruses: a review and proposed classification of GBV-A, GBV-C (HGV), and GBV-D in genus Pegivirus within the family Flaviviridae. J. Gen. Virol. *92*, 233–246.

Stark, R., Rumenapf, T., Meyers, G., and Thiel, H.-J. (1990). Genomic Localization of Hog Cholera Virus Glycoproteins. Virology *174*, 286–289.

Stark, R., Meyers, G., Rümenapf, T., and Thiel, H.J. (1993). Processing of Pestivirus Polyprotein: Cleavage Site between Autoprotease and Nucleocapsid Protein of Classical Swine Fever Virus. J. Virol. *67*, 7088–7095.

Sutter, G., Ohlmann, M., and Erfle, V. (1995). Non-replicating vaccinia vector efficiently expresses bacteriophage T7 RNA polymerase. FEBS Lett. *371*, 9–12.

Syed, G.H., Khan, M., Yang, S., and Siddiqui, A. (2017). Hepatitis C Virus Lipoviroparticles Assemble in the Endoplasmic Reticulum (ER) and Bud off from the ER to the Golgi Compartment in COPII Vesicles. J. Virol. *91*.

Tanaka, T., Kato, N., Cho, M.J., and Shimotohno, K. (1995). A novel sequence found at the 3′-terminus of hepatitis C virus genome. Biochem. Biophys. Res. Commun. *215*, 744–749.

Tanaka, T., Kato, N., Cho, M.J., Sugiyama, K., and Shimotohno, K. (1996). Structure of the 3' terminus of the hepatitis C virus genome. J. Virol. *70*, 3307–3312.

Tanji, Y., Hijikata, M., Satoh, S., Kaneko, T., and Shimotohno, K. (1995). Hepatitis C virus-encoded nonstructural protein NS4A has versatile functions in viral protein processing. J. Virol. *69*, 1575–1581.

Tautz, N., and Thiel, H.J. (2003). Cytopathogenicity of pestiviruses: Cleavage of bovine viral diarrhea virus NS2-3 has to occur at a defined position to allow viral replication. Arch. Virol. *148*, 1405–1412.

Tautz, N., Meyers, G., and Thiel, H.-J. (1993). Processing of Poly-ubiquitin in the Polyprotein of an RNA Virus. Virology *197*, 74–85.

Tautz, N., Meyers, G., Stark, R., Dubovi, E.J., and Thiel, H.-J. (1996). Cytopathogenicity of a Pestivirus Correlates with a 27-Nucleotide Insertion. J. Virol. *70*, 7851–7858.

Tautz, N., Elbers, K., Stoll, D., Meyers, G., and Thiel, H.-J. (1997). Serine Protease of Pestiviruses: Determination of Cleavage Sites. J. Virol. *71*, 5415–5422.

Tautz, N., Harada, T., Kaiser, A., Rinck, G., Behrens, S.-E., and Thiel, H.-J. (1999). Establishment and Characterization of Cytopathogenic and Noncytopathogenic Pestivirus Replicons. J. Virol. *73*, 9422–9432.

Tautz, N., Kaiser, A., and Thiel, H.-J. (2000). NS3 Serine Protease of Bovine Viral Diarrhea Virus: Characterization of Active Site Residues, NS4A Cofactor Domain, and Protease–Cofactor Interactions. Virology *273*, 351–363.

Tautz, N., Tews, B.A., and Meyers, G. (2015). The Molecular Biology of Pestiviruses. In Advances in Virus Research, pp. 47–160.

Tedbury, P.R., and Harris, M. (2007). Characterisation of the Role of Zinc in the Hepatitis C Virus NS2/3 Auto-cleavage and NS3 Protease Activities. J. Mol. Biol. *366*, 1652–1660.

Tellinghuisen, T.L., Marcotrigiano, J., Gorbalenya, A.E., and Rice, C.M. (2004). The NS5A Protein of Hepatitis C Virus Is a Zinc Metalloprotein. J. Biol. Chem. *279*, 48576–48587.

Tellinghuisen, T.L., Marcotrigiano, J., and Rice, C.M. (2005). Structure of the zinc-binding domain of an essential component of the hepatitis C virus replicase. Nature *435*, 374–379.

Tellinghuisen, T.L., Paulson, M.S., and Rice, C.M. (2006). The NS5A Protein of Bovine Viral Diarrhea Virus Contains an Essential Zinc-Binding Site Similar to That of the Hepatitis C Virus NS5A Protein. J. Virol. *80*, 7450–7458.

Tellinghuisen, T.L., Foss, K.L., and Treadaway, J. (2008). Regulation of Hepatitis C Virion Production via Phosphorylation of the NS5A Protein. PLoS Pathog. *4*, e1000032.

Tews, B.A., and Meyers, G. (2007). The Pestivirus Glycoprotein Erns Is Anchored in Plane in

the Membrane via an Amphipathic Helix. J. Biol. Chem. *282*, 32730–32741.

Thi, V.L.D., Granier, C., Zeisel, M.B., Guérin, M., Mancip, J., Granio, O., Penin, F., Lavillette, D., Bartenschlager, R., Baumert, T.F., et al. (2012). Characterization of hepatitis C virus particle subpopulations reveals multiple usage of the scavenger receptor BI for entry steps. J. Biol. Chem. *287*, 31242–31257.

Thiel, H.-J., Stark, R., Weiland, E., Rümenapf, T., and Meyers, G. (1991). Hog Cholera Virus: Molecular Composition of Virions from a Pestivirus. J. Virol. *65*, 4705–4712.

Thiel, H.J., Plagemann, P.G.W., and Moennig, V. (1996). Pestiviruses. In Fields Virology: Vol. 3, B.N. Fields, D.M. Knipe, and P.M. Howley, eds. (New York: Lippincott-Raven Publishers), pp. 1059–1073.

Thomssen, R., Bonk, S., Propfe, C., Heermann, K.H., Köchel, H.G., and Uy, A. (1992). Association of hepatitis C virus in human sera with β-lipoprotein. Med. Microbiol. Immunol. *181*, 293–300.

Tscherne, D.M., Evans, M.J., MacDonald, M.R., and Rice, C.M. (2008). Transdominant Inhibition of Bovine Viral Diarrhea Virus Entry. J. Virol. *82*, 2427–2436.

Tsukiyama-Kohara, K., Iizuka, N., Kohara, M., and Nomoto, A. (1992). Internal Ribosome Entry Site within Hepatitis C Virus RNA. J. Virol. *66*, 1476–1483.

Vassilev, V.B., Collett, M.S., and Donis, R.O. (1997). Authentic and Chimeric Full-Length Genomic cDNA Clones of Bovine Viral Diarrhea Virus That Yield Infectious Transcripts. J. Virol. *71*, 471–478.

Wakita, T., Pietschmann, T., Kato, T., Date, T., Miyamoto, M., Zhao, Z., Murthy, K., Habermann, A., Kräusslich, H.-G., Mizokami, M., et al. (2005). Production of infectious hepatitis C virus in tissue culture from a cloned viral genome. Nat. Med. *11*, 791–796.

Walther, T. (2017). Experimentelle Charakterisierung des pestiviralen NS2 Membranproteins. Universität zu Lübeck.

Walther, T., Fellenberg, J., Klemens, O., Isken, O., and Tautz, N. (2021). Membrane Topology of Pestiviral Nonstructural Protein 2 and Determination of the Minimal Autoprotease Domain. J. Virol. *95*.

Wang, A., Thurmond, S., Islas, L., Hui, K., and Hai, R. (2017). Zika virus genome biology and molecular pathogenesis. Emerg. Microbes Infect. *6*, e13.

Wang, Z., Nie, Y., Wang, P., Ding, M., and Deng, H. (2004). Characterization of classical swine fever virus entry by using pseudotyped viruses: E1 and E2 are sufficient to mediate viral entry. Virology *330*, 332–341.

Warrener, P., and Collett, M.S. (1995). Pestivirus NS3 (p80) Protein Possesses RNA Helicase Activity. J. Virol. *69*, 1720–1726.

Webster, D.P., Klenerman, P., and Dusheiko, G.M. (2015). Hepatitis C. Lancet *385*, 1124–1135.

Weiskircher, E., Aligo, J., Ning, G., and Konan, K. V (2009). Bovine viral diarrhea virus NS4B protein is an integral membrane protein associated with Golgi markers and rearranged host membranes. Virol. J. *6*, 185.

Welbourn, S., Green, R., Gamache, I., Dandache, S., Lohmann, V., Bartenschlager, R., Meerovitch, K., and Pause, A. (2005). Hepatitis C virus NS2/3 processing is required for NS3 stability and viral RNA replication. J. Biol. Chem. *280*, 29604–29611.

Welply, J.K., Shenbagamurthi, P., Lennarz, W.J., and Naider, F. (1983). Substrate Recognition by Oligosaccharyltransferase - Studies on Glycosylation of Modified Asn-X-Thr/Ser Tripeptides. J. Biol. Chem. *268*, 11856–11863.

Wessel, D., and Flügge, U.I. (1984). A Method for the Quantitative Recovery of Protein in Dilute Solution in the Presence of Detergents and Lipids. Anal. Biochem. *138*, 141–143.

Wiskerchen, M., and Collett, M.S. (1991). Pestivirus Gene Expression : Protein p80 of Bovine Viral Diarrhea Virus Is a Proteinase Involved in Polyprotein Processing. Virology *184*, 341–350.

Wrensch, F., Crouchet, E., Ligat, G., Zeisel, M.B., Keck, Z.Y., Foung, S.K.H., Schuster, C., and Baumert, T.F. (2018). Hepatitis C virus (HCV)-apolipoprotein interactions and immune evasion and their impact on HCV vaccine design. Front. Immunol. *9*.

Wu, M.-J., Shanmugam, S., Welsch, C., and Yi, M. (2019). Palmitoylation of Hepatitis C Virus NS2 Regulates Its Subcellular Localization and NS2-NS3 Autocleavage. J. Virol. *94*, e00906-19.

Wu, X., Lee, E.M., Hammack, C., Robotham, J.M., Basu, M., Lang, J., Brinton, M.A., and Tang, H. (2014). Cell Death-Inducing DFFA-Like Effector b Is Required for Hepatitis C Virus Entry into Hepatocytes. J. Virol. *88*, 8433–8444.

Xu, J., Mendez, E., Caron, P.R., Lin, C., Murcko, M.A., Collett, M.S., and Rice, C.M. (1997). Bovine Viral Diarrhea Virus NS3 Serine Proteinase: Polyprotein Cleavage Sites, Cofactor Requirements, and Molecular Model of an Enzyme Essential for Pestivirus Replication. J. Virol. *71*, 5312–5322.

Yamashita, T., Kaneko, S., Shirota, Y., Qin, W., Nomura, T., Kobayashi, K., and Murakami, S. (1998). RNA-dependent RNA polymerase activity of the soluble recombinant hepatitis C virus NS5B protein truncated at the C-terminal region. J. Biol. Chem. *273*, 15479–15486.

Yao, N., Reichert, P., Taremi, S.S., Prosise, W.W., and Weber, P.C. (1999). Molecular views of viral polyprotein processing revealed by the crystal structure of the hepatitis C virus bifunctional protease-helicase. Structure *7*, 1353–1363.

Yi, M., and Lemon, S.M. (2003a). Structure-function analysis of the 3′ stem-loop of hepatitis C virus genomic RNA and its role in viral RNA replication. RNA *9*, 331–345.

Yi, M., and Lemon, S.M. (2003b). 3′ Nontranslated RNA Signals Required for Replication of Hepatitis C Virus RNA. J. Virol. *77*, 3557–3568.

Yi, M., Ma, Y., Yates, J., and Lemon, S.M. (2007). Compensatory Mutations in E1, p7, NS2, and NS3 Enhance Yields of Cell Culture-Infectious Intergenotypic Chimeric Hepatitis C Virus. J. Virol. *81*, 629–638.

Yi, M., Ma, Y., Yates, J., and Lemon, S.M. (2009). trans-Complementation of an NS2 Defect in a Late Step in Hepatitis C Virus (HCV) Particle Assembly and Maturation. PLoS Pathog *5*, 1000403.

Yost, S.A., and Marcotrigiano, J. (2013). Viral precursor polyproteins: Keys of regulation from replication to maturation. Curr. Opin. Virol. *3*, 137–142.

Yu, H., Grassmann, C.W., and Behrens, S.-E. (1999). Sequence and Structural Elements at the 3' Terminus of Bovine Viral Diarrhea Virus Genomic RNA: Functional Role during RNA Replication. J. Virol. *73*, 3638–3648.

Yu, H., Isken, O., Grassmann, C.W., and Behrens, S.-E. (2000). A Stem-Loop Motif Formed by the Immediate 5′ Terminus of the Bovine Viral Diarrhea Virus Genome Modulates Translation as well as Replication of the Viral RNA. J. Virol. *74*, 5825–5835.

Yu, Y., Scheel, T.K.H., Luna, J.M., Chung, H., Nishiuchi, E., Scull, M.A., Echeverría, N., Ricardo-Lax, I., Kapoor, A., Lipkin, I.W., et al. (2017). miRNA independent hepacivirus variants suggest a strong evolutionary pressure to maintain miR-122 dependence. PLOS Pathog. *13*, e1006694.

Zahid, M.N., Turek, M., Xiao, F., Dao Thi, V.L., Guérin, M., Fofana, I., Bachellier, P., Thompson, J., Delang, L., Neyts, J., et al. (2013). The postbinding activity of scavenger receptor class B type I mediates initiation of hepatitis C virus infection and viral dissemination. Hepatology *57*, 492–504.

Zhong, J., Gastaminza, P., Cheng, G., Kapadia, S., Kato, T., Burton, D.R., Wieland, S.F.,

Uprichard, S.L., Wakita, T., and Chisari, F. V (2005). Robust hepatitis C virus infection in vitro. Proc. Natl. Acad. Sci. U. S. A. *102*, 9294–9299.

Zhong, W., Gutshall, L.L., and Del Vecchio, A.M. (1998). Identification and Characterization of an RNA-Dependent RNA Polymerase Activity within the Nonstructural Protein 5B Region of Bovine Viral Diarrhea Virus. J. Virol. *72*, 9365–9369.

Zhong, W., Uss, A.S., Ferrari, E., Lau, J.Y.N., and Hong, Z. (2000). De Novo Initiation of RNA Synthesis by Hepatitis C Virus Nonstructural Protein 5B Polymerase. J. Virol. *74*, 2017–2022.

Zhu, Q., and Casey, J.R. (2007). Topology of transmembrane proteins by scanning cysteine accessibility mutagenesis methodology. Methods *41*, 439–450.

8 Supplements

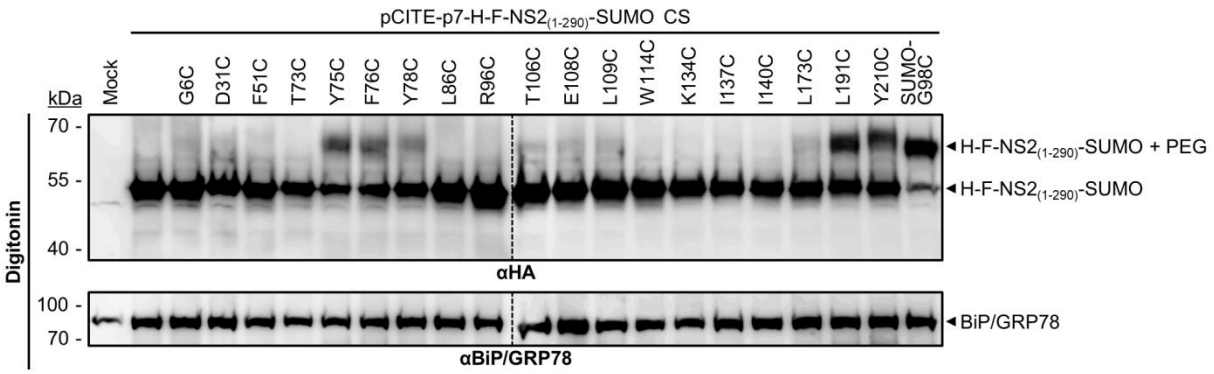

Fig. S 1: Analysis of PEGylation of H-F-NS2$_{(1-290)}$-SUMO CS derivatives after treatment with Digitonin (accessibility for PEG-Mal modification after selective PM permeabilization). Protein samples were separated by SDS-PAGE followed by western blot analyses using an αHA primary antibody. The cysteine-free NS2 derivative and the SUMO-G98C variant served as negative or positive control, respectively. Mock refers to cell lysates without transfected plasmid DNA. Positions of the PEGylated (H-F-NS2$_{(1-290)}$-SUMO + PEG) and the unmodified (H-F-NS2$_{(1-290)}$-SUMO) protein products are indicated on the right. The detection of BiP/GRP78 served as loading control. The molecular mass standards in kilodalton (kDa) are given on the left.

9 Acknowledgment

First and foremost, I would like to thank my doctoral supervisor Prof. Dr. Norbert Tautz for the opportunity to do my doctorate at the Institute of Virology and Cell Biology as well as for issuing the topic and supervising my work. I thank him for the inspiring discussions, his enthusiasm for science, the many advice and ideas as well as for his constant motivation and support.

My special thanks go to Dr. Olaf Isken for inspiring scientific discussions, advice and continuous support, which I appreciate very much. I sincerely thank him for his help in proofreading this work and for his support in writing scientific publications.

My sincere thanks go to my fellow doctoral students and former colleagues Dr. Danilo Dubrau, Jonas Fellenberg and Jan Knickmann for their constant support, the motivating talks and the exchange in the lab and at the seminars as well as for the many funny moments and nice memories.

I would like to thank all staff members of the Institute of Virology and Cell Biology for their helpfulness, collaboration and the pleasant working atmosphere. I am especially grateful to Barbara Bruhn for her tireless support during experiments and to Heiko Steenbock for his constant assistance and good advice concerning technical equipment.

I would like to thank Prof. Dr. Enno Hartmann and Susanne Allan from the Institute of Biology for providing the Odyssey Imaging System.

I would like to thank my parents and my parents-in-law for their support, interest and encouragement during my studies and doctorate.

Last but not least, I would like to especially thank my wife Anna, who has unconditionally supported me and had my back during the past years. I thank her for her love and belief in me.

Curriculum Vitae

Name: Thomas Walther né Kühne
Date of birth: 16th August 1983
Place of birth: Dresden

Doctorate:

01/2018 – 03/2021 **Research Associate/Doctoral Student**
Research group Tautz, Institute of Virology and Cell Biology, University of Luebeck; Director: Prof. Dr. Norbert Tautz

Studies:

10/2015 – 12/2017 **Master of Science in Molecular Life Science, University of Lübeck**

- Grade: 1.3
- Master's thesis: "Experimental characterization of the pestiviral NS2 membrane protein", Research group Tautz, Institute of Virology and Cell Biology, University of Luebeck

10/2012 – 09/2015 **Master of Science in Molecular Life Science, University of Lübeck**

- Grade: 1.5
- Bachelor's thesis: "Functional characterization of Gαq/11-coupled receptors in primary brain endothelial cells ", Research group Schwaninger, Institute for Experimental and Clinical Pharmacology and Toxicology, University of Luebeck

Internships:

01/2017 – 03/2017 **Intern at the Institute of Biochemistry, University of Lübeck**

- Subject: "Compartment-dependent crystallization of human nicastrin in living insect cells"
- Supervisor: Prof. Dr. Lars Redecke

10/2012 – 09/2015 **Intern at the Heinrich Pette Institute, Hamburg**

- Research department "Antiviral Strategies", Prof. Dr. Joachim Hauber
- Subject: "Generation of HIV latency reporter cell lines through CRISPR/Cas9-mediated genome editing"
- Supervisor: Dr. Dr. Ulrike Lange

School graduation:

06/2003 **German High School Diploma (A-levels)**
Berufliche Schulen des Kreises Herzogtum Lauenburg, Moelln